

# METHODS FOR MULTILoop CALCULATIONS AND HIGGS BOSON PRODUCTION AT THE LHC

Zur Erlangung des akademischen Grades eines  
DOKTORS DER NATURWISSENSCHAFTEN  
von der Fakultät für Physik des Karlsruher Instituts für Technologie  
(KIT)

genehmigte DISSERTATION

von

Dipl.-Phys. Jens Simon Hoff  
aus Speyer

Tag der mündlichen Prüfung: 30. Januar 2015

Referent: Prof. Dr. Matthias Steinhauser  
Korreferent: Prof. Dr. Johann Kühn



# CONTENTS

---

1	INTRODUCTION	7
2	FEYNMAN INTEGRAL FAMILIES	11
2.1	Definition and notation	11
2.1.1	Topology: integral class or family	11
2.1.2	From integrals to graphs	14
2.1.3	Completeness	17
2.1.4	Linear independence	19
2.1.5	Coefficient matrix	20
2.1.6	Different types	21
2.2	Linear dependence	22
2.2.1	Gröbner bases	22
2.2.2	Partial fractioning relations	27
2.3	Parametric representations	30
2.3.1	Symanzik polynomials	30
2.3.2	Properties	34
2.3.3	Recursiveness	35
2.3.4	Scalefulness	37
2.4	Canonically ordered polynomials	40
2.4.1	Topology identification	41
2.4.2	Canonical ordering	44
2.4.3	Application to topologies	50
2.4.4	Subtopologies	52
2.4.5	Finding momenta shifts	55
2.4.6	Symmetries	57
2.4.7	Mapping relations	59
2.5	The package TopoID	61
2.5.1	Example: massless propagators to five loops	62
2.6	Laporta's algorithm	68
2.6.1	Integration-by-parts relations	70
2.6.2	Integral reduction	72
2.6.3	Asset of TopoID	75
2.7	Completing topologies	76
2.7.1	Irreducible scalar products	76
2.7.2	Supertopologies	76
2.7.3	Revealing non-trivial relations	79
3	REVERSED UNITARITY	81
3.1	Optical theorem and Cutkosky's rules	83
3.1.1	Optical theorem	83
3.1.2	Cutkosky's rules	85
3.1.3	Extension	89
3.2	Handling cut diagrams	90

3.2.1	Detecting cuts	90
3.2.2	Cut integral reduction	101
4	HIGGS BOSON PRODUCTION	103
4.1	Introduction	103
4.1.1	General procedure	104
4.1.2	Anatomy of the total cross section	106
4.1.3	Status of theoretical predictions	110
4.2	Computational techniques	114
4.2.1	Effective theory	114
4.2.1.1	Renormalization	115
4.2.1.2	Matching coefficient	116
4.2.2	Mass factorization	117
4.2.2.1	Singular structure	117
4.2.2.2	Redefinition of the PDFs	119
4.2.2.3	DGLAP evolution equation	120
4.2.2.4	Parton splitting functions	123
4.3	Cross sections to NNLO	126
4.3.1	Setup of the calculation	127
4.3.2	Definition of topologies	128
4.3.3	Results	131
4.3.3.1	Harmonic polylogarithms	134
4.4	Convolutions of NNLO cross sections	136
4.4.1	Transition functions to N <sup>3</sup> LO	136
4.4.2	Collinear counterterms to N <sup>3</sup> LO	139
4.4.3	Systematic approach to convolution integrals	141
4.4.3.1	Mellin transform and harmonic sums	142
4.4.3.2	Regularized derivative	143
4.5	Contributions to Higgs boson production at N <sup>3</sup> LO	148
4.5.1	Fermionic contribution in the $qq'$ -channel	149
4.5.2	The complete $qq'$ -channel	155
4.5.2.1	Definition of topologies	155
4.5.2.2	Finding additional relations	160
4.5.3	Roadmap to the full calculation	165
5	OTHER APPLICATIONS	167
5.1	Higgs boson pair production	167
5.1.1	Top quark mass corrections	168
5.1.1.1	Large mass expansion	169
5.1.2	Towards NNLO corrections	171
5.1.2.1	Mapping of topologies	171
5.2	Drell-Yan process	172
5.2.1	Treatment of $\gamma_5$	174
5.2.2	Results	175
6	CONCLUSION	177
A	FEYNMAN INTEGRAL FAMILIES	179

A.1	Massless propagators at five loops	179
B	HIGGS BOSON PRODUCTION	185
B.1	Splitting functions at NNLO	185
B.2	Collinear counterterms at N <sup>3</sup> LO	187
C	SAMPLE CODE	191
C.1	Generic topologies	191
C.2	Basic topologies	193
C.3	Mapping topologies	196
C.3.1	Configuration for exp	196
C.3.2	Signature file	199
C.3.3	Non-factorizing topologies	200
C.3.4	Factorizing topologies	202
	Bibliography	205



## INTRODUCTION

---

In the summer of 2012 ATLAS and CMS at CERN announced the discovery of a scalar boson, see Refs. [1, 2]. But it remains an open question whether the discovered particle is indeed the Higgs boson of the Standard Model (SM). In forthcoming years the couplings of the found boson to the various gauge bosons and fermions will be measured with improved precision in order to verify their compatibility with the values dictated within the SM.

One fundamental property of theories such as Quantum Electrodynamics (QED) and Quantum Chromodynamics (QCD), which are experimentally confirmed, is *gauge invariance*. The correct description also of weak interactions requires *massive* vector bosons  $W^\pm$  and  $Z^0$ . In contrast, photons  $\gamma$  in QED and gluons  $g$  in QCD are massless. However, introducing masses (of vector bosons and fermions) directly as parameters of a theory that includes also weak interactions violates gauge invariance. Instead, a scalar doublet field accompanied by a potential is considered. The form of the potential gives rise to a non-vanishing vacuum expectation value which is phrased as “spontaneous symmetry breaking”. After a reparametrization of the theory, the “broken phase” of the SM, massless photons but massive  $Z^0$ - and  $W^\pm$ -bosons emerge. QED and weak interactions are *unified* in this electroweak theory and in addition a massive scalar particle remains, the *Higgs boson*. All masses of fermions and vector bosons are generated by their couplings to this Higgs boson.

The main subject of this thesis is the inclusive cross section of the SM Higgs boson in the gluon fusion production mode. Even though gluon fusion is dominant at the LHC other partonic production modes have to be accounted for, too. The complete list reads:

- gluon fusion ( $gg \rightarrow H$ ),
- vector boson fusion ( $qq \rightarrow qqH$ ),
- Higgs strahlung ( $q\bar{q}' \rightarrow HW^\pm$  and  $q\bar{q}, gg \rightarrow HZ^0$ ),
- production in association with top quark pairs ( $q\bar{q}, gg \rightarrow t\bar{t}H$ ).

Weighting the partonic cross sections with the corresponding parton distribution functions (PDFs) and integrating over the momentum fractions gives the hadronic cross sections. Then, in order to relate the hadronic cross section to the signals experimenters *actually measure*, a vast program of theoretical and experimental techniques comes into play.

From theoretical side these are:

- combination with the partial width of each decay mode (fermion and gauge boson pairs) to form a hard subprocess,

- parton showers (radiation cascades) for the initial and final state particles of the hard subprocess,
- hadronization and hadronic decay chains of unstable into (meta)stable particles,
- underlying events for the incoming hadron's remains not taking part in the hard scattering,
- multiple parton interactions involving a hard subprocess

to arrive at a full event presenting itself in the detector.

The decays  $H \rightarrow b\bar{b}, \tau\bar{\tau}, W^+W^-, Z^0Z^0, \gamma\gamma$  are of most interest since they either dominate numerically (like  $b\bar{b}, \tau\bar{\tau}$  and  $W^+W^-$ ) or allow by clear signatures (of subsequent decays) for a good identification and separation from background processes (like  $\gamma\gamma, W^+W^- \rightarrow 2l2\nu$  and  $Z^0Z^0 \rightarrow 4l$ ).

Before actually producing a Higgs boson partons may emit additional quarks or gluons, not relevant for the hard subprocess but modifying the provided energy. For the final state partons the situation is similar and in both cases Monte Carlo parton showers give a quantitative description. Followed by hadronization and hadronic decays the evolution to smaller energy scales and higher-multiplicity final states in the detector is done.

Sample events generated in this way used together with detector simulations enable experimentalists to tune their machinery for event reconstruction. Only then the set of signals recorded by the different components of the detector can be translated into a snapshot of kinematic quantities of a multi-particle final state and finally put into data analysis. These sets of recorded events from experiment enable extraction of distributions for quantities that, in the end, are confronted with the respective theoretical predictions (made on the basis of Monte Carlo events, too).

We emphasize that the total cross section for Higgs boson production via gluon fusion is merely one puzzle piece needed to connect the abstract picture of elementary interactions described by Quantum Field Theory (QFT) to physical reality. However, the Higgs boson cross section is an important puzzle piece, itself put together from various ingredients.

#### WHY HIGHER-ORDER CORRECTIONS?

Within the next decade the data acquired by the LHC and its upgrades will reduce statistical errors. Ultimately, the remaining uncertainties in the measurement of the Higgs boson cross section will challenge the precision of available theoretical predictions which is about 10%. Theory uncertainties are partly due to the PDFs, partly due to unknown higher-order corrections in the perturbation series of the partonic cross section. The leading order (LO), next-to-leading order (NLO) and next-to-next-to leading order (NNLO) terms of the perturbation series are known but rather slow convergence of the series was found. Therefore, the next-to-next-to-next-to-leading ( $N^3LO$ ) term is the objective at present. Albeit, the  $N^3LO$  calculation is a testing ground for new theoretical methods.



## OUTLINE

Chapters 2 and 3 of this thesis lay the technical foundation for calculations of inclusive partonic cross sections which are topic of Chapters 4 and 5. In Chapter 2 a very detailed discussion of methods to handle classes of Feynman diagrams is given. Reversed unitarity, enabling treatment of real corrections as loop integrals, is explained in Chapter 3. Chapter 4 is devoted to higher-order corrections to Higgs boson production. Chapter 5 describes two more applications of the techniques described before: Higgs boson pair production and the Drell-Yan process.



## FEYNMAN INTEGRAL FAMILIES

---

The following is the first of two technical chapters giving a pedagogical introduction to analytic methods used in nowadays calculations of matrix elements in terms of Feynman diagrams. Commonly, it is preferred to work initially with families of Feynman integrals which will be subject of this chapter. We lay out the notation for quantities, derive and motivate some of their useful properties and also formulate precisely algorithms for systematic solutions to particular problems arising in such kind of calculations. All of this is illustrated by numerous examples from real applications. These are selected to be as simple as possible without their characteristic features going astray.

### 2.1 DEFINITION AND NOTATION

With the beginning of this section we shall give a clear definition of a Feynman diagram class, alternatively called Feynman integral family or plainly referred to as “topology”. Even though the term topology in this context is actually an abuse of the name for an area of mathematics, we will stick to it. The mathematics behind “our” topologies is a mixture of rather elementary linear algebra and graph theory.

#### 2.1.1 Topology: integral class or family

We will denote topologies by capital letters, e.g.  $T, T_1, T_2$  and so on. A topology is a collection of  $N_f$  scalar factors  $\{F_i\}$  raised to arbitrary powers  $\{a_i\}$ , usually referred to as “indices”. In these sets we do not allow for duplicates, viz. factors with the same representation in momentum space are immediately identified. If the indices  $\{a_i\}$  are fixed to particular values we have a definite Feynman integral which we denote by capital letters, e.g.  $I, I_1, I_2$  and so on to distinguish from topologies. Symbols used for indices with subscripts omitted are to be understood as the sum of all indices,

$$a = \sum_{i=1}^{N_f} a_i. \quad (1)$$

If one considers a particular index  $a_j \leq 0$ , we speak of  $F_j =: N_j$  as a “pure numerator” or “irreducible scalar product” with which we will concern shortly. Reversely, if the sign of  $a_j$  is not restricted we call  $F_j =: D_j$  a “real denominator” or “propagator”. Usually indices can be regarded as integers but for some applications even complex numbers are admissible. As an example consider the recursive integration of massless one-loop propagators appearing as subintegral. The result of each integration has the form of

a propagator raised to a power involving  $\epsilon$ , a complex number describing the deviation from four space-time dimensions. Accordingly,  $N_d$  and  $N_n$  are the numbers of real denominators and pure numerators, respectively, and we have:

$$N_f = N_d + N_n. \quad (2)$$

The  $N_d$  propagators  $\{D_i\}$  with  $a_i$  unrestricted depend in general on  $N_d$  masses  $\{m_i\}$  assigned to corresponding particles and “line momenta”  $\{q_i\}$  flowing through these real denominators, such that we can write

$$\frac{1}{D_i} =: d_i = m_i^2 \pm q_i^2 \quad (3)$$

for the quadratic forms  $\{d_i\}$ . Therefore, the  $\{d_i\}$  are of mass dimension two. The plus sign in Eq. (3) applies when working with Euclidean momenta and the minus sign applies when working with Minkowskian momenta. Compared to the usual form of a scalar Feynman propagator

$$\frac{1}{P_i} := q_i^2 - m_i^2 + i\epsilon, \quad (4)$$

we omitted the  $+i\epsilon$ -prescription merely for convenience. Furthermore, we implicitly multiply all integrals by a factor  $(-1)^a$  because then we do not have to care about additional sign changes induced by switching between Minkowski and Euclidean space via Wick-rotation.

The line momenta  $\{q_i\}$  are linear combinations with the integer coefficients  $\{c_{ij}\}$  and  $\{d_{ij}\}$  of the  $N_p$  independent external momenta  $\{p_i\}$  and the  $N_k$  internal or integration momenta  $\{k_i\}$  of the Feynman integral whose graph always has  $N_L = N_k$  loops:

$$q_i = \sum_{j=1}^{N_p} c_{ij} p_j + \sum_{j=1}^{N_k} d_{ij} k_j \quad \text{with} \quad c_{ij}, d_{ij} \in \mathbb{Z}. \quad (5)$$

The notation with a  $(N_p + N_k)$ -dimensional vector of common momenta  $v$  and a common coefficient  $N_d \times (N_p + N_k)$  matrix  $C$  is a more compact alternative:

$$q_i = C_{ij} v_k \quad \text{with} \quad (6)$$

$$v = \left( p_1, \dots, p_{N_p}, k_1, \dots, k_{N_k} \right) \quad \text{and} \quad C_{ij} = c_{ij}, \quad C_{i, N_p+j} = d_{ij}.$$

For a particular kinematic setup, i.e. given external and internal momenta, supplemented by optional constraints, e.g. putting particles on-shell, one can form all possible scalar products

$$x_{p_i, p_j} := p_i \cdot p_j, \quad s_{p_i, k_j} := p_i \cdot k_j, \quad s_{k_i, k_j} := k_i \cdot k_j, \quad (7)$$

where  $\{x_{p_i, p_j}\}$  are external scalar products or invariants,  $\{s_{p_i, k_j}\}$  and  $\{s_{k_i, k_j}\}$  are internal or mixed scalar products. From expressions containing the external scalar products  $\{x_{p_i, p_j}\}$  one usually defines the (generalized) Mandelstam variables. The momentum symbols  $p$  and  $k$  may also be omitted if

there is no danger of confusion. Internal and mixed scalar products can then be labeled collectively  $\{s_{ij}\}$ . To obtain the maximum number of possible internal scalar products  $\hat{N}_{\text{sp}}$  (cf. Tab. 1 on Page 16) one has to combine each of the external with each of the internal momenta and form additionally all sorted pairs of internal momenta:

$$\hat{N}_{\text{sp}} = N_p N_k + N_k \frac{N_k + 1}{2} = \frac{N_k}{2} (2N_p + N_k + 1). \quad (8)$$

$\hat{N}_{\text{sp}}$  must be reduced by the number of imposed scalar conditions  $N_{\text{sc}}$  to give the number of actually appearing scalar products  $N_{\text{sp}}$ :

$$N_{\text{sp}} = \hat{N}_{\text{sp}} - N_{\text{sc}}. \quad (9)$$

An example follows below.

Scalar products occur linearly in all the  $\{f_i\}$  where

$$1/F_i =: f_i, \quad (10)$$

especially as some arbitrary linear combination in the pure numerators

$$\frac{1}{N_i} =: n_i \quad \text{with} \quad a_i \leq 0. \quad (11)$$

Combining all these notations, we have for a topology  $T$  in  $D = 4 - 2\epsilon$  dimensions:

$$\begin{aligned} T(a_1, \dots, a_{N_f}) &= \prod_{i=1}^{N_k} \int dk_i^D \left\{ \prod_{j=1}^{N_f} \frac{1}{f_j^{a_j}} \right\} = \\ &T(a_1, \dots, a_{N_d}, a_{N_d+1}, \dots, a_{N_d+N_n}) \\ &= \prod_{i=1}^{N_k} \int dk_i^D \left\{ \prod_{j=1}^{N_d} \frac{1}{d_j^{a_j}} \right\} \left\{ \prod_{j=N_d+1}^{N_d+N_n} n_j^{-a_j} \right\} \\ &= \prod_{i=1}^{N_k} \int dk_i^D \left\{ \prod_{j=1}^{N_d} \frac{1}{[m_j^2 \pm q_j^2]^{a_j}} \right\} \left\{ \prod_{j=N_d+1}^{N_d+N_n} n_j^{|a_j|} \right\}, \end{aligned} \quad (12)$$

where the factor  $\mu^{2\epsilon N_k}$  fixing the mass dimension of the integration measure is here and also the following suppressed, as well as the dependence on dimension  $D$  and external invariants  $\{x_{p_i, p_j}\}$  in the argument of  $T$ . Even though the  $\{f_i\}$  are strictly speaking the reciprocal topology factors, we will often call them the topology factors.

**Example 1.** The topology  $T_{H, \text{NLO}}^{\text{basic}}$  is defined below. It appears in our calculation for the NLO corrections to Higgs boson production via forward scattering. This means we have four external legs with momenta  $p_1, \dots, p_4$  fixed by  $p_1$  and  $p_2$  only:

$$p_3 = p_1, \quad p_4 = p_2.$$

In addition, all external particles are put on-shell:

$$p_1^2 = p_2^2 = 0.$$

Here, we have  $N_k = 1$  and  $N_p = 3$  resulting in  $\hat{N}_{\text{sp}} = 4$ . Our kinematic setup demands that

$$p_3 \cdot k_1 = p_1 \cdot k_1,$$

meaning  $N_{\text{sc}} = 1$  and thus  $N_{\text{sp}} = 3$  ( $p_4$  is not independent). This leaves us explicitly with the scalar products

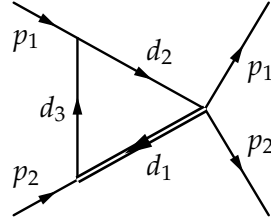
$$\begin{aligned} \{x_{ij}\} &= \{p_1 \cdot p_2 = -s/2\}, \\ \{s_{ij}\} &= \{p_1 \cdot k_1, p_2 \cdot k_1, k_1^2\}. \end{aligned}$$

Inspecting all diagrams for Higgs boson production at NLO, we find a single topology with  $N_f = N_d = 3$  and  $N_n = 0$  for

$$\begin{aligned} m_1 &= m_H, & q_1 &= k_1, \\ m_2 &= 0, & q_2 &= p_1 + p_2 + k_1, \\ m_3 &= 0, & q_3 &= p_2 + k_1. \end{aligned}$$

All in all, this can be represented as follows:

$$T_{H,\text{NLO}}^{\text{basic}}(a_1, a_2, a_3) = \int dk_1^D \frac{1}{d_1^{a_1} d_2^{a_2} d_3^{a_3}} =$$



$$\begin{aligned} \text{with } d_1 &= m_H^2 + k_1^2, \\ d_2 &= (p_1 + p_2 + k_1)^2 = -s + 2p_1 \cdot k_1 + 2p_2 \cdot k_1 + k_1^2, \\ d_3 &= (p_2 + k_1)^2 = 2p_2 \cdot k_1 + k_1^2. \end{aligned}$$

Labels on external lines state the momenta flowing in and out, labels on internal lines their corresponding topology factors. Simple plain black lines represent massless propagators (corresponding to quarks or gluons), the double black line a massive propagator (for the Higgs boson). Arrows indicate the directions of line momentum flow.

### 2.1.2 From integrals to graphs

Topologies usually have a diagrammatic representation. However, these representations are not unique (cf. Example 2) and certain propagators and

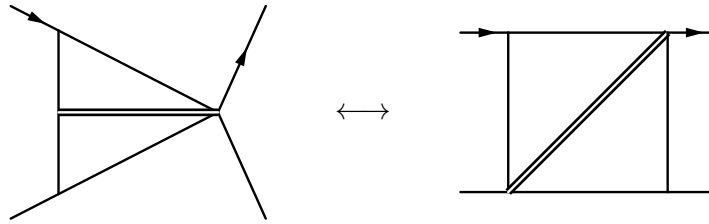
kinematic conditions cannot be envisioned as graph elements, e.g. the propagators of linear form in heavy quark effective theory (HQET):

$$\frac{1}{-2v \cdot q + i\epsilon'} \quad (13)$$

where  $q$  is a line momentum and  $v$  the velocity of a heavy quark. Therefore, the graph of a topology does not give a complete definition but is at least more tangible in practical use than just a mere list of quadratic forms.

In most cases topologies are deduced directly from Feynman diagrams. The lines in a diagram correspond to propagators and are also called edges. These edges are oriented due to the direction of the momentum flowing from a start vertex to an end vertex. It is admissible for multiple edges to connect to the same pair of vertices (one can think of self-energy insertions). In graph language this property is termed as “non-simple” or the corresponding graph as “multigraph”. Thus, the graphs we are dealing with in the context of QFTs are *directed* and *non-simple*.

**Example 2.** In the calculation for Higgs boson production via forward scattering two non-isomorphic diagrams appear that can both be attached to the same topology (this example will reappear in greater detail later on Page 43 and is also discussed in Ref. [3]):



The notation is as in Example 1 with the exception that arrows on external legs show entrance and exit only for momentum  $p_1$  since this is sufficient.

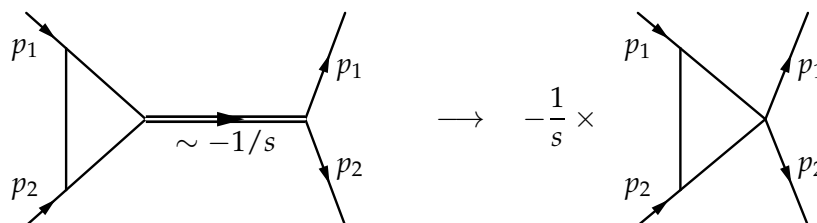
One should not confuse the number of internal lines  $N_I$  with the number of propagators  $N_d$ . Internal lines not part of a loop are not counted among the real propagators since they do not have to be considered in loop integrations and are “constants” in this sense. See Example 3, where  $N_I = 4$  but  $N_d = 3$ . Moreover, different edges of a graph could be associated with a single denominator factor of a topology (if they have the same mass in addition to the same momenta flow), resulting in a double counting. See Example 4, again with  $N_I = 4$  but  $N_d = 3$ .

**Example 3.** The topology associated with virtual NLO corrections for Higgs boson production contains a massive propagator without loop momentum

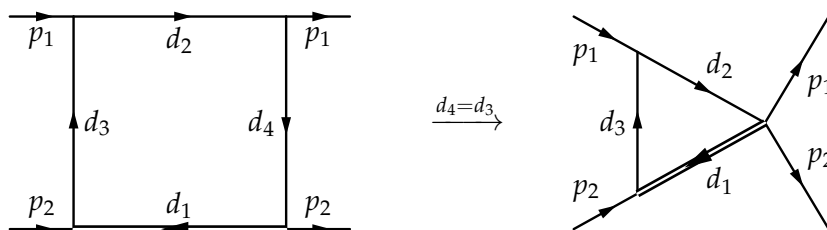
**Table 1:** Equations (8) and (14) applied for illustration purposes to various values of  $N_p$  and  $N_k$ . Note that the results for  $\hat{N}_I$  are meaningless for  $N_E = N_p + 1 \leq 2$  and  $N_L = N_k = 0$ , it is more sensible to define  $\hat{N}_I = 0$  in these cases.

$\hat{N}_{\text{sp}}, \hat{N}_I$	$N_k = 0$	$N_k = 1$	$N_k = 2$	$N_k = 3$	$N_k = 4$	$N_k = 5$
$N_p = 0$	0, -2	1, 1	3, 4	6, 7	10, 10	15, 13
$N_p = 1$	0, -1	2, 2	5, 5	9, 8	14, 11	20, 14
$N_p = 2$	0, 0	3, 3	7, 6	12, 9	18, 12	25, 15
$N_p = 3$	0, 1	4, 4	9, 7	15, 10	22, 13	30, 16
$N_p = 4$	0, 2	5, 5	11, 8	18, 11	26, 14	35, 17

which can be contracted immediately (giving a constant  $-1/s$ ) and is not part of the topology:



**Example 4.** There is an alternative picture for  $T_{H,\text{NLO}}^{\text{basic}}$  from Example 1 as planar box diagram that has two propagators with identical line momenta (and masses) which can be identified readily, viz. one line is contracted:



The maximum number of internal lines or edges  $\hat{N}_I$  of a graph (cf. Tab. 1) can be derived from the number of external lines or legs  $N_E$  ( $= N_p + 1$  due to momentum conservation) and the number of loops  $N_L = N_k$ . Quantities with a hat refer to the possible maximum value within a kinematic setup, corresponding quantities without hat refer to a particular topology. We assume the number of edges connecting to a vertex, called *vertex degree*, is three for all vertices. Let us call such graphs *complete* or *maximal*. Graphs with higher-degree vertices can always be obtained by contracting edges in maximal graphs. Imposing the condition  $N_E > 2$  for  $N_L = 0$ , this means

$$\hat{N}_I = N_E + 3(N_L - 1) = N_p + 3N_k - 2. \quad (14)$$

With  $N_L = 1$  the maximum number of internal lines equals the number of external legs which is incremented by one compared to the number of independent external momenta  $N_p$ . For every additional loop one has to



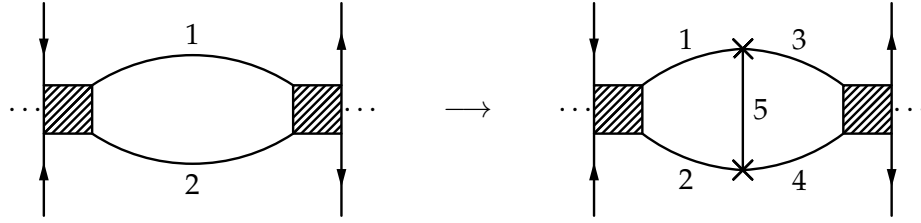


**Figure 1:** Generic graph where one loop is added by insertion of a line at the cuts of two edges. This guarantees that graphs built up in this manner have the possible maximum number of edges (otherwise higher-degree vertices would appear). Dashed areas denote generic parts of the graph kept unchanged.

insert an extra line by intersecting two present lines (giving two additional lines, see Fig. 1). Vacuum graphs can be understood as having one external leg with no momentum. The number of internal lines  $N_I$  of an arbitrary graph is related to the number of vertices  $N_V$  and  $N_L$  via

$$N_I = N_V + N_L - 1. \quad (15)$$

Adding to  $N_V$  connected vertices one additional edge is bound to result in one additional loop (consider the right diagram in Fig. 1).

In Tab. 1 we show the maximum numbers of scalar products  $\hat{N}_{\text{sp}}$  and internal lines  $\hat{N}_I$  for various configurations of external and internal momenta  $N_p$  and  $N_k$ . It can be seen that  $\hat{N}_{\text{sp}}$  grows more rapidly with  $N_k$  than  $\hat{N}_I$  (quadratically compared to linearly; this issue will be addressed later). Some of the most complicated problems of interest at the moment are four-loop on-shell propagator integrals ( $N_p = 1$  and  $N_k = 4$ ), Higgs boson production in the effective theory via forward scattering ( $N_{\text{sc}} = N_k$ ) at three-loop level ( $N_p = 2$  and  $N_k = 3$ ) or Higgs boson production in association with one jet at two loops in the full theory. The number of masses appearing in a process has also strong impact on the complexity.

### 2.1.3 Completeness

**Definition 1.** If all internal scalar products  $\{s_{ij}\}$  can be expressed by linear combinations of the factors  $\{f_i\}$  of a topology, we call the topology “complete”, otherwise we call it “incomplete”.

It is possible to start with a set  $\{f_i\} = \{d_i\}$  directly inferred from the  $N_d$  unique denominators of a certain diagram that is in the sense of Definition 1 still incomplete. One then joins to this set the missing scalar products  $\{n_i\}$  (or linear combinations of scalar products involving the missing ones) in such a way that the resulting set is complete where at least  $N_{\text{sp}} - N_d$  of these irreducible scalar products are needed.

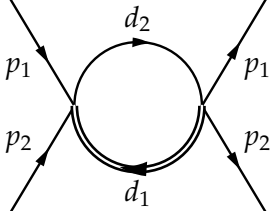
**Example 5.** If we invert the expressions for  $d_1$ ,  $d_2$  and  $d_3$  in  $T_{H,\text{NLO}}^{\text{basic}}$  from Example 1 for the scalar products  $k_1^2$ ,  $p_1 \cdot k_1$  and  $p_2 \cdot k_1$ , we find:

$$k_1^2 = d_1 - m_H^2,$$

$$p_1 \cdot k_1 = \frac{1}{2} (d_2 + s - 2 p_2 \cdot k_1 - k_1^2) = \frac{1}{2} (d_2 - d_3 + s),$$

$$p_2 \cdot k_1 = \frac{1}{2} (d_3 - k_1^2) = \frac{1}{2} (d_3 - d_1 + m_H^2).$$

Hence, we know that  $T_{H,\text{NLO}}^{\text{basic}}$  is a complete topology. Now, let us remove  $d_3$  and observe what changes:

$$\int dk_1^D \frac{n_3^{-a_3}}{d_1^{a_1} d_2^{a_2}} =$$


with

$$k_1^2 = d_1 - m_H^2,$$

$$p_1 \cdot k_1 = \frac{1}{2} (d_2 + s - 2 p_2 \cdot k_1 - k_1^2) = \frac{1}{2} (d_2 - d_1 - 2 n_3 + m_H^2 + s),$$

$$p_2 \cdot k_1 = n_3.$$

After removing  $d_3$  one scalar product (we chose  $p_2 \cdot k_1$  instead of  $p_1 \cdot k_1$ ) could not be expressed by denominator factors. Therefore, we introduced a  $n_3 = p_2 \cdot k_1$  which can only appear in the numerator. This choice is arbitrary; another suggestion would have been

$$n_3 = (p_2 \pm k_1)^2 = \pm 2 p_2 \cdot k_1 + k_1^2.$$

By contracting  $d_3$  we not only made the topology incomplete, we also made it impossible to express integrals with more than two propagators within the contracted topology. By introducing  $n_3$  we remedied the incompleteness of the topology but  $n_3$  cannot represent a propagator and we have to restrict its power  $a_3 \leq 0$ .

In general, one cannot contract an arbitrary propagator in an arbitrary topology to transform a topology with  $n$  external legs to one with  $(n - 1)$  external legs; such a property depends on the considered kinematics. This works in Example 5 since we have forward scattering.

As will be explained later in more detail (see Section 2.6), we require at certain steps of our calculation complete topologies. Put briefly: for technical reasons in the numerators of expressions for individual diagrams constituting the amplitude, all scalar products may appear. But more fundamental is the fact that the same holds for the integration-by-parts relations. Scalar products also appear as parts of the denominators but for the integral reduction it is beneficial to operate on a representation by factor symbols  $\{f_i\}$  exclusively. Thus, we need to express the  $\{s_{ij}\}$  completely in terms of the  $\{f_i\}$ . Note that after this notation change the  $\{n_i\}$  only appear in the numerator, that is with negative indices, see Eq. (12).

Inspecting Eqs. (8) and (14), one can see that the number of scalar products  $\hat{N}_{\text{sp}}$  grows with  $N_k^2$  compared to the number of candidate propagators  $\hat{N}_I$  growing with  $N_k$ . It follows that the problem of initially incomplete

topologies becomes more complex when going to more loops. It can even get worse, e.g., when one deals with diagrams containing effective higher-degree vertices (for example in Higgs boson pair production, see Section 5.1). Then, it may happen that only incomplete or non-maximal graphs occur which give less propagators than complete graphs (containing only degree-three vertices).

#### 2.1.4 Linear independence

**Definition 2.** If there exist linear relations among the factors of a topology  $\{f_i\}$ , possibly involving masses  $\{m_i\}$  and external quantities  $\{x_{ij}\}$ , we label the topology as “linearly dependent” or just “dependent”, otherwise as “linearly independent” or just “independent”.

**Example 6.** Besides  $T_{H,NLO}^{\text{basic}}$ , introduced in Example 1 on Page 13, the topology  $T_{H,NLO}^{\text{generic}}$  shown below also appears when computing diagrams of NLO contributions to Higgs boson production. It differs from  $T_{H,NLO}^{\text{basic}}$  by an additional denominator  $d_4$  whereby it becomes a box diagram with external momenta  $p_1$  and  $p_2$  passing through in a non-planar way.

$$T_{H,NLO}^{\text{generic}}(a_1, a_2, a_3, a_4) = \int dk_1^D \frac{1}{d_1^{a_1} d_2^{a_2} d_3^{a_3} d_4^{a_4}}$$

=

with

$$d_1 = m_H^2 + k_1^2,$$

$$d_2 = (p_1 + p_2 + k_1)^2 = -s + 2 p_1 \cdot k_1 + 2 p_2 \cdot k_1 + k_1^2,$$

$$d_3 = (p_2 + k_1)^2 = 2 p_2 \cdot k_1 + k_1^2,$$

$$d_4 = (p_1 + k_1)^2 = 2 p_1 \cdot k_1 + k_1^2.$$

We can choose the same inversion for internal scalar products as for  $T_{H,NLO}^{\text{basic}}$  written down in Example 5 which is accompanied by one scalar relation among the  $\{d_i\}$ :

$$d_1 + d_2 - d_3 - d_4 = m_H^2 - s.$$

Above relation can be used to perform a partial fractioning as we will see in Section 2.2.

Imposing external conditions such as vanishing external momenta or forward scattering that afflict the number of mixed external-internal scalar products  $\{s_{p_i, k_j}\}$  gives rise to linear dependence relations. Another circumstance for linearly dependent propagators are different masses, for example

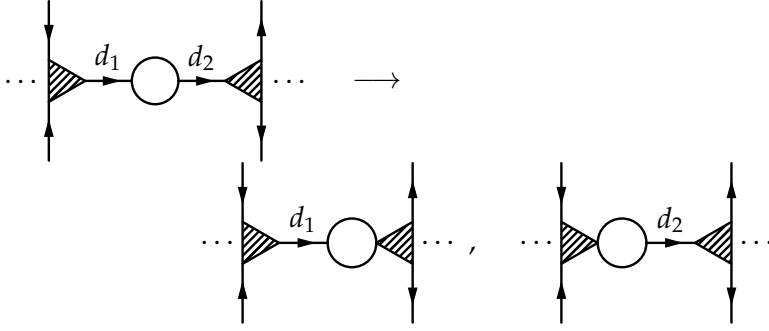


**Figure 2:** Typical graph with a self-energy insertion. If the two propagators  $d_1$  and  $d_2$  connecting to the bubble subgraph have the same masses  $m_1 = m_2$ , they can immediately be identified because they carry the same momenta  $q$ . Otherwise they are related via  $d_1 - d_2 = m_1^2 - m_2^2$ . Partial fractioning gives two contributions, each involving only one of the propagators and its respective mass. In any case a vertex of degree four arises.

on lines connecting to self-energy insertions, see Fig. 2. In the first case the dimension of the space of scalar products spanned by the propagators is reduced, whereas in the latter case the space of propagators is augmented.

The planar box representation for  $T_{H,\text{NLO}}^{\text{basic}}$  in Example 4 or topologies of the type as in Fig. 2 with  $m_1 = m_2$  can also be seen as trivial examples for linearly dependent topology factors (where partial fractioning turns out to be just an identification of equal propagators).

The issue with linearly dependent topologies is that one cannot *uniquely* express internal scalar products  $\{s_{ij}\}$  in terms of the topology factor symbols  $\{f_i\}$ , there may be several possibilities. We will encounter this issue again later in Section 2.6 where the reduction of integral families is described and linearly independent topologies are a prerequisite. But single dependent topologies can *always* be related, via partial fraction decomposition, to sets of independent topologies and the systematic solution to this problem will be presented in the next section, Section 2.2.

### 2.1.5 Coefficient matrix

We close this Section by giving merely an alternative bookkeeping device for topology factors  $\{f_i\}$ , namely the coefficient matrix of a topology  $T$  denoted by  $\tilde{M}$ . If we define the vector of all quadratic quantities

$$\begin{aligned} \tilde{s} &= (m^2, x, s) \\ &= (m_1^2, m_2^2, \dots, x_{p_1, p_1}, x_{p_1, p_2}, \dots, \\ &\quad s_{p_1, k_1}, s_{p_1, k_2}, \dots, s_{k_1, k_1}, s_{k_1, k_2}, \dots), \end{aligned} \quad (16)$$

then we can write all topology factors as

$$f_i = \tilde{M}_{ij} \tilde{s}_j. \quad (17)$$

Thus, we can fit the complete description of a topology into such a “topology matrix”. If we drop all columns associated with masses and external scalar

products we obtain the  $N_f \times N_{\text{sp}}$  matrix  $M$ , the “reduced topology matrix”. Its rank can be used together with the numbers of scalar products  $N_{\text{sp}}$  and topology factors  $N_f$  to reformulate the properties of completeness and independence of topology  $T$ :

$$\begin{aligned} T \text{ is complete} &\Leftrightarrow \text{rank}M = N_{\text{sp}}, \\ T \text{ is independent} &\Leftrightarrow \text{rank}M = N_f. \end{aligned} \tag{18}$$

**Example 7.** Applied to  $T_{H,\text{NLO}}^{\text{generic}}$  of Example 6 with rows corresponding to the vector  $f = (d_1, d_2, d_3, d_4)$  and columns to  $\tilde{s} = (m_H^2, s, p_1 \cdot k_1, p_2 \cdot k_1, k_1^2)$ , we find for the topology matrices:

$$\tilde{M} = \left( \begin{array}{cc|ccc} 1 & 0 & 0 & 0 & 1 \\ 0 & 1 & 2 & 2 & 1 \\ 0 & 0 & 0 & 2 & 1 \\ 0 & 0 & 2 & 0 & 1 \end{array} \right), \quad M = \begin{pmatrix} 0 & 0 & 1 \\ 2 & 2 & 1 \\ 0 & 2 & 1 \\ 2 & 0 & 1 \end{pmatrix} \quad \text{with } \text{rank}M = 3.$$

Clearly,  $T_{H,\text{NLO}}^{\text{generic}}$  is complete ( $N_{\text{sp}} = 3$ ) but linearly dependent ( $N_f = 4$ ). Deleting the last rows gives us directly the results for  $T_{H,\text{NLO}}^{\text{basic}}$  which was complete and linearly independent. Removing yet another row would leave us obviously with an incomplete topology of only rank two.

### 2.1.6 Different types

Lastly, we fix a manner of speech for different types of topologies.

**Definition 3.** *Generic topologies* or *diagram topologies* may in general be incomplete and also linearly dependent. As the name indicates they act as mapping patterns for Feynman diagrams and are usually constructed in a direct one-to-one correspondence to scalar denominators from a particular diagram. See the planar box representation for  $T_{H,\text{NLO}}^{\text{basic}}$  in Example 4 on Page 16 or the non-planar box for  $T_{H,\text{NLO}}^{\text{generic}}$  in Example 6 on Page 19.

**Definition 4.** In contrast, *Basic topologies* or *reduction topologies* need to be linearly independent and complete. Here, the name indicates that they are in an appropriate form to be passed to a reduction algorithm, e.g. Laporta’s algorithm, cf. Section 2.6. See  $T_{H,\text{NLO}}^{\text{basic}}$  in Example 1 on Page 13, Example 3 on Page 15 or Example 5 on Page 17 after completion with  $n_3$ .

Note that each basic topology is also a generic topology but in practice not always used as such. This is justified by basic topologies appearing as “subtopologies” to generic topologies, hence they are included by construction in the treatment of generic topologies whose number should not be too large. The precise definition of a subtopology follows in Section 2.4.4 on Page 52.

## 2.2 LINEAR DEPENDENCE

As mentioned before the problem of linearly dependent topologies and their partial fractioning can be solved in a systematic way. By partial fractioning of a topology we mean partial fractioning of expressions that involve arbitrary powers of linearly dependent propagators. This involves Gröbner bases which we introduce in Section 2.2.1. Originally this idea was presented by A. Pak in Ref. [3], we provide here a more elaborate access to it. The following is loosely based on Refs. [4–8] but much more literature can be found on the subject of Gröbner bases.

### 2.2.1 Gröbner bases

Gröbner bases are sets of multivariate polynomials with certain appealing properties. These properties often enable elegant solutions to problems from different fields of mathematics being unrelated at first sight. For us the most prominent application are algebraic relations among polynomials and their manipulation. But first of all we have to give two basic definitions.

**Definition 5.** If we have the set of polynomials  $F = \{f_1, \dots, f_m\}$  in variables  $\{x_1, \dots, x_n\}$ , then the *ideal*  $\langle F \rangle$  is the set spanned by all polynomial linear combinations of “basis polynomials” from  $F$ ,

$$\langle F \rangle = \left\{ \sum_{i=1}^m p_i f_i : f_i \in F, p_i \in K[x_1, \dots, x_n] \right\}, \quad (19)$$

where  $K$  denotes a field of numbers (e.g. rationals  $\mathbb{Q}$ ),  $K[x_1, \dots, x_n]$  the collection of polynomials built up from variables  $x_1, \dots, x_n$  and coefficients from  $K$ . The ideal  $\langle F \rangle$  can be thought of as the space of relations constructed algebraically from elements in the set  $F$ , thus containing the exact same information as  $F$ .

**Definition 6.** For the monomials  $x^a := \prod_{i=1}^n x_i^{a_i}$  we adopt a *total ordering* which can also be understood as acting on their exponent vectors  $a$ . If within this ordering a monomial  $x^a$  comes before a monomial  $x^b$  or is “simpler”, we denote this by the relation  $x^a \prec x^b$ . Such an ordering (admissible for Gröbner bases) must be multiplicative for monomials  $x^a$  and  $x^b$  or additive for their respective exponent vectors  $a$  and  $b$ ,

$$x^a \prec x^b \quad \Rightarrow \quad x^{a+c} \prec x^{b+c} \quad \forall x^c, \quad (20)$$

and it must begin with 1 as the “smallest” monomial,

$$1 \prec x^a \quad \forall x^a \neq 1. \quad (21)$$

Furthermore, we demand that monomials are positioned within polynomials in descending order from left to right where the “highest-ranked” term (coefficient times monomial) on the very left is the *leading term*. Symbolically we denote the leading term by LT and in explicit examples we underline it.

**Example 8.** Two common orderings also used in the following examples are

$$\begin{array}{l} \text{lexicographic} \\ \dots \prec x_2 \prec x_1 x_2 \prec x_1^2 x_2 \prec \dots, \end{array} \quad \begin{array}{l} 1 \prec x_1 \prec x_1^2 \prec \dots \\ \dots \prec x_2 \prec x_1 x_2 \prec x_1^2 x_2 \prec \dots, \end{array} \quad (22)$$

$$\begin{array}{l} \text{degree-lexicographic} \\ \prec x_1^2 \prec x_1 x_2 \prec x_2^2 \prec \dots \end{array} \quad \begin{array}{l} 1 \prec x_1 \prec x_2 \\ \prec x_1^2 \prec x_1 x_2 \prec x_2^2 \prec \dots \end{array} \quad (23)$$

Both are easier understood when writing exponent vectors,

$$\begin{array}{l} \text{lexicographic} \\ \dots \prec (0, 1) \prec (1, 1) \prec (2, 1) \prec \dots, \end{array} \quad \begin{array}{l} (0, 0) \prec (1, 0) \prec (2, 0) \prec \dots \\ \dots \prec (0, 1) \prec (1, 1) \prec (2, 1) \prec \dots, \end{array} \quad (24)$$

$$\begin{array}{l} \text{degree-lexicographic} \\ \prec (2, 0) \prec (1, 1) \prec (0, 2) \prec \dots \end{array} \quad \begin{array}{l} (0, 0) \prec (1, 0) \prec (0, 1) \\ \prec (2, 0) \prec (1, 1) \prec (0, 2) \prec \dots \end{array} \quad (25)$$

In case of degree-lexicographic ordering we first sort by the sums of exponents. If the sums agree, we sort by the exponents of the first variable. If the first exponents agree, we sort by the second exponents and so on.

With this in mind we note that the outcome of polynomial division or *reduction* of multivariate polynomials depends on the ordering adopted for monomials. The polynomial reduction step of  $h_0$  modulo  $f$  resulting in  $h_1$  subtracts from  $h_0$  a suitable (monomial) multiple of  $f$  such that some term in  $h_0$  cancels against the leading term  $\text{LT}(f)$ . This is written as

$$h_1 = h_0 \bmod f \quad \text{or} \quad h_0 \rightarrow_f h_1. \quad (26)$$

There are several possibilities of picking an  $f \in F$  with differing results  $h_1$  to reduce some  $h_0$ . This step can be iterated by reducing resulting polynomials further and further modulo polynomials from  $F$  until all terms are “simpler” than any leading term present in  $F$ , according to our ordering. We write for this sequence of operations:

$$h_0 \rightarrow_F h_F. \quad (27)$$

Not a single term in  $h_F$  can be reproduced by multiplication of a leading term from  $F$  with some monomial. It is known that an iteration of this kind always terminates but its result is in general not unambiguous. It depends on the reduction chain, enabling

$$h_0 \rightarrow_F h_F, \quad h_0 \rightarrow_F h'_F \quad \text{but} \quad h_F \neq h'_F. \quad (28)$$

**Example 9.** Observe the possible outcomes of polynomial divisions for the polynomial  $h$  by polynomials from the set  $F$  assuming degree-lexicographic ordering, see Eq. (23). Concretely:

$$\begin{array}{l} h = \underline{x^2 y^3}, \\ F = \{f_1, f_2\} = \left\{ \underline{-y^3 + x^2}, \underline{y^2 + x} \right\}. \end{array}$$

The two different possibilities of reduction terminate immediately after only one step because no leading term in  $F$  allows for further simplification:

$$\begin{aligned} h &\rightarrow_{f_1} \underline{x^2y^3} + x^2 \left( \underline{-y^3} + x^2 \right) = \underline{x^4} \\ h &\rightarrow_{f_2} \underline{x^2y^3} - x^2y \left( \underline{y^2} + x \right) = \underline{-x^3y}. \end{aligned}$$

With additional combinations of elements from  $F$ , e.g.  $f_1 + yf_2 = \underline{xy} + x^2$ , the reduction could of course lead further.

**Definition 7.** One possible definition of *Gröbner bases* is by the property to yield a *unique* reduction of any polynomial  $h_0$ , assuming an acceptable convention for monomial ordering, see Eqs. (20) and (21):

$$h_0 \rightarrow_G h_G, \quad h_0 \rightarrow_G h'_G \quad \Rightarrow \quad h_G = h'_G. \quad (29)$$

This definition is not of constructive nature, it does not even allow one to check in practice if a basis is a Gröbner basis since one cannot perform all reductions of all polynomials. Luckily, there exist many equivalent definitions, also constructive ones.

**Example 10.** Now, take the Gröbner basis  $G$  below as given and perform all possible polynomial divisions by elements of  $G$  for the same polynomial  $h$  as in Example 9:

$$\begin{aligned} h &= x^2y^3, \\ G &= \{g_1, g_2\} = \left\{ \underline{y^2} + x, \underline{x^2} - y \right\}. \end{aligned}$$

For  $G$  the two initially different reduction paths meet again and terminate with the same result:

$$\begin{aligned} h &\rightarrow_{g_1} \underline{x^2y^2} - x^2y \left( \underline{y^2} + x \right) = \underline{-x^3y} \\ &\rightarrow_{g_2} \underline{-x^3y} + xy \left( \underline{x^2} - y \right) = \underline{-xy^2}, \\ h &\rightarrow_{g_2} \underline{x^2y^3} - y^3 \left( \underline{x^2} - y \right) = \underline{y^4} \\ &\rightarrow_{g_1} \underline{y^4} - y^2 \left( \underline{y^2} + x \right) = \underline{-xy^2}, \\ \underline{-xy^2} &\rightarrow_{g_1} \underline{-xy^2} + x \left( \underline{y^2} + x \right) = \underline{x^2} \\ &\rightarrow_{g_2} \underline{x^2} - \left( \underline{x^2} - y \right) = \underline{y}. \end{aligned}$$

Coming back to ideals, the “*main problem of ideal theory*”, namely whether a polynomial  $h$  lies within some ideal  $\langle F \rangle$  can be answered for a Gröbner basis  $F = G$  trivially by checking if successive reduction terminates in zero:

$$h \in \langle G \rangle \quad \Leftrightarrow \quad h \rightarrow_G 0. \quad (30)$$



For  $G$  the reduction leads uniquely to zero or not, meaning each single reduction path gives the right answer. For an arbitrary polynomial basis  $F$  some reductions may lead to zero while others do not, making assertion of membership to  $\langle F \rangle$  a way harder problem. For a Gröbner basis, interpreted as set of basic relations, we can thus answer directly if and how its elements allow to reexpress any given polynomial.

**Example 11.** Using the same Gröbner basis  $G$  as in Example 10 one may assert that all possible reduction paths (we do not show them here explicitly) of the polynomial  $h = \underline{xy^4} + y^3$  end indeed in 0. Thus,  $h$  lies within the ideal of  $G$ .

The Buchberger algorithm, stated below, gives for any polynomial basis  $F$  a Gröbner basis  $G$  that generates the same ideal as  $F$ , although the number of elements in each base may differ:

$$F \xrightarrow{\text{Buchberger}} G: \langle F \rangle = \langle G \rangle. \quad (31)$$

It is constructive, i.e. it generates Gröbner bases, and it is also a simple device for checking whether a given set of polynomials forms already such a basis. The algorithm can be stated easily as soon as we specify what subtraction polynomials or “S-polynomials” are.

**Definition 8.** The *S-polynomial* denoted by  $S[f_1, f_2]$  is the difference of polynomials  $f_1$  and  $f_2$  multiplied each by appropriate monomial factors such that their leading terms drop out:

$$S[f_1, f_2] := \text{LCM}(\text{LT}(f_1), \text{LT}(f_2)) \left( \frac{f_1}{\text{LT}(f_1)} - \frac{f_2}{\text{LT}(f_2)} \right), \quad (32)$$

where LCM is the least common multiple of two monomials. Note that this least common multiple of leading terms corresponds to the “simplest” polynomial allowing in principle for branching reduction chains.

Starting from an arbitrary finite set of polynomials  $F$ , the Buchberger algorithm can always transform this set in a finite number of steps to a Gröbner basis  $G$ . This algorithm is a generalization of the Euclidean algorithm, computing the greatest common divisor of univariate polynomials, and the Gaußian algorithm, solving linear systems of equations.

**Algorithm 1** (Buchberger). The Gröbner basis is initialized with  $G = F$ . Then, for some pair  $(f_1, f_2)$  from  $G$  compute the reduction of their S-polynomial with respect to  $G$ , giving  $h$ :

$$S[f_1, f_2] \rightarrow_G h. \quad (33)$$

Only if  $h \neq 0$  join  $h$  to  $G$  and iterate these steps for the new  $G$  until also all new pairs have been checked.

Gröbner bases are not required to be minimal, viz. a subset of  $G$  could generate the same ideal as  $G$  and would thereby be a Gröbner basis by itself. The minimal form, additionally fulfilling restrictions on the coefficients of leading monomials and on the trailing monomials, is called the reduced Gröbner basis but we will not cope with it in more detail.

**Example 12.** Using  $G$  from Example 10 one more time, one can compute the single S-polynomial

$$S[g_1, g_2] = \underline{y^3} + x^2$$

and verify easily that all possible reductions end up in zero, asserting  $G$  to be a Gröbner basis:

$$\begin{aligned} \underline{y^3} + x^3 &\rightarrow_{g_1} \underline{y^3} + x^3 - y(\underline{y^2} + x) = \underline{x^3} - xy \\ &\rightarrow_{g_2} \underline{x^3} - xy - x(\underline{x^2} - y) = 0, \\ \underline{y^3} + x^3 &\rightarrow_{g_2} \underline{y^3} + x^3 - x(\underline{x^2} - y) = \underline{y^3} + xy \\ &\rightarrow_{g_1} \underline{y^3} + xy - y(\underline{y^2} + x) = 0. \end{aligned}$$

To mention another nice property of Gröbner bases, solving the “elimination problem”, note that

$$\langle G \rangle \cap K[x_1, \dots, x_i] = \langle G \cap K[x_1, \dots, x_i] \rangle \quad \forall i \leq n, \quad (34)$$

meaning the ideal for elimination of  $x_1, \dots, x_i$  on the left-hand side is just the ideal spanned by the elements from  $G$  involving only  $x_1, \dots, x_i$  on the right-hand side. If we are interested in the set of roots of a system  $F$ , its *variety*, we compute its Gröbner basis  $G$  which has the same ideal and solutions. In  $G$  we can simply start by inspecting a subset of univariate equations, substitute their solutions in the next bigger subset involving also the second variable and continue in this manner until all solutions are determined. The *elimination property* of Gröbner bases presumes of course an appropriate ordering such as the lexicographic ordering in Eq. (22) used in the following example.

**Example 13.** Suppose we want all solutions to a system of polynomial relations  $F$  equating zero, e.g.

$$F = \left\{ -\underline{xy^2} + x^2y, \underline{y^2} + x^2 - 1 \right\}.$$

$F$  exposes the same variety as its Gröbner basis

$$G = \left\{ \underline{2y^5} - 3y^3 + y, \underline{2y^4} - 2y^2 + xy, \underline{y^2} + x^2 - 1 \right\}.$$

Taking only the first relation from  $G$ , we find all solutions for  $y$  to be

$$y \in \left\{ 0, \pm 1, \pm \frac{1}{\sqrt{2}} \right\}.$$

These we can substitute into the remaining two equations from  $G$  to find all sets of solutions

$$(y, x) \in \left\{ (0, -1), (\pm 1, 0), \left( \pm \frac{1}{\sqrt{2}}, \mp \frac{1}{\sqrt{2}} \right) \right\}.$$

The initial system  $F$  is in this case not very complicated and one can solve it also directly. The solution via a Gröbner basis is, however, algorithmic and works also in more complicated cases.

To conclude, Gröbner bases are a powerful tool with a plethora of applications, e.g. in commutative algebra (system solvability, polynomial ideals, diophantine equations, etc.), invariant theory, partial differential equations, hypergeometric functions, symbolic summation. Another interesting application, directly from our field of research, is the “S-bases approach” for Feynman integral reduction, see Refs. [9–11]. As a sidenote: it was observed that an S-bases reduction performs good for cases where a Laporta reduction (cf. Section 2.6) struggles and vice versa. Both approaches complement one another. Our next step is to apply Gröbner bases to the problem of partial fractioning of linearly dependent topologies (or more precisely: their propagators).

### 2.2.2 Partial fractioning relations

Expressions stemming from scalar diagrams as in Fig. 2 on Page 20 could involve terms containing

$$d_1^2 d_2, d_1/d_2, d_2^2/d_1, \dots$$

with linearly dependent topology factors  $d_1$  and  $d_2$  related by

$$d_1 - d_2 = m_1^2 - m_2^2,$$

where  $m_1$  and  $m_2$  denote different particle masses. These diagram expressions can be simplified by transforming terms with dependent factors to sums of terms where each involves only independent factors. We can work out such a system of transformation rules from the linear dependence relation:

$$\begin{aligned} d_2 &\rightarrow -m_1^2 + m_2^2 + d_1, \\ \frac{d_1}{d_2} &\rightarrow \frac{m_1^2}{d_2} - \frac{m_2^2}{d_2} + 1, \\ \frac{1}{d_1 d_2} &\rightarrow -\frac{1}{m_1^2 - m_2^2} \frac{1}{d_1} + \frac{1}{m_1^2 - m_2^2} \frac{1}{d_2}. \end{aligned}$$

Clearly, all possible combinations of positive and negative powers of  $d_1$  and  $d_2$  will be reduced by these rules to terms containing solely  $d_1$  or  $d_2$  each.

In the aforementioned case it is trivial to find the set of partial fractioning relations for propagators. For the general case it is, however, often laborious

to arrive at a complete (applying to all kinds of monomials, including also negative powers) and terminating (repeated execution without loops) system of decomposition rules. We have to consider simplification of products of arbitrary powers  $\{a_i\}$  of topology factors  $\{f_i\}$ ,

$$\prod_{i=1}^{N_f} f_i^{a_i} \quad \text{with} \quad a_i \in \mathbb{Z}, \quad (35)$$

employing  $N_f - \text{rank}M$  possible linear relations (the topology matrix  $M$  was defined in Section 2.1.5 on Page 20) containing masses  $\{m_i\}$  and external invariants  $\{x_{ij}\}$ ,

$$\sum_{i=1}^{N_f} c_i (f_i - m_i^2) = \sum_{i \leq j}^{N_p} d_{ij} x_{ij}, \quad \text{with} \quad c_i, d_{ij} \in \mathbb{Q}. \quad (36)$$

In order to facilitate the use of Gröbner bases, we first need to rewrite negative powers of topology factors in terms of  $F_i = 1/f_i$  and treat them as independent variables. Products of arbitrary powers of topology factors can then be written as

$$\prod_{i=1}^{N_f} f_i^{a'_i} F_i^{b'_i} \quad \text{with} \quad (a'_i, b'_i) = \begin{cases} (a_i, 0), & \text{for } a_i \geq 0, \\ (0, -a_i), & \text{otherwise,} \end{cases} \quad (37)$$

supplemented by the additional relations,

$$f_i F_i = 1 \quad \text{with} \quad i = 1, \dots, N_f. \quad (38)$$

Furthermore, we have to formalize our notion of what is “simpler” by introducing a suitable ordering. One possibility is a linear weighting of an exponent vector  $\{a_i, b_i\}$  by lexicographically comparing component-wise  $Ma$  with  $Ma'$  for two such vectors  $a$  and  $a'$  where

$$M_{ij} = \begin{cases} 1, & \text{for } i \geq j, \\ 0, & \text{otherwise.} \end{cases} \quad (39)$$

The matrix  $M$  is just the lower left triangle matrix including the diagonal filled with ones and the rest with zeros, making the sum of exponents the primary criterion.

Based on this ordering one computes the Gröbner basis to the set of polynomial relations equating zero obtained from Eqs. (36) and (38). Our starting relations and the Gröbner basis contain the same information since both generate the same ideal which can be taken as all possibilities to algebraically manipulate these relations. But in the Gröbner basis these relations are rearranged as manifestly terminating equivalence rules. Each element (equating zero) can be reinterpreted as replacement rule with its most “complicated” monomial in the  $\{f_i, F_j\}$  as left-hand side.

The fact that this works becomes clearer if we mention another property of Gröbner bases that is essentially equivalent to its definition via unique polynomial division in Eq. (29). The *leading power property* of a Gröbner

basis  $G$  connotes that all leading monomials in the ideal  $\langle G \rangle$  are multiples of at least one of the leading monomials in  $G$ . Thus, we will find for all possible monomials in Eq. (37) at least one replacement rule resulting in easier monomials, given the monomial was not already in its simplest form. On each resulting term the same applies until an initial expression is in its final form completely mapped to terms of independent monomials.

**Example 14.** Returning to the generic box topology  $T_{H,\text{NLO}}^{\text{generic}}$  for NLO Higgs boson production of Example 6 with the linear dependence

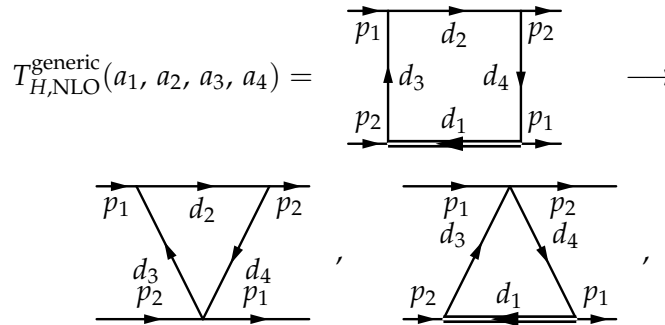
$$d_1 + d_2 - d_3 - d_4 = m_H^2 - s,$$

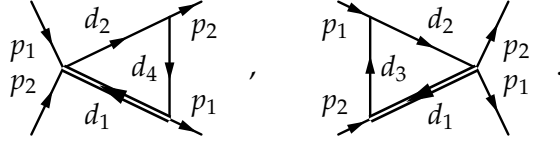
the method laid out in this subsection gives the rules

$$\begin{aligned} d_4 &\rightarrow -m_H^2 + s + d_1 + d_2 - d_3, \\ \frac{d_3}{d_4} &\rightarrow \frac{1}{d_4} (-m_H^2 + s + d_1 + d_2 - d_4), \\ \frac{d_2}{d_3 d_4} &\rightarrow \frac{1}{d_3 d_4} (m_H^2 - s - d_1 + d_3 + d_4), \\ \frac{d_1}{d_2 d_3 d_4} &\rightarrow \frac{1}{d_2 d_3 d_4} (m_H^2 - s - d_2 + d_3 + d_4), \\ \frac{1}{d_1 d_2 d_3 d_4} &\rightarrow \frac{1}{(m_H^2 - s) d_1 d_2 d_3 d_4} (d_1 + d_2 - d_3 - d_4). \end{aligned}$$

The right-hand sides in above transformation rules give rise to new terms. Note that each right-hand side term has either less or “simpler” denominators than the left-hand side. If the denominators in a right-hand side term are not simpler than on the left-hand side, the numerators of the right-hand side term are simpler than on the left-hand side. The transformation rules above represent the computed Gröbner basis where the leading term of each basis polynomial is now a left-hand side. In this case the Gröbner basis has five elements which equals the number of conditions from Eqs. (36) and (37). This is no generic feature.

The decomposition has a diagrammatic representation, namely the mapping of terms leads to each possible contraction of lines whose factors appear in the initial linear relations:





As a side note: in the application to Higgs boson production, contributions of the first two topologies would be discarded since they do not expose  $s$ -channel cuts through the massive line. The last two topologies are in fact symmetric and identical to the basic topology  $T_{H,\text{NLO}}^{\text{basic}}$ .

The outcome of this transformation of dependent monomials, from expressions attributed to generic topologies, into independent monomials can be seen as a set of expressions where each term attributes to a basic topology. It is the mapping of a generic topology onto a set of independent subtopologies. Candidates for such subtopologies can be readily identified by those subsets of rows from the coefficient matrix in Eq. (17) exposing the same matrix rank as the full matrix.

### 2.3 PARAMETRIC REPRESENTATIONS

In this section we state a well-known parametric representation for Feynman integrals, usually called alpha-representation. It is closely related to Feynman parametrization where denominator factors of an integrand are combined into a single (still quadratic) one. We, however, will use these names synonymously. This section is based on the books by V.A. Smirnov, see Refs. [12–14], and the educational review on Feynman integral polynomials in Ref. [15].

#### 2.3.1 Symanzik polynomials

All factors  $\{f_j\}$  of a scalar Feynman integral can be rewritten by means of the Schwinger-representation

$$\frac{1}{f_j^{a_j}} = \frac{i^{a_j}}{\Gamma(a_j)} \int_0^\infty d\alpha_j \alpha_j^{a_j-1} \exp[-if_j\alpha_j], \quad (40)$$

where integration over auxiliary variables  $\{\alpha_j\}$ , the Feynman or alpha-parameters, has been introduced. Now, the order of integration over  $N_k$  loop momenta  $\{k_i\}$  and  $N_f$  alpha-parameters  $\{\alpha_j\}$  can be interchanged, exponentials are combined and terms are collected by loop momenta. Then, we are left with  $D$ -dimensional Gaussian integrals which can be evaluated via

$$\int dk_i^D \exp[i(Ak_i^2 - 2B \cdot k_i)] = \left(\frac{\pi}{A}\right)^{D/2} \exp\left[\frac{i\pi}{2} \left(1 - \frac{D}{2}\right)\right] \exp\left[-i\frac{B^2}{A}\right], \quad (41)$$

where  $A$  is a number and  $B$  a linear combination of external and internal momenta involving the parameters  $\{\alpha_j\}$ .

**Example 15.** Applied to the one-loop massless propagator in Minkowski metric, we obtain

$$\begin{aligned}
 P_1(a_1, a_2) &= \begin{array}{c} \xrightarrow{p} \text{---} \bigcirc \text{---} \xrightarrow{p} \\ \quad \quad \quad \begin{array}{c} a_1 \\ \uparrow \\ \downarrow \\ a_2 \end{array} \end{array} = \int \mathrm{d}k^D \frac{1}{[-k^2]^{a_1}} \frac{1}{[-(p+k)^2]^{a_2}} \\
 &= \frac{i^{a_1+a_2}}{\Gamma(a_1)\Gamma(a_2)} \int_0^\infty \mathrm{d}\alpha_1 \mathrm{d}\alpha_2 \alpha_1^{a_1-1} \alpha_2^{a_2-1} \\
 &\quad \times \int \mathrm{d}k \exp[i((\alpha_1 + \alpha_2)k^2 + 2\alpha_2 p \cdot k + \alpha_2 p^2)] \\
 &= \pi^{D/2} \frac{\exp\left[\frac{i\pi}{2}\left(a_1 + a_2 + 1 - \frac{D}{2}\right)\right]}{\Gamma(a_1)\Gamma(a_2)} \\
 &\quad \times \int_0^\infty \mathrm{d}\alpha_1 \mathrm{d}\alpha_2 \frac{\alpha_1^{a_1-1} \alpha_2^{a_2-1}}{(\alpha_1 + \alpha_2)^{D/2}} \exp\left[-i \frac{p^2 \alpha_1 \alpha_2}{\alpha_1 + \alpha_2}\right].
 \end{aligned}$$

Above procedure can be generalized and written for all  $N_k$  loop integrations in the matrix form

$$\begin{aligned}
 &\prod_{i=1}^{N_k} \int \mathrm{d}k_i^D \exp\left[i\left(\sum_{m,n} A_{mn} k_m \cdot k_n + 2\sum_m B_m \cdot k_m\right)\right] \\
 &= \exp\left[N_k \frac{i\pi}{2}\left(1 - \frac{D}{2}\right)\right] \pi^{N_k D/2} (\det A)^{-D/2} \\
 &\quad \times \exp\left[-i \sum_{m,n} A_{mn}^{-1} B_m \cdot B_n\right], \tag{42}
 \end{aligned}$$

where  $A_{mn}$  now denotes a matrix of coefficients and  $B_m$  a linear combinations of external momenta. Applied to a general topology  $T$ , this results in the first form of the alpha-representation:

$$\begin{aligned}
 T(a_1, \dots, a_{N_f}) &= (-1)^a \pi^{N_k D/2} \exp\left[\frac{i\pi}{2}\left(a + N_k\left(1 - \frac{D}{2}\right)\right)\right] \\
 &\quad \times \left[\prod_{i=1}^{N_f} \Gamma(a_i)\right]^{-1} \prod_{j=1}^{N_f} \int_0^\infty \mathrm{d}\alpha_j \left[\prod_{i=1}^{N_f} \alpha_i^{a_i-1}\right] \mathcal{U}^{-D/2} \exp\left[-i \frac{\mathcal{V}}{\mathcal{U}}\right], \tag{43}
 \end{aligned}$$

where as usual  $a = a_1 + \dots + a_{N_f}$  is the sum of all indices and the factor  $(-1)^a$  is due to convention. Two polynomials, defined in graph-theoretical language and referred to as the first and second Symanzik or alpha-polynomials, enter this form as

$$\mathcal{U} = \sum_{\tau \in \tau^1} \prod_{j \notin \tau} \alpha_j, \quad \mathcal{V} = \sum_{\tau \in \tau^2} \prod_{j \notin \tau} \alpha_j p_\tau^2. \tag{44}$$

In these formulae  $\tau$  denotes a specific graph composed of several lines associated to alpha-parameters and belonging to a family of graphs. These families are the *(one-)trees*  $\tau^1$  and the *two-trees*  $\tau^2$ . (One-)Trees consist of



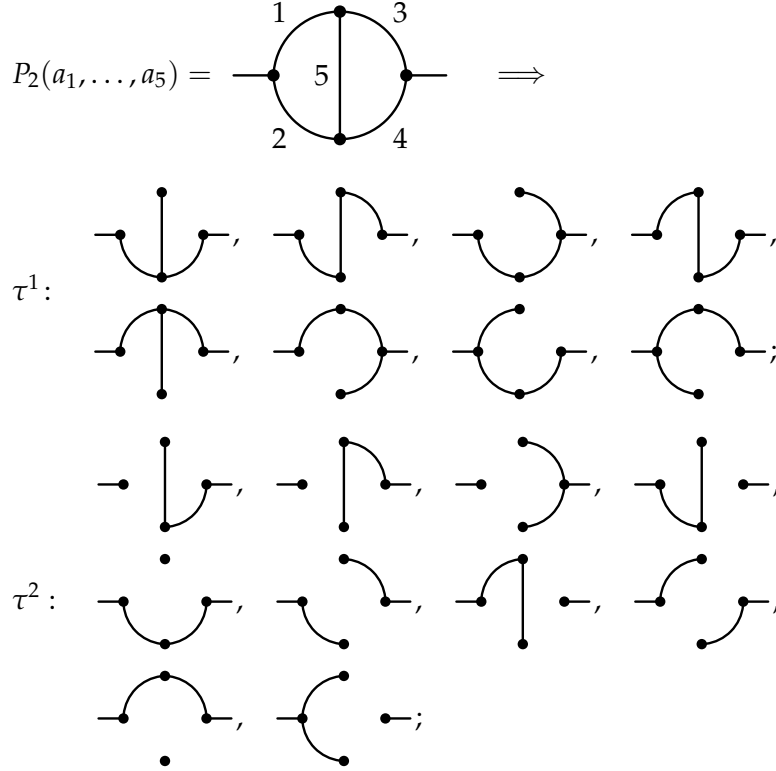


$$\times \int_0^\infty d\alpha_1 d\alpha_2 \delta(a_1 + a_2 - 1) \alpha_1^{a_1-1} \alpha_2^{a_2-1} \frac{(\alpha_1 + \alpha_2)^{a_1+a_2-D}}{(p^2 \alpha_1 \alpha_2)^{a_1+a_2+D/2}}.$$

This is in agreement with Eq. (46) up to the factor  $(-1)^{-a_1-a_2}$  which was due to convention in Eq. (43). The massless one-loop propagator integral for general powers of denominators can be expressed in terms of Gamma-functions:

$$i\pi^{D/2} \frac{\Gamma(2-\epsilon-a_1) \Gamma(2-\epsilon-a_2)}{\Gamma(a_1) \Gamma(a_2) \Gamma(4-a_1-a_2-2\epsilon)} \frac{\Gamma(a_1+a_2+\epsilon-2)}{(-p^2)^{a_1+a_2+\epsilon-2}}.$$

**Example 18.** An other example whose alpha-representation will be made use of later is the two-loop massless propagator topology:



$$\mathcal{U} = \alpha_{13} + \alpha_{14} + \alpha_{15} + \alpha_{23} + \alpha_{24} + \alpha_{25} + \alpha_{35} + \alpha_{45},$$

$$\mathcal{V} = p^2 (\alpha_{123} + \alpha_{124} + \alpha_{125} + \alpha_{134} + \alpha_{145} + \alpha_{234} + \alpha_{235} + \alpha_{345}).$$

Pictures for one- and two-trees are ordered according to terms in  $\mathcal{U}$  and  $\mathcal{V}$  where we used the abbreviation  $\alpha_{1\dots i} = \alpha_1 \dots \alpha_i$ . The fifth and ninth two-trees do not appear in  $\mathcal{V}$  since they each multiply a squared momentum equal to zero flowing between their two components.

**Example 19.** Also for one of our standard examples from Higgs boson production  $T_{H,\text{NLO}}^{\text{generic}}$  we show this diagrammatically:

$$T(a_1, a_2, a_3, a_4) = \begin{array}{c} \text{---} \bullet \text{---} \text{---} \bullet \text{---} \\ | \quad \quad | \\ \text{---} \bullet \text{---} \text{---} \bullet \text{---} \end{array} \begin{array}{c} 2 \\ 3 \quad 4 \\ 1 \end{array} \implies$$

$$\tau^1 : \begin{array}{cccc} \text{---} \bullet \text{---} \text{---} \bullet \text{---} & , & \text{---} \bullet \text{---} \text{---} \bullet \text{---} & , \\ | \quad \quad | & & \text{---} \bullet \text{---} \text{---} \bullet \text{---} & , \\ \text{---} \bullet \text{---} \text{---} \bullet \text{---} & & \text{---} \bullet \text{---} \text{---} \bullet \text{---} & ; \\ & & & \end{array}$$

$$\tau^2 : \begin{array}{cccc} \text{---} \bullet \text{---} \text{---} \bullet \text{---} & , & \text{---} \bullet \text{---} \text{---} \bullet \text{---} & , \\ | \quad \quad | & & \text{---} \bullet \text{---} \text{---} \bullet \text{---} & , \\ \text{---} \bullet \text{---} \text{---} \bullet \text{---} & & \text{---} \bullet \text{---} \text{---} \bullet \text{---} & ; \\ & & & \end{array}$$

$$\mathcal{U} = \alpha_1 + \alpha_2 + \alpha_3 + \alpha_4, \quad \mathcal{V} = -s(\alpha_{12} - \alpha_{34}).$$

Again, only some of all possible two-trees contribute, namely the first and the last one. In this case we used Minkowski space propagators for  $T_{H,\text{NLO}}^{\text{generic}}$ . The arrows in the first picture indicate the routing of external momentum  $p_1$ . We still have the same kinematics introduced before and thus  $(p_1 + p_2)^2 = -s$  and  $(p_1 - p_2)^2 = s$ .

### 2.3.2 Properties

Let us remark on some features which are apparent from above derivations and examples:

- All  $N_k$  integrations over the  $D$ -dimensional loop momenta have been carried out and traded for  $N_f$  integrations over scalar parameters. This representation for dimensionally regularized integrals is explicitly covariant and its integrand is unique up to renaming of the alpha-parameters.
- When starting from a graphical representation, the polynomials  $\mathcal{U}$  and  $\mathcal{V}$  can be read off directly in terms of trees and two-trees. Otherwise  $\mathcal{U}$  and  $\mathcal{V}$  can be computed algebraically as long as one deals with at maximum quadratic factors, viz. by completing the square as done above.
- The prefactor of the integral and the powers of  $\mathcal{U}$  and  $\mathcal{W}$  in Eq. (46) depend on the number of loops  $N_k$ , the number of dimensions  $D$  and the indices  $\{a_j\}$  only. The two characteristic polynomials themselves do not depend on the indices, they are universal in this sense for all integrals of the topology and their indices can be fixed later.

- The polynomial  $\mathcal{U}$  is linear and homogeneous in the  $\{\alpha_j\}$  with degree  $N_k$ , as are the polynomials  $\mathcal{V}$  and  $\mathcal{W}$  but with degree  $N_k + 1$ . The pair  $\mathcal{U}$  and  $\mathcal{V}$  encodes the information of possible graphs of a topology. In addition,  $\mathcal{V}$  has also information on the kinematic setup and  $\mathcal{W}$  on the mass configuration of lines of the topology.
- There is a strict correspondence between an alpha-parameter and its former topology factor or graph line. All topology factors can be treated on the same ground, regardless whether they are real denominators or pure numerators (restrictions on the signs of their indices).
- Working with propagators in Euclidean space (plus sign in Eq. (3)) results always in  $\mathcal{U}$  and  $\mathcal{V}$  having negative signs for each term, whereas Minkowski space propagators (minus sign in Eq. (3)) result in positive signs.

The alpha-representation is a good starting point for numerical evaluation, e.g., via sector decomposition. Singularities of the initial loop integral translate to singularities in the parametric integral and can be revealed systematically. But also analytic methods make use of the alpha-representation. For example, direct symbolic integration leading to special functions, see Refs. [16, 17], or reading off certain properties to derive canonical forms of differential equations, see Refs. [18, 19]. We, however, use the characteristic polynomials  $\mathcal{U}$  and  $\mathcal{W}$  as unique identifiers for Feynman integrals as will be explained in Section 2.4.

### 2.3.3 *Recursiveness*

Until now we encountered two ways of calculating Symanzik polynomials, firstly by explicit integration over loop momenta after rewriting propagators in Schwinger-representation and completing squares, secondly via correspondence to one- and two-trees of diagrammatic representations. Another possibility is to define the alpha-representation in a recursive way, see Ref. [15], and from this definition a useful property can be seen: contraction of a line or factor can be achieved by setting the corresponding alpha-parameter to zero. Related to this is factorization of integrals or corresponding disentangled loops in diagrams when both Symanzik polynomials factorize.

The recursive definition of  $\mathcal{U}$  and  $\mathcal{V}$  reads for topology  $T$ :

$$\mathcal{U}(T) = \mathcal{U}(T/j) + \alpha_j \mathcal{U}(T-j), \quad \mathcal{V}(T) = \mathcal{V}(T/j) + \alpha_j \mathcal{V}(T-j), \quad (48)$$

where  $T/j$  denotes contraction of line or factor  $j$  and  $T-j$  denotes deletion of  $j$  which should neither be “bridge” or “self-loop”. A bridge corresponds to a sole propagator connecting two parts of a graph. Such a propagator would not contain loop momenta and the corresponding graph would be one-particle reducible. We do not consider such cases. A tadpole, or self-loop in graph language, consists of a propagator connecting only to a single vertex. Upon contraction of a self-loop, the number of loops is effectively

lowered and corresponding to line deletion. The recursion ends in the “terminal forms”  $\mathcal{U}_0$  and  $\mathcal{V}_0$  which correspond to products of self-loops with the trivial one-tree (containing no lines) only and no two-trees:

$$\mathcal{U}_0 = \prod_{j=1}^{N_k} \alpha_j, \quad \mathcal{V}_0 = 0. \quad (49)$$

From Eq. (48) it can be seen that by setting  $\alpha_j$  to zero in the polynomials of a “full” topology  $T$  one gets the corresponding polynomials of the subtopology  $T/j$  with factor  $j$  contracted:

$$\mathcal{U}(T/j) = \mathcal{U}(T) |_{\alpha_j \rightarrow 0}, \quad \mathcal{V}(T/j) = \mathcal{V}(T) |_{\alpha_j \rightarrow 0}. \quad (50)$$

On the right-hand sides of Eq. (48),  $\alpha_j$  does not appear anywhere but in front of the second terms which thereby drop out. The same holds also for the polynomial  $\mathcal{W}$ , see Eq. (45). This is demonstrated in the next example.

**Example 20.** We return to  $T_{H,\text{NLO}}^{\text{generic}}$  from Example 19 and contract it to  $T_{H,\text{NLO}}^{\text{basic}}$ . Setting  $\alpha_4$  in the polynomials for  $T_{H,\text{NLO}}^{\text{generic}}$  to zero has the same effect as contracting line 4 in the graph and inspecting one- and two-trees anew:

$T_{H,\text{NLO}}^{\text{basic}}(a_1, a_2, a_3) =$

$\tau^1:$

$\tau^2:$

$\mathcal{U} = \alpha_1 + \alpha_2 + \alpha_3, \quad \mathcal{V} = -s\alpha_{12}.$

If line  $j$  is contracted one-trees containing this line will persist as will corresponding terms in  $\mathcal{U}$ . One-trees not containing  $j$  will inevitably form a loop and should therefore not contribute, their terms contain  $\alpha_j$  and thus drop out. For  $\mathcal{V}$  the reasoning is similar: two-trees not containing  $j$  turn upon contraction to one-trees and their terms again have an  $\alpha_j$ . This property holds also for sets of alpha-parameters.

For a factorizing integral in a diagrammatic or momentum-space representation, also its alpha-representation factorizes. The converse statement is not proven, however. If we compute the  $\mathcal{U}$  and  $\mathcal{V}$  (or  $\mathcal{W}$ ) polynomials for the  $N_F$  factors of the integral, numerated by subscripts, the combined polynomials are of the form

$$\mathcal{U} = \prod_{m=1}^{N_F} \mathcal{U}_m, \quad \mathcal{V} = \sum_{m=1}^{N_F} \mathcal{V}_m \prod_{n \neq m}^{N_F} \mathcal{U}_n. \quad (51)$$

Note, for factorizing graphs all possible combinations of one-trees (picking only one from each factor) are again one-trees relevant for  $\mathcal{U}$  and combining each two-tree of each factor with one-trees from the remaining factors gives all two-trees linked to  $\mathcal{V}$ . In practice, we use this property to check if an integral factorizes and to extract alpha-representations of its various factors instead of resorting to graph-based techniques.

**Example 21.** Contracting line 5 turns the two-loop massless propagator topology of Example 18 into a product of two one-loop bubbles and allows us to observe aforementioned property. Compare one- and two-trees of Example 16 to those shown below:

$$P_2(a_1, a_2, a_3, a_4, 0) = P_1(a_1, a_2) \times P_1(a_3, a_4) = \text{---} \begin{array}{c} \textcircled{1} \quad \textcircled{3} \\ \text{---} \quad \text{---} \\ \textcircled{2} \quad \textcircled{4} \end{array} \text{---} \implies$$

$$\tau^1: \text{---} \textcircled{1} \text{---}, \quad \text{---} \textcircled{2} \text{---}, \quad \text{---} \textcircled{3} \text{---}, \quad \text{---} \textcircled{4} \text{---};$$

$$\tau^2: \text{---} \textcircled{1} \text{---}, \quad \text{---} \textcircled{2} \text{---}, \quad \text{---} \textcircled{3} \text{---}, \quad \text{---} \textcircled{4} \text{---};$$

$$\mathcal{U} = (\alpha_1 + \alpha_2) (\alpha_3 + \alpha_4), \quad \mathcal{V} = p^2 [\alpha_{12} (\alpha_3 + \alpha_4) + \alpha_{34} (\alpha_1 + \alpha_2)].$$

#### 2.3.4 Scalefulness

The form of the Symanzik polynomials in Eqs. (44) and (45) can be used as tool to probe if an integral or a whole class of integrals lacks an inherent scale. Within dimensional regularization, see Ref. [20], such *scaleless* integrals vanish and can be discarded. The criterion we elaborate on here originated from Ref. [21] where it was used to identify relevant regions after expanding integrands of Feynman integrals in a given limit of external invariants. Regions usually refer to distinct scalings of integration momenta relative to external invariants but this transfers also to the scalings of alpha-parameters. The idea is to sum contributions from all regions integrated over the whole parameter space to obtain an equivalent to the Taylor expansion of the integral (without having to evaluate it exactly before).

Scalelessness implies existence of a rescaling of parameters or a subset of them that leaves the integrand invariant. This is connected to massless tadpoles amounting to zero within dimensional regularization, see Ref. [20]. In momentum space this means:

$$T(\{k_i\}_a, \{c k_i\}_b) = c^{D_T} T(\{k_i\}) \iff T(\{k_i\}) = 0, \quad (52)$$

where  $c \neq 0$  is some constant and  $D_T$  a scaling dimension of topology  $T$ . We emphasize the fact that we consider an explicit momentum space

representation of topology  $T$  by using the set of loop momenta  $\{k_i\}$  as argument. The indices  $a$  and  $b$  indicate disjunct subsets of loop momenta  $\{k_i\} = \{k_i\}_a \cup \{k_i\}_b$ .

**Example 22.** In the one-loop massless tadpole diagram with arbitrary power  $a$  for the propagator, we rescale the loop momentum  $k$  by  $c \neq 0$  and find that the integral must vanish:

$$P_1(a, 0) = \begin{array}{c} k, a \\ \circlearrowleft \\ \longrightarrow \end{array} = \int d^D k \frac{1}{[k^2]^a} \stackrel{k \rightarrow ck}{=} c^{D-2a} \int d^D k \frac{1}{[k^2]^a} = 0.$$

Above argument can be transferred to the polynomials  $\mathcal{U}$  and  $\mathcal{W}$  giving:

$$\begin{aligned} \mathcal{U}(\{\alpha_j\}_a, \{c\alpha_j\}_b) &= c^{D_{\mathcal{U}}} \mathcal{U}(\{\alpha_j\}), \\ \mathcal{W}(\{\alpha_j\}_a, \{c\alpha_j\}_b) &= c^{D_{\mathcal{W}}} \mathcal{W}(\{\alpha_j\}), \end{aligned} \quad (53)$$

where the same disjunct subset  $b$  is scaled for  $\mathcal{U}$  and  $\mathcal{W}$ . The symbol  $D$  with a subscript denotes the respective scaling dimension. Instead of two simultaneous scalings, we can evidently consider just the scaling of the product  $\mathcal{U} \times \mathcal{W}$ , see Eq. (46):

$$(\mathcal{U} \times \mathcal{W})(\{\alpha_j\}_a, \{c\alpha_j\}_b) = c^{D_{\mathcal{U} \times \mathcal{W}}} (\mathcal{U} \times \mathcal{W})(\{\alpha_j\}). \quad (54)$$

Upon inspecting Eq. (46), it is clear that all factors but the delta-function in the integrand produce scaling factors which can be moved in front of the integral sign.

By homogeneity the full set  $\{\alpha_j\}$  always produces trivial scaling factors for the Symanzik polynomials. Therefore, the subset of rescaled parameters  $\{\alpha_j\}_b$  should not coincide with the full set, we demand it to be a strict subset. The *Cheng-Wu theorem*, see Ref. [22], states that the integral is invariant under the replacement

$$\delta\left(\sum_{j=1}^{N_f} \alpha_j - 1\right) = \delta\left(\sum_{\alpha \in \{\alpha_j\}} \alpha - 1\right) \longrightarrow \delta\left(\sum_{\alpha \in \{\alpha_j\}_a} \alpha - 1\right), \quad (55)$$

where the sum over all alpha-parameters in the delta-function is changed into a sum over a subset  $\{\alpha_j\}_a$  corresponding to the non-scaled parameters. Integration for scaled parameters is thereby not anymore bounded from above by one which is still the case for non-scaled parameters (due to the delta-function). Details can also be found Ref. [14]. This shows that also the delta-function is compatible with the scaling of the polynomials.

To check if such a scaling exists, we can resort to geometrical arguments. Every term in  $\mathcal{U} \times \mathcal{W}$  in the variables  $\{\alpha_j\}$  can be interpreted as point in a  $N_f$ -dimensional space spanned by the exponent vectors  $v$  of monomials:

$$\prod_{j=1}^{N_f} \alpha_j^{v_j} \quad \text{with} \quad v = (v_1, \dots, v_{N_f})^T. \quad (56)$$

From homogeneity of  $\mathcal{U}$  and  $\mathcal{W}$  follows also homogeneity of  $\mathcal{U} \times \mathcal{W}$  and

$$\sum_{j=1}^{N_f} v_j = 2N_k + 1 \quad (57)$$

describes thereby an  $(N_f - 1)$ -dimensional hyperplane covering all points from the polynomial.

In a particular problem the points of  $\mathcal{U} \times \mathcal{W}$  have a complex hull with maximum dimensionality  $N_f - 1$  embedded in the plane given by Eq. (57). The dimension of this hull can be checked by computing the rank of a matrix made up of vectors connecting all points of the hull, denoted by  $\text{rank}[\mathcal{U} \times \mathcal{W}]$ . These vectors can for example be the vectors between all ridges of the convex hull or just the difference vectors to one arbitrary reference point from  $\mathcal{U} \times \mathcal{W}$ .

Now, suppose the hull dimensionality is less or equal to  $N_f - 2$ . Then, we can find at least one vector lying within the plane described by Eq. (57) but perpendicular to any edge or facet of the hull. These vectors correspond precisely to possible scalings of strict subsets of parameters. They characterize directions in exponent space orthogonal to all directions (differences of points) encoded in the polynomial.

We can formulate the criterion for scalefulness, or conversely scalelessness, by asking whether the volume given by  $\text{rank}[\mathcal{U} \times \mathcal{W}]$  is  $(N_f - 1)$ -dimensional or not:

$$\begin{aligned} \text{rank}[\mathcal{U} \times \mathcal{W}] < N_f - 1 &\Leftrightarrow \text{topology } T \text{ is scaleless,} \\ \text{rank}[\mathcal{U} \times \mathcal{W}] = N_f - 1 &\Leftrightarrow \text{topology } T \text{ is scaleful.} \end{aligned} \quad (58)$$

By construction the rank cannot be greater than  $N_f - 1$ . Note that even if an integral is scaleful, it could still be zero for other reasons.

**Example 23.** We contract lines 4 and 5 in the two-loop massless propagator topology from Example 18 to obtain a scaleless subtopology:

$$P_2(a_1, a_2, a_3, 0, 0) = \text{Diagram}$$

$$\begin{aligned} &\text{with } \mathcal{U} = \alpha_{13} + \alpha_{23}, \quad \mathcal{W} = -p^2 \alpha_{123}; \\ &\mathcal{U} \times \mathcal{W} = -p^2 (\alpha_1^2 \alpha_2^1 \alpha_3^2 + \alpha_1^1 \alpha_2^2 \alpha_3^1) \\ \Rightarrow &\text{points: } \left\{ \begin{pmatrix} 2 \\ 1 \\ 2 \end{pmatrix}, \begin{pmatrix} 1 \\ 2 \\ 2 \end{pmatrix} \right\}, \quad \text{rank} \begin{pmatrix} 1 \\ -1 \\ 0 \end{pmatrix} = 1 < 2 = N_f - 1. \end{aligned}$$

By “points” we mean the set of coordinates in exponent space from each term in the polynomial  $\mathcal{U} \times \mathcal{W}$ . For having two points in exponent space that mark just one direction we can freely choose a perpendicular direction  $w$  to this connection vector and within the homogeneity plane, see Eq. (57).

These rescaling vectors  $w$  are to be understood in the sense of  $\alpha_j \rightarrow c^{w_j} \alpha_j$ . For example  $w = (1, 1, -2)^T$  which is a linear combination of  $(1, 1, 0)^T$  and  $(0, 0, 1)^T$  corresponding to the obvious possible scalings for  $\mathcal{U} \times \mathcal{W}$  given by  $\alpha_{1,2} \rightarrow c \alpha_{1,2}$  and  $\alpha_3 \rightarrow c \alpha_3$ , respectively. These vectors are not perpendicular to the normal vector of the plane which is  $(1, 1, 1)^T$ . Applying the scaling  $w$  here results in  $\mathcal{U} \times \mathcal{W}$  changing by a factor  $1/c$ .

**Example 24.** In contrast to the previous example, if we contract lines 2 and 3 in the two-loop massless propagator topology the resulting subtopology remains scaleful. Here, one cannot construct a vector perpendicular to both, the normal of the homogeneity plane and the edges of the envelope of exponent vectors.

$$P_2(a_1, 0, 0, a_4, a_5) = \begin{array}{c} 1 \\ \circlearrowleft \\ 5 \\ \circlearrowright \\ 4 \end{array}$$

$$\text{with } \mathcal{U} = \alpha_{14} + \alpha_{15} + \alpha_{45}, \quad \mathcal{W} = -p^2 \alpha_{145};$$

$$\mathcal{U} \times \mathcal{W} = -p^2 \left( \alpha_1^2 \alpha_4^2 \alpha_5^1 + \alpha_1^2 \alpha_4^1 \alpha_5^2 + \alpha_1^1 \alpha_4^2 \alpha_5^2 \right)$$

$$\Rightarrow \text{points: } \left\{ \begin{pmatrix} 2 \\ 2 \\ 1 \end{pmatrix}, \begin{pmatrix} 2 \\ 1 \\ 2 \end{pmatrix}, \begin{pmatrix} 1 \\ 2 \\ 2 \end{pmatrix} \right\},$$

$$\text{rank} \begin{pmatrix} 1 & 1 \\ 0 & -1 \\ -1 & 0 \end{pmatrix} = 2 = N_f - 1.$$

To conclude, the criterion in Eq. (58) is simple, can be automated easily and it does not depend on graph information of an integral, even though we used massless tadpoles as illustrative examples. Together with the line contraction property of the alpha-representation for topologies mentioned in Section 2.3.3, one can readily identify all its vanishing subtopologies. Pure numerators of a topology can always be neglected for checking scalefulness. In momentum space representation the numerators can be expanded and in each resulting integral the scaling of the integration momenta will apply.

## 2.4 CANONICALLY ORDERED POLYNOMIALS

This section is devoted to the systematics behind topology classification. For that purpose the parametric representations for Feynman integrals derived in Section 2.3 are employed not for explicit evaluation but for constituting a proper identifier made up of the Symanzik polynomials.



## 2.4.1 Topology identification

One aspect of multi-loop problems is the vast complexity in form of the number of Feynman diagrams one has to handle and their individual intricacy with increasing number of loops. Even more so if the problem is in addition of multi-scale nature. This is partly due to the Feynman rules that leave arbitrariness to some degree by not fixing the routing of external and internal momenta completely.

The task is to reduce this complexity as much as possible to cope with the calculation of some process. A crude breakdown would be:

1. The large number of diagrams gives rise to a comparable number of common distinct integrals, in the ballpark of  $\mathcal{O}(10^{4-7})$ .
2. These diagrams or their integrals can be classified into a much smaller set of topologies, typically  $\mathcal{O}(10^{1-2})$ , which can be treated separately.
3. The reduction of the initial integrals within these topologies expresses each integral as a linear combination of only a few “master integrals”, typically of the order of the number of topologies.

This requires one to be able to decide for Feynman integral families  $T_1, T_2, \dots$  whether

- topologies  $T_1$  and  $T_2$  are equivalent (though their explicit definitions in momentum-space may differ)

$$T_1 \equiv T_2,$$

- topology  $T_1$  is contained in topology  $T_2$  (or  $T_1$  is a genuine subtopology to  $T_2$ )

$$T_1 \subset T_2,$$

- topology  $T_1$  is contained in or equivalent to topology  $T_2$  (combining the previous two statements)

$$T_1 \subseteq T_2,$$

- topology  $T_1$  can be expressed in topology  $T_2$  (all denominators of  $T_1$  can be mapped directly to those of  $T_2$  whereas numerators may require shifts of loop momenta)

$$T_1 \lesssim T_2.$$

And for specific Feynman integrals  $I_1, I_2, \dots$  (with fixed values of indices) if

- integrals  $I_1$  and  $I_2$  are one and the same (each represented as single integral in some topology),

$$I_1 \equiv I_2,$$

- integral  $I_1$  is member of topology  $T_2$  ( $I_1$  represented as single integral from  $T_2$ )

$$I_1 \in T_2.$$

- integral  $I_1$  can be expressed in topology  $T_2$  ( $I_1$  is a linear combination of integrals from  $T_2$ )

$$I_1 \lesssim T_2.$$

Here, let us complete the notation by also introducing newly constructed entities besides the previous relations between topologies and integrals:

- a greatest common subtopology of topologies  $T_1$  and  $T_2$

$$T_1 \cap T_2,$$

- a topology completely containing both topologies  $T_1$  and  $T_2$

$$T_1 \cup T_2.$$

The relations  $\cap$  and  $\cup$  for topologies can be understood in terms of all the integrals of a topology. For example in the last case: all integrals from  $T_1$  and all integrals from  $T_2$  are included in the integrals of  $T_1 \cup T_2$ .

The main pieces of technology making these tasks feasible are addressed in this section and based on a unique way of writing down parametric representations of Feynman integrals involving the Symanzik polynomials  $\mathcal{U}$  and  $\mathcal{W}$  discussed in Section 2.3. Before, we discuss briefly alternative ways to tackle these problems, their disadvantages and how we intend to improve upon them. Suppose the following situation: we are given two Feynman diagrams and explicit momentum-space representations for their integrals. How can we know if both integrals are equal?

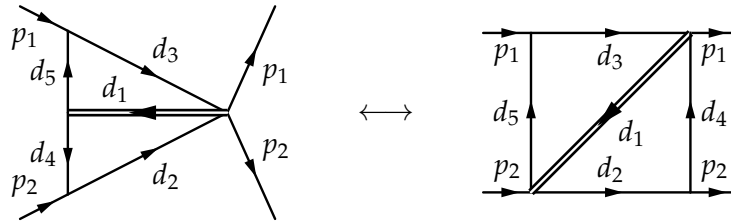
An obvious approach would be to try and transform one diagram into the other by renaming edges in all possible ways. Diagrammatically, this corresponds to repositioning vertices which leaves the adjacency structure intact. Graph identification in this sense is for example implemented in the program `exp`, see Refs. [23, 24]. This problem is computationally very demanding, checking isomorphism for (sub)graphs is of NP(-complete) complexity. Loosely speaking, this means the problem can be solved in a time Polynomially dependent on its size but only in a Non-deterministic way. Conversely, this means (probably) the problem cannot be solved deterministically more efficient than with exponential growth. The name “`exp`” hints to the program’s capabilities to perform also **exp**ansion in some limit of masses or invariants on diagram level.

There is also a very elegant way to encode a graph in a unique string of symbols, called the “Nickel-index”, see for example Ref. [25]. It is basically an ordered way of writing down the adjacency list of a graph (for each vertex a listing of vertices to which it connects) leaving out possible redundancies. Computing and comparing these strings then gives the answer but soon we

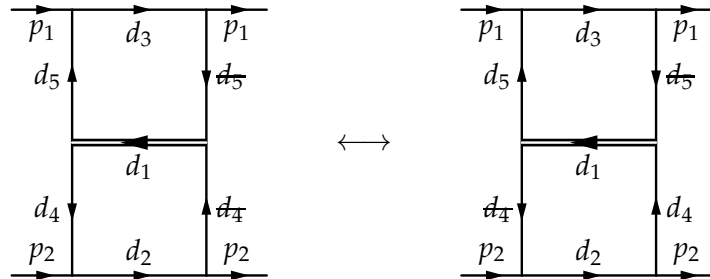
will realize that one should not rely too much on graph information. For this purpose let us return to Example 2 that was already used in Ref. [3], here we modified it slightly.

**Example 25.** Compared to Example 2, we explicitly label propagators of both graphs and fix a routing of loop momenta.

$$\begin{aligned} d_1 &= m_H^2 + k_1^2, \\ d_2 &= (p_2 + k_2)^2, \\ d_3 &= (p_1 + k_1 - k_2)^2, \\ d_4 &= k_2^2, \\ d_5 &= (k_1 - k_2)^2. \end{aligned}$$



Surprisingly, we find that the same set of propagators can be used for the two non-isomorphic graphs, meaning they are different representations of the same integral. This is explained below but there are cases where this is not possible. Both graphs can be embedded in a larger graph where, due to identical propagators and symmetries, only two diagrammatically distinct contractions are possible, each corresponding to one of the graphs. The right-most of the lines assigned  $d_5$  is contracted, indicated by a slashed symbol, together with one of the lines assigned  $d_4$ .



This example shows a basic fact: there can be various non-isomorphic graphs attached to one and the same topology (there is even more precariousness involved when coming back to this topic in Section 2.7) and for graph-based algorithms to give us a full solution to the question of membership in a topology, we would have to construct all valid graphs to a topology and operate on these. But eventually, there exists an alternative approach described below.

Comparing integrands is also a valid way: one has to match  $N_{d,1}$  propagators from the first topology to  $N_{d,2}$  propagators from the second topology. These propagators are given in terms of scalar products, viz. in explicit

momentum-space representations which can differ but are related by shifts in the loop momenta which will be topic in Section 2.4.5. Naively, one has to try all  $\binom{N_{d,1}}{N_{d,2}}$  ways of combining propagators and for each combination one must look for (discrete) shifts in the  $N_k$  loop momenta. Using restrictions from mass scales or external invariants appearing in propagators can improve the combinatorics to some extent. That is the philosophy behind the program `reg`, see Ref. [26]. We use this tool to find for each diagram a topology and the corresponding permutation of denominators together with the transformation of loop momenta. The name “reg” is an abbreviation of **regions**, referring to transformations on scalar products rather than graph lines.

#### 2.4.2 Canonical ordering

The following discussion is general for any multivariate polynomial and can thus be seen completely loosened from the context of  $\mathcal{U}$ - and  $\mathcal{W}$ -polynomials and alpha-parameters. It was first described in this connection by A. Pak in Ref. [3], here it is given in a more formal way with one important modification described below.

Given some polynomial  $P$  with constant coefficients  $\{c_i\}$  for  $m$  terms in  $n$  variables  $\{x_j\}$ , we look for a procedure that brings each polynomial  $P'$  obtained from  $P$  by applying an arbitrary permutation of variables  $\{x_{\sigma(j)}\}$ , also including the identical case  $P' = P$ , into a single unique form  $\hat{P}$  for all  $P'$ .

The procedure itself needs not to be unique for there could be various ways to rename the  $\{x_j\}$  in order to arrive from any  $P'$  at a fixed  $\hat{P}$ , i.e. if the polynomial exhibits symmetries in all or some of its variables. Moreover,  $\hat{P}$  by itself can be chosen to be any of the possible  $P'$ . This procedure of canonical ordering is achieved by defining a metric on a polynomial  $P'$  and picking one of those permutations of parameters  $\{x_{\sigma(j)}\}$  that maximize this metric. The metric of a polynomial  $P'$  should depend on its structure, i.e. on the coefficients  $\{c_i\}$  and the powers of variables  $\{x_j\}$  in monomials. For this purpose one needs an ordering of coefficients which can be fixed in any way. In a real implementation one can use for this mandatory ordering conveniently the one provided by the particular computer algebra system (CAS). But for the following discussion let us assume lexicalic ordering, see Eq. (22).

---

**Algorithm 2** (canonical ordering). The following steps describe the implementation of one suitable metric and its maximization, also constituting the very core of the Mathematica package `TopoID` presented in Section 2.5. A polynomial  $P$  on the input is converted to its canonical form  $\hat{P}$ .

1. Convert the polynomial  $P$  with  $m$  terms and  $n$  variables into the  $m \times (n + 1)$  matrix  $M^{(0)}$ . Each row corresponds to a term, the first column to the monomial coefficients  $\{c_i\}$ , the remaining columns to the non-negative integer powers of variables  $\{x_j\}$ . For simplicity, we assign the

first column the index zero, such that  $M_{i0}^{(0)} = c_i$  denotes the vector of constant coefficients. We write symbolically:

$$P(\{c_i\}, \{x_j\}) \rightarrow M_{ij}^{(0)}.$$

2. To start with the following considerations in the second column which we assign the index one, set the variable  $k$  to one and initialize the set of matrices  $S^{(k=1)}$  to contain only  $M^{(0)}$ :

$$S^{(1)} = \{M^{(0)}\}, \quad k = 1.$$

3. The set  $S^{(k)} = \{M^{(k),\sigma}\}$  contains all matrices still present in step  $k$ . For all these matrices  $M^{(k),\sigma}$  compute in addition all transpositions of column  $k$  (corresponding to  $x_k$ ) with all remaining columns  $l = k + 1, \dots, n$  (corresponding to  $x_{k+1}, \dots, x_n$ ) to obtain the set  $S'^{(k)} = \{M'^{(k),\sigma}\} \supset S^{(k)}$ . The index  $\sigma$  collects all the permutations applied to a specific matrix so far and  $\sigma(k, l)$  symbolizes incorporation of the transposition  $k \leftrightarrow l$  into the permutation  $\sigma$ . More specifically:

$$\begin{aligned} M'_{ik}{}^{(k),\sigma(kl)} &= M_{il}^{(k),\sigma}, & M'_{il}{}^{(k),\sigma(kl)} &= M_{ik}^{(k),\sigma}, \\ M'_{ij}{}^{(k),\sigma(kl)} &= M_{ij}^{(k),\sigma} & \text{for } j &\neq k, l. \end{aligned}$$

4. For each matrix in  $S'^{(k)}$  sort rows lexicographically by inspecting the first  $k$  columns only to obtain the set  $S''^{(k)} = \{M''^{(k),\sigma}\}$ :

$$M''^{(k),\sigma} = \text{sort}[1..m, 1..k] M'^{(k),\sigma},$$

with fixed ordering operation "sort" acting on  $M_{i,1..k}^{(k),\sigma}$  only.

5. Extract from each  $M''^{(k),\sigma}$  the vectors of column  $k$  and compare all  $m$  elements to determine the lexicographically largest one  $\hat{M}_{ik}''^{(k)}$ :

$$\hat{M}_{ik}''^{(k)} = \max \{M_{ik}''^{(k),\sigma}\}.$$

6. Keep all matrices from  $S''^{(k)}$  which exhibit the maximized column  $k$  in the set  $S^{(k+1)}$  and discard all with non-maximal column  $k$ . If  $k < n - 1$ , increment  $k$  by one and perform Steps 3 to 6 *iteratively*:

$$S^{(k+1)} = \{M''^{(k),\sigma} \mid M_{ik}''^{(k),\sigma} = \hat{M}_{ik}''^{(k)}\},$$

if  $k < n - 1$ : set  $k \rightarrow k + 1$ , go to Step 3.

7. When  $k = n - 1$  is reached the algorithm terminates and all the matrices in  $S^{(n)}$  encode the same polynomial  $\hat{P} = \hat{P}_\sigma$  with relabeled variables maximizing the metric corresponding to  $M^{(n),\sigma}$ . The requested permutations of variables  $\{x_{\sigma(j)}\}$  are precisely the set of remaining collective indices  $\hat{\sigma}$  in  $S^{(n)}$ .

These permutations  $\{x_{\sigma(j)}\}$  are in the following referred to as “canonical permutations”, “canonical (re-)orderings”, “canonical (re-)labelings”, etc. of variables and the polynomial  $\hat{P}$  onto which one of these permutations was leading as “canonical polynomial”.

In contrast to what is stated as Step (v) in Section 2 of Ref. [3], it is in Step 6 mandatory to proceed not recursively but iteratively. The difference may appear very subtle at first glance but it causes wrong results in the output. Recursion is usually understood as a branching of the algorithm whereby results of different branches are independent. Then, however, all matrices selected in Step 6 would in general not correspond to one and the same maximum column vector and the result could contain, besides all canonical permutations, also permutations for local maxima of the metric. So either one has to post-process the output from the procedure of Ref. [3] or assert that already during their build-up all permutations belong to the global maximum.

**Example 26.** It is in order to demonstrate the workings of this algorithm step-by-step for some simple polynomials, still without relation to any topology. The various steps are indicated by equation labels, also stating the number of iterations if applicable and a filled black box shows that the procedure has halted. For convenience, matrix blocks relevant for sorting rows in Step 4 are marked in Step 3 and maximized columns in Step 5 or Step 6 are highlighted in previous results of Step 4.

$$P = x_1^2 + 2x_1x_2 + x_2^2 + x_3^2 \quad \rightarrow \quad M^{(0)} = \begin{pmatrix} 1 & 2 & 0 & 0 \\ 2 & 1 & 1 & 0 \\ 1 & 0 & 2 & 0 \\ 1 & 0 & 0 & 2 \end{pmatrix}. \quad (\text{Step 1})$$

$$S^{(1)} = \{M^{(0)(123)} = M^{(0)}\}, \quad k = 1. \quad (\text{Step 2})$$

$$S'^{(1)} : \quad M'^{(1)(123)} = \begin{pmatrix} 1 & 2 & 0 & 0 \\ 2 & 1 & 1 & 0 \\ 1 & 0 & 2 & 0 \\ 1 & 0 & 0 & 2 \end{pmatrix}, \quad M'^{(1)(213)} = \begin{pmatrix} 1 & 0 & 2 & 0 \\ 2 & 1 & 1 & 0 \\ 1 & 2 & 0 & 0 \\ 1 & 0 & 0 & 2 \end{pmatrix},$$

$$M'^{(1)(321)} = \begin{pmatrix} 1 & 0 & 0 & 2 \\ 2 & 0 & 1 & 1 \\ 1 & 0 & 2 & 0 \\ 1 & 2 & 0 & 0 \end{pmatrix}.$$

(Step 3-1)

$$S''^{(1)} : M''^{(1)(123)} = \begin{pmatrix} 1 & \mathbf{0} & 0 & 2 \\ 1 & \mathbf{0} & 2 & 0 \\ 1 & \mathbf{2} & 0 & 0 \\ 2 & \mathbf{1} & 1 & 0 \end{pmatrix}, \quad M''^{(1)(213)} = \begin{pmatrix} 1 & \mathbf{0} & 2 & 0 \\ 1 & \mathbf{0} & 0 & 2 \\ 1 & \mathbf{2} & 0 & 0 \\ 2 & \mathbf{1} & 1 & 0 \end{pmatrix},$$

$$M''^{(1)(321)} = \begin{pmatrix} 1 & \mathbf{0} & 0 & 2 \\ 1 & \mathbf{0} & 2 & 0 \\ 1 & \mathbf{2} & 0 & 0 \\ 2 & \mathbf{0} & 1 & 1 \end{pmatrix}.$$

(Step 4-1)

$$\hat{M}''^{(1)} = \begin{pmatrix} 0 \\ 0 \\ 2 \\ 1 \end{pmatrix}.$$

(Step 5-1)

$$S^{(2)} = \{M''^{(1)(123)}, M''^{(1)(213)}\}, \quad k = 2. \quad (\text{Step 6-1})$$

$$S'^{(2)} : M'^{(2)(123)} = \begin{pmatrix} 1 & 0 & 0 & 2 \\ 1 & 0 & 2 & 0 \\ 1 & 2 & 0 & 0 \\ 2 & 1 & 1 & 0 \end{pmatrix}, \quad M'^{(2)(132)} = \begin{pmatrix} 1 & 0 & 2 & 0 \\ 1 & 0 & 0 & 2 \\ 1 & 2 & 0 & 0 \\ 2 & 1 & 0 & 1 \end{pmatrix},$$

$$M'^{(2)(213)} = \begin{pmatrix} 1 & 0 & 2 & 0 \\ 1 & 0 & 0 & 2 \\ 1 & 2 & 0 & 0 \\ 2 & 1 & 1 & 0 \end{pmatrix}, \quad M'^{(2)(231)} = \begin{pmatrix} 1 & 0 & 0 & 2 \\ 1 & 0 & 2 & 0 \\ 1 & 2 & 0 & 0 \\ 2 & 1 & 0 & 1 \end{pmatrix}.$$

(Step 3-2)

$$S''^{(2)} : M''^{(2)(123)} = \begin{pmatrix} 1 & 0 & \mathbf{0} & 2 \\ 1 & 0 & \mathbf{2} & 0 \\ 1 & 2 & \mathbf{0} & 0 \\ 2 & 1 & \mathbf{1} & 0 \end{pmatrix}, \quad M''^{(2)(132)} = \begin{pmatrix} 1 & 0 & 0 & 2 \\ 1 & 0 & 2 & 0 \\ 1 & 2 & 0 & 0 \\ 2 & 1 & 0 & 1 \end{pmatrix},$$

$$M''^{(2)(213)} = \begin{pmatrix} 1 & 0 & \mathbf{0} & 2 \\ 1 & 0 & \mathbf{2} & 0 \\ 1 & 2 & \mathbf{0} & 0 \\ 2 & 1 & \mathbf{1} & 0 \end{pmatrix}, \quad M''^{(2)(231)} = \begin{pmatrix} 1 & 0 & 0 & 2 \\ 1 & 0 & 2 & 0 \\ 1 & 2 & 0 & 0 \\ 2 & 1 & 0 & 1 \end{pmatrix}.$$

(Step 4-2)

$$\hat{M}''^{(2)} = \begin{pmatrix} 0 \\ 2 \\ 0 \\ 1 \end{pmatrix}.$$

(Step 5-2)

$$S^{(2)} = \{M''^{(2)(123)}, M''^{(2)(213)}\}. \quad (\text{Step 6-2})$$

$$\hat{P} = P = x_3^2 + x_2^2 + x_1^2 + 2x_1x_2, \quad \hat{\sigma} = \{(123), (213)\}. \quad \blacksquare \quad (\text{Step 7})$$

The polynomial  $P$  has an obvious symmetry under  $x_1 \leftrightarrow x_2$  which is also reproduced by the algorithm since two canonical permutations  $\{(123), (213)\}$  are returned. We also see that  $P$  was already in canonical form. The permu-

tation (213) denotes the simultaneous replacement  $(x_1, x_2, x_3) \rightarrow (x_2, x_1, x_3)$  transforming  $P$  into  $\hat{P}$ .

**Example 27.** Now, let us trade in  $P$  the term  $x_3^2$  for the term  $2x_2x_3$  and trace how the steps change.

$$P = x_1^2 + 2x_1x_2 + x_2^2 + 2x_2x_3 \rightarrow M^{(0)} = \begin{pmatrix} 1 & 2 & 0 & 0 \\ 2 & 1 & 1 & 0 \\ 1 & 0 & 2 & 0 \\ 2 & 0 & 1 & 1 \end{pmatrix}. \quad (\text{Step 1})$$

$$S^{(1)} = \{M^{(0)(123)} = M^{(0)}\}, \quad k = 1. \quad (\text{Step 2})$$

$$S'^{(1)} : M'^{(1)(123)} = \left( \begin{array}{ccc|cc} 1 & 2 & 0 & 0 & 0 \\ 2 & 1 & 1 & 0 & 0 \\ 1 & 0 & 2 & 0 & 0 \\ 2 & 0 & 1 & 1 & 0 \end{array} \right), \quad M'^{(1)(213)} = \left( \begin{array}{ccc|cc} 1 & 0 & 2 & 0 & 0 \\ 2 & 1 & 1 & 0 & 0 \\ 1 & 2 & 0 & 0 & 0 \\ 2 & 1 & 0 & 0 & 1 \end{array} \right),$$

$$M'^{(1)(321)} = \left( \begin{array}{ccc|cc} 1 & 0 & 0 & 2 & 0 \\ 2 & 0 & 1 & 1 & 0 \\ 1 & 0 & 2 & 0 & 0 \\ 2 & 1 & 1 & 0 & 0 \end{array} \right).$$

(Step 3-1)

$$S''^{(1)} : M''^{(1)(123)} = \left( \begin{array}{cccc} 1 & 0 & 2 & 0 \\ 1 & 2 & 0 & 0 \\ 2 & 0 & 1 & 1 \\ 2 & 1 & 1 & 0 \end{array} \right), \quad M''^{(1)(213)} = \left( \begin{array}{ccc|cc} 1 & 0 & 2 & 0 & 0 \\ 1 & 2 & 0 & 0 & 0 \\ 2 & 1 & 1 & 0 & 0 \\ 2 & 1 & 0 & 0 & 1 \end{array} \right),$$

$$M''^{(1)(321)} = \left( \begin{array}{cccc} 1 & 0 & 0 & 2 \\ 1 & 0 & 2 & 0 \\ 2 & 0 & 1 & 1 \\ 2 & 1 & 1 & 0 \end{array} \right).$$

(Step 4-1)

$$\hat{M}''^{(1)} = \begin{pmatrix} 0 \\ 2 \\ 1 \\ 1 \end{pmatrix}.$$

(Step 5-1)

$$S^{(2)} = \{M''^{(1)(213)}\}, \quad k = 2. \quad (\text{Step 6-1})$$

$$S'^{(2)} : M'^{(2)(213)} = \left( \begin{array}{ccc|cc} 1 & 0 & 2 & 0 & 0 \\ 1 & 2 & 0 & 0 & 0 \\ 2 & 1 & 1 & 0 & 0 \\ 2 & 1 & 0 & 1 & 0 \end{array} \right), \quad M'^{(2)(231)} = \left( \begin{array}{ccc|cc} 1 & 0 & 0 & 2 & 0 \\ 1 & 2 & 0 & 0 & 0 \\ 2 & 1 & 0 & 1 & 0 \\ 2 & 1 & 1 & 0 & 0 \end{array} \right).$$

(Step 3-2)



$$S''^{(2)} : M''^{(2)(213)} = \begin{pmatrix} 1 & 0 & 2 & 0 \\ 1 & 2 & 0 & 0 \\ 2 & 1 & 0 & 1 \\ 2 & 1 & 1 & 0 \end{pmatrix}, \quad M''^{(2)(231)} = \begin{pmatrix} 1 & 0 & 0 & 2 \\ 1 & 2 & 0 & 0 \\ 2 & 1 & 0 & 1 \\ 2 & 1 & 1 & 0 \end{pmatrix}. \quad (\text{Step 4-2})$$

$$\hat{M}''^{(2)} = \begin{pmatrix} 2 \\ 0 \\ 0 \\ 1 \end{pmatrix}. \quad (\text{Step 5-2})$$

$$S^{(2)} = \{M''^{(2)(213)}\}. \quad (\text{Step 6-2})$$

$$\hat{P} = x_2^2 + x_1^2 + 2x_1x_3 + 2x_1x_2, \quad \hat{\sigma} = \{(213)\}. \quad \blacksquare \quad (\text{Step 7})$$

By the change of terms we destroyed the former symmetry  $x_1 \leftrightarrow x_2$  and apparently this is why the algorithm produces thereafter only one canonical ordering.

Henceforth, we may understand the various steps of the algorithm in more general terms:

- By converting a polynomial  $P$  into a matrix  $M$  in Step 1 the arbitrary order of monomials of  $P$  translates into rearranging rows of  $M$  freely, whereas renaming pairs of variables  $(x_k, x_l)$  corresponds to interchanging columns  $(M_{ik}, M_{il})$ . However, in contrast to row interchanges, column interchanges must be kept track of (by the collective index  $\sigma$ ) for they give in the end the permutations we are interested in.
- Steps 2, 3 and 6 ensure that all possible permutations of the  $\{x_j\}$  are considered as candidate orderings and systematically excluded in each iteration to keep computational effort in check.
- As stated initially, this procedure depends on monomial coefficients  $\{c_i\}$  and powers of variables  $\{x_j\}$ . As one can see from Step 4 and Step 5 in the above examples, the ordering works such that for the “first” variables “more complicated” coefficients are preferred as primary criterion and higher powers as secondary criterion. However, this depends on the internal implementation in a CAS of “sort” in Step 4 and “max” in Step 5 that do not need to bother us any further as long as they provide a unique ordering. We assumed a simple lexical ordering in the examples. Changing this ordering will surely change the canonical form resulting in the end but not the fact that it is unambiguously defined.
- Later, in context of  $\mathcal{U}$ - and  $\mathcal{W}$ -polynomials, it will become clear that the  $\{c_i\}$  encode the kinematics and mass configuration of a Feynman diagram topology and the exponents of the  $\{x_j\}$  the graph structure itself.

Considering canonically reordered polynomials appears to be mathematically equivalent (or at least related) to the usage of matroids, structures

which generalize the notion of linear dependency. A special class of matroids, cycle matroids, have in general multiple graph representations in analogy to topologies. The public code `Reduze`, see Ref. [27], is based on such matroids.

### 2.4.3 Application to topologies

We have seen in Section 2.3 that for any given topology, or Feynman integral with specified values for powers of denominators and numerators from such a topology, one can readily write down the alpha- or Feynman parametrization in terms of the two Symanzik polynomials  $\mathcal{U}$  and  $\mathcal{W}$ . As already mentioned, these representations have the advantage that integration over loop momenta has already been carried out. Thus, one got rid of the to some extent arbitrary routing of loop momenta that had to be introduced according to the Feynman rules. While this ambiguity is resolved, the one associated with relabeling of alpha-parameters corresponding to renaming of lines in the graph or factors in the integral remains.

Now, this last freedom can also be removed by employing the technique described in Section 2.4.2 for the polynomials  $\mathcal{U}$  and  $\mathcal{W}$ . Thereafter one can use these canonically reordered  $\hat{\mathcal{U}}$ - and  $\hat{\mathcal{W}}$ -polynomials together as unique identifier for a topology. This property applies to all different kinds of topologies and subtopologies, regardless if complete or incomplete, linearly dependent or independent and also to specific Feynman integrals, taking their reordered vector of indices into account.

The ordering procedure was defined in Section 2.4.2 only for a single polynomial but now we want to apply it to the pair  $(\mathcal{U}, \mathcal{W})$ . In the case of multiple polynomials one can introduce just as many auxiliary variables (considered part of monomial coefficients) as there are polynomials, form the sum of polynomials weighted with their respective marker and finally apply our procedure. It proved sufficient in practice to use either  $\mathcal{U} \times \mathcal{W}$  or  $\mathcal{U} + \mathcal{W}$  as characteristic polynomial. The product  $\mathcal{U} \times \mathcal{W}$  was suggested by A. Pak in Ref. [3] and has the advantage that one can also infer scalefulness from it (see Section 2.3.4). For comparison purposes this is less efficient than the sum  $\mathcal{U} + \mathcal{W}$  where the total number of terms is only the sum of the numbers of terms in  $\mathcal{U}$  and  $\mathcal{W}$  and not their product, in the worst case. Additionally, uniqueness is for the polynomial expression  $\mathcal{U} + \mathcal{W}$  evident since the degrees of homogeneity differ for  $\mathcal{U}$  and  $\mathcal{W}$  by one. On the contrary, it is not obvious that one can always factorize  $\mathcal{U} \times \mathcal{W}$  uniquely to reconstruct the characteristic pair  $(\mathcal{U}, \mathcal{W})$  and one cannot exclude misidentification.

In the following we want to demonstrate this reordering on some of the simplest examples available, namely one-loop propagator topologies and the basic and generic topologies for Higgs boson production  $T_{H,\text{NLO}}^{\text{basic}}$  and  $T_{H,\text{NLO}}^{\text{generic}}$ , we encountered in Example 1 and Example 6, respectively. Since we work now with Feynman parametrizations for propagators defined in Euclidean metrics, we label graph lines with numbers corresponding to Feynman parameters and refrain from giving directions for the flows of line momenta. Canonically reordered topologies are denoted with an additional hat on their



$$\begin{aligned}\hat{U} &= -\alpha_1 - \alpha_2 - \alpha_3, \\ \hat{W} &= -m_H^2 \alpha_1^2 - m_H^2 \alpha_1 \alpha_2 - m_H^2 \alpha_1 \alpha_3 + s \alpha_1 \alpha_3.\end{aligned}$$

We had to apply (132) to the initial order of factors and alpha-parameters to arrive at the canonically reordered topology  $\hat{T}_{H,NLO}^{\text{basic}}$ . For  $T_{H,NLO}^{\text{generic}}$  we find again a symmetry, reflected in the two orderings  $\{(1342), (1432)\}$ . Both orderings give:

$$\hat{T}_{H,NLO}^{\text{generic}}(a_1, a_2, a_3, a_4) = \begin{array}{c} \begin{array}{ccc} \begin{array}{c} \rightarrow p_1 \\ | \\ 4 \\ | \\ 2 \\ | \\ \rightarrow p_2 \end{array} & \begin{array}{c} \diagdown \\ \diagup \end{array} & \begin{array}{c} \rightarrow p_1 \\ | \\ 3 \\ | \\ \rightarrow p_2 \end{array} \\ & & \end{array} \quad \Longrightarrow \end{array}$$

$$\begin{aligned}\hat{U} &= -\alpha_1 - \alpha_2 - \alpha_3 - \alpha_4, \\ \hat{W} &= -m_H^2 \alpha_1^2 - m_H^2 \alpha_1 \alpha_2 - m_H^2 \alpha_1 \alpha_3 - m_H^2 \alpha_1 \alpha_4 + s \alpha_1 \alpha_4 - s \alpha_2 \alpha_3.\end{aligned}$$

In this example we did not explicitly state the characteristic polynomials since especially the products become already quite lengthy.

In Example 29 both choices of characteristic polynomials give the same answers for reordering which is unfortunately no generic feature. In the following we will stick for reordering to the more manageable sum of Symanzik polynomials alone.

#### 2.4.4 Subtopologies

As explained in Section 2.3.3 the alpha-representation to a subtopology can be readily obtained by setting all but the alpha-parameters corresponding to factors of the subtopology to zero. In case these factors are depictable as lines in a graph this corresponds to contraction of these lines. Naturally, the question arises if the alpha-representation once brought into canonical form by means of the procedure discussed in Section 2.4.2 will still be in canonical form after applying contractions. First, let us see by an easy counter-example that it is unfortunately not possible to define an ordering of variables that implements this property. One can, however, handle the problem of subtopology classification by different means that will be laid out thereafter.

**Example 30.** The polynomial  $P_{(1234)}$  in variables  $x_1, \dots, x_4$  is ordered according to our procedure,

$$P_{(1234)} = \hat{P}_{(1234)} = x_1 x_2^2 x_3 + x_1^2 x_2 x_4.$$

There is a symmetry in simultaneously changing  $x_1 \leftrightarrow x_2$  and  $x_3 \leftrightarrow x_4$ , reflected in the canonical orderings  $\{(1234), (2143)\}$ . If we now apply the contraction  $x_3 = 0$ , corresponding to the permutation (124), and the contraction  $x_4 = 0$ , corresponding to the permutation (123), we obtain:

$$P_{(124)} = x_1^2 x_2 x_3, \quad P_{(123)} = x_1 x_2^2 x_3.$$

Here, the terms of  $P_{(1234)}$  were simply separated into both contractions. After the contraction  $x_3 = 0$  in  $P_{(124)}$  also the renaming  $x_4 \rightarrow x_3$  has been applied. Inspecting both contracted polynomials more closely, we find the canonical orderings:

$$\sigma_{P_{(124)}} = \{(123), (132)\}, \quad \sigma_{P_{(123)}} = \{(213), (231)\}.$$

Hence, the canonical ordering is destroyed by the contraction (123). Now, let us try to understand why this happened and if one can circumvent it by applying a different ordering prescription. Writing down the matrix  $M^{(0)}$ , which would be the starting point for every sensible metric construction, we get:

$$M^{(0)} = \begin{pmatrix} 1 & 1 & 2 & 1 & 0 \\ 1 & 2 & 1 & 0 & 1 \end{pmatrix}.$$

Based on this matrix it is always possible to define uniquely an order of present variables. However, upon contraction of any variable, say  $x_k$ , all terms involving  $x_k$  are removed or equally any row  $l$  in  $M^{(0)}$  with  $M_{lk}^{(0)} \neq 0$  and thereafter the column  $M_{ik}^{(0)}$  itself:

$$M_{(124)}^{(0)} = (1 \ 2 \ 1 \ 1), \quad M_{(123)}^{(0)} = (1 \ 1 \ 2 \ 1), \quad M_{(124)}^{(0)} \neq M_{(123)}^{(0)}.$$

It becomes obvious that by contraction of  $x_k = 0$  the relative importance of all  $x_{j \neq k}$  present in terms involving  $x_k$  gets changed in general. Or equally for  $x_j$  if there is an  $l$  with  $M_{lj}^{(0)} \neq 0$  and  $M_{lk}^{(0)} \neq 0$ .

We have to realize that it is impossible to devise a specific ordering of variables in a polynomial that persists after the contraction of arbitrary variables. There is no contraction property for canonically ordered polynomials.

We want to compare Feynman integrals or classes of them in order to identify a minimal set of the objects we had in the beginning. This means topologies present as subtopology in an arbitrary topology with more factors or as alternative momentum space representation can immediately be dropped. To check if some topology  $T_1$  is isomorphic to a subtopology of some other topology  $T_2$  with more lines than  $T_1$ , in the sense of  $T_1 \subset T_2$ , the following steps are necessary:

- Perform all possible contractions leaving  $T_2$  with the same number of lines as  $T_1$ .
- Bring the corresponding alpha-representations of subtopologies into canonical form.
- Finally, compare to the canonical form of alpha-representation of  $T_1$ .

Alternatively but more efficient, we determine for each and every possible contraction of factors of a topology the canonical permutation of alpha-parameters in the corresponding subtopology and store only the resulting

“canonical contraction” or “canonical subset”. Applying these reordered contractions onto the canonical Symanzik polynomials of the initial topology results then in canonical representations also for the subtopologies.

**Example 31.** Observe in Example 30 that if we had applied one of the reordered versions of the contraction (123) to  $P_{(1234)}$ , in this case just (213) or (231), the resulting polynomials  $P_{(213)} = P_{(231)} = x_1^2 x_2 x_3$  would have been in canonical form.

In general, upon performing a contraction, denoted by a subset of factors of a topology (or their positions), we can freely choose the order of selected factors and still end up with the same subtopology. We can make use of this freedom and incorporate into the contraction one of the canonical reorderings valid for the emerging subtopology, while the other reorderings represent its symmetries. By this strategy also different contractions leading to identical subtopologies can be found and grouped. Together with the criterion for scalelessness a complete classification of a topology into groups of equivalent subtopologies is possible, one group describing all scaleless subtopologies.

**Example 32.** If we apply the canonical reordering (23451) to the massless two-loop propagator topology of Example 18 (in Euclidean metrics), we find:

$$\hat{P}_2(a_1, \dots, a_5) = \text{---} \begin{array}{c} 2 \\ \circ \\ 1 \\ \circ \\ 3 \end{array} \begin{array}{c} 4 \\ \circ \\ 1 \\ \circ \\ 5 \end{array} \text{---} ,$$

$$\hat{U} = \alpha_{12} + \alpha_{13} + \alpha_{14} + \alpha_{15} + \alpha_{24} + \alpha_{25} + \alpha_{34} + \alpha_{35} ,$$

$$\hat{W} = p^2 (\alpha_{123} + \alpha_{125} + \alpha_{134} + \alpha_{145} + \alpha_{234} + \alpha_{235} + \alpha_{245} + \alpha_{345}) .$$

Note that the reordering of alpha-parameters also applies to lines in the graph. By the technique described before we can classify all its distinct and vanishing subtopologies encoded in the following sets of subsets of lines:

distinct groups of identical subsets:

$$\begin{aligned} & \{ \{(12345)\} , \\ & \quad \{(2345)\} , \\ & \quad \{(1254) , (1345) , (1432) , (1523)\} , \\ & \quad \{(125) , (134)\} \} , \end{aligned}$$

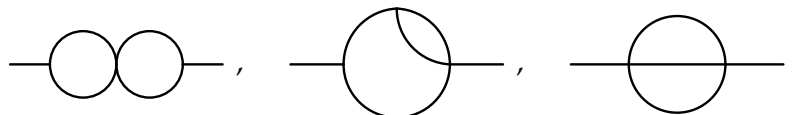
vanishing subsets:

$$\{ (123) , (124) , (135) , (145) , (234) , (235) , (245) , (345) \} .$$

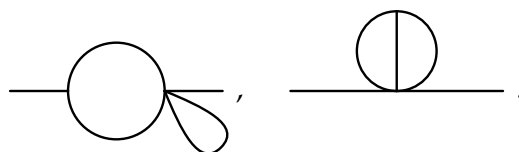
The first group contains the full topology, i.e. the identity. Each of the following groups gives subsets of lines to be considered equivalent, they have identical  $\hat{U}$ - and  $\hat{W}$ -polynomials. The last group is made up of subsets

corresponding to scaleless integrals where even smaller subsets of these were left out intentionally for not providing anything new. In this example each group corresponds to a class of isomorphic graphs (due to symmetries of the subtopology) shown below. In general there can be multiple classes of isomorphic graphs for each group.

Non-vanishing subtopologies :



Vanishing subtopologies :



For demonstration purposes we apply (1254) and (1432), corresponding to the second non-vanishing topology illustrated above, to  $\hat{\mathcal{U}}$  and  $\hat{\mathcal{W}}$ :

$$\begin{aligned}\hat{\mathcal{U}}_{(1254)} &= \hat{\mathcal{U}}_{(1432)} = \alpha_{12} + \alpha_{13} + \alpha_{14} + \alpha_{23} + \alpha_{24}, \\ \hat{\mathcal{W}}_{(1254)} &= \hat{\mathcal{W}}_{(1432)} = p^2 (\alpha_{123} + \alpha_{134} + \alpha_{243}).\end{aligned}$$

As intended both contractions have the same outcome. The general recipe for a canonical contraction is just the application of a canonical ordering in the subtopology (given as inverse permutation) on the corresponding subset. The subset (1235) gives as reorderings (1423) and (4123). Permuting the subset by the first reordering gives (1523), as in the previous complete classification list, but also (5123) from the second reordering would be valid and produce equal polynomials due to the symmetry of lines 1 and 5 once line 4 is absent.

More complex examples of this kind of classification are presented in Chapter 4 devoted to Higgs boson production and Section 2.5 explaining the usage of some features of TopoID. Details on the implementation of techniques described in this chapter will be published elsewhere, see Ref. [28].

#### 2.4.5 Finding momenta shifts

It has already been mentioned on several occasions that a topology can be represented in different ways in momentum space since one can always shift integration momenta  $\{k_i\}$  by (integer) amounts of other integration momenta or external momenta  $\{p_i\}$ . In analogy to Eq. (5), we write

$$k_i \rightarrow k'_i = \sum_{j=1}^{N_p} c_{ij}^k p_j + \sum_{j=1}^{N_k} d_{ij}^k k_j \quad \text{with} \quad c_{ij}^k, d_{ij}^k \in \mathbb{Z}. \quad (59)$$

In addition we can admit transformations on (independent) external momenta,

$$p_i \rightarrow p'_i = \sum_{j=1}^{N_p} c_{ij}^p p_j \quad \text{with} \quad c_{ij}^p \in \mathbb{Z}. \quad (60)$$

Such general transformations on external momenta can be used to connect topologies of different kinematic configurations, e.g. vertex type topologies (with independent external momenta  $p_1$  and  $p_2$ ) with propagator type topologies (by  $p'_1 = p_1 + p_2$ ,  $p'_2 = 0$ ). For implementing crossing of external momenta it suffices to allow permutations:

$$p_i \rightarrow p'_i = p_{\sigma(i)}. \quad (61)$$

In any case, transformations on both kinds of momenta in Eqs. (59) and (60) can be encoded in a single matrix:

$$\begin{pmatrix} p'_1 \\ \vdots \\ p'_{N_p} \\ k'_1 \\ \vdots \\ k'_{N_k} \end{pmatrix} = \begin{pmatrix} c^p & 0 \\ \hline c^k & d^k \end{pmatrix} \cdot \begin{pmatrix} p_1 \\ \vdots \\ p_{N_p} \\ k_1 \\ \vdots \\ k_{N_k} \end{pmatrix} \quad \text{or} \quad v' = C v, \quad (62)$$

where we defined implicitly common vectors of momenta  $v^{(l)}$  and a common transformation matrix  $C$ . Note that the (linear) transformation of integration momenta comes with the Jacobian factor  $\det c^k$ . When comparing vectors of factors  $\{f_i\}$  and  $\{f'_i\}$  of two topologies with the same number of factors (e.g. one topology before and after shifting momenta), shifts in Eq. (62) can generate permutations  $\sigma$  such that

$$f_i = f'_{\sigma(i)}. \quad (63)$$

The other way around, suppose we want to find such permutation of topology factors and corresponding momenta shifts. One could test all possible permutations and some restricted set of discrete momenta shifts by brute force. Our approach answers this question more elegantly since from canonical reordering the relation between both sets of factors is known readily. Thereby the only thing left to do is comparing coefficients in these sets to obtain the transformations in Eqs. (59) and (60).

In conclusion, it does not matter in which way one routes external and internal momenta through the lines of a topology. Once the procedure of canonical ordering is applied to any momentum-space representation, always the same characteristic polynomial from the Feynman parametrization will emerge. However, one has to take care for different choices of irreducible scalar products. On the one hand, this can be achieved by neglecting topology numerators in the characteristic polynomials (by contraction). If correspondence of denominators can be established and a shift of integration momenta exists (this is not guaranteed), then two topologies are related



in the sense of  $T_1 \subsetneq T_2$ . On the other hand, if we can relate the full set of factors of two topologies, in the sense of  $T_1 \equiv T_2$ , momenta shifts are not necessary.

**Example 33.** Using one more time the two-loop massless propagator topology of Example 32 for which we know the correspondence of all subtopologies, e.g. (1254) and (1523), we first have to give a momentum-space definition of factors:

$$\begin{aligned} q_1 &= k_1 + k_2, & d_1 &= k_1^2 + 2k_1 \cdot k_2 + k_2^2, \\ q_2 &= k_1, & d_2 &= k_1^2, \\ q_3 &= p - k_1, & \implies d_3 &= p^2 - 2p \cdot k_1 + k_1^2, \\ q_4 &= k_2, & d_4 &= k_2^2, \\ q_5 &= p + k_2. & d_5 &= p^2 + 2p \cdot k_2 + k_2^2. \end{aligned}$$

Hence, we can equate representations for the subsets (1254) and (1523) (the latter is distinguished with primed variables):

$$\begin{aligned} k_1^2 + 2k_1 \cdot k_2 + k_2^2 &= k_1'^2 + 2k_1' \cdot k_2' + k_2'^2, \\ k_1^2 &= p^2 + 2p \cdot k_2' + k_2'^2, \\ p^2 + 2p \cdot k_2 + k_2^2 &= k_1'^2, \\ k_2^2 &= p^2 - 2p \cdot k_1' + k_1'^2. \end{aligned}$$

We can simply read off  $k_1' = p + k_2$  and  $k_2' = p - k_1$ . This transformation can now be applied to integrals (with numerators) from (1523) to map them completely onto subtopology (1254). For example:

$$\begin{aligned} P_2(1, 1, 1, -1, 2) &= \int dk_1' dk_2' \frac{d_4}{d_1 d_2 d_3 d_5^2} = \int dk_1' dk_2' \frac{k_2'^2}{d_1 d_2 d_3 d_5^2} = \\ &= \int dk_1 dk_2 \frac{p^2 - 2pk_1 + k_1^2}{d_1 d_2^2 d_4 d_5} = \int dk_1 dk_2 \frac{d_3}{d_1 d_2^2 d_4 d_5} = P_2(1, 2, -1, 1, 1). \end{aligned}$$

This case corresponds to a global symmetry of  $P_2$ , namely the last one of the global reorderings  $\{(12345), (13254), (14523), (15432)\}$ .

In general, when mapping an integral  $I_1$  of a topology  $T_1$  to a subtopology of another topology  $T_2$ , one obtains multiple terms on the right-hand side after reexpressing scalar products in the numerator of  $I_1$  by topology factors of  $T_2$ .

#### 2.4.6 Symmetries

We already saw that the set of all canonical orderings of a topology corresponds to its symmetries. The contraction property of Feynman parameters, see Eq. (50), together with a single canonical ordering for each subtopology allowed us to define canonical contractions to give a complete classification. If we combine all reorderings in a subtopology with the corresponding con-

traction, we obtain the symmetries in this subtopology. One can consider symmetries of different subsets of lines that lead to equal subtopologies separately or combined for such subsets. We opted for the latter. In contrast to the structure for subtopology classification (see Example 32), the structure build up for symmetries can for example contain groups of subsets that are already completely incorporated in a group of subsets with more lines. This means there is a contraction that does not allow for new symmetries. Groups of subsets of this kind are discarded.

Symmetries are useful for simplification of expressions. If variables (symmetric integrals within some topology in this case) are identified, their coefficients can be combined and the expression becomes more manageable. However, from all possible representations of one integral originating from symmetries one particular must be preferred to the others. This preferred form is dictated by an underlying strict ordering on the indices of integrals. E.g. for lexicalic ordering and a symmetry  $\{(123), (231)\}$ , the integral representation  $T_{H,NLO}^{\text{basic}}(1, 2, -1)$  would be preferred to  $T_{H,NLO}^{\text{basic}}(2, -1, 1)$ .

In general, a symmetry is present if we are free to rearrange denominators of a (sub)topology, possibly supplied with additional transformations. By the latter we can distinguish different attributes of symmetries:

**Global symmetry** All factors of the topology give multiple canonical reorderings. See Example 28 and  $\hat{T}_{H,NLO}^{\text{generic}}$  in Example 29.

**Sector symmetry** Different selections of topology factors resulting in the same characteristic polynomial which can be used to classify the complete structure of distinct subtopologies. See the third and fourth identical groups in Example 32.

**Subtopology symmetry** Different reorderings of the same subset of topology factors or their combination with all sector symmetries. An example will follow.

**Momenta shift symmetries** Rearrangement of (a subset of) denominators that comes together with a transformation of momenta (optionally external). See Example 33.

**Direct symmetry** Rearrangement of (a subset of) factors without shift in momenta. Thereby, no completely generic numerator can be present, only numerator factors included in the symmetry itself. As an example consider  $P_2(1, 1, 1, 0, 2)$  which lacks a numerator and therefore requires no shifts of loop momenta in Example 33.

**External or crossing symmetry** A transformation of topology factors that comes together with a linear transformation of external momenta reflected in the invariants  $\{x_{ij}\}$ . For example  $\{p_1, p_2\} \rightarrow \{p_2, p_1\}$ .

**Mass symmetry** A transformation of topology factors together with a permutation of masses  $\{m_i\}$  present in the problem.

**Jacobian symmetry** A transformation of topology factors together with a non-unit Jacobian factor of  $\det c^k$  in Eq. (62).

**Master integral symmetry** Possible functional dependence on masses and kinematic invariants not yet covered by crossing and mass symmetries.

Crossing and mass symmetries can be detected with our techniques by comparing characteristic polynomials after transforming the  $\{x_{ij}\}$  and  $\{m_i\}$ . Jacobian and master integral symmetries are listed only for completeness.

**Example 34.** The symmetries of the massless two-loop propagator topology  $P_2$  from before are:

$$\begin{aligned} & \{(\# = 4) \\ & \quad \{(12345), (13254), (14523), (15432)\}, \\ & \quad (\# = 8) \\ & \quad \{(1234), (1325), (1452), (1543), (2451), (3541), (4231), (5321)\}, \\ & \quad (\# = 8) \\ & \quad \{(2345), (2354), (3245), (3254), (4523), (4532), (5423), (5432)\}, \\ & \quad (\# = 12) \\ & \quad \{(125), (134), (143), (152), (215), (251), (314), (341), (413), \\ & \quad \quad (431), (512), (521)\} \end{aligned}$$

We indicated the number of elements each group has in parentheses. In the first group valid for all lines, the “top-level” or global symmetries are listed. The second group corresponds to a subtopology with one line contracted. The third group gives different ways to represent the double-bubble graph, the last group belongs to the sunrise graph. The latter are examples of subtopology symmetries, whereas the corresponding groups in Example 32 are sector symmetries. Here, we have for example (2345) and (2354) in the third group which are different reorderings of the same subset.

The knowledge of all existing symmetries of a topology is advantageous for various reasons. The number of integrals in an expression can be reduced drastically by applying symmetries of the corresponding topology. Also, the coefficients of the integrals tend to simplify or cancel for some integrals even completely. Therefore, the amount of expressions and their complexity is decreased. This concerns both, the calculation of Feynman diagrams in terms of scalar integrals from a topology and the subsequent reduction of the integrals within this topology to master integrals. We will comment on the practical use of symmetries in Section 2.6.

#### 2.4.7 Mapping relations

Dealing with sets of topologies, it becomes necessary to introduce a notation for relations among different (sub)topologies. This means we want to describe how a subset of factors of one topology is related to a subset of factors of another topology. We need to generalize and combine our notation for permutations and subsets using the symbol  $\sigma$ .

We defined a subtopology  $T_\sigma$  to topology  $T$  via the subset  $\sigma$  of factors or lines:

$$T_\sigma(a_1, \dots, a_{N_f}) \subseteq T(a_1, \dots, a_{N_f}) \quad \text{with} \quad \forall i \notin \sigma: a_i \leq 0. \quad (64)$$

In contrast to this, a (sub)sector  $T_\rho$  is usually defined via a subset of factors  $\rho$  in the following way:

$$T_\rho(a_1, \dots, a_{N_f}) \quad \text{with} \quad \begin{cases} a_i \leq 0, & \text{if } i \notin \rho, \\ a_i > 0, & \text{otherwise.} \end{cases} \quad (65)$$

The difference is that sectors are mutually exclusive, whereas subtopologies contain all those subtopologies which have less factors. This is a consequence of  $a_i$  for  $i \in \sigma$  not being restricted in Eq. (64). An alternative notation via a set of *directions*  $\{d_i\}$  with  $d_i = \pm 1$  in the space of indices translates to the sector notation by:

$$d = (d_1, \dots, d_{N_f}) \quad \text{with} \quad (a_i - 1/2) d_i > 0, \quad (66)$$

where  $d_i = +1$  for  $a_i > 0$  and  $d_i = -1$  for  $a_i \leq 0$ .

Before,  $\sigma$  was a permutation for canonical reorderings or a subset of integers for subtopologies. We extend the notation by allowing  $\sigma$  to be a multiset of non-negative integers, meaning elements may repeat. A zero denotes contraction of a line, duplicate positive integers mean identification of lines. Such a multiset gives a directed relation between (sub)topologies with respect to a “source” and a “target” topology. Rearrangement of elements is understood in the sense of an *inverse permutation*: the position of an element refers the order of factors in the source, the value of an element refers to the order of factors in the target. For definiteness, if topologies  $T_{\text{source}}$  and  $T_{\text{target}}$  are related by

$$T_{\text{source}}(\{a_i\}) = T_{\text{target}}(\sigma(\{a_i\})), \quad (67)$$

we denote this by

$$T_{\text{source}} \xrightarrow{\sigma} T_{\text{target}}. \quad (68)$$

Mappings can be composed, i.e. two or multiple of them can be combined into a single one. Note that if a mapping incorporates a contraction or identification of lines, it is in general not possible to reverse it unambiguously.

**Example 35.** We illustrate the notion of mappings by the different cases mentioned in the text and Examples 28 and 29, using  $p = p_1 + p_2$  for  $\hat{P}_{1,m}$ .

**Pure (canonical) permutation**

$$\begin{array}{l} T_{H,\text{NLO}}^{\text{basic}} \xrightarrow{(132)} \hat{T}_{H,\text{NLO}}^{\text{basic}}, \\ T_{H,\text{NLO}}^{\text{generic}} \xrightarrow{(1342)} \hat{T}_{H,\text{NLO}}^{\text{generic}} \quad T_{H,\text{NLO}}^{\text{generic}} \xrightarrow{(1432)} \hat{T}_{H,\text{NLO}}^{\text{generic}}. \end{array}$$

**Line contraction**

$$\hat{T}_{H,\text{NLO}}^{\text{basic}} \xrightarrow{(102)} \hat{P}_{1,m},$$

$$\hat{T}_{H,\text{NLO}}^{\text{generic}} \xrightarrow{(1002)} \hat{P}_{1,m}.$$

**Line identification**

$$\hat{T}_{H,\text{NLO}}^{\text{generic}} \xrightarrow{(1223)} \hat{T}_{H,\text{NLO}}^{\text{basic}}.$$

**Reverse mapping**

$$\hat{P}_{1,m} \xrightarrow{(13)} \hat{T}_{H,\text{NLO}}^{\text{basic}}, \quad \hat{P}_{1,m} \xrightarrow{(14)} \hat{T}_{H,\text{NLO}}^{\text{generic}},$$

$$\hat{T}_{H,\text{NLO}}^{\text{basic}} \xrightarrow{(124)} \hat{T}_{H,\text{NLO}}^{\text{generic}}, \quad \hat{T}_{H,\text{NLO}}^{\text{basic}} \xrightarrow{(134)} \hat{T}_{H,\text{NLO}}^{\text{generic}}.$$

**Composed mapping**

$$T_{H,\text{NLO}}^{\text{generic}} \xrightarrow{(1342)} \hat{T}_{H,\text{NLO}}^{\text{generic}} \xrightarrow{(1223)} \hat{T}_{H,\text{NLO}}^{\text{basic}} = T_{H,\text{NLO}}^{\text{generic}} \xrightarrow{(1232)} \hat{T}_{H,\text{NLO}}^{\text{basic}}.$$

Analogously to a symmetry within one topology, a mapping can coincide with a momentum shift transformation or not. Especially for mappings between subtopologies of different topologies such shifts of momenta need not to exist necessarily.

## 2.5 THE PACKAGE TOPOID

All the techniques and algorithms described in the previous sections have been implemented in the Mathematica, see Ref. [29], package TopoID (the name refers to **T**opology **I**Dentification). This implementation was one of the mayor pieces of work done in context of this thesis. In the last part of this chapter we summarize capabilities built into TopoID. Also in some of the next chapters we will encounter examples for tasks it can handle. A dedicated user manual and full documentation (especially of the generated code) would be rather technical and exceed the scope of this thesis. Thus, it will appear elsewhere, see Ref. [28].

TopoID is a generic, process independent tool that aims to bridge the gap in the calculation workflow between Feynman diagrams and unrenormalized results expressed in terms of master integrals. By this we mean *actual* master integrals, i.e. taking into account non-trivial relations discussed in Section 2.7.3 in a completely automatic way. In principle, one can also perform the operations of TopoID manually but with numerous topologies this quickly becomes tedious and error-prone. It is written as a package for Mathematica which offers a high-level programming environment and the demanded algebraic capabilities. However, for the actual calculation FORM code, see Refs. [30–32], is generated to process the diagrams in a more efficient way. TopoID also generates configuration files for the programs exp,

see Refs. [23, 24], and `reg`, see Ref. [26], which are used to map each diagram to a topology. An implementation of Laporta’s algorithm is not part of `TopoID` but useful properties of a topology such as symmetries, unitarity cuts and scaleless subtopologies can be provided to assist in the reduction of integrals by an external code. Results obtained with the external code can then be post-processed by `TopoID` to give a minimal set of master integrals.

Let us briefly summarize features the package has to offer:

- *topology identification* and construction of minimal sets of topologies,
- classification of distinct and scaleless subtopologies,
- treatment of properties such as completeness, linear dependence, etc.,
- construction of partial fractioning relations,
- revealing symmetries (completely within all levels of subtopologies),
- graph manipulation, treatment of unitarity cuts, factorizing topologies,
- *FORM code generation* (diagram mapping, topology processing, Laporta integral reduction),
- *master integral identification* (arbitrary base changes, non-trivial relations).

### 2.5.1 Example: massless propagators to five loops

Let us demonstrate one application of `TopoID` by the identification of all topologies necessary for the calculation of massless propagator integrals up to five loops. In a first step we generate the diagrams with `QGRAF`, see Ref. [33]. For topology identification it is not necessary to work in “real” QCD. A simplified theory containing only gluons is sufficient and results in a much smaller number of diagrams which improves the combinatorics for `TopoID`. Let us briefly introduce some of the functions we need for this identification process:

`Setup`

- Information on the kinematic setup is given once at the beginning to the command `Setup[<rules>]` to initialize a data structure that can later be passed to functions that need this information. By `<rules>` we denote a list of rules specifying external and internal momenta, masses and constants, kinematic constraints and transformation rules (for introduction of a notation). Some of the entries in `<rules>` are optional. A self-explanatory example is given below.

`GetDiagrams`

- The function `GetDiagrams[<file>]` reads and parses `QGRAF` output into the internal data structure for topologies. This is bound to the standard `.sty` file coming together with `TopoID`. Alternatively, another included `.sty` file allows to generate directly `TopoID` compatible `QGRAF` output that can be read simply with `Get[<file>]`.

- `MapDiagramToTopology[<top(s)>, <setup>]` first constructs from the routing of line momenta produced by QGRAF, particle masses and kinematic constraints specified in <setup> a list of quadratic propagators. Identical propagators can immediately be identified after this step. Then, the canonical alpha-representation is derived and propagators reordered accordingly. Single topologies or whole sets can be passed as input. The output contains also information on the applied reorderings in the form of mappings (exemplified below). MapDiagramTo-  
Topology
- The command `MinimizeTopologies[<tops>]` can be invoked to minimize a given set of topologies. The output consists of the new, minimal set of topologies and a set of mappings that relates the topologies in the input and output. In the course of minimization, the complete subtopology structure is revealed for each topology in the output. MinimizeTopolo-  
gies
- A simple way to obtain graphical representations for topologies are the commands `TopologyPlot[<top>]` and `TopologyGrid[<tops>]`. The output may not always be aesthetically appealing but is in practice indispensable. TopologyPlot  
TopologyGrid

Massless propagator topologies are by construction linear independent. Propagators carrying the same momentum can be readily identified and there are no conditions on external momenta. Therefore, we need not take care of linear independence in this application. Nevertheless, the topologies still need to be completed.

**Example 36.** A typical Mathematica session for the identification process looks as shown below. The code has to be modified only marginally to proceed from one to five loops. Therefore, we show and comment only the three-loop case. We give, however, the final results produced from one to four loops below and in Figs. 3 and 4. Results to five loops are given in Appendix A.1.

```
In[1]:= << TopoID';
```

```

-----
--->---+--- |__  __| ----- | | | _ \ ---+--->---
      \   | |  --  ---  | | | | \ \ |
      +   | | / \ | _ \ / \ | | | | \ \ |
      | \  | | / \ | | \ \ / \ | | | | / / +--->---
      | \  | | \ \ / | | \ / \ \ / | | | | \ / /
      | \  | | \ \ / | | \ / \ \ / | | | | \ / /
      | \  | | \ \ / | | \ / \ \ / | | | | \ / /
      | \  | | \ \ / | | \ / \ \ / | | | | \ / /
      | \  | | \ \ / | | \ / \ \ / | | | | \ / /
-----+-----+-----+-----+-----+----->---

```

```

PACKAGE:
  TopoID -- [Topo]logy [ID]entification
VERSION:
  1.2 (2014-10-16)
AUTHORS:
  Jens Hoff & Alexey Pak
MAILTO:
  [jens.hoff@kit.edu]

```

## DESCRIPTION:

- Starting from Feynman diagrams, the underlying generic topologies are identified and their set is minimized. These are decomposed into (linearly independent) Laporta topologies.
- FORM code can be generated in order to map diagrams onto them and to process both types of topologies.
- Afterwards emerging sets of master integrals can be minimized. This includes base changes.
- Usage information is available through `?TopoID`, for instance. Provided functions and used symbols are listed in the variables `$TopoIDFunctions` and `$TopoIDSymbols`.
- The debugging mode can be enabled with `$TopoIDDebug = True;` before loading the package.

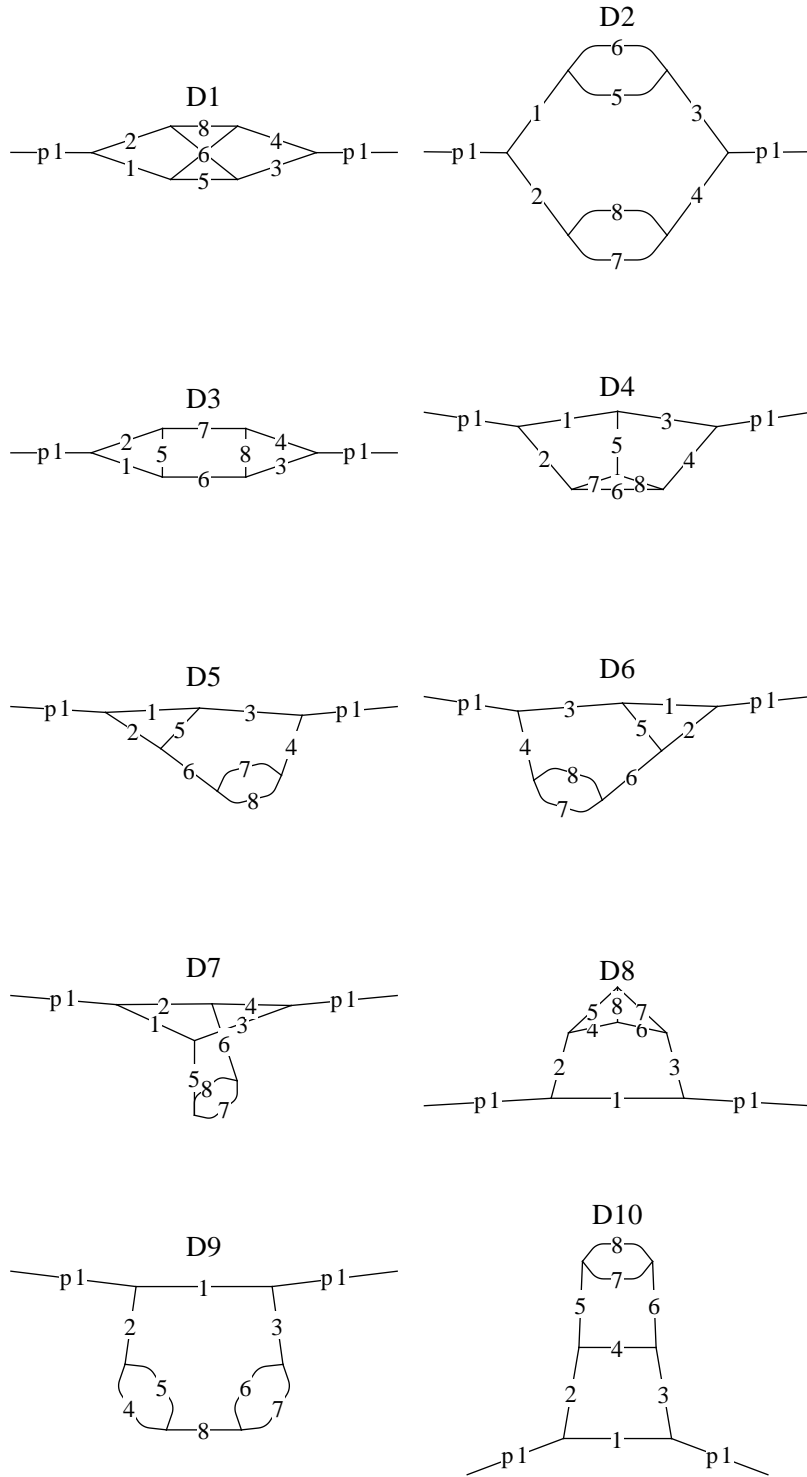
```
In[2]:= setup3 = Setup[
  Externals -> {p1},          (* one external momentum *)
  Internals -> {v1, v2, v3},  (* three internal momenta *)
  Masses -> {"gl" -> 0}];  (* only gluons with mass 0 *)
```

```
In[3]:= dias3 = GetDiagrams["3.gg.raw"]; (* generated by QGRAF *)
Read 10 diagrams.
```

```
In[4]:= TopologyGrid[
  dias3, 2,
  ImageSize -> {140, 100},
  PlotLabel -> Automatic]
```



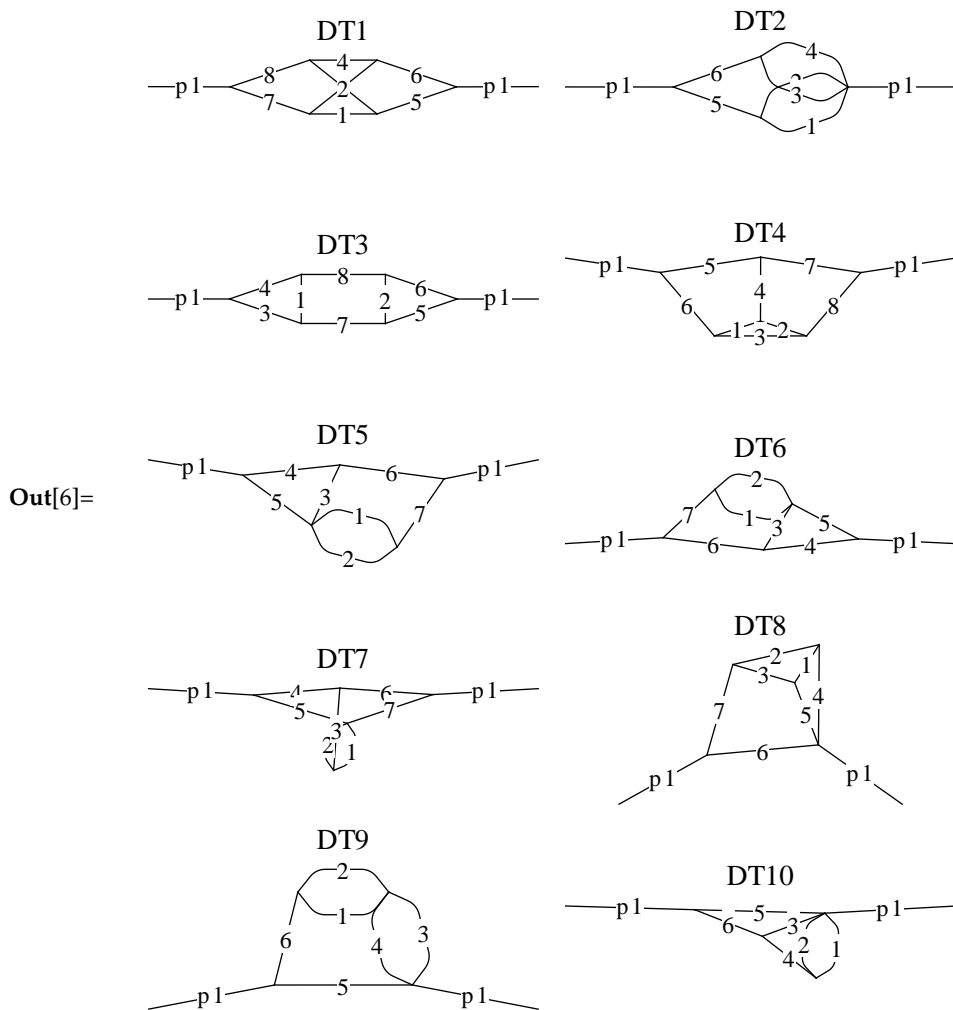
Out[4]=



```
In[5]:= {dmaps3, dtops3} = MapDiagramToTopology[dias3, setup3];
Map 10 diagrams to topologies.
Created 10 mappings and 10 topologies.
```

```
In[6]:= TopologyGrid[
  dtops3, 2,
  ImageSize -> {140, 70},
```

PlotLabel -> Automatic]

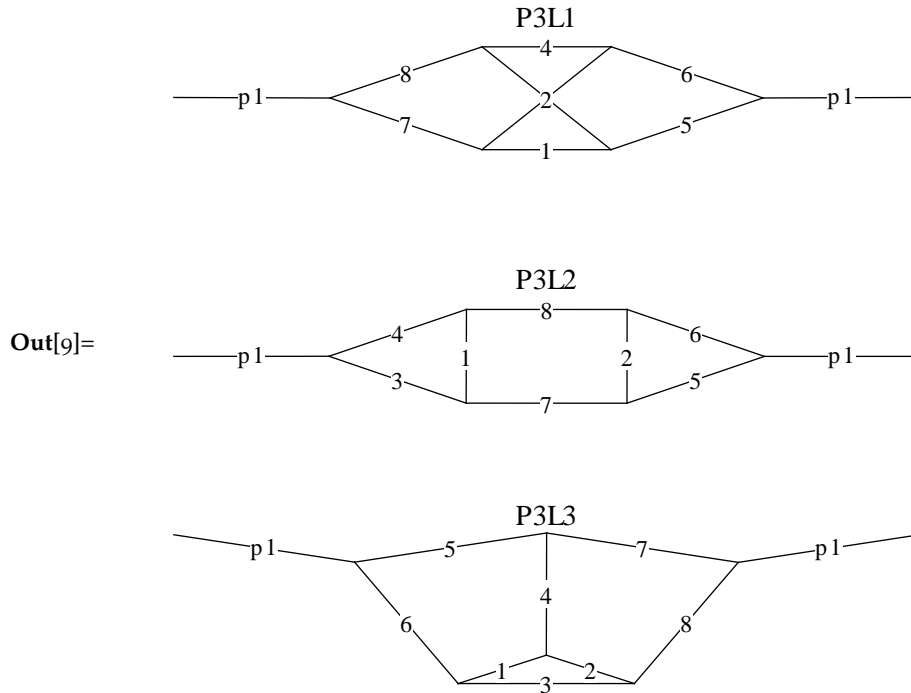


```
In[7]:= Scan[Print, dmaps3];
{fr -> "D1", to -> "DT1", id -> {7, 8, 5, 6, 1, 2, 3, 4}}
{fr -> "D2", to -> "DT2", id -> {5, 6, 5, 6, 2, 1, 4, 3}}
{fr -> "D3", to -> "DT3", id -> {3, 4, 5, 6, 1, 7, 8, 2}}
{fr -> "D4", to -> "DT4", id -> {5, 6, 7, 8, 4, 3, 1, 2}}
{fr -> "D5", to -> "DT5", id -> {4, 5, 6, 7, 3, 7, 2, 1}}
{fr -> "D6", to -> "DT6", id -> {4, 5, 6, 7, 3, 7, 2, 1}}
{fr -> "D7", to -> "DT7", id -> {4, 5, 6, 7, 3, 3, 2, 1}}
{fr -> "D8", to -> "DT8", id -> {6, 7, 7, 2, 3, 4, 5, 1}}
{fr -> "D9", to -> "DT9", id -> {5, 6, 6, 2, 1, 4, 3, 6}}
{fr -> "D10", to -> "DT10", id -> {5, 6, 6, 3, 4, 4, 2, 1}}
```

```
In[8]:= {gmaps3, gtops3} = MinimizeTopologies [
  dtops3,
  Naming -> Iterate["P3L"]]; (* how topologies are named *)
Minimize set of 10 topologies.
Minimized 10 to 3 topologies.
```

```
In[9]:= TopologyGrid[
```

```
gtops3, 1,
ImageSize -> {280, 90},
PlotLabel -> Automatic]
```



```
In[10]:= Scan[Print, gmaps3];
{fr -> "DT1", to -> "P3L1", id -> {1, 2, 3, 4, 5, 6, 7, 8}}
{fr -> "DT10", to -> "P3L1", id -> {1, 5, 4, 3, 7, 8}}
{fr -> "DT2", to -> "P3L1", id -> {1, 2, 3, 4, 7, 8}}
{fr -> "DT3", to -> "P3L2", id -> {1, 2, 3, 4, 5, 6, 7, 8}}
{fr -> "DT5", to -> "P3L2", id -> {1, 3, 2, 6, 5, 8, 7}}
{fr -> "DT6", to -> "P3L2", id -> {1, 3, 2, 6, 5, 8, 7}}
{fr -> "DT9", to -> "P3L2", id -> {1, 3, 2, 5, 8, 7}}
{fr -> "DT4", to -> "P3L3", id -> {1, 2, 3, 4, 5, 6, 7, 8}}
{fr -> "DT7", to -> "P3L3", id -> {1, 2, 4, 5, 6, 7, 8}}
{fr -> "DT8", to -> "P3L3", id -> {1, 2, 3, 4, 6, 7, 8}}
```

Note that in the topologies produced by `MapDiagramToTopology` propagators connecting formerly to self-energy insertions are contracted. We also printed the mapping information from `dmaps3` and `gmaps3`. The key `fr` indicates the “source” topology, the key `to` the “target” topology. We use `id` to assign propagators of the source (by the position of a number in the list) to propagators of the target (via the value of the number in the list). This allows for retracing the identification process. In D10 for example, lines 2 and 3 carry the same momentum. Therefore, they can both be assigned to the propagator 6 in DT10. The values of `id` in `dmaps3` appear completely reshuffled which is a consequence of the canonical reordering. In `gmaps3` we can see that DT10 is identified with a subset of 6 lines in P3L1.

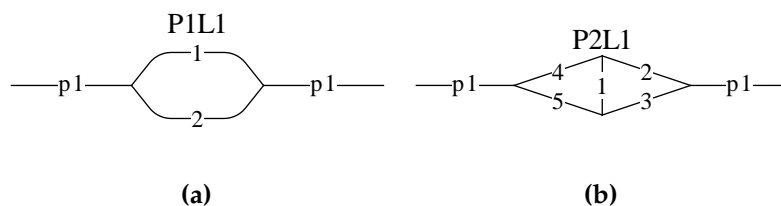


**Figure 3:** Minimal sets of massless propagator topologies identified by TopoID at one loop in Fig. a and at two loops in Fig. b. In both cases, the set consists of only one topology. Each graph is labeled by the generated topology name. Labels on external legs indicate the single external momentum, labels on internal lines number the propagators which are massless in this case.

As expected, at one and two loops only one topology is found respectively, see Fig. 3. Three topologies are identified at three loops in Example 36 and eleven topologies at four loops, see Fig. 4. For the 64 topologies at five loops see Appendix A.1.

As one can also read off in Tab. 1 with  $N_p = 1$  and  $N_k = 1, \dots, 5$  we have the following numbers of propagators for each identified topology at each loop order: 2 at one loop, 5 at two loops, 8 at three loops, 11 at four loops and 14 at five loops. All topologies have “maximal” graphs, consisting only of three-valent vertices without any self-loops.

All the code needed to perform actual calculations with the found topologies and its properties can be obtained with TopoID:

- |                                     |   |
|-------------------------------------|---|
| <code>topsel.&lt;problem&gt;</code> | <ul style="list-style-type: none"> <li>• exp configuration file for mapping diagrams on “diagram topologies” at the level of graph representations,</li> </ul>        |
| <code>&lt;topology&gt;.EXP</code>   | <ul style="list-style-type: none"> <li>• FORM code transforming diagram topologies to generic topologies,</li> </ul>  |
| <code>&lt;problem&gt;.reg</code>    | <ul style="list-style-type: none"> <li>• reg configuration file for mapping diagrams on generic topologies at the level of momentum space representations,</li> </ul> |
| <code>&lt;topology&gt;.gen</code>   | <ul style="list-style-type: none"> <li>• FORM code for processing generic topologies and their mapping to basic topologies,</li> </ul>                                |
| <code>&lt;topology&gt;.def</code>   | <ul style="list-style-type: none"> <li>• FORM code for processing basic topologies and as input for the Laporta algorithm rows.</li> </ul>                            |

It can be found in electronic form in the supplementary material to this thesis, see Ref. [34]. Sample code generated for the case of Higgs boson production at NNLO is given in Appendix C but the structure of the generated code is independent of the considered process.

## 2.6 LAPORTA’S ALGORITHM

In this section, we want to convey the idea of integral reduction and also sketch one driving component, Laporta’s algorithm, that made calculations over the last decade feasible that were impossible before.

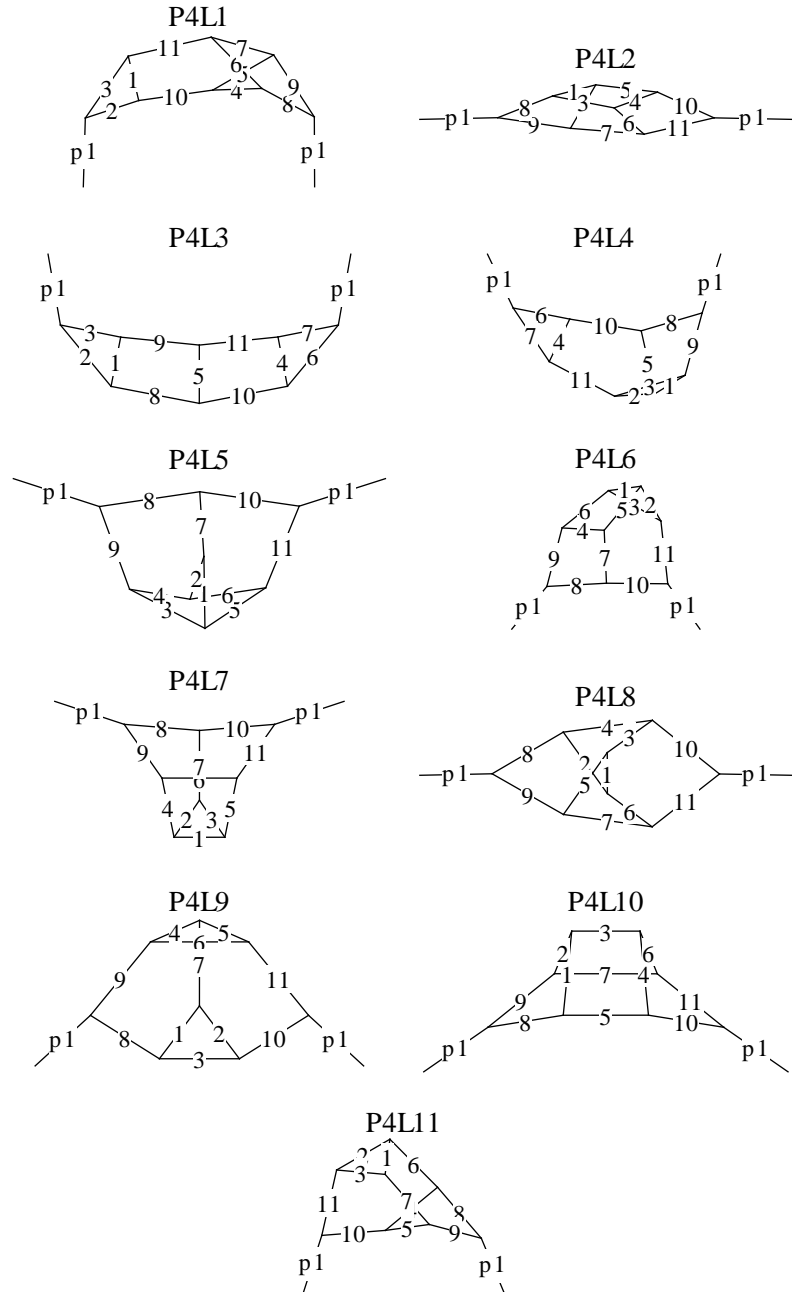


**Figure 4:** Minimal set of massless propagator topologies at four loops.

## 2.6.1 Integration-by-parts relations

We introduce integration-by-parts identities (IBPs) for classes of Feynman integrals, see Refs. [35, 36]:

$$T(\{a_i\}) = \prod_{i=1}^{N_k} \int dk_i^D t(\{a_j\}) \quad \text{with} \quad t(\{a_j\}) = \prod_{j=1}^{N_f} f_j^{-a_j}, \quad (69)$$

where we abbreviated in comparison to Eq. (12) the integrand by the symbol  $t$ . Then, we have

$$0 = \prod_{i=1}^{N_k} \int dk_i^D \frac{\partial}{\partial k_m^\mu} [v_n^\mu t(\{a_j\})], \quad (70)$$

where the divergence is taken with respect to a loop momentum  $k_m$  and  $v_n$  is a component of the vector of all momenta  $v_n = (p_1, \dots, k_1, \dots)$ . Equation (70) can be understood as consequence of Gauß's theorem since the surface term vanishes with infinite integration bounds. We can rewrite Eq. (70) as

$$0 = \prod_{i=1}^{N_k} \int dk_i^D \left[ D \delta_{k_m, v_n} + \sum_{l=1}^{N_f} \left( \frac{-a_l}{f_l} \right) v_n^\mu \frac{\partial f_l}{\partial k_m^\mu} \right] t(\{a_j\}). \quad (71)$$

If we have quadratic topology factors  $\{f_i\}$  and demand that the topology  $T(\{a_i\})$  is a complete one, then  $v_n^\mu \partial f_l / \partial k_m^\mu$  (in general leading to all possible scalar products) can always be rewritten in terms of the  $\{f_i\}$  (integrals stay within their family):

$$\begin{aligned} v_n^\mu \frac{\partial f_l}{\partial k_m^\mu} &= \sum_{p=1}^{N_{ei}} c_{mnlp} x_p + \sum_{p=1}^{N_{sp}} d_{mnlp} s_p \\ &= \sum_{p=1}^{N_p} b'_{mnlp} m_p + \sum_{p=1}^{N_{ei}} c'_{mnlp} x_p + \sum_{p=1}^{N_f} d'_{mnlp} f_p, \end{aligned} \quad (72)$$

where the vector of  $N_{ei}$  (independent) external invariants is denoted by  $x$  and the vectors of scalar products and masses by  $s$  and  $m$ , respectively. The coefficients  $c$ ,  $d$ ,  $b'$ ,  $c'$  and  $d'$  are just numbers. Hence, Eq. (71) can be applied to obtain recurrence relations which allow to linearly express many different integrals from a family in terms of only a few integrals, so-called master integrals.

Let us define "index-shift" operators  $\mathbf{1}^\pm, \mathbf{2}^\pm, \dots$  such that

$$\mathbf{p}^\pm T(a_1, \dots, a_p, \dots, a_{N_f}) = T(a_1, \dots, a_p \pm 1, \dots, a_{N_f}) \quad (73)$$

increases or decreases a specific index  $p$ . Plugging Eqs. (72) and (73) into Eq. (71), we find:

$$0 = \left[ D \delta_{m, N_p+n} - \sum_{l=p=1}^{N_f} a_l d_{mnlp} \mathbf{1}^+ \mathbf{p}^- \right] T(\{a_j\}). \quad (74)$$

Indices are raised or lowered at most by one. Note that Eq. (74) for a particular choice of  $m, n$  and an index  $a_i \leq 0$  can never result in a term where  $a_i > 0$ . A contracted line cannot reappear due to IBP relations.

The requirement for completeness of a topology is thus related to building up a recurrence structure and therefore essential to integral reduction. The same holds for the Laporta algorithm, soon to be explained. Linear independence of topologies is not an essential requirement for integral reduction but it makes life easier to consider independent topologies that have fewer indices than a common dependent topology and which are less entangled.

Equation (74) can be studied systematically for certain classes of integrals to find a set of recurrence relations that terminates for arbitrary integrals as input in a linear combination of fixed master integrals as output. This implies some ordering prescription on integrals to distinguish reducible integrals from master integrals. The two most prominent examples for this approach are MINCER, see Refs. [37, 38] and Example 36, for massless propagator topologies to three loops and MATAD, see Ref. [39], for massive tadpole topologies to three loops.

Recent studies on IBPs have shown that their generating operators  $O_{mn} = \partial/\partial k_m \cdot v_n$  form a Lie algebra, see Ref. [40]. This means, not all  $N_k \times (N_p + N_k)$  IBP relations generated by Eq. (74) are independent, there exists a basis of only  $N_p + N_k + 1$  relations. Moreover, a second class of recurrence relations, so-called Lorentz invariance identities (LIs), is entirely determined by IBPs, thus providing no additional information. In Ref. [41], it was proven that the number of master integrals is finite and a technique to calculate this number has been developed in Ref. [40] (the corresponding code is named MINT).

**Example 37.** Let us show the IBPs for  $T_{H,\text{NLO}}^{\text{basic}}$  of Example 1, employing the inversion of Example 5. We start from Eq. (71) and reexpress the scalar products  $\{p_1 \cdot k_1, p_2 \cdot k_1, k_1^2\}$  in  $v_n \cdot \partial d_1/\partial k_m$  by topology factors  $\{d_1, d_2, d_3\}$ . Using index-shift operators from Eq. (73), we find:

$$0 = (-a_2 + a_3) - a_1 \mathbf{1}^+ - a_1 \mathbf{1}^+ \mathbf{2}^- + a_1 \mathbf{1}^+ \mathbf{3}^- + a_2 \mathbf{2}^+ \mathbf{3}^- - a_3 \mathbf{2}^- \mathbf{3}^+, \quad (R_1)$$

$$0 = (a_1 - a_3) - a_1 x \mathbf{1}^+ + a_2(1-x) \mathbf{2}^+ - a_3 x \mathbf{3}^+ - a_1 \mathbf{1}^+ \mathbf{3}^- + a_2 \mathbf{1}^- \mathbf{2}^+ - a_2 \mathbf{2}^+ \mathbf{3}^- + a_3 \mathbf{1}^- \mathbf{3}^+, \quad (R_2)$$

$$0 = (D - 2a_1 - a_2 - a_3) + 2a_1 x \mathbf{1}^+ - a_2(1-x) \mathbf{2}^+ + a_3 x \mathbf{3}^+ - a_2 \mathbf{1}^- \mathbf{2}^+ - a_3 \mathbf{1}^- \mathbf{3}^+ \quad (R_3)$$

for the IBP operators  $\partial/\partial k_1 \cdot p_1$ ,  $\partial/\partial k_1 \cdot p_2$  and  $\partial/\partial k_1 \cdot k_1$ , respectively.

At this level of complexity, we can manipulate above equations into a useful recursive definition of integrals  $T_{H,\text{NLO}}^{\text{basic}}(a_1, a_2, a_3)$  terminating in master integrals. Since in this case lines 1 and 2 are cut, all integrals with  $a_1 \leq 0$  or  $a_2 \leq 0$  vanish. Let us form the linear combinations  $R_1 + R_2 + R_3$  with  $a_1 \rightarrow a_1 - 1$  for  $a_3 = 0$  and  $R_1 + R_2$  for  $a_3 \rightarrow a_3 - 1$ :

$$0 = (1-x)(1-a_1) + (5-2\epsilon - a_1 - 2a_2) \mathbf{1}^- + (1-a_1) \mathbf{2}^-, \quad (R_4)$$

$$0 = (1 - a_1)(x - \mathbf{1}^- + \mathbf{2}^-) + (a_1 - a_2)\mathbf{3}^- - a_1(1 + x + \mathbf{2}^-)\mathbf{3}^-\mathbf{1}^+ + a_2(1 - x + \mathbf{1}^-)\mathbf{3}^-\mathbf{2}^+. \quad (R_5)$$

According to  $R_4$  and assuming  $a_3 = 0$ , either  $a_1$  or  $a_2$  will reduce to zero. Therefore, repeated application of  $R_4$  will operate as  $T_{H,NLO}^{\text{basic}}(a_1, a_2, 0) \rightarrow T_{H,NLO}^{\text{basic}}(1, 1, 0)$ . For  $a_3 \neq 0$  relation  $R_5$  will always lower the sum of all indices. Then,  $a_3$  can always be reduced to zero according to the rule  $T_{H,NLO}^{\text{basic}}(a_1, a_2, a_3) \rightarrow T_{H,NLO}^{\text{basic}}(a_1, a_2, 0)$  and where  $R_4$  applies again. There will be no new master integral apart from  $T_{H,NLO}^{\text{basic}}(1, 1, 0)$ . Note that the linear combinations of IBPs  $R_4$  and  $R_5$  we picked correspond to contraction with the momenta flowing through lines 2 and 3, respectively.

Surely, other sets of recurrence relations exist for this case which may lead with fewer steps to a reduced result. We only wanted to demonstrate a terminating set of relations. Unfortunately, this strategy cannot be transferred to higher loop orders easily which demands for adoption of Laporta's strategy. Quite logically, a Laporta reduction for above topology (including cuts) ends up in the same single master integral  $T_{H,NLO}^{\text{basic}}(1, 1, 0)$ .

### 2.6.2 Integral reduction

The foundation of a problem independent approach to integral reduction was laid by S. Laporta in Ref. [42]. The basic idea is not to try and solve the generic IBP relations (in symbolic  $\{a_i\}$ ) but to consider a linear homogeneous system of equations generated from a restricted set of specific integrals, so-called "seeds". The selection of seeds can be related to the integrals to be reduced.

To date many implementations of Laporta's algorithm have been written. Public codes include:

- AIR, see Ref. [43], written in the CAS Maple,
- FIRE, see Refs. [44–46], written in Mathematica and C++ (also employing S-bases) and
- Reduze, see Refs. [27, 47], written in C++.

But many more private codes exist, e.g. Crusher by P. Marquard and D. Seidel. Here, we give some details on rows which originated from A. Pak, see Ref. [48]. We adapted and improved some aspects of rows for our purposes in this work, see Ref. [49]. One can regard the strategy of Ref. [42] not as clear-cut but as merely stating the necessary ingredients for a working integral reduction:

- recurrence relations (from IBPs and/or LIs),
- generation of seed integrals,
- ordering or complexity of integrals,



- Gauß elimination.

In practice, one's computing resources are limited and different schemes for management and processing of reduction tables had to be devised by the different authors of Laporta algorithm codes. This concerns for example parallel processing of parts of the table or database storage. However, some ingredients like GiNaC/CLN, see Ref. [50], for algebraic operations in C++ or Fermat, see Ref. [51], for fast polynomial GCD (greatest common divisor) computations are a common part of most implementations.

In contrast to Laporta's algorithm more systematic treatments include

- Baikov's method implemented in the private FORM code BAICER, see Refs. [52–56],
- S-bases/Gröbner bases, see Refs. [9–11],
- LiteRed, see Refs. [57, 58], using heuristic rules to “solve” IBPs symbolically before specifying indices to integer values.

We also want to mention the idea to use a mapping to prime fields for improved simplification of polynomial coefficients in the Gauß elimination, see Refs. [59, 60].

**COMPLEXITY OF INTEGRALS** Complexity of integrals can be defined in many ways but it must be unique, complete and should preferably reflect the intuitive notion of “simple” and “complicated”. The details of this ordering determine the form of master integrals remaining in the end of the reduction. We define for index-vectors  $\{a_i\}$  the number of denominators  $N_+$ , the (absolute) sums of denominator indices  $S_+$  and numerator indices  $S_-$ :

$$N_+(\{a_i\}) = \sum_{i=1}^{N_f} \theta(a_i - 1/2), \quad (75)$$

$$S_+(\{a_i\}) = \sum_{i=1}^{N_f} a_i \theta(a_i - 1/2), \quad S_-(\{a_i\}) = - \sum_{i=1}^{N_f} a_i \theta(-a_i). \quad (76)$$

Imposing a complete ordering on two sets of indices  $\{a_i\}$  and  $\{b_i\}$  proceeds for rows by the following comparisons:

1.  $N_+(\{a_i\}) < N_+(\{b_i\})$ ,
2.  $S_+(\{a_i\}) < S_+(\{b_i\})$ ,
3.  $S_-(\{a_i\}) < S_-(\{b_i\})$ ,
4.  $\{a_i\} \prec_{\text{lexicolic}} \{b_i\}$ .

Whenever a condition brings no decision (the = case) we go to the next one until we find a decision (the < or > cases). Then, we can say  $\{a_i\}$  is simpler than  $\{b_i\}$ , written  $\{a_i\} \prec_{\text{rows}} \{b_i\}$ , or the other way around. We denoted the Laporta ordering by the symbol  $\prec_{\text{rows}}$  and lexicographic ordering by  $\prec_{\text{lexicolic}}$ . In human language this reads: fewer lines are simpler, fewer “dots”

are simpler, less numerators are simpler and for any two integrals with the same first three properties decide by lexicographic ordering.

These criteria are in rows encoded as single-valued function  $O$  returning a unique positive integer for each index-vector  $\{a_i\}$ . This can be achieved by using numbers of base  $2N$  where  $N$  is larger than any absolute value of  $N_+$ ,  $S_{\pm}$  or  $\{a_i\}$ ,  $N > \max[N_+(\{a_i\}), S_{\pm}(\{a_i\}), \{a_i\}]$  and we have:

$$O(\{a_i\}) = (2N)^{N_f+2}N_+ + (2N)^{N_f+1}S_+ + (2N)^{N_f}S_- \\ + (2N)^{N_f-1}(a_1 + N) + \dots + (2N)^0(a_{N_f} + N). \quad (77)$$

This function can be inverted easily, meaning a complexity value can be decoded to retrieve an index-vector  $O^{-1}(O(\{a_i\})) = \{a_i\}$ . This allows for using index-vector and complexity in an interchangeable way.

**SEED GENERATION** We discuss seed generation only briefly and how it works in rows. We note that it is mandatory to constrain the system of IBP relations. The selection of seed integrals  $A$  to be plugged into the IBPs must be related to the set of integrals  $B$  appearing in an unreduced result. On the one hand, the table's size must still be manageable and it should not be crowded by integrals that are irrelevant for  $B$ . On the other hand, a complete reduction of all integrals  $B$  to only a few master integrals is desired.

The observation after Eq. (74), that the IBPs (together with the ordering of integrals) cannot restore lines once contracted, means that integrals  $a \in A$  with  $N_+^A = N_+(\{a_i\})$  will be reduced only by integrals  $b \in B$  with  $N_+^A \geq N_+(\{b_i\})$ . The maximal absolute sums of positive and negative indices  $S_{\pm}^{\max,A} = \max[S_{\pm}(\{a_i\}) | N_+(\{a_i\}) = N_+^A]$  are used to delimit seeds within each such subset. The vectors of minimal and maximal indices  $\{a_i\}^{\min}$  and  $\{a_i\}^{\max}$  can be taken as absolute bounds (over all integrals in  $A$ ) to further constrain the set of generated seeds.

The index of an irreducible numerator  $n_i$  has never to be considered positive, the same holds for corresponding seed integrals. There is much space for improvement in above prescription. For example, within each subtopology one could consider bounds for index vectors  $\{a_i\}^{\min,A}$  and  $\{a_i\}^{\max,A}$  individually. One could also generate less relations for each seed integral using Lee's ideas, see Ref. [40].

**GAUSS ELIMINATION** Since Gauß elimination can be assumed as well-known to the reader, we remark only on some aspects of this final step of the Laporta algorithm.

- The order in which relations are placed in the table is crucial to the performance of the implementation. A rather good choice for this ordering is to use the complexity of the seed integral.
- When normalizing relations with respect to the highest-complexity integral and performing substitutions into other relations, the most time-consuming operation is the simplification of integral coefficients. This involves computation of GCDs of polynomials in the space-time dimension  $D$  and  $N_{\text{iv}} = N_{\text{ei}} - 1$  independent (scaleless) variables.

- The implementation rows allows for sequential updates to a table. Undiagonalized relations can be appended to the table before Gauß elimination is performed anew. Thus, a table can be grown to the desired range of reduced integrals.

As one can see, Laporta's reduction scheme can be varied easily in many aspects. This can be exploited to optimize an implementation with regard to a special class of problems.

### 2.6.3 Asset of TopoID

The asset to integral reduction that comes from TopoID (apart from automatic topology definition) is the total symmetrization of integrals and detection of scaleless subtopologies. The philosophy is: nowhere and never keep identical representations of an integral (within each topology). The various steps of a calculation are affted by this as follows:

- Unreduced scalar integrals appearing in the *sum of diagrams* are symmetrized and scaleless integrals are discarded before handing them over to the reduction.
- Based on the previous step, *seed integrals* are selected and subsequently simplified again by the rules from TopoID (identification of identical and vanishing integrals).
- The same simplification is applied to integrals appearing in the generated *IBP relations*.

The advantage of this symmetrization scheme is that less expressions of smaller individual size arise in a calculation, resulting in a significant speed-up.

The symmetrization procedure itself works such that we allow for change of notation between each and every symmetric representation of each unique (sub)topology. The used CAS (FORM or Mathematica) picks one of the proposed notations as its preferred one. Symmetries valid for more lines are applied before those valid for less lines. Application of symmetries in this order is repeated until the notation for an integral undergoes no more change. This is guaranteed to always terminate in a minimal form for an expression. We observed that it is sufficient to include symmetries without momenta shifts only (global, sector and subtopology symmetries, see Section 2.4.6) for the procedure to be exhaustive. This, however, is also related to the choice of IBPs generated for each seed. The results for all reductions performed with symmetries from TopoID never contained different representations of the same master integral. This is a strong check for complete symmetrization.

## 2.7 COMPLETING TOPOLOGIES

In the last section we saw that the IBPs require complete topologies. Let us return to the issue of completing topologies already mentioned in Section 2.1.3.

### 2.7.1 Irreducible scalar products

One can freely choose how to incorporate irreducible scalar products. E.g., in case  $p_1 \cdot k_2$  cannot be expressed in terms of propagators of the topology, one can use it directly as additional factor of the topology. Let us call this choice “pure scalar products”.

In our case, another natural choice is  $(p_1 \pm k_2)^2 = \pm p_1 \cdot k_2 + k_2^2$  where external momenta are on-shell and  $p_1^2 = p_2^2 = 0$ . Such a choice guarantees that the scalar product  $p_1 \cdot k_2$  can be expressed in the new, extended set of topology factors. We name this choice “pseudo-propagator” or “inverse propagator” with reference to the fact that a flow of momenta can be attached to this construction which is of quadratic form. This is not the case for the irreducible scalar product itself.

**Definition 9.** If the scalar product  $v \cdot k$ , where  $v$  is an external or internal momentum  $v \in \{p_i\} \cup \{k_i\}$  and  $k$  is an internal momentum  $k \in \{k_i\}$ , is irreducible, we need to complete the topology. Three possible choices for a new topology factor  $n$  that guarantee completion are:

$$\text{pure scalar product: } n := v \cdot k, \quad (78)$$

$$\text{pseudo- or inverse propagator: } n := (v \pm k)^2. \quad (79)$$

In practice pseudo-propagators seem superior to pure scalar products. One reason is that pseudo-propagators have a greater potential for admitting symmetries in the topology. Picking pure scalar products on the other hand, restricts symmetries to those which transform pure scalar products into one another.

It depends on the particular routing of momenta in the real propagators of a topology whether “plus” or “minus” pseudo-propagators are more advantageous. By advantageous we mean that a pseudo-propagator can be represented as line in the graph (possibly after contractions).

### 2.7.2 Supertopologies

A more sophisticated idea is to merge or “stack” topologies, resulting in “supertopologies”. They can be regarded as unified sets of propagators, such that particular subsets of propagators correspond to topologies that have been merged. By this we mean not the naive joining of sets of propagators in momentum space representation. We require minimality and ask for the smallest set of propagators that allows to represent all topologies that have been merged.

Suppose we want to merge two topologies in canonical form  $\hat{T}_1$  and  $\hat{T}_2$  whose subtopologies have been classified completely, see Section 2.4.4. Multiple topologies can be handled by iterating the procedure to be described. We can pick a greatest common subtopology  $\hat{T}_1 \cap \hat{T}_2$  for which we have in each topology at least one momentum space representation  $\hat{T}'_1 \equiv \hat{T}'_2 \equiv \hat{T}_1 \cap \hat{T}_2$  (there can be multiple due to symmetries) and compute transformations of the momenta  $v = (p_1, \dots, k_1, \dots)$  that relate the two momentum space representations  $T'_1$  and  $T'_2$ , see Eq. (62),

$$\hat{T}'_1 \xrightarrow{v'=Cv} \hat{T}'_2. \quad (80)$$

Applying the same shift to those factors  $f_i$  of topology  $\hat{T}_1$  that are *not* included in the greatest common subtopology  $f_i \in \hat{T}_1 \setminus \hat{T}'_1$  gives a set of propagators “fitting” to the routing of momenta in  $\hat{T}_2$ . This set forms together with  $\hat{T}_2$  a supertopology  $\hat{T}_1 \cup \hat{T}_2$ . A supertopology can in general be linearly dependent, even if the initial topologies were linearly independent. Note an interesting mathematical property in this context: topologies can have ambiguous greatest common subtopologies.

These ideas are implemented as yet experimental features of the package TopoID. The functions `TopologyIntersection(s)`, `TopologyComplement(s)` and `UnionTopology` give access to the corresponding generalized set operations for topologies. In a future version `SuperTopology` will be available as an extension to `UnionTopology`. The routine `TopologyGraphs` reconstructs for a set of propagators all existing graphs which serves as a sufficient check for the construction of the supertopology. TopoID can handle supertopologies in the same way as “ordinary” topologies. Therefore, we are confident in the validity of this approach. However, supertopologies still have to prove their value in a real calculation.

**Example 38.** The three massless topologies from Example 36 have 8 independent propagators each. But with one external and three internal momenta, there exist 9 scalar products. The above procedure results indeed in a single complete supertopology with 9 propagators. For simplicity, we write only the line momenta, not the quadratic propagators and give the three graphical representations:

$$\begin{aligned} q_1 &= k_1, \\ q_2 &= p - k_1, \\ q_3 &= k_2, \\ q_4 &= p - k_1 - k_2, \\ q_5 &= k_3, \\ q_6 &= p - k_1 - k_2 - k_3, \\ q_7 &= k_1 + k_2 + k_3, \\ q_8 &= k_1 + k_2, \\ q_9 &= k_1 + k_3. \end{aligned}$$

$$P_3(a_1, \dots, a_8, 0) = \text{Diagram 1},$$

$$P_3(a_1, 0, a_3, \dots, a_9) = \text{Diagram 2},$$

$$P_3(a_1, \dots, a_7, 0, a_9) = \text{Diagram 3}.$$

The greatest common subtopology is obtained by contracting the line with  $q_8$  for the planar ladder topology, the line with  $q_5$  of the Benz topology and the line with  $q_9$  for the non-planar topology. In this case, it can be seen that the construction is related to contracting a propagator such that a four-valent vertex arises which is subsequently pulled in a different way into two separate vertices again. There are always three possible ways to pull such a vertex, corresponding to  $s$ -,  $t$ - and  $u$ -channel type subgraphs. However, it is not clear if such a graphical procedure is in general able to create the  $N_{\text{sp}} - N_I$  new propagators that are needed for completion of a topology.

Note that the same construction applies to a massive four-loop tadpole which can be seen by connecting external legs in this example by an additional propagator.

All 9 factors of the supertopology are real propagators but one has never to consider an integral with 9 positive indices. Only integrals in one of the three distinct subtopologies (12345678), (13456789) and (12345679) are relevant for physical quantities. An integral with nine positive indices cannot result from any diagram in this case.

The unification of topologies can also happen accidentally when using pseudo-propagators. In context of diagram cuts this issue has to be handled with care. *All* valid cuts of *all* possible diagrammatic representations of the topology have to be accounted for.

### 2.7.3 *Revealing non-trivial relations*

Let us close this chapter by presenting some ideas that connect topology completeness, linear dependency and supertopologies to the problem of linear relations among “master” integrals. In a calculation with multiple topologies it may happen that a subset of all the master integrals among the topologies is related in a linear way. That is, some integrals are actually no master integrals since they can be expressed by the other integrals in this subset. Either direct evaluation of integrals or conditions on independent contributions (e.g. from the gauge parameter or different fermion numbers) can hint to such relations.

Let us assume the master integrals in each topology taken separately are indeed “local” master integrals, they are minima of the complexity function used by the Laporta algorithm. But a Laporta algorithm usually works only on a single (complete and independent) topology and it is usually not the case that such relations can be expressed within a single topology. Therefore, the Laporta algorithm (in the described flavor) alone cannot reveal these relations.

One possible way to circumvent this problem will be discussed together with its application to a real problem in Section 4.5.2.2. Here, we merely want to point out further possibilities to find non-trivial relations, both employing supertopologies. The central idea is to have a supertopology for all topologies in a certain problem or an independent subclass. If the supertopology should still be incomplete, it must be completed by the means described in Section 2.7.1. In general it will contain linearly dependent propagators to be dealt with partial fractioning relations obtained via the techniques described in Section 2.2.

**SUPERTOPOLOGY PARTIAL FRACTIONING** The reduction is done in the usual way: independently for each ordinary topology. The partial fractioning relations for the supertopology can be used to systematically map propagators of remaining integrals to a preferred subset of propagators of the supertopology. As result one has in general multiple terms on the right-hand sides which can be rewritten in terms of a subset of initial topologies. A subsequent reduction may be necessary but the result are the demanded linear dependencies among former master integrals.

**SUPERTOPOLOGY REDUCTION** The mapping of supertopology denominators described above (via the set of always terminating rules from the Gröbner basis) can also be incorporated directly into the Laporta algorithm. A single table would cover the whole calculation. An excellent management of computing resources and parallelization is mandatory if this strategy is to be followed.

**SUPERSECTOR INTEGRAL REDUCTION** The reduction of integrals which lie within a “supersector” could also lead to linear relations of integrals formerly taken as master integrals. Therefore, the picked integral must be

completely reducible to Feynman integrals (which have a diagrammatic representation). Since the IBP reduction usually leads from more complicated integrals to simpler ones, integrals from a supersector have the potential to reduce to integrals from different ordinary topologies.



## REVERSED UNITARITY

All calculations described in this thesis are based on the technique of reversed unitarity introduced in Ref. [61] for the NNLO computation of the total cross section for Higgs boson production via gluon fusion. We want to proceed in this process to N<sup>3</sup>LO and apply the same techniques also in the process of Higgs boson pair production at NLO and NNLO. From the technical point of view, the Drell-Yan process is almost equivalent to single Higgs boson production, suggesting itself as another application.

Usually, the optical theorem is understood to relate the imaginary part of a forward scattering amplitude to the total production cross section of all considered intermediate states. It is a direct consequence of the unitarity of the  $S$ -matrix or the intuition that the probability for a state to propagate unchanged is complementary to the probability to undergo any interaction. In the context of perturbation theory, the optical theorem applies to single Feynman diagrams and to individual contributions of intermediate states to the imaginary part. The Cutkosky rules relate specific sets of propagators put on-shell, so-called *cuts*, to these contributions to the imaginary part.

One possible way to apply the optical theorem is to obtain a total cross section or decay width by computing the complete amplitude in forward scattering kinematics and taking the imaginary part of the full result at the very end. Being interested in inclusive cross sections for a selection of final states, we will apply it in a slightly different way. For Higgs boson production at N<sup>3</sup>LO, these states consist of a single Higgs boson in association with up to three additional partons. We trade computation of different squared amplitudes and their integration over different phase spaces for computation of the related imaginary parts of the forward scattering amplitude. These imag-

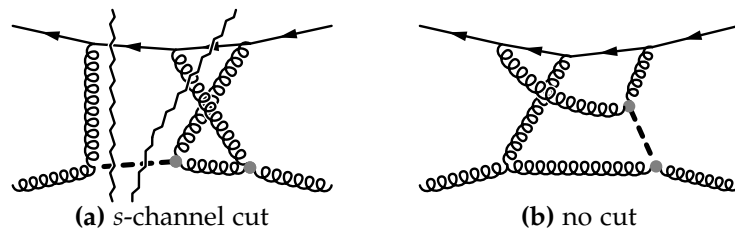


**Figure 5:** Candidate diagrams for contributions to single Higgs boson production at NNLO in the  $gq$ -channel. Curly lines are gluons, straight lines quarks and the thick dashed line represents the Higgs boson. Zigzag lines denote possible cuts of the diagram. Both diagrams contain a single Higgs boson but the second one can be discarded since it gives a zero contribution. Only the first one has valid cuts. That is through the Higgs boson and additional quarks and gluons, separating all incoming from all outgoing momenta (the  $s$ -channel) such that exactly two connected remains emerge.

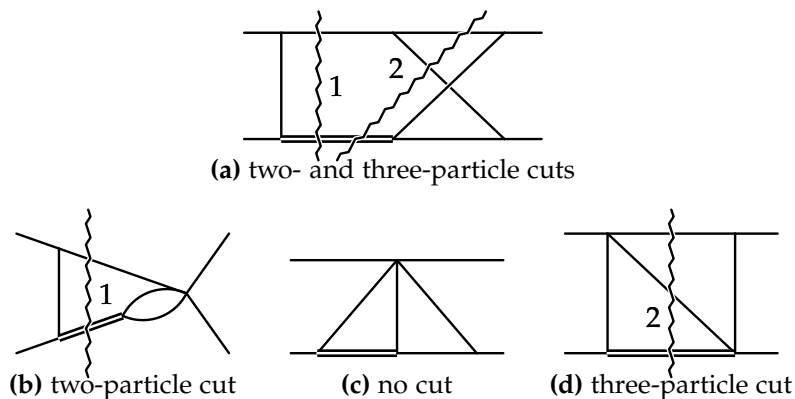


**Figure 6:** Figure a shows a topology that can be inferred from the diagram in Fig. 5a. The lower line shows subtopologies for possible contractions of propagators. Single lines are massless, the double line is massive and cuts are labeled by integers. The subtopologies in Fig. b and Fig. d correspond each to one of the cuts the “parent” topology has, whereas the topology in Fig. c has none of the cuts and can be neglected. Not a single integral from this topology is relevant for Higgs boson production.

inary parts are distinguished by cuts matching the selection of final states as mentioned before. In the diagram in Fig. 5a, the drawn cuts contribute to the production of a Higgs boson together with a quark and an additional gluon.

In greater detail, this facilitates us to proceed as follows:

1. Neglect diagrams part of the forward scattering amplitude but without any contributing cut from the very start, see Fig. 5.
2. Discard complete subtopologies not exhibiting cuts during the reduction of scalar integrals to master integrals, see Fig. 6.
3. Compute the different phase space contributions to a master integral only at the end (for that purpose think of the topology in Fig. 6a as a master integral with both cuts).

For example, the topology in Fig. 6a describes at the same time classes of contributions with one and two additionally produced partons. It is a box-topology in simplified kinematics without special reference to phase spaces (with exception of its cuts). The same is true for all other topologies we need. Hence, all the technology developed for multi-loop integrals is still applicable. Thus, the number of scalar integrals can be reduced drastically by employing Laporta’s algorithm based on IBP relations. Only for the small number of remaining master integrals, we make the transition back to phase space integrals to evaluate them. In summary, we can treat different kinds of phase space integrals in a unified way.

This chapter first reviews the optical theorem and the Cutkosky rules and then moves on to the realization of an algorithm that checks a given diagram for relevant cuts. This algorithm acts as filter for diagrams in Step 1, subtopologies in Step 2 and specific cuts in Step 3.

## 3.1 OPTICAL THEOREM AND CUTKOSKY'S RULES

The following is mostly based on the more pedagogical discussions given in Refs. [62–65] compared to Cutkosky's original publication in Ref. [66].

First, we explore the connection between the imaginary part of the forward scattering amplitude and the total cross section which follows directly from the unitarity of the  $S$ -matrix. This is the optical theorem as it is usually understood. It can also be regarded as consequence of a more fundamental statement applicable for single Feynman integrals that appear in the expansion of  $S$ -matrix elements.

The imaginary part of each diagram can have various contributions which leads us to Cutkosky's rules relating these contributions to cuts, specific sets of propagators in the diagram put on-shell. They turn out to allow for a diagrammatic interpretation: cut propagators dissect the diagram into two parts, each connected to either all incoming or all outgoing legs. Cutkosky also showed how to compute the contribution of an individual cut (there can be multiple) of a single diagram, closely related to the computation of a phase space integral. This results in the optical theorem holding also separately for specific classes of cuts.

## 3.1.1 Optical theorem

From the unitarity of the  $S$ -matrix,  $S^\dagger S = 1$ , and the decomposition in terms of the unit matrix and the transition matrix  $T$  between states,  $S = 1 + iT$ , one finds

$$-i(T - T^\dagger) = T^\dagger T. \quad (81)$$

Taking the matrix element  $\mathcal{M}$  of transitions between the states  $|a\rangle$  and  $|b\rangle$ , subsequently inserting a complete set of (intermediate) states, gives

$$\begin{aligned} & -i[\mathcal{M}(a \rightarrow b) - \mathcal{M}^*(b \rightarrow a)] \\ &= \sum_f \int d\Pi_f \mathcal{M}^*(b \rightarrow f) \mathcal{M}(a \rightarrow f) \delta(\sum \{p_f\} - \sum \{p_{a,b}\}), \end{aligned} \quad (82)$$

where  $f$  denotes all possible intermediate states with momenta  $\{p_f\}$  and both sides are understood to include a delta-function that ensures total momentum conservation. The Lorentz invariant phase space integral in the equation above is defined as

$$\int d\Pi_f = \int dp_f^D (2\pi)^D \delta(p_f^2 - m_f^2) \delta(p - \sum \{p_f\}), \quad (83)$$

where  $p$  is the total incoming momentum and  $\{m_f\}$  are the masses of the intermediate state particles.

In forward scattering, initial and final states are the same. Therefore, we set  $a = b = i$  to show the connection with the total cross section  $\sigma_{\text{tot}}$ :

$$\text{Im } \mathcal{M}(i \rightarrow i) = \frac{1}{2} \sum_f \int d\Pi_f |\mathcal{M}(i \rightarrow f)|^2 = 2 E_{\text{cm}} p_{\text{cm}} \sigma_{\text{tot}}(i \rightarrow f), \quad (84)$$

with the total energy  $E_{\text{cm}}$  and the modulus of three-momentum of an incoming particle  $p_{\text{cm}}$  in the center-of-mass frame. The flux factor  $E_{\text{cm}} p_{\text{cm}}$  stems from the definition of a cross section. In our setting with massless on-shell particles in the initial state  $p_{1,2} = (E_{\text{cm}}/2, 0, 0, \pm E_{\text{cm}}/2)$ , the prefactor can be expressed as  $2 E_{\text{cm}} p_{\text{cm}} = E_{\text{cm}}^2 = -s$  with  $s > 0$ . Equation (84) can also be represented in a graphical way:

$$\begin{aligned}
 \text{Diagram with zigzag cut} &\propto \sum_f \int d\Pi_f \text{Diagram with two circles} \\
 &= \sum_f \int d\Pi_f \left| \text{Diagram with one circle} \right|^2,
 \end{aligned} \tag{85}$$

where the zigzag line represents imaginary parts (or cuts or discontinuities) associated with states which are intermediate in the forward scattering amplitude but final for the squared modulus of the production amplitudes.

Below the threshold  $s_0$  of the lightest intermediate multiparticle state, the amplitude as function of the center-of-mass energy  $\sqrt{s}$  is manifestly real:

$$\mathcal{M}(s) = [\mathcal{M}(s^*)]^*. \tag{86}$$

The analytic continuation of Eq. (86) for  $s$  above the threshold  $s_0$  and near the positive real axis, parametrized by an infinitesimal  $\epsilon$ , such that  $\mathcal{M}(s + i\epsilon)$  acquires an imaginary part, gives

$$\text{Re } \mathcal{M}(s + i\epsilon) + i \text{Im } \mathcal{M}(s + i\epsilon) = \text{Re } \mathcal{M}(s - i\epsilon) - i \text{Im } \mathcal{M}(s - i\epsilon). \tag{87}$$

Starting at the threshold  $s_0$ , we have a branch cut singularity associated with the discontinuity

$$\text{disc } \mathcal{M}(s) = \mathcal{M}(s + i\epsilon) - \mathcal{M}^*(s - i\epsilon) = 2i \text{Im } \mathcal{M}(s). \tag{88}$$

Equations (84) and (88) obviously hold separately in each order of perturbation theory and for each appearing diagram, if regarded as an analytic function. The only source of imaginary parts in the Feynman diagrams can be the  $i\epsilon$ -prescription relevant for virtual particle propagators put on-shell together with an overall factor  $i$  from the definition of  $\mathcal{M}$  (as an expansion in terms of Feynman diagrams). We have seen that only branch cut type singularities contribute and that the magnitude is intimately linked to the discontinuity across the branch cut. What remains to be answered, is how to expose these singularities in an arbitrary multi-loop diagram and calculate the discontinuities systematically.

## 3.1.2 Cutkosky's rules

We focus on the derivation given by 't Hooft and Veltman in Refs. [63–65]. Cutkosky's original work in Ref. [66] is formulated in the language of the Landau equations, see Ref. [67], and therefore not very illuminating for our purposes.

Propagators  $P_F(q)$  in momentum space ( $q$ -space) are treated with the usual Feynman prescription for their poles. They are of the form:

$$P_F(q) = \frac{i}{q^2 - m^2 + i\epsilon}. \quad (89)$$

Via a  $D$ -dimensional Fourier transformation, we get  $P_F(x)$  in coordinate space ( $x$ -space) from Eq. (89):

$$P_F(x) = \int \frac{dq^D}{(2\pi)^D} \frac{i \exp(-iq \cdot x)}{q^2 - m^2 + i\epsilon}. \quad (90)$$

Since the scalar propagator is the time-ordered amplitude for a free particle moving some distance  $x$ , we split Eq. (89). Each of the two terms captures separately the behavior for  $x^0 > 0$  and  $x^0 < 0$  associated with positive and negative energy flow, respectively:

$$P_F(x) = \theta(x^0) P_F^+(x) + \theta(-x^0) P_F^-(x). \quad (91)$$

For the functions  $P_F^+(x)$  and  $P_F^-(x)$  we also have representations in terms of Fourier transforms:

$$P_F^\pm(x) = 2\pi \int \frac{dq^D}{(2\pi)^D} \theta(\pm q^0) \delta(q^2 - m^2) \exp(-iq \cdot x). \quad (92)$$

One can verify above representation by evaluating the  $q^0$  integrals in Eq. (90) with the  $i\epsilon$ -prescription and Eq. (91) with Eq. (92) plugged in. Obviously, we have for  $P_F^\pm(x)$  and  $P_F(x)$  the following behavior under complex conjugation:

$$[P_F^\pm(x)]^* = P_F^\mp(x) = P_F^\pm(-x), \quad (93)$$

$$[P_F(x)]^* = \theta(x^0) P_F^-(x) + \theta(-x^0) P_F^+(x), \quad (94)$$

where Eq. (94) follows from Eq. (93). In  $q$ -space, we have from Eq. (92) additional Feynman rules for *on-shell* propagators:

$$P_F^\pm(q) = 2\pi \theta(\pm q^0) \delta(q^2 - m^2) = 2\pi \delta^\pm(q^2 - m^2). \quad (95)$$

Note that compared to Refs. [63–65], we omitted the generalization via the Källén-Lehmann spectral function and adapted the notation to our number of space-time dimensions, metric and definition of a scalar propagator as of the form in Eq. (89).

In the  $x$ -space representation of some scalar Feynman integral  $I$ , each of the  $N_V$  vertices comes with a coordinate variable  $x_j$ . We have a simple product of  $x$ -space propagators for edges in the corresponding diagram:

$$I(\{x_j\}) = i^{N_V} \prod_{j \leq k} P_F(x_j - x_k) M_{jk}, \quad (96)$$

where we neglected coupling constants. The adjacency matrix  $M$  encodes a connection of vertices  $j$  and  $k$  as  $M_{jk} = 1$  if there is an edge between them and  $M_{jk} = 0$  otherwise. One arrives at the  $q$ -space form of  $I$  by integration over all  $\{x_j\}$  after multiplying with plane wave functions for the amputated external legs. A momentum  $p_i$  incoming at a vertex  $x_j$  gives  $\exp(-ip_i \cdot x_j)$  and  $\exp(ip_i \cdot x_j)$  in case it is outgoing.

**Example 39.** Take an integral just as in Fig. 6a whose  $x$ -space representation, see Eq. (96), reads:

$$\begin{aligned}
 I(x_1, \dots, x_6) &= \begin{array}{c} p_1 \text{---} x_1 \text{---} x_5 \text{---} x_3 \text{---} p_1 \\ | \quad \quad \quad \diagdown \quad \quad \diagup \\ p_2 \text{---} x_2 \text{---} x_6 \text{---} x_4 \text{---} p_2 \end{array} \\
 &= (-1) P_F(x_1 - x_2) P_F(x_1 - x_5) P_F(x_2 - x_6) \\
 &\quad \times P_F(x_3 - x_5) P_F(x_3 - x_6) P_F(x_4 - x_6).
 \end{aligned}$$

We introduce the concept of *underlined variables*  $\underline{x}_k$  and  $\underline{x}_l$  which denote vertices that belong to the complex conjugate of an amplitude. We modify the original expression for

$$I(\{x_j\}) = I(x_1, \dots, x_k, \dots, x_l, \dots, x_{N_V}) \quad (97)$$

according to a set of rules, using a shorthand notation for the distances  $x = x_k - x_l$ ,

$$\begin{aligned}
 P_F(x) &\rightarrow P_F(x) && \text{if } x_k \text{ and } x_l, \\
 P_F(x) &\rightarrow P_F^+(x) && \text{if } \underline{x}_k \text{ and } x_l, \\
 P_F(x) &\rightarrow P_F^-(x) && \text{if } x_k \text{ and } \underline{x}_l,
 \end{aligned} \quad (98)$$

$$\begin{aligned}
 P_F(x) &\rightarrow P_F^*(x) && \text{if } \underline{x}_k \text{ and } \underline{x}_l, \\
 i &\rightarrow -i && \text{in Eq. (96) for each } \underline{x}_k \text{ or } \underline{x}_l.
 \end{aligned} \quad (99)$$

The rule in Eq. (99) means to replace for every underlined vertex  $x_k$  or  $x_l$  a factor of  $i$  in Eq. (96) by a factor of  $-i$ . Equations (98) and (99) can be taken as complex conjugation of a subset of vertices (the underlined variables) and the propagators they connect. Variables not underlined are referred to as *plain variables*.

Now suppose, we start from an integral  $I$  without any underlinings and for which we know  $x_k^0$  to be the largest time component amongst all  $\{x_j\}$ . For this we write  $x_k^0 = \max \{x_j^0\}$ . We create two versions of  $I$ , both with the same arbitrary variables underlined or not but  $x_k$  plain in one and underlined in the other version. Then, we have the so-called *largest time equation*:

$$I(\dots, x_k, \dots) = -I(\dots, \underline{x}_k, \dots), \quad (100)$$

where the minus sign is purely due to Eq. (99).

**Example 40.** For clarity, let  $x_6$  have the largest time component in Example 39 and consider

$$I(x_1, x_2, \underline{x_3}, x_4, \underline{x_5}, x_6) = -I(x_1, x_2, \underline{x_3}, x_4, \underline{x_5}, \underline{x_6}).$$

The minus sign is caused by the numbers of underlined variables differing by one on both sides. Any additional difference would come from propagators connecting to  $x_6$ :

$$\begin{aligned} I(x_1, x_2, \underline{x_3}, x_4, \underline{x_5}, x_6) &= \text{Diagram 1} \\ &= \dots P_F(x_2 - x_6) P_F^+(x_3 - x_6) P_F(x_4 - x_6) \dots \\ &= \dots P_F^-(x_2 - x_6) P_F^+(x_3 - x_6) P_F^-(x_4 - x_6) \dots, \end{aligned}$$

$$\begin{aligned} I(x_1, x_2, \underline{x_3}, x_4, \underline{x_5}, \underline{x_6}) &= \text{Diagram 2} \\ &= \dots P_F^-(x_2 - x_6) P_F^*(x_3 - x_6) P_F^-(x_4 - x_6) \dots \\ &= \dots P_F^-(x_2 - x_6) P_F^+(x_3 - x_6) P_F^-(x_4 - x_6) \dots, \end{aligned}$$

where we circled vertices corresponding to underlined variables. From Eqs. (92), (93) and (94), we see that propagators involving the largest time always reduce to  $P_F^\pm(x)$ . This verifies the largest time equation in Eq. (100) not only for this particular case but also in general.

Detached from some largest component under time ordering, Eq. (100) leads directly to

$$\sum_{\text{underlinings}} I(\{x_k\}, \{\underline{x_l}\}) = 0, \quad (101)$$

where the sum runs over all  $2^{N_V}$  possible ways to partition  $N_V$  vertices  $\{x_j\}$  into a plain set  $\{x_k\}$  and an underlined set  $\{\underline{x_l}\}$  of variables. For some  $x_k$  with the largest time component, there exist in Eq. (101) always a term with  $x_k$  plain and a term with  $x_k$  underlined which cancel by virtue of Eq. (100).

Transforming Eq. (101) into  $q$ -space will result in loop integrals involving propagators of the form of Eqs. (89) and (95) with appropriate routing of internal momenta. Two of these integrals stand out: the Fourier transforms of  $I$  with plain variables only and with underlined variables only. By the rules of Eqs. (98) and (99), the latter is precisely the complex conjugate of the former. Only certain other terms will survive and give non-zero contributions in the end. The reason is the collection of Heaviside theta-functions  $\theta(\pm q_i^0)$  from Eq. (95) where the line momenta  $\{q_i\}$  involve now linear combinations of external momenta  $\{p_i\}$  and integration momenta  $\{k_i\}$ . The configuration of these on-shell propagators indicates a directed boundary over which energy

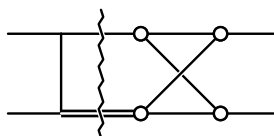
is to be transferred, always from uncircled to circled vertices. However, this can conflict with momentum conservation and thereby restrain the region for loop integrations to a volume of effectively zero.

Ultimately, we arrive at the so-called *cutting equation*:

$$I(\{p_i\}) + [I(\{p_i\})]^* = - \sum_{c \in \text{cuts}} I_c(\{p_i\}), \quad (102)$$

where we have on the left-hand side the two terms which are complex conjugate to each other and on the right-hand side terms which give a non-zero contribution from Eq. (101). The sum runs over all possible “cuts”, special ways to dissect the diagram along the aforementioned boundaries such that the sum of momenta passing this threshold is compatible with total momentum conservation.

**Example 41.** The two examples for configurations of circled vertices from Example 40 give zero in our kinematic setup. In both cases only  $p_1$  is transported over the cut. In principle, cuts with different numbers of external legs on each side are valid but since we consider forward scattering, these cases drop out. For us all outgoing legs need to be attached to circled vertices. In contrast, the configuration



clearly contributes. All incoming legs connect uncircled vertices, all outgoing legs connect circled vertices. Both types of vertices form connected regions whose boundary line is a diagrammatic cut that is crossed by  $p_1 + p_2$ . The case



gives again zero. On the one hand, external momenta are directed from the left to the right through the graph. On the other hand, the three propagators involving the circled vertex require energy to flow towards it. This is a contradiction.

#### CONCLUDING REMARKS

- Equation (102) strongly resembles Eq. (81) and in fact we can regard unitarity of the  $S$ -matrix as consequence of the cutting equation for single Feynman integrals. This is true, because the expansion of the transition matrix  $T$  in terms of Feynman graphs comes with an additional factor of  $-i$ .



- The two components of a cut diagram form together an interference term of diagrams one would have to account for when computing the cross section via the right-hand side of Eq. (84). For the different final state phase spaces separately, contributions to the amplitudes of various orders in the perturbation series mix to appear in a given order of its squared modulus.
- There is no  $q$ -space equivalent to Eq. (100) that implies a time ordering since one has to integrate over all coordinates and thereby also all times. Loosely speaking, in momentum space one can not isolate discontinuities easily.
- The discussions in Refs. [63, 64] handle the case of self-energy insertions via the Källén-Lehmann representation. The problem arises when a propagator on one side of an insertion is put on-shell and we have an equivalent propagator on the other side that gives a pole. We omitted this for simplicity but for correct treatment of these insertions Eqs. (90), (92) and (95) need only slight modification.
- We did not discuss the case of non-scalar, e.g. fermionic, on-shell propagators since in practice we only need to cope with scalar integrals. All non-scalar structures in diagrams can be handled without any modification in the usual way.
- For propagators of the form of Eq. (4), Eq. (95) acquires an additional factor of  $i$ . In practice this means that we can freely replace on-shell propagators by their discontinuity in the manner of

$$\frac{1}{m^2 - q^2} \longleftrightarrow 2\pi i \theta(q^0) \delta(m^2 - q^2). \quad (103)$$

This presumes we know which particles' propagators are to be put on-shell. Propagators raised to higher powers must be reduced to simple denominators before applying above replacement.

- The algorithm we describe in the following Section 3.2.1 works along a very similar line of thought that lead to the cutting equation in Eq. (102).
- In Ref. [66], the problem is basically translated into the solvability of a system of equations, namely Landau's conditions for an integral to develop a singularity. After that, it is shown how to reparametrize generically such an integral as a phase space integral for those propagators that are put on-shell.

### 3.1.3 Extension

The discussion so far applied to total cross sections but there exists a powerful generalization for differential quantities. The method pioneered by

Anastasiou and Melnikov in Ref. [61] was extended and applied in Refs. [68–71] to rapidity distributions for Higgs boson production and the Drell-Yan process up to NNLO.

The main idea is to introduce an additional delta-function in the phase space integrals. This delta-function is chosen such that it catches the dependence on a selected kinematic variable  $x$  which must be expressed in a covariant way in terms of incoming external momenta  $\{p_i^{\text{in}}\} = \{p_i\}$  and final state momenta of the phase space integral  $\{p_i^{\text{out}}\}$ :

$$\delta\left(x' - f\left(\{p_i^{\text{in}}\}, \{p_i^{\text{out}}\}\right)\right). \quad (104)$$

These delta-functions can be replaced in the same way as delta-functions imposing on-shell conditions as in Eq. (103). Final state momenta of the phase space integral now become linear combinations of internal and external momenta in such propagators.

For example, the rapidity  $y$  of a final state particle with momentum  $p_y^{\text{out}}$  is defined in the rest frame of the hadrons as

$$y = \frac{1}{2} \ln\left(\frac{p_y^{0,\text{out}} + p_y^{3,\text{out}}}{p_y^{0,\text{out}} - p_y^{3,\text{out}}}\right). \quad (105)$$

By change to the variable  $u$ , one gets rid of the exponential function and arrives at

$$u = \frac{x_1}{x_2} \exp(-2y) = \frac{p_1 \cdot p_y^{\text{out}}}{p_2 \cdot p_y^{\text{out}}}, \quad (106)$$

where  $x_1$  and  $x_2$  are the momentum fractions of incoming partonic momenta  $p_1$  and  $p_2$ , respectively. Accordingly, one can choose a delta-function capturing the correct dependence on  $u$  and replace it by a propagator, e.g.

$$\delta\left(\frac{p_y^{\text{out}} \cdot (p_1 - u p_2)}{p_y^{\text{out}} \cdot p_2}\right) \longleftrightarrow \frac{p_y^{\text{out}} \cdot p_2}{p_y^{\text{out}} \cdot (p_1 - u p_2)}. \quad (107)$$

Obviously, these propagators introduce in general extra scales in comparison to a total cross section computation and are not of the standard form of Eq. (4). In the example above, even a scalar product appears in the numerator. However, these propagators are still polynomial in external and internal momenta. Thus, standard reduction techniques, like Laporta's algorithm, can be applied. Note, for each single distribution one is interested in, this insertion of a new propagator with subsequent reduction must be done from scratch.

## 3.2 HANDLING CUT DIAGRAMS

### 3.2.1 Detecting cuts

We present an algorithm that allows us to work with the concept of cuts of Feynman diagrams. Its abstract formalization is followed by some descriptive examples that should clarify the way it works. We encourage the reader

to look ahead into the examples which follow the same enumeration and notation as the algorithm in order to understand its steps. Its first version was due to A. Pak and applied in calculations described in Refs. [72, 73]. In this PhD thesis it has been extended to work also in the case of Higgs boson pair production and was generalized in some aspects.

**Algorithm 3** (find cuts). The problem is posed as follows: given the graph  $G$  of a Feynman diagram and a specification of ranges how often which particle is allowed to be cut, does the diagram have allowed cuts and if it has, how are these cuts defined?

For definiteness, the graph is given by a list of edges  $\{e_i\}$ , each denoted by a pair of vertex labels  $(v_i^{\text{in}}, v_i^{\text{out}})$  and having attached a particle type  $p_i$ :

$$G = \{e_i\}, \quad e_i = \left\{ \left( v_i^a, v_i^b \right), p_i \right\}. \quad (108)$$

The superscripts “a” and “b” indicate the two vertices of an edge which are elements of the whole set of internal vertices of the graph  $\{v_1, \dots, v_{N_V}\}$ . Moreover, we have for all particle types  $\{p_j\}$  ranges  $\{r(p_j)\}$  for the valid number of cuts:

$$r(p_j) = [r_1(p_j), r_2(p_j)]. \quad (109)$$

1. From the ranges  $\{r(p_j)\}$  we can classify each edge  $e_i$  by a value of  $c(p_i)$  obtained according to

$$c(p_i) = \begin{cases} \text{N}, & \text{if } r_1(p_i) = r_2(p_i) = 0, \\ \text{C}, & \text{if } r_1(p_i) = 0 < r_2(p_i), \\ \text{M}, & \text{if } 0 < r_1(p_i) \leq r_2(p_i). \end{cases} \quad (110)$$

The letters “N”, “C” and “M” abbreviate that a line is **N**ot to be cut, **C**an be cut or **M**ust be cut, respectively. For external legs we have  $c(p_i) = \text{N}$ , irrespective of particle species  $p_i$  since they cannot be cut by definition.

2. Depending on the nature of demanded cuts (in  $s$ -,  $t$ - or  $u$ -channel or a generalization thereof), we assign external vertices of incoming and outgoing legs to either a “source” vertex  $v_+$  or a “sink” vertex  $v_-$ . For simplicity, we map the set of vertices  $(v_+, v_-, v_1, \dots, v_{N_V})$  to the set of integers  $(1, 2, 3, \dots, N_V + 2)$ .
3. Next, we have to build the symmetric adjacency matrix  $M$  of the graph. Rows and columns correspond to vertex labels, matrix entries to edge classifications. If vertex  $j$  connects via edge  $e_i$  to vertex  $k$  and vice versa, we set  $M_{jk} = M_{kj} = c(p_i)$ , otherwise  $M_{jk} = M_{kj} = 0$ .

Stricly speaking, this can only be done for simple graphs, viz. any pair of vertices is only connected by a single edge; no loop is spanned

between two vertices only. For this reason we need to merge cut-conditions imposed on non-simple edges according to the rules:

$$\begin{aligned}
 C \wedge c(p_i) &\rightarrow c(p_i) && \text{for } c(p_i) \in \{N, C, M\}, \\
 M \wedge c(p_i) &\rightarrow M && \text{for } c(p_i) \in \{C, M\}, \\
 N \wedge c(p_i) &\rightarrow N && \text{for } c(p_i) \in \{N, C\}, \\
 M \wedge N &\rightarrow \emptyset && \text{(no cut is possible).}
 \end{aligned} \tag{111}$$

Or graphically:

$$\begin{aligned}
 \begin{array}{c} ? \\ \text{---} \end{array} &\rightarrow \begin{array}{c} ? \\ \text{---} \end{array}, \\
 \begin{array}{c} \text{---} \\ \text{---} \end{array} &\rightarrow \begin{array}{c} \text{---} \\ \text{---} \end{array}, \\
 \begin{array}{c} \text{---} \\ \text{---} \end{array} &\rightarrow \begin{array}{c} \text{---} \\ \text{---} \end{array}, \\
 \begin{array}{c} \text{---} \\ \text{---} \end{array} &\rightarrow \emptyset.
 \end{aligned} \tag{112}$$

Here, we introduce the notation for line classes as: thin for lines that can be cut, dashed for lines that must be cut and thick for lines that cannot be cut.

At this stage, if a non-simple edge is classified as  $\emptyset$ , we can readily infer that the graph in question has not a single cut whatsoever, regardless of its nature. For example, one can think of a Higgs loop attached to a top-quark propagator or its counter-part in the EFT, a Higgs tadpole:

$$\begin{array}{c} \text{---} \\ \text{---} \end{array} \rightarrow \emptyset, \quad \begin{array}{c} \text{---} \\ \text{---} \end{array} \rightarrow \emptyset.$$

Both will lead to contradictions and thus no cuts. In the first case edges cannot be merged. The second case is discarded later, more precisely in Step 4, because the vertices have to be in different classes for the attached Higgs line being cut. This is impossible for a tadpole or a self-loop in the language of graph theory which has only one vertex.

What follows is the stepwise coloring of the vertices of the underlying simple graph by connectivity components. Generally speaking, by coloring we mean the assignment of properties to elements of a graph. Vertices that connect by an uncut line belong to the same class, vertices connecting with a cut edge are assigned different classes. In the end, if a graph can be dissected completely and in a correct way, only two vertex classes remain, one for each side of the cut. For intermediate steps we make use of temporary classes.

For a completely unclassified graph with  $N_V + 2$  vertices (also counting source and sink) one would naively assume  $N_V + 2$  possible classes (if all edges are cut). But we will make use of classes labeled by the integers  $-N_V - 2, \dots, N_V + 2$  which allows us to encode in the sign if two adjoining

vertices are located on the same or opposite sides of the cut. Classes  $N_V + 2$  and  $-N_V - 2$  are reserved as vertex classes for the source and the sink and unconstrained vertices are of class 0. The complete list of classes and their meaning is:

$$\begin{aligned}
0: & \text{ unconstrained,} \\
j \in (1, N_V + 1]: & \text{ same side as } j - 1, \\
j \in [-N_V - 1, -1): & \text{ opposite side to } -j + 1, \\
N_V + 2: & \text{ class of the source, vertex 1,} \\
-N_V - 2: & \text{ class of the sink, vertex 2.}
\end{aligned} \tag{113}$$

Assigned classes for the vertices in a graph are stored in a vector  $V = (N_V + 2, -N_V - 2, \dots)$  of length  $N_V + 2$  where the first two components are fixed to the classes of source and sink. Thus, the vector is initialized as  $V = (N_V + 2, -N_V - 2, 0, \dots, 0)$ .

4. The initial constraints (of lines that must or must not be cut) based on the adjacency matrix  $M$  are applied to the vertex classes  $V$ . Therefore, we basically iterate over each vertex  $j$  and each adjacent vertex  $k$  and distinguish different cases for the values of  $M_{jk}$ ,  $V_j$  and  $V_k$  as depicted in Pseudocode 1 below.

The value of  $f$  is the sign of vertex classes encoding the relative position of vertices with respect to a cut. Every combination of the two vertices being classified or not is checked. Whenever the setting of a vertex class cannot be ensured, the graph has no cuts. If a value for a vertex class is set, iteration over adjacent vertices of vertex  $j$  is halted and conditions are applied recursively to vertices adjacent to vertex  $k$ . In the case of vertex  $j$  depending on vertex  $k$ , nothing is done for that iteration step.

In the first two graphs on the right-hand side of the diagrammatic formula in Example 14 on Page 29 or in the graph in Fig. 6c on Page 82, ensuring correct setting of vertex classes would not succeed. There is a conflict whenever a vertex exists connecting to both, incoming and outgoing external legs. If a line that must be cut links vertices, on their part connecting to external legs of the same side, we have another situation without cut. Both cases are revealed at this step of the algorithm.

5. The previous step will in general leave some subset of vertices unclassified, i.e. they will have  $V_j = 0$ . For these we will basically have to test every possible assignment to either source or sink vertex class. When these vertices are fixed, an assignment for dependent vertices (previously in temporary classes) can be concluded from the definition of vertex classes in Eq. (113) and proceeds by an iteration. Setting  $M_{j,k} = 0$  for each vertex pair with  $V_j \neq V_k$  applies the constraints back

onto the adjacency matrix. For details on both steps, see Pseudocode 2. Note that this and the next step is understood to operate on copies of  $M$  and  $V$  obtained after Step 4.

At this point the only classes appearing in  $V$  are either  $N_V + 2$  or  $-N_V - 2$  and  $M$  contains no more “M”-entries for lines that must be cut since these have been deleted.

6. All vertices are now put definitely on one side of the cut. However, it is not clear yet if all vertices on either side form a single connectivity component. Starting from some vertex connected to the source and aided by the modified matrix  $M$ , we seek all connected vertices. The same is done for the sink and in the end we check if any vertices are left over. See Pseudocode 3 and Pseudocode 4. If it is not the case that a vertex is left over, we found a candidate for a valid cut.

At this stage the diagram in Fig. 5b would be discarded since the vertex connecting to the upper right external quark leg gives a third connectivity component. Knowing which vertices lie on which side of the cut, we would simply not find a way to connect the two vertices to the right of the cut.

7. Last but not least, we translate vertex classifications returned in Step 6 back to selections of diagram propagators that are cut. Cut propagators have vertices with vertex classes of opposite sign, propagators with vertices of classes of equal sign are not cut and the sign tells us to which side of the cut they belong. After that, we can impose the counting conditions  $\{r(p_j)\}$  on the particle types appearing in the diagram.
-

```

Constrain Classes( $j$ )
  for  $k = 1$  to  $N_V + 2$  do
    if  $M_{jk} = N$  then                                     (encode link type in  $f$ )
      |  $f \leftarrow 1$ 
    else if  $M_{jk} = M$  then
      |  $f \leftarrow -1$ 
    else                                                    (no link between  $j$  and  $k$ )
      | return
    if  $V_j = 0$  then                                       (handle independent classes)
      | if  $V_k = 0$  then
      |   |  $V_k \leftarrow f(j+1)$ 
      |   | Constrain Classes( $k$ )
      | else
      |   | ensure  $V_k = f(j+1)$ 
    else                                                    (handle dependent classes)
      | if  $V_k = 0$  then
      |   | if  $V_j = f(k+1)$  then                          ( $j$  depends on  $k$ )
      |   |   | continue
      |   | else
      |   |   |  $V_k \leftarrow fV_j$ 
      |   |   | Constrain Classes( $k$ )
      | else
      |   | ensure  $V_k = fV_j$ 

```

**Pseudocode 1:** Apply constraints on vertex classes  $V$  starting from vertex  $j$ .

```

for  $j = 1$  to  $N_V + 2$  do                                  (fix dependent vertex classes)
  | if  $V_j \in \{N_V + 2, -N_V - 2\}$  then
  |   | continue
  | if  $V_j > 0$  then
  |   |  $V_j \leftarrow V_{j-1}$ 
  | else if  $V_j < 0$  then
  |   |  $V_j \leftarrow -V_{-j-1}$ 

for  $j, k = 1$  to  $N_V + 2$  do                              (apply constraints back to  $M$ )
  | if  $V_j \neq V_k$  then
  |   |  $M_{jk} \leftarrow 0$ 

```

**Pseudocode 2:** Fix dependent vertex classes in  $V$  and apply constraints to  $M$ .

```

Connect Vertices( $j$ )
┌
│   for  $k = 1$  to  $N_V + 2$  do
│   │   if  $M_{jk} = 0$  then                                (no link present)
│   │   │   continue
│   │   if  $V_k = 0$  then                                (claim unrestricted vertex)
│   │   │    $V_k \leftarrow V_j$ 
│   │   │   Connect Vertices( $k$ )
│   │   │   continue
│   │   ensure  $V_j = V_k$                                 (conflicting classifications in  $M$  and  $V$ )
└
    
```

**Pseudocode 3:** Color component connected to vertex  $j$  by adjacency matrix  $M$ .

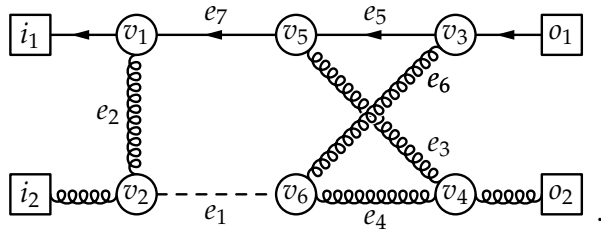
```

 $V \leftarrow (N_V + 2, -N_V - 2, 0, \dots, 0)$ 
 $(l, m) \leftarrow (0, 0)$ 
for  $k = 3$  to  $N_V + 2$  do                                (find source and sink start vertices)
┌
│   if  $M_{k1} \neq 0$  and  $l = 0$  then
│   │    $l \leftarrow k$ 
│   │    $V_k \leftarrow N_V + 2$ 
│   if  $M_{k2} \neq 0$  and  $m = 0$  then
│   │    $m \leftarrow k$ 
│   │    $V_k \leftarrow -N_V - 2$ 
└
Connect Vertices( $l$ )
Connect Vertices( $m$ )
ensure  $0 \notin V$                                 (check that no unmapped vertices remain)
    
```

**Pseudocode 4:** Map components connected to source and sink.



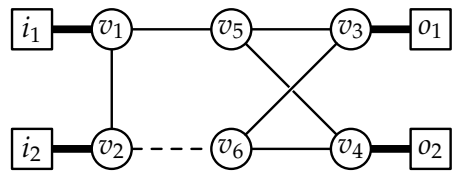
**Example 42.** We give a demonstration of this algorithm where we stress the point of vertex classification and conclude with some explanations in this regard. Consider the topology introduced in Fig. 6a:



We explicitly show labels for external and internal vertices and also edges. The particle type  $p_i$  can as usual be seen from the line style.

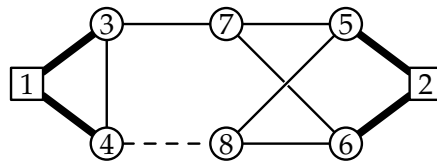
1. In single Higgs boson production we have  $r(H) = [1, 1], r(g) = r(q) = [0, \infty)$  and thereby  $c(H) = M, c(g) = c(q) = C$ . Each graph must contain exactly one cut Higgs boson line and can have arbitrarily many cuts through parton lines. For Higgs boson pair production we have  $r(H) = [2, 2], r(g) = r(q) = [0, \infty)$  and thus again  $c(H) = M$  and  $c(g) = c(q) = C$  since we always have a cut with two Higgs bosons plus optional partons. Working in the full theory where top-quarks persist which cannot be cut for our purposes, we set  $r(t) = [0, 0]$  and get  $c(t) = N$ .

This translates to the graph of the topology as follows:



2. In our case of forward scattering, external vertices of all incoming legs are identified with the source and those of all outgoing legs with the sink.

This identification and mapping to integer vertex labels (from 1 to 8) gives:

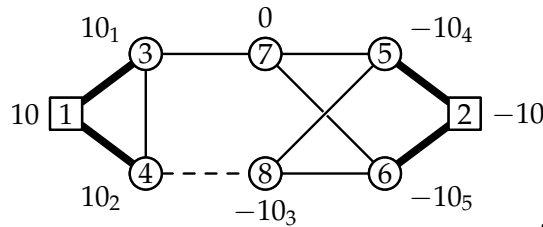


3. In this example no merging of edges is necessary. The symmetric adjacency matrix and the initial vector of vertex classes (from  $-10$  to  $10$ ) read:

$$M = \begin{pmatrix} 0 & 0 & N & N & 0 & 0 & 0 & 0 \\ & 0 & 0 & 0 & N & N & 0 & 0 \\ & & 0 & C & 0 & 0 & C & 0 \\ & & & 0 & 0 & 0 & 0 & M \\ & & & & 0 & 0 & C & C \\ & & & & & 0 & C & C \\ & & & & & & 0 & 0 \\ & & & & & & & 0 \end{pmatrix},$$

$$V = (10, -10, 0, 0, 0, 0, 0, 0).$$

4. Application of initial constraints to the vertex classes  $V$  gives:

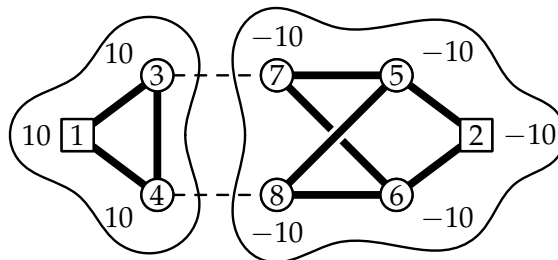


$$V = (10, -10, 10, 10, -10, -10, 0, -10).$$

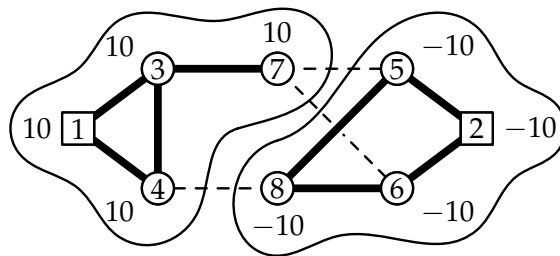
We indicated vertex classes and the order in which they have been assigned by subscripts also in the graph.

- 5./6. The next to last component in  $V$  is  $0$ . Thus, we have the two alternatives  $-10$  and  $10$ . Here, no fixing of dependent vertices is needed and how constraints apply back onto  $M$  can also be seen from the graphs for both alternatives:

- a)  $V = (10, -10, 10, 10, -10, -10, -10, -10)$ :



b)  $V = (10, -10, 10, 10, -10, -10, 10, -10)$ :



Coloring of the two connected components succeeds obviously in both cases, leaving us with two candidates.

7. Translating the vectors  $V$  back to particle labels in the graph we started from, we find that in the first case the Higgs boson and a quark are cut. In the second case the Higgs boson, a quark and a gluon are cut. All particle counts lie within their respective ranges. Therefore both candidates also pass this last condition and we found two valid cuts, identical to those in Fig. 6a. We denote the two-particle cut by  $(e_1, e_7)$  and the three-particle cut by  $(e_1, e_3, e_5)$ , see the first diagram of this example.

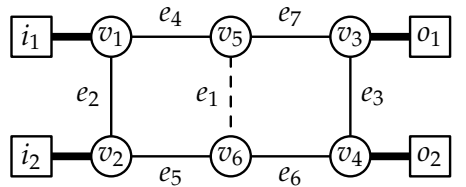
#### CONCLUDING REMARKS

- The number of loops  $N_L$ , together with the requirement to cut a diagram into two connected pieces, allows for the total number of cuts to be at most  $N_L + 1$ .
- As can be seen in Pseudocode 1 and Pseudocode 3, various steps of this algorithm are backtracking recursions.
- This algorithm has been implemented in `Per1` to efficiently filter output of the Feynman diagram generator `QGRAF`, see Ref. [33], for diagrams with valid cuts. Another implementation exists in the `Mathematica` package `TopoID` and allows to inspect topologies for cuts.
- In practice we found this algorithm to be very effective. We applied it to five-loop diagrams relevant for Higgs boson pair production. Filtering of  $\mathcal{O}(10^7)$  diagrams takes roughly a day and leaves only about  $\mathcal{O}(10^5)$ . Usually, information on the cuts of a single diagram is returned almost instantaneously.
- The main ingredient for this good performance are the (intermediate) vertex classification and propagating of constraints in Step 4 and Step 5. This improves combinatorics drastically and leaves only very few possibilities compared to a brute force approach (based on checking for connectivity components of a graph). Before using trial-and-error, we build “islands” of connected and “canals” of disconnectes portions of the graph.

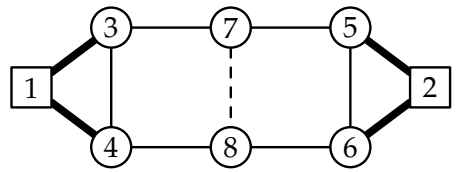
- Alternatively, one could try to set particles on-shell and demand that the total momentum is still preserved at each vertex. This is equivalent to checking whether all conditions from delta- and theta-functions can be satisfied simultaneously in a phase space integral.
- Our algorithm works on a graph whose edges are colored by a correct routing of external and internal momenta. This graph coloring and momentum conservation at each vertex are essentially interchangeable.

**Example 43.** Let us consider a second topology appearing in NNLO Higgs boson production where some cases occur that have been missing so far.

1. In the graph we use the notation for lines that can, cannot or must be cut:



2. Vertex relabeling and identification with source and sink give:

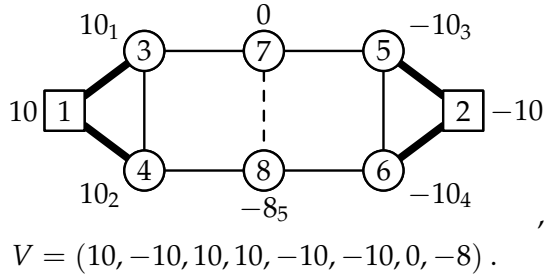


3. Again, no edge merging is necessary and we have for  $M$  and  $V$ :

$$M = \begin{pmatrix} 0 & 0 & N & N & 0 & 0 & 0 & 0 \\ 0 & 0 & 0 & 0 & N & N & 0 & 0 \\ & 0 & C & 0 & 0 & 0 & C & 0 \\ & & 0 & 0 & 0 & 0 & 0 & C \\ & & & 0 & C & C & 0 & \\ & & & & 0 & 0 & C & \\ & & & & & 0 & M & \\ & & & & & & 0 & 0 \end{pmatrix},$$

$$V = (10, -10, 0, 0, 0, 0, 0, 0).$$

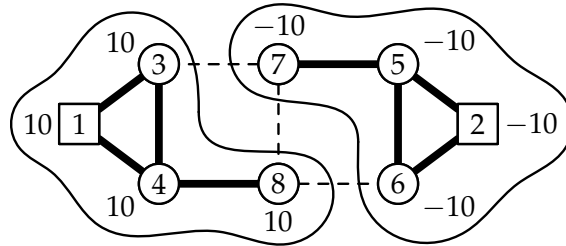
4. After imposing constraints, we have the classification:



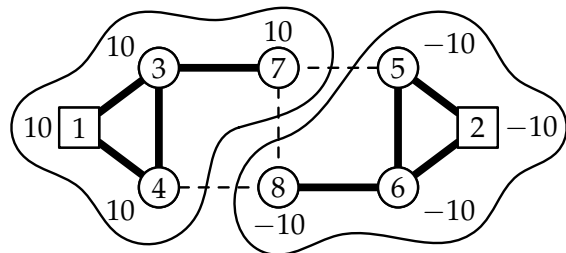
In this case, the order of assignments is slightly different compared to Example 42 and the case of dependent classes can be observed for vertex 8. The assignment of this class can be understood from the definition of vertex classes in Eq. (113) and Pseudocode 1.

5./6. Again, we have two alternatives for the next to last vertex class. Picking one, the dependence of the last vertex class can be fixed as prescribed in Pseudocode 2.

- a)  $V = (10, -10, 10, 10, -10, -10, -10, -8)$   
 $\rightarrow V = (10, -10, 10, 10, -10, -10, -10, 10):$



- b)  $V = (10, -10, 10, 10, -10, -10, 10, -8)$   
 $\rightarrow V = (10, -10, 10, 10, -10, -10, 10, -10):$



7. After successful coloring of vertices, we find here two symmetric three-particle cuts  $(e_1, e_4, e_6)$  and  $(e_1, e_5, e_7)$ .

### 3.2.2 Cut integral reduction

Having at hand a list of valid cuts for a topology we use this knowledge during the reduction (and classification) procedure. Suppose we have a sin-

gle cut, then every integral where one of the cut propagators is completely absent or appears only in the numerator is zero. This is true because these integrals do not contribute to the imaginary part one is interested in. If there are multiple cuts, every possibility for a cut must be excluded before an integral can be set to zero.

Boolean algebra helps to translate the list of cuts into a more useful form: a list of subtopologies that do not expose any cut and are therefore zero. These can also be combined with scaleless subtopologies, see Section 2.3.4. Note that taking into account valid cuts renders operations such as subtopology classification, symmetrization, partial fractioning, etc. as described in Chapter 2 much more efficient. The total amount of objects is simply less, by a factor of  $\mathcal{O}(10^{-1})$  to  $\mathcal{O}(10^{-2})$  in the case of Higgs boson production at N<sup>3</sup>LO. Laporta algorithms work such that more complicated integrals are expressed in terms of simpler ones, a lot of those simpler integrals can immediately be discarded when they have no cut.

We are given the list of cuts in the form  $C = \{C_i\}$  where  $C_i = (b_j)_i$  is a list of boolean variables  $b_j$  denoting that an edge  $e_j$  part of cut  $C_i$  exists in the graph (compared to before, we just replaced edges by boolean variables). Then, the condition that *no* cut is possible in the corresponding (sub-)topology can be formulated as

$$\text{no cut} \hat{=} \bigwedge_i \neg \bigwedge_{b \in C_i} b = \bigwedge_i \bigvee_{b \in C_i} \neg b, \quad (114)$$

where  $b$  runs over the boolean variables of each line in each cut. The symbol  $\wedge$  denotes logical conjunction,  $\vee$  logical disjunction and  $\neg$  logical negation. One specific cut is impossible if one of its propagators is missing and this has to hold for all valid cuts. This condition can be brought into disjoint normal form where each alternative states a subtopology without any of the demanded cuts. The boolean variable  $b_j$  is linked to the index  $a_j$  of a propagator  $p_j$  via  $b_j = a_j > 0$ . Only for a positive index of a propagator one can assign it also to an edge in a graph (which can then be cut).

**Example 44.** We can operate on the cuts of the topology from Example 42 stated in terms of edges of its graph:  $(e_1, e_7)$  and  $(e_1, e_3, e_5)$ . The condition for no cuts is then

$$\begin{aligned} \neg (b_1 \wedge b_7) \wedge \neg (b_1 \wedge b_3 \wedge b_5) &= (\neg b_1 \vee \neg b_7) \wedge (\neg b_1 \vee \neg b_3 \vee \neg b_5) \\ &= \neg b_1 \vee (\neg b_3 \wedge \neg b_7) \vee (\neg b_5 \wedge \neg b_7). \end{aligned}$$

The three alternatives on the right-hand side give precisely the subtopologies without cuts. In the notation of line subsets, they are given by (234567), (12456) and (12346). Note that (12346) is shown in Fig. 6c on Page 82.

## HIGGS BOSON PRODUCTION

---

We open this chapter by a general description of the process in Section 4.1. As motivated in Chapter 1, the focus lies on the inclusive production rate for the Higgs boson via gluon fusion in the SM. We expose the analytic structure that underlies the partonic cross section and that allows for a breakdown of contributions. Simultaneously, we review available theoretical predictions. After that, we describe necessary theoretical tools in Section 4.2. Section 4.3 describes the calculation of cross sections up to NNLO while Section 4.4 shows how LO to NNLO cross sections enter collinear subtraction terms at N<sup>3</sup>LO. The chapter is closing by Section 4.5, discussing completed parts of the calculation in the  $qq'$ -channel at N<sup>3</sup>LO and our strategy for the full calculation.

### 4.1 INTRODUCTION

In the SM the coupling of the Higgs boson to strongly interacting particles is mediated predominantly by the top quark's large mass. The process starts at order  $\alpha_s$  with one-loop diagrams which contain already three scales: the partonic center-of-mass energy  $\sqrt{s}$ , the Higgs mass  $m_H$  and the top quark mass  $M_t$ . See the diagram on the left-hand side in Fig. 7. The LO result for the total partonic cross section  $\sigma_{gg}^{(0)}$  reads:

$$\begin{aligned} \sigma_{gg}^{(0)}(s, m_H^2, M_t^2) &= \frac{\pi}{4v^2 N_g^2} \left(\frac{\alpha_s}{\pi}\right)^2 \delta\left(1 - \frac{m_H^2}{s}\right) \\ &\quad \times \frac{16M_t^4}{m_H^4} \left[1 + \left(1 - \frac{4M_t^2}{m_H^2}\right) \arcsin^2\left(\frac{m_H}{2M_t}\right)\right]^2, \quad (115) \end{aligned}$$

with the Higgs field vacuum expectation value  $v$ . The factor  $1/N_g^2$  stems from averaging over the number of gluons  $N_g = N_c^2 - 1 = 8$  ( $N_c$  is the number of colors).

Including higher-order corrections means not only to compute virtual but also real corrections. Meaning, one has to consider more loops as well as additional partons in the final state. For virtual corrections we have  $s = m_H^2$ , as for the LO process. Hence, for virtual corrections the three scales are not independent. It is beyond scope of present calculational technology in our field to directly compute diagrams relevant beyond NLO exactly in the three scales. However, at NNLO calculations are available, see Refs. [72–77] where the full dependence on the three scales has been reconstructed.

One alternative is to work within an effective field theory (EFT) where the top quark is integrated out by assuming  $M_t^2 \gg m_H^2, s$ . In this way, a separation of scales is achieved and the dependence on  $M_t$  is absorbed into the effective coupling  $C_1$ . We deal with a new set of Feynman rules where

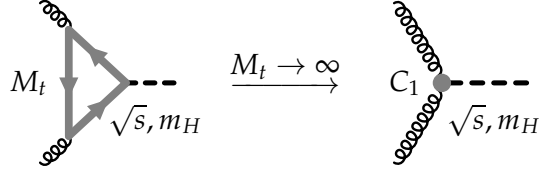


**Figure 7:** LO diagram for Higgs boson production via gluon fusion in the full theory on the left-hand side and in the EFT on the right-hand side. Curly lines represent gluons, the dashed line the Higgs boson and the thick gray lines top quarks. The transition between theories corresponds to the limit  $M_t \rightarrow \infty$  and can be visualized as contraction of the top quark loop to an effective vertex, denoted by a gray dot.

the Higgs boson couples directly to gluons. This modification is sketched in the right-hand side of Fig. 7 and makes Higgs boson production a process of Drell-Yan type where we have dependence only on  $m_H^2$  and  $s$ . Expanding Eq. (115) in the parameter  $m_H^2/M_t^2$  leads to

$$\sigma_{gg}^{(0)}(s, m_H^2, M_t^2 \rightarrow \infty) = \frac{\pi}{9v^2 N_g^2} \left(\frac{\alpha_s}{\pi}\right)^2 \delta\left(1 - \frac{m_H^2}{s}\right), \quad (116)$$

which allows us to infer  $C_1^2 = \alpha_s^2/(9\pi^2)$  at LO. We give further details on the EFT and  $C_1$  sufficient for Higgs boson production at N<sup>3</sup>LO in Section 4.2.1.

The total cross section is given in terms of squared amplitudes for the various final states at higher orders integrated over the full corresponding phase space. Instead of computing these contributions separately, one can employ the optical theorem, presented in great detail in Chapter 3. Let us take a different point of view depicted in Fig. 8. Squaring diagrams in one specific contributing amplitude generates various interference terms. Each term is interpreted as forward scattering diagram with a cut that corresponds to the final state of its dedicated amplitude. Among all squared amplitudes there are interference terms that generate the same forward scattering diagram but with different cuts.

#### 4.1.1 General procedure

In the approach we chose, that is within the EFT and using the optical theorem, we need to calculate diagrams with four external legs, two scales ( $m_H$  and  $\sqrt{s}$ ) and three loops for N<sup>3</sup>LO. We have forward scattering kinematics  $p_3 = p_1$  and  $p_4 = p_2$  where  $p_1, \dots, p_4$  are the momenta of external legs. External momenta are put on-shell  $p_1^2 = p_2^2 = 0$  and  $p_1 \cdot p_2 = s/2$ . We have only one massive propagator with the Higgs mass  $m_H$  in the diagrams but need to consider all possible cuts through the Higgs line and additional parton lines. The problem can be fully described by a single dimensionless variable  $x = m_H^2/s$ . We state our general strategy for calculating the described diagrams:

1. Integrals appearing in the set of all diagrams are reduced in “full kinematics”, that is full dependence on the variable  $x$ , to fewer and simpler “master integrals”.



$$\begin{aligned}
& \int d\Pi_1 \left| \begin{array}{c} \text{diagram 1} \\ + \\ \text{diagram 2} \\ + \dots \end{array} \right|^2 \\
& + \int d\Pi_2 \left| \begin{array}{c} \text{diagram 3} \\ + \\ \text{diagram 4} \\ + \dots \end{array} \right|^2 \\
& + \int d\Pi_3 \left| \begin{array}{c} \text{diagram 5} \\ + \\ \text{diagram 6} \\ + \dots \end{array} \right|^2 + \dots \\
& = \text{diagram 7} + \text{diagram 8} + \dots + \text{diagram 9} \\
& \quad + \dots + \text{diagram 10} + \dots + \text{diagram 11} + \dots
\end{aligned}$$

**Figure 8:** Schematics of the optical theorem applied to the inclusive cross section for Higgs boson production in the EFT. Terms abbreviated by dots stand for omitted diagrams within an order, higher orders of an amplitude or further amplitudes as a whole. The left-hand side of the equation shows the sum of partial cross sections for a Higgs boson together with zero partons, one parton and so on. Phase spaces with different multiplicity are therefore denoted by  $d\Pi_i$ . The right-hand side shows interference terms originating from squared amplitudes with phase space integrations translated to cuts. The last two interference diagrams are the same but differ in the cut that has to be taken. The first stems from an interference of diagrams in the amplitude with one additional parton, the second from the amplitude with two additional partons.

2. For these master integrals we construct a system of (in general coupled) differential equations in  $x$ .
3. As boundary conditions for these differential equations we use the “soft limit”  $x \rightarrow 1$  where only soft partons are produced besides the Higgs boson.

In Step 1 we utilize the techniques described in Chapter 2. Steps 2 and 3 are not subject of this thesis but will be discussed in the thesis of M. Höschele, see Ref. [78]. Nevertheless, we give here a very brief survey.

The method of differential equations for Feynman integrals was introduced in Refs. [79–82] and nicely reviewed in Ref. [83]. See also the recent review by Henn in Ref. [18]. The central idea is very simple: the derivative of some master integral with respect to one of its kinematic invariants (or equivalently to a dimensionless variable) raises the powers of some denom-

inators. The resulting integrals are subsequently reduced to master integrals again by the methods of Step 1. Thus, one obtains a coupled system of first order differential equations. Recently, see Ref. [84], J. Henn identified a canonical form of differential equations,

$$\frac{d}{dx} f_j(\{x_i\}, \epsilon) = \epsilon A_{jk}(\{x_i\}) f_k(\{x_i\}, \epsilon) \quad \text{with } x \in \{x_i\}, \quad (117)$$

where  $f(\{x_i\}, \epsilon)$  is a vector of master integrals and  $A(\{x_i\})$  the matrix of the coupled system. In this form, the dependence on kinematic variables  $\{x_i\}$  and the dimensional regulator  $\epsilon$  is factorized and one can thereby integrate the system order-by-order in  $\epsilon$ . The matrix  $A(\{x_i\})$  has a special form linked to the ‘‘alphabet’’ (see Section 4.3.3.1 on Page 134) of the functions appearing in the solution of  $f(\{x_i\}, \epsilon)$ . However, the existence of master integrals obeying a canonical form of differential equations is a conjecture and it is not proven that such a basis of master integrals  $f(\{x_i\}, \epsilon)$  exists for all kind of topologies at all orders. Partially systematic methods for constructing this kind of basis were developed in Refs. [19, 85] and there exists a claim for a complete algorithmic solution in Ref. [86].

In general, it is not straightforward to perform the soft expansion  $x \rightarrow 1$ . One cannot simply expand propagators under the integral sign, contributing regions of loop momenta have to be inspected carefully. In Refs. [21, 87] this task was fulfilled on completely general grounds using a geometrical formulation and providing also an algorithm called *asy.m*. Otherwise, the soft expansion has to be constructed case-by-case, as was done in Refs. [88, 89] for example. Our course of action is to perform the soft expansion in the Mellin-Barnes representation of an integral to evaluate the leading term and a few subleading terms (if possible).

#### 4.1.2 Anatomy of the total cross section

Expressions for Higgs boson production cross sections at each order expose a rich structure one can exploit to partition the computation into smaller blocks. This is inevitable, being confronted with the numbers of diagrams and topologies at N<sup>3</sup>LO being approximately 180 000 and 200.

Partonic channels are labeled by the particles in the initial state which can be quarks  $q$ , quarks of different flavor  $q'$ , antiquarks  $\bar{q}$  and gluons  $g$ . In total there are five:  $gg$  starting at LO,  $q\bar{q}$  and  $qg$  contributing on from NLO, completed by  $qq'$  and  $q\bar{q}$  opening up at NNLO. This is demonstrated in Fig. 9. Note that we need not to consider indistinguishable contributions separately. For example  $qg$ ,  $q'g$  and  $\bar{q}g$  are equivalent, as are  $qq'$  and  $q\bar{q}'$  and so forth. For the  $qq$ -channel initial states are equal and there are additional crossed diagrams compared to the  $qq'$ -channel.

With every additional order on top of the first non-vanishing order of a channel, apart from the  $gg$ -channel at tree-level, there come fermionic contributions we can distinguish by powers of the number of light quark flavors  $n_l$ . For example  $n_l$  and  $n_l^2$  in the  $qg$ -channel at N<sup>3</sup>LO. See also Tab. 3 on Page 127 and Tab. 4 on Page 149. The quark channels  $qq'$ ,  $qq$  and  $q\bar{q}$  can furthermore

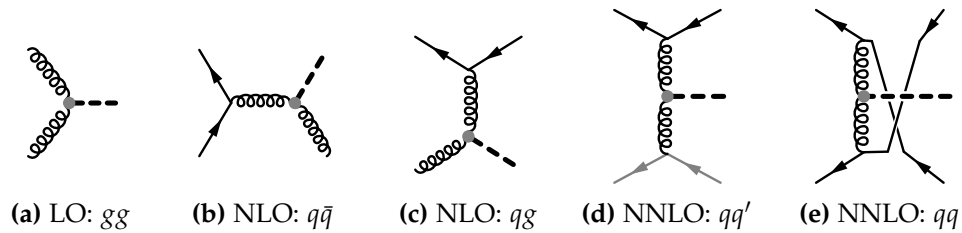


**Figure 9:** Sample diagram for each channel at its first relevant order. These are the  $gg$ -channel at LO in Fig. a, the  $q\bar{q}$ - and  $qg$ -channels at NLO in Figs. b and c, the  $qq'$ - and  $qq$ -channels at NNLO in Figs. d and e. Curly lines represent gluons, straight lines quarks, the dashed line is the Higgs boson with its effective coupling to gluons marked with a gray dotted vertex. A quark of different flavor is represented by a gray line in Fig. e. We hold on to this notation in the following.

**Table 2:** Contributions from different cuts in each partonic channel. The letter “T” for the  $gg$ -channel at LO signals that it is a Tree-level contribution. All other contributions are combinations of **Virtual** and **Real** corrections denoted by powers of “V” and “R”, respectively. T, R, VV,  $R^2$ , VRV and  $R^3$  stem from squares of amplitudes.

Channel(s)	Order			
	LO	NLO	NNLO	$N^3LO$
$qq', qq$	–	–	$R^2$	$VR^2, R^3$
$q\bar{q}, qg$	–	R	$RV, R^2$	$VRV, V^2R, VR^2, R^3$
$gg$	T	V, R	$VV, V^2, RV, R^2$	$VV^2, V^3, VRV, V^2R, VR^2, R^3$

be split into singlet and non-singlet type contributions. But this is more important for the Drell-Yan process as we will see in Section 5.2.

Furthermore, we can classify contributions within a channel by the nature of its cuts which correspond to interference terms in the modulus square of production amplitudes, see Tab. 2. We have the following interference classes of  $N^3LO$  corrections:

$VV^2$  one-loop virtual times two-loop virtual,

$V^3$  three-loop virtual times tree-level,

$VRV$  one-loop virtual with one real emission squared (self-interference),

$V^2R$  two-loop virtual with one real emission times tree-level,

$VR^2$  one-loop virtual with two real emissions times tree-level,

$R^3$  three real emissions (self-interference).

For sample diagrams see Fig. 10. Note that purely virtual corrections exist only for the  $gg$ -channel. Each purely virtual diagram can be assigned either to  $VV^2$  or  $V^3$ . On the other hand, contributions involving real radiation mix. Diagrams can have cuts of different multiplicity classes, see also Figs. 10c, 10d and 10e. Only diagrams with self-energy insertions from classes  $VRV$ ,  $V^2R$  or  $VR^2$  can possibly have a single kind of cut in

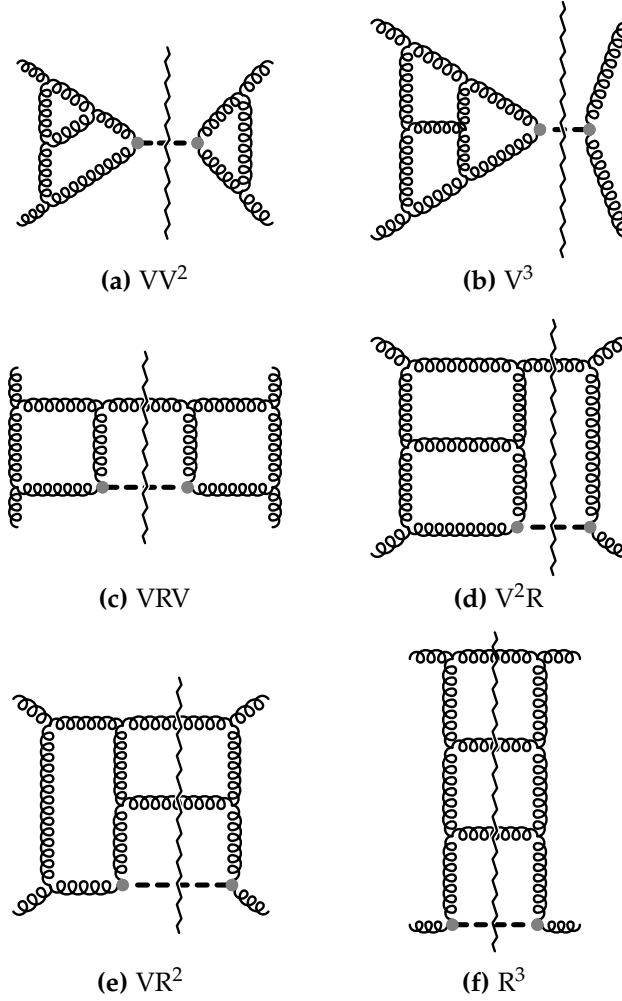


**Figure 10:** Sample diagrams from the  $gg$ -channel at  $N^3\text{LO}$ . The notation is as in Fig. 9 but with the zigzag line indicating the contribution of a specific cut. Figures a and b show purely virtual corrections, Fig. f shows a purely real correction, Figs. c, d and e show different virtual-real mixed corrections. Note that the latter have also other contributing cuts not drawn here.

In this setting we can have three kinds of singularities. Ultraviolet (UV) divergences from the loop integrations extending to infinity are removed systematically by renormalization of the strong coupling constant  $\alpha_s$  and the operator  $\mathcal{O}_1$  of the effective coupling of the Higgs boson to gluons. Soft singularities occur when a massless particle of vanishing momentum is emitted by a parton before participating in the hard process. If an initial state parton emits a parton under a vanishing angle we have a collinear singularity. Soft and collinear singularities can mix and belong both into the infrared (IR) category. UV and collinear divergences manifest themselves in simple poles  $1/\epsilon$ , whereas soft divergences come with double poles  $1/\epsilon^2$ . The soft double poles cancel by the Kinoshita-Lee-Nauenberg (KLN) theorem between virtual and real corrections once they are added. The remaining simple collinear poles are absorbed into a redefinition of the PDFs by mass factorization.

For purely virtual contributions we have  $s = m_H^2$ . Hence, they enter the partonic cross section with a factor  $\delta(1-x)$ . Real contributions to the partonic cross section diverging in the soft limit  $x \rightarrow 1$  can be identified in phase space and have the form  $(1-x)^{-1+b\epsilon}$  with some integer  $b$ . They need to be regularized properly in terms of delta-distributions  $\delta(1-x)$  and plus-distributions  $\left[\frac{\ln^k(1-x)}{1-x}\right]_+$  via the prescription

$$(1-x)^{-1+b\epsilon} = \frac{\delta(1-x)}{b\epsilon} + \left[\frac{1}{1-x}\right]_+ + b\epsilon \left[\frac{\ln(1-x)}{1-x}\right]_+ + \frac{(b\epsilon)^2}{2} \left[\frac{\ln^2(1-x)}{1-x}\right]_+ + \mathcal{O}(\epsilon^3). \quad (118)$$

This prescription will be derived in Section 4.2.2. Exactly due to Eq. (118) soft divergences coincide with double poles and come with delta-functions while collinear singularities have single poles and plus-distributions. Since only the  $gg$ -channel has a purely virtual component and the sum with real corrections is required to be finite, only the  $gg$ -channel has terms with plus-distributions in its result. All other channels are regular at the threshold for  $x = 1$ .

In the spirit of Ref. [90], let us factor out the LO dependence and denote corrections to the finite partonic cross section as

$$\sigma_{ij} = \frac{\pi C_1^2}{v^2 N_g^2} \left[ \tilde{\sigma}_{ij}^{(0)} + \frac{\alpha_s}{\pi} \tilde{\sigma}_{ij}^{(1)} + \left(\frac{\alpha_s}{\pi}\right)^2 \tilde{\sigma}_{ij}^{(2)} + \left(\frac{\alpha_s}{\pi}\right)^3 \tilde{\sigma}_{ij}^{(3)} + \mathcal{O}(\alpha_s^4) \right], \quad (119)$$

such that  $\tilde{\sigma}_{ij}^{(0)} = \delta_{ig}\delta_{jg} \delta(1-x)$ .  $C_1$  is given explicitly on Page 116.

All divergences shall be subtracted by a common UV and IR counterterm  $\delta\tilde{\sigma}_{ij}^{(k)}$  from the bare cross section  $\tilde{\sigma}_{ij}^{0,(k)}$  at each order,

$$\tilde{\sigma}_{ij}^{(k)} = \tilde{\sigma}_{ij}^{0,(k)} + \delta\tilde{\sigma}_{ij}^{(k)}, \quad (120)$$

where quantities on the right-hand side now contain only poles up to  $\mathcal{O}(\epsilon^{-k})$  since real and virtual contributions have been summed. The structure of phase space integrals in the soft limit for a cut through the Higgs line and up to  $k$  partons gives singular behaviors like

$$\left\{ (1-x)^{-2\epsilon}, (1-x)^{-3\epsilon}, \dots, (1-x)^{-2k\epsilon} \right\}. \quad (121)$$

Together with Eq. (118) and accounting also for regular terms in the limit  $x \rightarrow 1$ , we can write

$$\begin{aligned} \tilde{\sigma}_{ij}^{(k)} &= \tilde{\sigma}_{ij}^{(k),S} + \tilde{\sigma}_{ij}^{(k),R} \\ &= \delta(1-x) \tilde{\sigma}_{ij}^{(k,-1),S} + \sum_{l=0}^{2k-1} \left[ \frac{\ln^l(1-x)}{1-x} \right]_+ \tilde{\sigma}_{ij}^{(k,l),S} \\ &\quad + \sum_{l=0}^{2k-1} \ln^l(1-x) \tilde{\sigma}_{ij}^{(k,l),R}, \end{aligned} \quad (122)$$

where  $\tilde{\sigma}_{ij}^{(k,l),S}$  and  $\tilde{\sigma}_{ij}^{(k,l),R}$  denote coefficients of singular and regular terms, respectively. Analogous expansions can be written down for counterterms and bare quantities in Eq. (120).

### 4.1.3 Status of theoretical predictions

In this subsection, we give a short review of selected results gathered by several groups over the years, leading to N<sup>3</sup>LO calculations for Higgs boson production being presently in focus or providing ingredients for these calculations. For a complete review of Higgs boson production cross sections (and decay widths) we refer to Ref. [91] in case of inclusive quantities and to Ref. [92] in case of differential quantities.

**LO AND NLO CROSS SECTIONS** The LO process, see Fig. 7, has already been computed right after the beginnings of quantum field theory and the Standard Model half a century ago. It is known with exact dependence on the Higgs boson and top quark masses, see Refs. [93–96]. Also at NLO such an exact computation was realized about twenty years ago in Refs. [97–99]. For the LHC, the NLO correction has the same size as the LO cross section. The K-factor, defined as ratio of the NLO result (including LO) and the LO result, amounts roughly to two. For this reason information on NNLO corrections was mandatory.

**NNLO CORRECTIONS IN THE EFT** An exact calculation for the partonic cross section at NNLO requires massive three-loop triangle, two-loop box and one-loop pentagon amplitudes. Even nowadays, such a calculation is not feasible. The NNLO corrections were therefore obtained within the EFT about ten years ago by three independent collaborations, see Refs. [61, 100, 101]. Working out the NLO corrections in the same EFT framework, leads only to a very small deviation of about 2% relative to the exact NLO result for  $m_H < 2M_t$ . This justified the use of the EFT at NNLO. Moreover, it was observed in Ref. [100] that the majority of the NNLO corrections can be encapsulated by an expansion around the soft limit  $x \rightarrow 1$ . Already the third expansion term, proportional to  $(1 - x)^1$ , leaves an error of only 1% relative to the exact result.

**NNLO CORRECTIONS BEYOND THE EFT** Strictly speaking, since  $\sqrt{s}$  is only constrained by the beam energy that is much larger at the LHC than the top quark mass, the limit  $M_t^2 \gg s$  is not valid. However, the gluon luminosity accentuates effects at low values of the momentum fraction  $x \approx 0.1$  which could lead to a suppression in the region where  $M_t^2 \approx s$ . Nevertheless, this questions the validity of the EFT which has been addressed in Refs. [72–77, 102]. Asymptotic expansions were used in a full theory setup with the top quark to compute subleading terms in the small parameter  $m_H^2/M_t^2$ . The procedure of asymptotic expansion allows to reduce the four-loop three-scale diagrams in the full theory to products of simpler diagrams; in the sense of less loops and less scales. Virtual contributions were obtained by computing triangle graphs in Refs. [74, 75]. Real corrections were computed via the optical theorem in Ref. [72] and by computing amplitudes with one or two additional partons in Ref. [76]. These results reached up to four terms in the expansion in  $m_H^2/M_t^2$ . In Refs. [73, 77], they were matched

to the high-energy behavior of the partonic cross section first computed in Ref. [102] since in this region the  $m_H^2/M_t^2$  expansion shows no convergence. It was found that corrections due to a finite top quark mass at NNLO amount only to about 1% which encouraged the proceeding within the EFT to N<sup>3</sup>LO.

**EFFECTIVE COUPLING AND RENORMALIZATION** The Wilson coefficient  $C_1$ , also called effective coupling or matching coefficient, depends only on the masses of particles which have been integrated out. Thus, in case of the SM it depends only on the top quark mass and solely via  $\ln(\mu^2/M_t^2)$ . Three-loop results for  $C_1$  in the SM can be found in Refs. [103, 104], see also Ref. [105]. In Ref. [103] the four-loop coefficient has been inferred via a low-energy theorem from the three-loop decoupling constant of the strong coupling, whereas in Refs. [106, 107] a genuine four-loop computation lead to the same result. For N<sup>3</sup>LO Higgs boson production  $C_1$  is needed to four-loop order, viz.  $\mathcal{O}(\alpha_s^4)$ . The renormalization of the operator  $\mathcal{O}_1$ , responsible for the direct coupling of gluons to the Higgs boson, is entirely determined by the QCD beta-function, see Ref. [108]. Thus, we need only the renormalization constant of the strong coupling to three-loop order which was first published in Refs. [109, 110]. We collect necessary results for the matching coefficient  $C_1$  and the renormalization of  $\mathcal{O}_1$  in Section 4.2.1 on Page 114.

#### COLLINEAR SINGULARITIES

- The NNLO or three-loop parton splitting functions in the singlet and non-singlet cases, describing collinear emission of partons, were computed in Refs. [111, 112].
- Higher orders in the  $\epsilon$ -expansion of the NNLO master integrals were calculated in Refs. [73, 113].
- Accordingly, the NNLO cross sections have been computed to higher orders in  $\epsilon$  in Refs. [90, 114]. More specifically: at LO to  $\mathcal{O}(\epsilon^3)$ , at NLO to  $\mathcal{O}(\epsilon^2)$  and at NNLO to  $\mathcal{O}(\epsilon)$ . The LO to NNLO cross sections including higher orders in  $\epsilon$  are needed for the UV renormalization at N<sup>3</sup>LO.
- These higher  $\epsilon$ -orders, together with the NNLO splitting functions, allowed to form all convolution integrals necessary for N<sup>3</sup>LO. They were evaluated systematically in Refs. [90, 114, 115]. In Ref. [115] also results applying to the Drell-Yan process and a public code performing convolution integrals were given.
- In Ref. [114], the appearing convolution integrals were combined to proper collinear counterterms at N<sup>3</sup>LO. Including also the UV counterterms, this allowed for a prediction of the complete scale dependence at N<sup>3</sup>LO. The authors estimate the residual scale uncertainty at N<sup>3</sup>LO to lie between 2% and 8% percent.

The requirement for all poles of the known counterterm  $\delta\tilde{\sigma}_{ij}^{(k)}$  and the unknown bare cross section  $\tilde{\sigma}_{ij}^{0,(k)}$  to cancel, fixes in the finite cross section in

Eq. (120) all coefficients proportional to  $\ln^l(\mu^2/s)$  for  $1 \leq l \leq k$ . The scale dependence of  $\tilde{\sigma}_{ij}^{0,(k)}$  is caused by  $1/\epsilon^l$ -poles multiplying factors of  $(\mu^2/s)^{k\epsilon}$  which are expanded as

$$\left(\frac{\mu^2}{s}\right)^{k\epsilon} = \sum_{l=0}^{\infty} \frac{(k\epsilon)^l}{l!} \ln^l\left(\frac{\mu^2}{s}\right). \quad (123)$$

Hence, we have a system of equations from the coefficients of poles in  $\epsilon$ :

$$\tilde{\sigma}_{ij}^{0,(k)} = \left(\frac{\mu^2}{s}\right)^{k\epsilon} \sum_{l=-k}^{\infty} \epsilon^l \tilde{\sigma}_{ij}^{0,(k,l)} = -\delta\tilde{\sigma}_{ij}^{(k)} = -\sum_{l=-k}^{\infty} \epsilon^l \delta\tilde{\sigma}_{ij}^{(k,l)}, \quad (124)$$

where we defined coefficients  $\tilde{\sigma}_{ij}^{0,(k,l)}$  with  $(\mu^2/s)^{k\epsilon}$  unexpanded. We can solve this system for the coefficients of the  $\ln^l(\mu^2/s)$  terms appearing in the finite contribution  $\tilde{\sigma}_{ij}^{(k,0)}$ . The highest power of the renormalization scale logarithm  $\ln^k(\mu^2/s)$  is fixed by the highest pole of the counterterm  $\delta\tilde{\sigma}_{ij}^{(k,-k)}$ . The next lower power  $\ln^{k-1}(\mu^2/s)$  can be determined from the two lowest poles  $\delta\tilde{\sigma}_{ij}^{(k,-k)}$  and  $\delta\tilde{\sigma}_{ij}^{(k,-k+1)}$ . This reconstruction of the renormalization scale dependence at N<sup>3</sup>LO was done in Ref. [114].

### N<sup>3</sup>LO RESULTS

- The Gluon and quark form factors to three loops were calculated in Refs. [116, 117]. The gluon form factor gives the purely virtual contributions  $VV^2$  and  $V^3$  in Figs. 10a and 10b. (The quark form factor is the counter part for the Drell-Yan process.)
- In Ref. [89], contributions of type VRV in Fig. 10c were computed in full kinematics as expansion in  $\epsilon$  and to all orders in  $\epsilon$  for the first coefficients in the expansion around the threshold. In Ref. [118], coefficients in the threshold expansion were computed to  $\mathcal{O}(\epsilon)$  and then used to reconstruct the result with full  $x$ -dependence.
- Corrections to the single-soft current operator to two-loop order were computed in Ref. [119] to  $\mathcal{O}(\epsilon^2)$  and even to all orders in  $\epsilon$  in Ref. [120]. This quantity is universal in the sense that it describes the emission of a soft parton in presence of two hard partons. It describes contributions of type V<sup>2</sup>R in Fig. 10d in the soft limit, that is to the coefficient of  $\delta(1-x)$  in Eq. (122).
- The V<sup>2</sup>R contributions were computed in full kinematics in Ref. [121]. In Ref. [122], the two-loop splitting amplitudes were computed. They describe the factorization of QCD when two external partons become collinear. This result was also applied in order to obtain the full  $x$ -dependence for the V<sup>2</sup>R contribution.
- The first terms in the threshold expansion for type VR<sup>2</sup> contributions, shown in Fig. 10e, were considered in Refs. [123, 124]. In Ref. [124] they have been calculated to all orders in  $\epsilon$ .



- The  $R^3$  type contributions, exemplified in Fig. 10f, are known only as an expansion to second order around the threshold, see Ref. [88]. The relevant region for an expansion by regions on integrand level has also been identified in Ref. [88]. This could be proof beneficial in order to calculate subleading terms in the expansion.
- In Ref. [19], all master integrals of a particular topology of  $R^3$  type, the “sea snake”, have been calculated retaining also full  $x$ -dependence. There, also an algorithm has been devised to transform coupled systems of differential equations into canonical form.
- In Refs. [123, 125], the complete first and second terms in the threshold expansion are given. They include contributions from all final state multiplicities in Fig. 10, see also Ref. [126]. The first term of the expansion around  $x \rightarrow 1$  is the complete singular part in Eq. (122), that is all coefficients of delta- and plus-distributions. The second term is given by the coefficient  $\tilde{\sigma}_{ij}^{(k,l),R}$  of  $\ln^0(1-x)$ . The authors of Refs. [123, 125] claim that the situation at  $N^3LO$  differs substantially from NNLO where the soft expansion provided for a good approximation to the full result. According to them, the soft expansion in its currently available depth does not allow to make a reliable prediction. From the full  $x$ -dependence of all  $N^3LO$  counterterms and the VRV and  $V^2R$  contributions, the authors of Ref. [125] could also determine the coefficients  $\tilde{\sigma}_{ij}^{(3,l),R}$  for  $l \in \{3, 4, 5\}$  in Eq. (122) for full kinematics.

**RESUMMATIONS** Driven by the large NLO and NNLO corrections, over the last ten years many groups have contributed to various resummed results aiming to improve the convergence of the perturbation series. Before the NNLO calculation was available, this has already been done for the NLO case in Ref. [105]. The starting point is to identify certain structures recurring at each order in the perturbation series, such as logarithms or terms proportional to  $\pi^2$ . Then, these structures are resummed to all orders in the perturbative expansion which is formally equivalent to a redefinition of the expansion parameter. Higgs production seems to be dominated by contributions where only soft additional partons are emitted. This is the reason why the expansion around the threshold  $x = 1$  works so well up to NNLO. Resummation of soft radiation effects were studied in Refs. [127–136] to improve the fixed-order calculations. Soft radiation is related to the structure of Eq. (122) and resummations give access to the contributions in the threshold expansion. Therefore, the coefficients of plus-distributions  $\tilde{\sigma}_{ij}^{(k,l),S}$  were already known from Ref. [129], constituting the soft  $N^3LO$  approximation. Since the coefficient of the delta-function  $\tilde{\sigma}_{ij}^{(k,0),S}$  was calculated in Ref. [123] it has also been taken into account in Refs. [137–140] to construct resummations based on this  $N^3LO$  soft-virtual approximation. The mentioned studies differ mostly in the precise resummation prescription (often performed in Mellin space) or in the way knowledge on the top quark mass dependence and on the high-energy limit  $s \rightarrow \infty$  is included. In Refs. [130, 132, 133],

resummations were performed by working in the soft-collinear effective theory (SCET). “Conventional” resummation and SCET at NNLO are compared in Ref. [141]. The coefficients  $\tilde{\sigma}_{ij}^{(3,l),R}$  for  $l \in \{3, 4, 5\}$  calculated in Ref. [125] were predicted correctly in Ref. [140].

In view of current results for the threshold expansion, see Refs. [123, 125, 126], and the ambiguities involved in resummations, a computation of the N<sup>3</sup>LO cross section with full dependence on  $x$  or more terms in the soft expansion are still required. Missing ingredients to the former are only due to contributions of types VR<sup>2</sup> and R<sup>3</sup>.

## 4.2 CALCULATIONAL TECHNIQUES

We briefly discuss the two essential theoretical techniques for this calculation already mentioned in the previous section.

### 4.2.1 Effective theory

The effective field theory (EFT) where the top quark is integrated out is an indispensable ingredient for computing higher order corrections to Higgs boson production. The number of scales, loops and also diagrams is diminished in the EFT. The heavy top quark EFT is constructed via an operator product expansion (OPE).

In the first step, an effective Lagrangian  $\mathcal{L}'$  is assumed that has the same structure of the full Lagrangian  $\mathcal{L}$  but without dependence on the heavy fields  $\{\Phi_i\}$ . The fields  $\{\phi'_i\}$  and parameters  $\{x'_i\}$  in the EFT are related to light fields  $\{\phi_i\}$  and parameters  $\{x_i\}$  in the full theory via so-called decoupling relations:

$$\phi'_i = \zeta_i \phi_i, \quad x'_i = \zeta_i x_i. \quad (125)$$

The decoupling constants  $\{\zeta_i\}$  are defined analogously to renormalization constants but are finite.

In the second step, local operators  $\{\mathcal{O}_i\}$  are constructed from the light fields  $\{\phi_i\}$  to mediate interactions due to heavy fields  $\{\Phi_i\}$  that were integrated out. The  $\{\mathcal{O}_i\}$  appear in the effective Lagrangian multiplied by corresponding Wilson coefficients  $\{C_i\}$ . The  $\{C_i\}$ , also referred to as effective couplings, contain the residual dependence on the heavy degrees of freedom (the same is true for the  $\{\zeta_i\}$ ). In general, the  $\{\mathcal{O}_i\}$  mix under renormalization, as do the  $\{C_i\}$ .

In our case of Higgs boson production in the  $M_t \rightarrow \infty$  EFT only one composite operator is relevant:

$$\mathcal{O}_1 = \frac{1}{4} G_{\mu\nu}^a G^{a,\mu\nu}, \quad (126)$$

where  $G_{\mu\nu}^a$  is the gluon field strength tensor. The other operators, see for example Refs. [103, 104], are either not gauge-invariant and do not contribute

to observables or are suppressed by light quark masses. Hence, we calculate within five-flavor QCD with an additional interaction term:

$$\mathcal{L} = \mathcal{L}_{\text{QCD}}^{(5)} + \mathcal{L}_{Y,\text{eff}} \quad \text{with} \quad \mathcal{L}_{Y,\text{eff}} = -\frac{H}{v} C_1 \mathcal{O}_1, \quad (127)$$

where  $H$  is the Higgs field and  $v$  its vacuum expectation value.

#### 4.2.1.1 Renormalization

The renormalization of all  $\{\mathcal{O}_i^0\}$  and  $\{C_i\}$  is given in terms of QCD renormalization constants, see Ref. [108]. For  $\mathcal{O}_1^0$  and  $C_1^0$  it is entirely determined by the QCD beta-function and related via

$$C_1^0 \mathcal{O}_1^0 = (Z_{\mathcal{O}_1}^{-1} C_1^0) (Z_{\mathcal{O}_1} \mathcal{O}_1^0) = C_1 \mathcal{O}_1, \quad (128)$$

where

$$\begin{aligned} Z_{\mathcal{O}_1} &= 1 + \alpha_s \frac{\partial \ln Z_{\alpha_s}}{\partial \alpha_s} \\ &= 1 - \frac{\alpha_s}{\pi} \frac{\beta_0}{\epsilon} + \left(\frac{\alpha_s}{\pi}\right)^2 \left(\frac{\beta_0^2}{\epsilon^2} - \frac{\beta_1}{\epsilon}\right) \\ &\quad + \left(\frac{\alpha_s}{\pi}\right)^3 \left(-\frac{\beta_0^3}{\epsilon^3} + \frac{2\beta_0\beta_1}{\epsilon^2} - \frac{\beta_2}{\epsilon}\right) + \mathcal{O}(\alpha_s^4). \end{aligned} \quad (129)$$

$$(130)$$

The perturbative expansion of the QCD beta-function up to three loops reads, see Refs. [109, 110, 142]:

$$\begin{aligned} \beta(\alpha_s) &= -\left(\frac{\alpha_s}{\pi}\right)^2 \sum_{i=0}^{\infty} \left(\frac{\alpha_s}{\pi}\right)^i \beta_i = \\ &\quad -\left(\frac{\alpha_s}{\pi}\right)^2 \left[ \beta_0 + \frac{\alpha_s}{\pi} \beta_1 + \left(\frac{\alpha_s}{\pi}\right)^2 \beta_2 + \mathcal{O}(\alpha_s^3) \right], \end{aligned} \quad (131)$$

where

$$\beta_0 = \frac{1}{4} \left( \frac{11}{3} C_A - \frac{4}{3} T_F n_l \right), \quad (132)$$

$$\beta_1 = \frac{1}{16} \left( \frac{34}{3} C_A^2 - \frac{20}{3} C_A T_F n_l - 4 C_F T_F n_l \right), \quad (133)$$

$$\begin{aligned} \beta_2 &= \frac{1}{64} \left( \frac{2857}{54} C_A^3 - \frac{1415}{27} C_A^2 T_F n_l - \frac{205}{9} C_A C_F T_F n_l + \frac{158}{27} C_A T_F^2 n_l^2 \right. \\ &\quad \left. + 2 C_F^2 T_F n_l + \frac{44}{9} C_F T_F^2 n_l^2 \right). \end{aligned} \quad (134)$$

Here and in the following:

$$C_F = \frac{N_c^2 - 1}{2N_c} = \frac{N_g}{2N_c} = \frac{4}{3}, \quad C_A = N_c = 3, \quad (135)$$

denote the Casimir invariants of the  $SU(N_c)$  gauge group in fundamental and adjoint representation, respectively.  $T_F = 1/2$  is the normalization of the trace in fundamental representation.  $N_c = 3$  is the number of colors,  $N_g = N_c^2 - 1 = 8$  the number of gluons or generators in the adjoint representation.

## 4.2.1.2 Matching coefficient

In principle,  $C_1$  can be computed by matching any Green's function involving  $\mathcal{O}_1$  calculated in the EFT to its counter-part in the full theory. This matching is performed in the limit of vanishing external momenta  $p_i = 0$ , justified by  $M_t \rightarrow \infty$ . One possible choice is the computation of corrections to the vertex of two gluons and a Higgs boson for external momenta set to zero, see Fig. 7 on Page 104. See Ref. [104] for a comprehensive explanation of the matching procedure between full and effective theory.

Furthermore, an alternative approach to calculate  $C_1$  is via the low-energy theorem (LET), see Refs. [103, 104, 143], that relates  $C_1$  to the decoupling constant of the strong coupling  $\zeta_{\alpha_s}$  and reads for renormalized quantities:

$$C_1 = -\frac{M_t^2}{2} \frac{\partial \ln \zeta_{\alpha_s}}{\partial M_t^2}. \quad (136)$$

This is possible since matching coefficients and decoupling constants are both calculated via the same set of Green's functions.  $\zeta_{\alpha_s}$  depends only via logarithms  $\ln^i(\mu^2/M_t^2)$  on the top quark mass. These logarithms can be reconstructed via renormalization group methods to one order higher than  $\zeta_{\alpha_s}$  is available (currently four loops, see Refs. [106, 107]). Therefore, a five loop expression is known for  $C_1$  involving, however, presently unknown coefficients of the beta-function.

The LET can also be motivated by the observation that

$$m_t^2 \frac{\partial}{\partial m_t^2} \frac{1}{q - m_t} = \frac{1}{q - m_t} \frac{m_t}{2} \frac{1}{q - m_t}. \quad (137)$$

The derivative acting on a top quark propagator generates the top quark Yukawa vertex with nullified momentum for the Higgs boson. This connects for example the gluon self-energy which enters  $\zeta_{\alpha_s}$  and the triangle graph in Fig. 7 on Page 104 which enters  $C_1$ .

The matching coefficient  $C_1$  expressed by the strong coupling with five active flavors  $\alpha_s = \alpha_s^{(5)}$  and the on-shell mass of the top quark  $M_t$  up to  $\mathcal{O}(\alpha_s^3)$  reads:

$$\begin{aligned} C_1 = & -\frac{\alpha_s}{3\pi} \left\{ 1 + \frac{\alpha_s}{\pi} \left( -\frac{3}{4}C_F + \frac{5}{4}C_A \right) \right. \\ & + \left( \frac{\alpha_s}{\pi} \right)^2 \left[ \frac{27}{32}C_F^2 - \frac{25}{12}C_FC_A - \frac{1}{12}C_FT_F + \frac{1063}{576}C_A^2 - \frac{5}{96}C_AT_F \right. \\ & \quad \left. + T_F n_l \left( -\frac{5}{16}C_F - \frac{47}{144}C_A + \frac{1}{2}C_F \ln \left( \frac{\mu^2}{M_t^2} \right) \right) \right. \\ & \quad \left. \left. + \left( -\frac{11}{16}C_FC_A + \frac{7}{16}C_A^2 \right) \ln \left( \frac{\mu^2}{M_t^2} \right) \right] \right\}. \quad (138) \end{aligned}$$

Results up to  $\mathcal{O}(\alpha_s^4)$  needed for N<sup>3</sup>LO Higgs boson production can be found in, e.g., Refs. [103, 104, 106, 107].

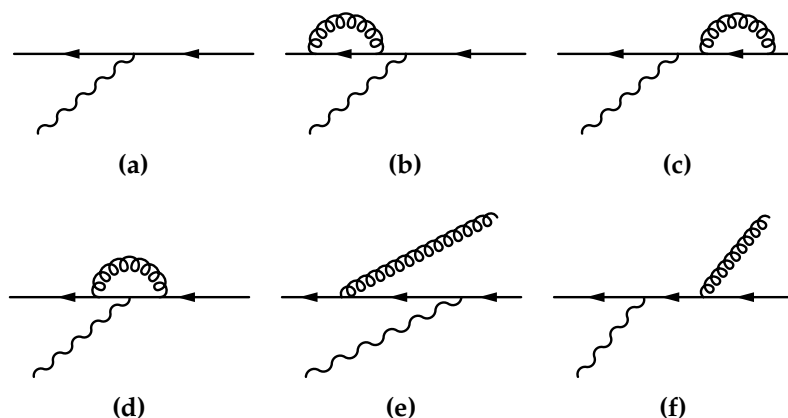


**Figure 11:** Relevant diagrams for scattering of a virtual photon off a quark (partonic subprocess to DIS) at tree-level in Fig. a and at NLO in Figs. b, c, d, e and f. Figures b, c and d show virtual propagator and vertex corrections, Figs. e and f show corrections due to real radiation.

#### 4.2.2 Mass factorization

There are two types of IR singularities which can both be linked to special configurations of momenta in a diagram: soft singularities (vanishing energy of a particle) and collinear singularities (vanishing angle between particles).

There are general theorems, the Bloch-Nordsieck theorem for QED and the Kinoshita-Lee-Nauenberg theorem for QCD, that state the cancellation of purely soft singularities in the sum of virtual and real contributions to a scattering process.

Mass factorization terms the systematic removal of collinear infrared singularities from partonic cross sections. These divergences are present in *massless* QCD and universal for all processes computed in this approximation. In this sense, mass factorization accomplishes for these IR singularities the same as renormalization does for UV singularities.

##### 4.2.2.1 Singular structure

To get a rough idea, consider deep inelastic scattering (DIS) of an electron  $e$  off a proton  $p$ :  $e + p \rightarrow e + X$  where  $X$  is a hadronic state subject to further decays. The partonic subprocess is scattering of a virtual photon  $\gamma^*$  off a quark  $q$ :  $q(p) + \gamma^*(q) \rightarrow q(p')$  beginning at Born level,  $q(p) + \gamma^*(q) \rightarrow q(p') + g(p_g)$  starting at NLO and so on. We indicated the momenta of the respective particles in parentheses. There are real and virtual corrections to the tree-level process, as one can see in Fig. 11. We do not give a rigorous treatment of these diagrams here. Detailed discussions can instead be found in most textbooks on collider physics, e.g. Refs. [144, 145].

Taking a closer look at the  $t$ -channel type real radiation diagram in Fig. 11e, we see that the propagator carries the momentum  $p - p_g$ . If we parametrize

the external momenta in the center-of-mass system (CMS) of the incoming momenta  $p$  and  $q$ , we have

$$p = |\vec{p}| (1, 0, 0, 1), \quad p_g = |\vec{p}_g| (1, 0, -\sin \theta, -\cos \theta). \quad (139)$$

The angle between the spacial components of  $p$  and  $p'$  is given by  $\theta$ . Since  $p'$  and  $p_g$  always point in opposite directions, a single parameter  $\theta$  suffices to describe the angular dependence in these kinematics. Therefore, the denominator of the propagator with momentum  $p - p_g$  becomes

$$(p - p_g)^2 = -2p \cdot p_g = -2|\vec{p}| |\vec{p}_g| (1 + \cos \theta), \quad (140)$$

leading to two different kinds of divergences which are called:

**Soft** for vanishing energy of the additionally emitted particle (in this case: a gluon with  $|\vec{p}_g| \rightarrow 0$ ),

**Collinear** for configurations of parallel momenta (here: quark and gluon momenta are parallel,  $\vec{p} \parallel \vec{p}_g$  or  $\cos \theta \rightarrow -1$ ).

As for UV divergences, dimensional regularization (DREG) is used to cope with above soft-collinear divergences. A calculation of the NLO diagrams in Fig. 11 involves bubble (Figs. 11b and 11c) and triangle (Fig. 11d) loop integrals for the virtual contributions. The real contributions at NLO require a two-particle phase space integration (Figs. 11e and 11f).

Bubble integrals with external momentum  $p_1^2 \neq 0$  contribute via self-energy insertions in the quark propagator. They contain only simple poles in  $\epsilon$ , see Example 17 on Page 32:

$$\int dk_1^D \frac{1}{k_1^2} \frac{1}{(k_1 + p_1)^2} \sim \frac{\Gamma^2(1 - \epsilon)}{\Gamma(2 - 2\epsilon)} \frac{(-p_1^2)^{-\epsilon}}{\epsilon}. \quad (141)$$

The computation of virtual vertex corrections involves scalar triangle diagrams with incoming momenta  $p_1^2 = 0$ ,  $p_2^2 \neq 0$  and outgoing momentum  $p_3^2 = (p_1 + p_2)^2 = 0$  which have double poles in  $\epsilon$ :

$$\int dk_1^D \frac{1}{k_1^2} \frac{1}{(k_1 + p_1)^2} \frac{1}{(k_1 - p_2)^2} \sim \frac{\Gamma^2(1 - \epsilon)}{\Gamma(1 - 2\epsilon)} \frac{(-p_2^2)^{-1-\epsilon}}{\epsilon^2}. \quad (142)$$

Both types of integrals can be evaluated easily in an expansion in  $\epsilon$  using Feynman parameters (presented in Section 2.3). We extracted all poles in  $\epsilon$  from the Gamma-functions, defined in Eq. (47) on Page 32, using the identity

$$\Gamma(1 + z) = z\Gamma(z). \quad (143)$$

Real radiation corrections demand for two-particle phase space integrations. The Lorentz invariant two-particle phase space in  $D = 4 - 2\epsilon$  dimensions reads:

$$\int d\Pi_2 = \int dp'^D dp_g^D (2\pi)^D \delta(p + q - p' - p_g)$$

$$\sim s^{-\epsilon} \frac{1}{\Gamma(1-\epsilon)\Gamma(1+\epsilon)} \int_0^1 dy \frac{1}{[y(1-y)]^\epsilon}, \quad (144)$$

where  $y = (1 + \cos \theta)/2$  contains the dependence on the polar angle  $\theta$  introduced earlier. Contributions of the type as in Fig. 11f with propagators like Eq. (140) give for example the integral

$$\int_0^1 dy \frac{1}{[y(1-y)]^\epsilon} \frac{1}{y} = -\frac{\Gamma^2(1-\epsilon)}{1-2\epsilon} \frac{1}{\epsilon} \quad (145)$$

which has a simple pole in  $\epsilon$ . This still has to be combined with the factors  $s^{-\epsilon}$  and  $1/(|\vec{p}| |\vec{p}_g|)$ . With the virtuality of the photon  $q^2 = -Q^2$  and the variable  $z$  defined as the fraction of the initial quark momentum that is probed by the photon  $p - p_g = zp$ , these factors give rise to

$$\frac{s^{-\epsilon}}{|\vec{p}| |\vec{p}_g|} \sim (1-z)^{-1-\epsilon}. \quad (146)$$

For details on the kinematics describing DIS, let us refer to Ref. [144]. We simply want to point out that Eq. (146) has to be expanded via Eq. (118) and combined with Eq. (145) also leads to a double pole in  $\epsilon$ . If the propagator were not soft, the factor  $(1-z)^{-1}$  would be absent and the divergence purely collinear.

In the actual calculation the numerators of diagrams involve also traces over the gamma-matrices giving non-singular terms in  $\epsilon$  and cancellation of poles may occur. We just wanted to show how singular different divergences can possibly be:

**Soft** divergences lead to double poles  $1/\epsilon^2$ ,

**Collinear** divergences lead to simple poles  $1/\epsilon$ .

The former may occur for vanishing energy of propagators, regardless whether they appear in a loop integral or a phase space integral.

#### 4.2.2.2 Redefinition of the PDFs

The sum of the Born contribution and all NLO corrections gives for the partonic structure function  $F_2^0$ , see Refs. [144, 145] for its precise definition, a result which is free of  $1/\epsilon^2$ -poles but not of  $1/\epsilon$ -poles:

$$\frac{F_2^0(z, Q^2)}{x} = \delta(1-z) - \frac{\alpha_s}{\pi} \left\{ P_{qq}(z) \left[ \frac{1}{\epsilon} + \ln \left( \frac{\mu_r^2}{\mu_f^2} \right) \right] + (\dots) \right\}, \quad (147)$$

where  $x = Q^2/(2P \cdot q)$  is the Bjorken variable and  $x/z$  is the momentum fraction of the proton passed to the quark  $p = x/z P$ . Contributions with a pole were identified with the quark-quark splitting function  $P_{qq}$ , given below in Eq. (181). We introduced the *factorization scale*  $\mu_f$ , not to be confused with the renormalization scale  $\mu_r$ . All terms collected in ellipses are finite and can

depend on the ratios of  $\mu_r^2$ ,  $\mu_f^2$ , and  $Q^2$ . The hadronic structure function  $F_{2,h}$  is obtained after weighting  $F_2^0$  with the quark distribution function  $\phi_q^0$ :

$$\frac{F_{2,h}(x, Q^2)}{x} = \int_x^1 \frac{dz}{z} \phi_q^0\left(\frac{x}{z}\right) \frac{F_2^0(z, Q^2)}{x}, \quad (148)$$

where the superscript 0 indicates bare quantities.

Formally, the  $1/\epsilon$ -term in Eq. (147) can be absorbed into the quark distribution  $\phi_q^0$  by defining its “mass factorized” version  $\phi_q$ :

$$\begin{aligned} \phi_q(x) &= \phi_q^0(x) - \frac{\alpha_s}{\pi} \int_x^1 \frac{dz}{z} \phi_q^0\left(\frac{x}{z}\right) \\ &\times \left\{ P_{qq}(z) \left[ \frac{1}{\epsilon} + \ln\left(\frac{\mu_r^2}{\mu_f^2}\right) \right] + (\dots) \right\}, \end{aligned} \quad (149)$$

where  $(\dots)$  stands for the constant finite terms absorbed into the redefinition of quantities within the  $\overline{\text{MS}}$ -scheme. We insert Eqs. (147) and (149) into Eq. (148) to find

$$\begin{aligned} \frac{F_{2,h}(x, Q^2)}{x} &= \int_x^1 \frac{dz}{z} \phi_q\left(\frac{x}{z}\right) \left[ \delta(1-z) - \frac{\alpha_s}{\pi} C_q(z) \right] \\ &= \int_x^1 \frac{dz}{z} \phi_q\left(\frac{x}{z}\right) \frac{F_2(z, Q^2)}{x}, \end{aligned} \quad (150)$$

with the so-called coefficient function  $C_q$  which is finite since collinear singularities have been factorized off. Notice that  $C_q$  depends on  $\mu_r$  and  $\mu_f$ . The expression in brackets in the first line of Eq. (150) is  $F_2/x$ , the finite version of  $F_2^0/x$ .

**CONVOLUTION INTEGRALS** The convolution integral is usually abbreviated with the symbol  $\otimes$  and defined as

$$\begin{aligned} [f \otimes g](x) &= \int_0^1 dx_1 dx_2 \delta(x - x_1 x_2) f(x_1) g(x_2) \\ &= \int_x^1 \frac{dx_1}{x_1} f(x_1) g\left(\frac{x}{x_1}\right). \end{aligned} \quad (151)$$

The lower integration bound  $x$  in the second line of Eq. (151) is due to the initial integration bounds of  $[0, 1]$ . Note that convolutions are commutative. This notation allows for more compact formulae.

#### 4.2.2.3 DGLAP evolution equation

We can rewrite Eq. (149) with the abbreviation introduced in Eq. (151):

$$\phi_q(x) = \left[ \Gamma_{qq} \otimes \phi_q^0 \right](x), \quad (152)$$

introducing the “transition function”  $\Gamma_{qq}$ :

$$\Gamma_{qq}(x) = \delta(1-x) - \frac{\alpha_s}{\pi} \left\{ P_{qq}(x) \left[ \frac{1}{\epsilon} + \ln\left(\frac{\mu_r^2}{\mu_f^2}\right) \right] + (\dots) \right\}. \quad (153)$$



As bare quantity,  $\phi_q^0$  does not depend on the scale  $\mu_f$  where the factorization is performed. Thus, we can *motivate* the DGLAP (Dokshitzer-Gribov-Lipatov-Altarelli-Parisi) evolution equation at NLO:

$$\begin{aligned} \frac{d}{d\ln \mu_f^2} \phi_q(x) &= \left[ \frac{d\Gamma_{qq}}{d\ln \mu_f^2} \otimes \phi_q^0 \right](x) \\ &= \left[ \frac{d\Gamma_{qq}}{d\ln \mu_f^2} \otimes \Gamma_{qq}^{-1} \otimes \phi_q \right](x) = \frac{\alpha_s}{\pi} [P_{qq} \otimes \phi_q](x). \end{aligned} \quad (154)$$

#### CONCLUDING REMARKS

- It is not sufficient to consider only quark-quark transitions. The distributions of all partons are coupled by the splitting functions  $P_{ij}$ :

$$\frac{d}{d\ln \mu_f^2} \phi_q = \frac{\alpha_s}{\pi} [P_{qq} \otimes \phi_q](x) + \frac{\alpha_s}{\pi} [P_{qg} \otimes \phi_g](x), \quad (155)$$

$$\frac{d}{d\ln \mu_f^2} \phi_g = \frac{\alpha_s}{\pi} [P_{gq} \otimes \phi_q](x) + \frac{\alpha_s}{\pi} [P_{gg} \otimes \phi_g](x). \quad (156)$$

See also Fig. 12. This can be written as single matrix equation in the space of parton species:

$$\frac{d}{d\ln \mu_f^2} \phi_i = \frac{\alpha_s}{\pi} [P_{ij} \otimes \phi_j](x). \quad (157)$$

Only (flavor) non-singlet quark distributions evolve independently from the singlet distributions of quarks and gluons.

- Solving the DGLAP equations corresponds to resummation of  $\alpha_s \ln(\mu_f^2/Q^2)$  contributions. These can be thought of as cascades or chains of multiple splittings, see Fig. 12.
- Replacing  $\alpha_s$  in Eq. (154) with the running coupling  $\alpha_s(Q^2)$  accounts for leading logarithmic contributions from vertex and propagator insertions.
- The DGLAP equation can be proven rigorously to all orders in perturbation theory with an OPE.

**DELTA- AND PLUS-DISTRIBUTIONS** Results for partonic cross sections and splitting functions can contain delta- and plus-distributions since the conversion to hadronic cross sections involves convolution integrals with the PDFs. Both distributions are a remnant of the phase space integration: the delta-distribution alone in case of purely virtual corrections that come with a one-particle phase space and a combination of delta- and plus-distributions in case of real corrections with multiple additional particles in the final state.

The definition of the plus-distribution reads:

$$\int_0^1 dx \left[ \frac{\ln^i(1-x)}{1-x} \right]_+ f(x) = \int_0^1 dx \frac{\ln^i(1-x)}{1-x} [f(x) - f(1)], \quad (158)$$

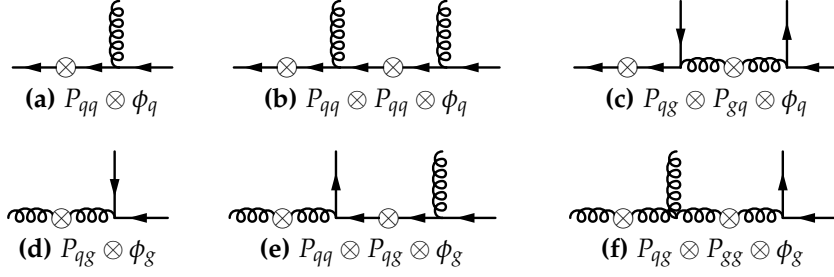


**Figure 12:** Sketch of the coupled evolution of parton distributions exemplified by the quark case. The left-most lines in each diagram can be thought of as the parton distributions on the right-hand side of Eq. (155). These are convoluted with splitting functions  $P_{ij}$  which is represented by the symbol  $\otimes$ . The right-most lines are then the quark distribution on the left-hand side of Eq. (155). Figures a and d correspond to logarithmic contributions to the evolution. Figures b, c, e and f correspond to double-logarithmic contributions.

where  $f(x)$  is a smooth test function and the effect is subtraction of the divergence at  $x = 1$ . One often finds the alternative notation

$$\mathcal{D}_i^+(1-x) = \left[ \frac{\ln^i(1-x)}{1-x} \right]_+ . \quad (159)$$

In general, products of regular functions in the limit  $x \rightarrow 1$  and plus-distributions can be split into terms, each completely regular or proportional to a plus-distribution.

**Example 45.** Using the definition in Eq. (158) it is easy to show that

$$\begin{aligned} x \left[ \frac{\ln^i(1-x)}{1-x} \right]_+ &= \left[ \frac{\ln^i(1-x)}{1-x} \right]_+ - \ln^i(1-x), \\ \frac{1}{x} \left[ \frac{\ln^i(1-x)}{1-x} \right]_+ &= \left[ \frac{\ln^i(1-x)}{1-x} \right]_+ + \frac{\ln^i(1-x)}{x}. \end{aligned}$$

These formulae (and similar ones for other regular functions) can be applied repeatedly to separate regular and irregular behavior of expressions. This functionality is also implemented in the package MT, see Ref. [115].

The expansion in Eq. (118) can be motivated by the following chain of equations, see also Ref. [146]:

$$\begin{aligned} &\int_0^1 dx (1-x)^{-a+b\epsilon} f(x) \\ &= \int_0^1 dx (1-x)^{-a+b\epsilon} [f(x) - f(1)] + \int_0^1 dx (1-x)^{-a+b\epsilon} f(1) \\ &= \int_0^1 dx (1-x)^{-a} \left[ \sum_{i=0}^{\infty} \frac{(b\epsilon)^i}{i!} \ln^i(1-x) \right] [f(x) - f(1)] + \frac{f(1)}{1-a+b\epsilon} \end{aligned}$$

$$\begin{aligned}
 &= \int_0^1 dx \left\{ \sum_{i=0}^{\infty} (1-x)^{1-a} \frac{(b\epsilon)^i}{i!} \left[ \frac{\ln^i(1-x)}{1-x} \right]_+ f(x) \right. \\
 &\quad \left. + \frac{\delta(1-x)}{1-a+b\epsilon} f(x) \right\}. \tag{160}
 \end{aligned}$$

In the first step, we split off the divergency for  $\epsilon = 0$  and  $x \rightarrow 1$ . In the second step, we wrote a Taylor series in  $\epsilon$  for the first terms and integrated the last term. In the last step, we identified the definitions of the delta- and plus-distributions. Thus, we have

$$(1-x)^{-a+b\epsilon} = \frac{\delta(1-x)}{1-a+b\epsilon} + (1-x)^{1-a} \sum_{i=0}^{\infty} \frac{(b\epsilon)^i}{i!} \left[ \frac{\ln^i(1-x)}{1-x} \right]_+. \tag{161}$$

Equation (118) is just the special case of Eq. (161) for  $a = 1$ . Plus-distributions enter partonic cross sections and splitting functions through the expansion of  $(1-x)^{-1+b\epsilon}$  factors from the phase space in DREG via Eq. (161). Hence, divergences of the form  $1/(1-x)$  in the unregularized phase space are re-expressed as  $\delta(1-x)/\epsilon + \dots$  with regulator  $\epsilon$ .

#### 4.2.2.4 Parton splitting functions

Let us briefly address the parton splitting functions at higher orders since they will be an important ingredient in what follows. In principle, they can be extracted from each process that shows collinear divergences. The easiest choice is deep inelastic scattering of a probe particle on a parton.

The distributions  $\phi_{q_i}$  and  $\phi_{\bar{q}_i}$  of quarks  $q_i$  and antiquarks  $\bar{q}_i$  have hadron dependent ‘‘valence’’ parts  $\phi_{q_i}^V$  and  $\phi_{\bar{q}_i}^V$ , as well as independent ‘‘sea’’ parts  $\phi_{q_i}^S$  and  $\phi_{\bar{q}_i}^S$ . Hence, one can write

$$\phi_{q_i} = \phi_{q_i}^V + \phi_{q_i}^S, \quad \phi_{\bar{q}_i} = \phi_{\bar{q}_i}^V + \phi_{\bar{q}_i}^S. \tag{162}$$

Accordingly, the quark and antiquark splitting functions  $P_{q_i\bar{q}_j}$  and  $P_{q_i q_j}$  are, using charge conjugation,

$$P_{q_i q_j} = P_{\bar{q}_i \bar{q}_j} = \delta_{ij} P_{qq}^V + P_{qq}^S, \quad P_{q_i \bar{q}_j} = P_{\bar{q}_i q_j} = \delta_{ij} P_{q\bar{q}}^V + P_{q\bar{q}}^S. \tag{163}$$

The coupled evolution equations for the PDFs are further simplified by a decomposition of quark and antiquark distributions into singlet and non-singlet under the  $SU(n_l)$  flavor symmetry for  $n_l$  massless quarks. The non-singlet type contributions are distributions of flavor differences or asymmetries  $\phi_{\text{ns},q_i q_k}^{\pm}$  and the total valence distribution  $\phi_{\text{ns}}^V$ . They evolve independently, as does the singlet type contribution  $\phi_s$ . These distributions are defined as

$$\phi_{\text{ns},q_i q_k}^{\pm} = (\phi_{q_i} \pm \phi_{\bar{q}_i}) - (\phi_{q_k} \pm \phi_{\bar{q}_k}), \quad \phi_{\text{ns}}^V = \sum_{i=1}^{n_l} (\phi_{q_i} - \phi_{\bar{q}_i}), \tag{164}$$

$$\phi_s = \sum_{i=1}^{n_l} (\phi_{q_i} + \phi_{\bar{q}_i}). \tag{165}$$

This translates directly to splitting functions governing their evolution and reads:

$$P_{\text{ns}}^{\pm} = P_{qq}^{\text{V}} \pm P_{q\bar{q}'}^{\text{V}}, \quad (166)$$

$$P_{\text{ns}}^{\text{V}} = P_{qq}^{\text{V}} - P_{q\bar{q}}^{\text{V}} + n_l \left( P_{qq}^{\text{S}} - P_{q\bar{q}}^{\text{S}} \right) = P_{\text{ns}}^{-} + P_{\text{ns}}^{\text{S}}, \quad (167)$$

$$P_{qq}^{\text{S}} = P_{qq}^{\text{V}} + P_{q\bar{q}}^{\text{V}} + n_l \left( P_{qq}^{\text{S}} + P_{q\bar{q}}^{\text{S}} \right) = P_{\text{ns}}^{+} + P_{\text{ps}}, \quad (168)$$

where  $P_{qq}^{\text{S}}$  is the quark singlet splitting function and we implicitly defined  $P_{\text{ns}}^{\text{S}}$  and the ‘‘pure singlet’’:  $P_{\text{ps}}$

$$P_{\text{ns}}^{\text{S}} = n_l \left( P_{qq}^{\text{S}} - P_{q\bar{q}}^{\text{S}} \right), \quad P_{\text{ps}} = n_l \left( P_{qq}^{\text{S}} + P_{q\bar{q}}^{\text{S}} \right). \quad (169)$$

One can choose any independent set of four quark splitting functions in Eqs. (163), (166), (167), (168) and (169) to fully describe parton evolution. In the results from Refs. [111, 112] we need for our purposes, these are provided by  $P_{\text{ns}}^{\pm}$ ,  $P_{\text{ns}}^{\text{S}}$  and  $P_{\text{ps}}$ . The quark singlet  $P_{qq}^{\text{S}}$  is coupled to the gluonic splitting functions  $P_{qg}$ ,  $P_{gq}$  and  $P_{gg}$ . The former two are related to their corresponding single quark quantities by:

$$P_{qg} = n_l P_{q_i g}, \quad P_{gq} = P_{g q_i}, \quad (170)$$

where in  $P_{qg}$  the final state is not fixed by the initial state and the contrary is true for  $P_{gq}$ .

The calculation performed in Refs. [111, 112] also employed the optical theorem to circumvent phase space integration. They considered deep inelastic scattering of certain ‘‘probe’’ particles on partons. These were photons  $\gamma$ ,  $W$ -bosons and scalars coupling directly to the gluon  $\phi$  giving full access to all seven contributions in Eqs. (166), (169) and (170) and  $P_{gg}$ . They operated in Mellin space and obtained symbolic results for the Mellin moments of the partonic structure functions which can be related by an inverse Mellin transform to results in momentum space. The universal part, expressed by the splitting functions, can be extracted from these. For more information on the methods used in Refs. [111, 112], see Refs. [147, 148]. We will encounter the Mellin transform in more detail later in Section 4.4.

To accomplish factorization of collinear singularities in the quark channels  $qq$ ,  $qq'$  and  $q\bar{q}$ , we need to map the splitting functions  $P_{\text{ns}}^{\pm}$ ,  $P_{\text{ns}}^{\text{S}}$  and  $P_{\text{ps}}$  onto splitting functions corresponding to our ‘‘physical’’ production channels. Starting from Eq. (163) and using the inversion of Eqs. (166) and (169), we obtain for these:

$$P_{qq} = P_{qq}^{\text{V}} + P_{qq}^{\text{S}} = \frac{1}{2} \left( P_{\text{ns}}^{+} + P_{\text{ns}}^{-} \right) + \frac{1}{2n_l} \left( P_{\text{ps}} + P_{\text{ns}}^{\text{S}} \right), \quad (171)$$

$$P_{q\bar{q}} = P_{q\bar{q}}^{\text{V}} + P_{q\bar{q}}^{\text{S}} = \frac{1}{2} \left( P_{\text{ns}}^{+} - P_{\text{ns}}^{-} \right) + \frac{1}{2n_l} \left( P_{\text{ps}} - P_{\text{ns}}^{\text{S}} \right), \quad (172)$$

$$P_{qq'} = \frac{1}{2n_l} \left( P_{\text{ps}} + P_{\text{ns}}^{\text{S}} \right), \quad (173)$$

$$P_{q\bar{q}'} = \frac{1}{2n_l} \left( P_{\text{ps}} - P_{\text{ns}}^{\text{S}} \right). \quad (174)$$

Here, we distinguished only two different quark flavors denoted by  $q$  and  $q'$ . Note that we will somewhat deviate from the standard notation concerning higher orders, also used in Refs. [111, 112]. We will shift superscripts indicating the order of the perturbation series by 1 so that the sum of orders of all factors in a term of the cross section will give the term's total order. Moreover, for Higgs boson production we do not need  $P_{q\bar{q}'}$  in Eq. (174) but it appears in vector boson production. Since the Higgs boson carries no electric charge, we have for its partonic cross sections  $\sigma_{q\bar{q}'} = \sigma_{q\bar{q}}$ . For the  $W$ -boson the situation is not that simple which will be relevant in Section 5.1 on Page 167.

It is instructive to inspect the first non-zero contributions to the splitting functions.  $P_{qg}$ ,  $P_{gq}$ ,  $P_{gg}$  and  $P_{qq}^S$  start already at tree-level which is the LO. This is also true for  $P_{ns}^+$  and  $P_{ns}^-$  for which we have  $P_{ns}^{+(1)} = P_{ns}^{-(1)} = P_{qq}^{S(1)} = P_{qq}^{(1)}$ . At NLO  $P_{ns}$  starts to contribute, as well as  $P_{q\bar{q}}$  and  $P_{qq'}$  and we have three different quark splitting functions:

$$P_{qq}^{(2)} = \frac{1}{2} \left( P_{ns}^{+(2)} + P_{ns}^{-(2)} \right) + \frac{1}{2n_l} P_{ps}^{(2)}, \quad (175)$$

$$P_{q\bar{q}}^{(2)} = \frac{1}{2} \left( P_{ns}^{+(2)} - P_{ns}^{-(2)} \right) + \frac{1}{2n_l} P_{ps}^{(2)}, \quad (176)$$

$$P_{qq'}^{(2)} = P_{q\bar{q}'}^{(2)} = \frac{1}{2n_l} P_{ps}^{(2)}. \quad (177)$$

We have  $P_{qq'}^{(2)} = P_{q\bar{q}'}^{(2)}$  since  $P_{ns}^S$  begins to appear at NNLO where it contains a new color structure  $d_{abc}d^{abc}$  that was absent in other contributions so far. For completeness, we list the first non-zero orders of the different  $P_{ij}$ :

$$P_{qg}^{(1)} = T_F \frac{1 - 2x + 2x^2}{2}, \quad (178)$$

$$P_{gq}^{(1)} = C_F \frac{2 - 2x + x^2}{2x}, \quad (179)$$

$$P_{gg}^{(1)} = C_A \left[ \frac{1}{1-x} \right]_+ + \delta(1-x) \left( C_A \frac{11}{12} - T_F \frac{n_l}{3} \right) + C_A \frac{1 - 2x + x^2 - x^3}{x}, \quad (180)$$

$$P_{qq}^{(1)} = C_F \left[ \frac{1}{1-x} \right]_+ + C_A \frac{3}{4} \delta(1-x) - C_F \frac{1+x}{2}, \quad (181)$$

$$P_{qq'}^{(2)} = C_F T_F \left( \frac{(1-x)(10+x+28x^2)}{18x} + \frac{3+15x+8x^2}{12} H_0(x) - \frac{1+x}{2} H_{0,0}(x) \right), \quad (182)$$

$$P_{q\bar{q}}^{(2)} = C_F^2 \left( H_{0,0}(x) \frac{1+x^2}{2(1+x)} - H_{-1,0}(x) \frac{1+x^2}{1+x} + H_0(x) \frac{1+x}{2} - \frac{\pi^2}{12} \frac{1+x^2}{1+x} + \frac{1-x^2}{1+x} \right) + C_A C_F \left( -H_{0,0}(x) \frac{1+x^2}{4(1+x)} + H_{-1,0}(x) \frac{1+x^2}{2(1+x)} \right)$$

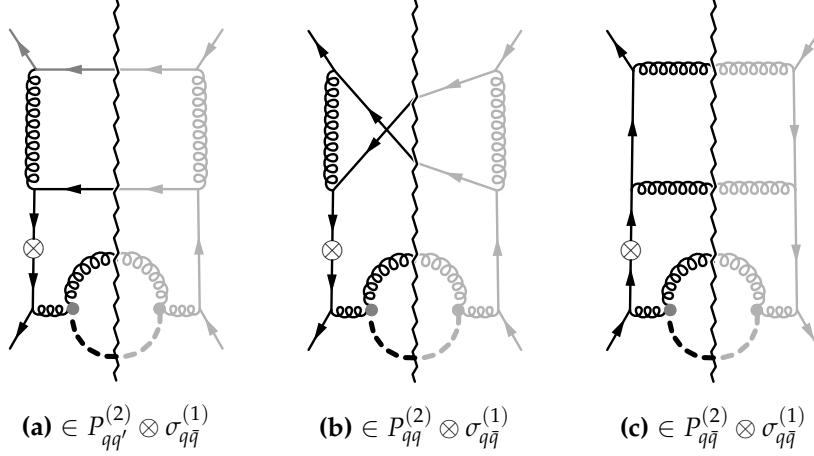


**Figure 13:** Distinct convolution contributions to the  $qq'$ -,  $qq$ - and  $q\bar{q}$ -channels at  $N^3\text{LO}$ . The left-hand sides of the cuts show a collinear singularity arising in the subprocess where two quarks scatter to produce a Higgs boson in association with three partons. The right-hand sides of the cuts are faded and only meant to show the twisting of quark lines in Fig. b. In the left-hand sides those parts of the diagrams above the convolution symbol  $\otimes$  represent contributions to the quark splitting functions at NLO. The parts below  $\otimes$  stand for the partonic cross section in the  $q\bar{q}$ -channel at NLO. Figure a is a contribution from  $P_{ps}^{(2)}$  or  $P_{qq'}^{(2)}$  which consist only of diagrams of this type. Figures b and c cannot be linked directly to the other non-singlet and singlet pieces  $P_{ns}^{\pm}$  and  $P_{ns}^S$  but they clearly represent two independent classes.  $P_{qq}^{(2)}$  receives corrections of the types in Figs. a and b,  $P_{q\bar{q}}^{(2)}$  from the types in Figs. a and c.

$$\begin{aligned}
 & -\frac{1+x}{4} H_0(x) + \frac{\pi^2}{24} \frac{1+x^2}{1+x} - \frac{1-x^2}{2(1+x)} \\
 & + C_F T_F \left( -H_{0,0}(x) \frac{1+x}{2} + H_0(x) \frac{3+15x+8x^2}{12} \right. \\
 & \quad \left. + \frac{(1-x)(10+x+28x^2)}{18x} \right). \tag{183}
 \end{aligned}$$

The remaining splitting functions up to two loops can be found in Appendix B.1. Note the appearance of delta- and plus-distributions introduced in Section 4.2.2 and of the harmonic polylogarithms  $H_{\dots}(x)$  which will be subject in Section 4.3.3.1 on Page 134. To get an impression of the three distinct quark splitting functions relevant to Higgs boson production, we sketched in Fig. 13 some convolutions appearing in the quark channels.

### 4.3 CROSS SECTIONS TO NNLO

At NNLO all five distinct partonic channels contribute, for the number of diagrams in each channel see Tab. 3. Let us describe the generic setup of our calculation first and then come to the generation of topologies with TopoID.

**Table 3:** Number of diagrams appearing up to NNLO in each channel and in their sum. The numbers in the right columns indicate dissection in fermionic contributions. Gluonic channels include also diagrams with ghosts as incoming and outgoing particles. Purely virtual diagrams in the  $gg$ -channel are listed for completeness.

Order	Channel	Number of diagrams (fermionic loops)		
LO	$gg$	#1		
NLO	$q\bar{q}$	#1		
	$qg$	#1		
	$gg_{\text{virt}}$	#10		
	$gg_{\text{real}}$	#38		
	$\Sigma$	#50		
NNLO	$qq'$	#1		
	$qq$	#2		
	$q\bar{q}$	#84	= #81	+ #3 $n_l$
	$qg$	#124	= #122	+ #2 $n_l$
	$gg_{\text{virt}}$	#294	= #252	+ #42 $n_l$
	$gg_{\text{real}}$	#2458	= #2293	+ #165 $n_l$
	$\Sigma$	#2964	= #2752	+ #212 $n_l$

#### 4.3.1 Setup of the calculation

The effective Lagrangian in Eq. (127) contains three vertices mediating the coupling of the Higgs boson to two, three and four gluons which we denote by  $g^2H$ ,  $g^3H$  and  $g^4H$ , respectively. At LO only  $g^2H$  is relevant. At NLO also  $g^3H$  contributes and at NNLO finally  $g^4H$ . The vertices  $g^3H$  and  $g^4H$  are not implemented as higher-degree vertices but via  $g\sigma H$  and  $\sigma^2H$  vertices where  $\sigma$  is an auxiliary field with a momentum independent propagator. The same trick (and the same field  $\sigma$ ) is used in pure QCD to split the four-gluon vertex  $g^4$  into two  $g^2\sigma$  vertices such that each diagram has a global color factor, see Ref. [149]. The  $g^3H$  vertex, for example, is obtained from a  $g\sigma H$  and a  $g^2\sigma$  vertex. Note that this splitting of higher-degree vertices increases the number of Feynman diagrams on the one hand. But their handling is simplified on the other hand.

Color algebra, contraction of Lorentz indices and traces over Dirac gamma-matrices are treated with a code written in FORM. Since we need to compute higher orders in the dimensional regulator  $\epsilon$  we list the crucial steps of our calculation where  $\epsilon$ -dependence enters:

- application of projectors (discussed below),
- traces over gamma-matrices,
- reduction of scalar integrals (usually expanded in  $\epsilon$ ).

PROJECTORS AND PHYSICAL POLARIZATIONS We need to apply projectors  $P_i P_j$  depending on the considered initial state particles  $i$  and  $j$ .

$$P_q = a_q \left[ \not{p}_q + m_q \right] \delta^{ij}, \quad P_{\bar{q}} = a_q \left[ \not{p}_q^T + m_q \right] \delta^{ij}, \quad (184)$$

$$P_g = a_g g^{\mu\nu} \delta^{ab}, \quad P_c = P_{\bar{c}} = a_c \delta^{ab}, \quad (185)$$

where  $p_q$  and  $m_q$  are momentum and mass of a quark or antiquark, respectively. We have  $m_q = 0$  in our case. Each projector comes with an ‘‘averaging factor’’  $a_i$ . They are the reciprocal number of averaged states, including color and polarizations. Quarks and antiquarks have two spin states and  $N_c = C_A = 3$  color states. Gluons and ghosts have  $N_g = (N_c^2 - 1) = 2C_F C_A = 8$  color states. They have no longitudinal component and thus  $D - 2$  polarizations in  $D$  dimensions. This leaves us with:

$$a_q = \frac{1}{2N_c} = \frac{1}{2C_A}, \quad (186)$$

$$a_g = a_c = \frac{1}{2(1 - \epsilon)N_g} = \frac{1}{4(1 - \epsilon)C_F C_A}. \quad (187)$$

It is not sufficient to consider ghosts only as internal particles, we always need to include channels with ghosts and antighosts in the initial state whenever we consider a gluonic channel. Only thereby we subtract unphysical degrees of freedom completely. Otherwise we needed to construct a more complicated projector for the gluon than Eq. (185). Gauge invariance violating terms in the scalar amplitude surviving  $P_g$  are precisely canceled by the contributions from the ghost-channels. In summary, we have for physical polarizations:

$$\sigma_{qg}^{\text{phys}} = \sigma_{qg} + \sigma_{cg} - \sigma_{\bar{c}g} \quad (188)$$

$$\sigma_{gg}^{\text{phys}} = \sigma_{gg} + 2\sigma_{cc} - 2\sigma_{c\bar{c}} - 4\sigma_{cg}. \quad (189)$$

The full  $\epsilon$ -dependence of the LO result is only due to averaging of the two gluon polarizations and the trace over gamma-matrices,

$$\tilde{\sigma}_{gg}^{(0)} = \delta(1 - x) \frac{1}{1 - \epsilon} = \delta(1 - x) \left( 1 + \epsilon + \epsilon^2 + \epsilon^3 + \mathcal{O}(\epsilon^4) \right). \quad (190)$$

### 4.3.2 Definition of topologies

A detailed description of the generation of topologies with TopoID will be given in Section 4.5.2 on Page 155. Here, we show instead the connection between generic and basic topologies as they were introduced in Section 2.1.6 on Page 21. We use a scheme in which generic topologies need not to be complete.

Using diagrams provided by QGRAF for the simplified QCD model without fermions, TopoID finds 16 generic topologies, see Fig. 15. These topologies (named NNLOrGT1, NNLOrGT2, ...) are in general incomplete and linearly dependent. Subsequently, linearly independent subtopologies are identified



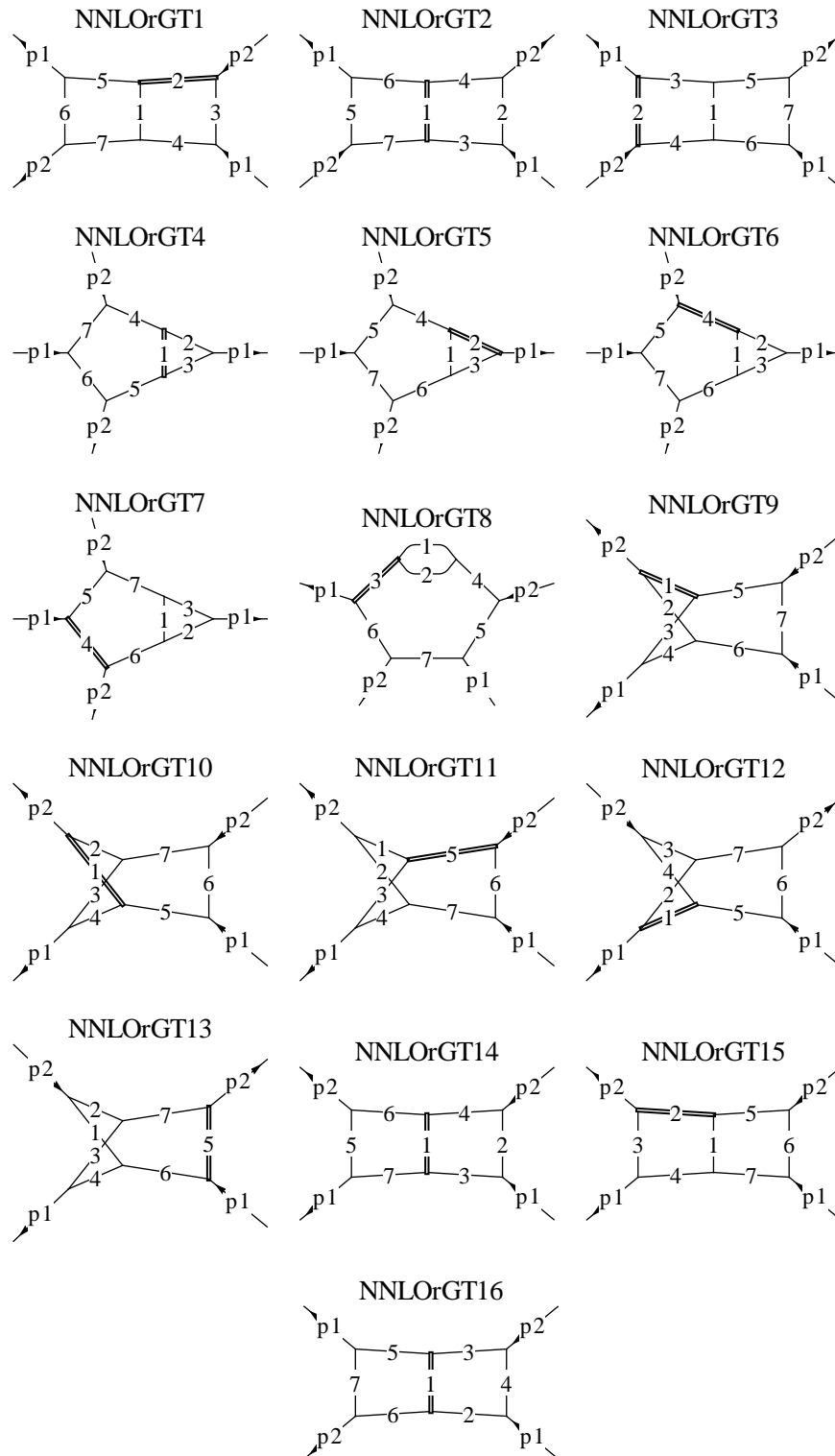


**Figure 14:** Minimal set of 16 generic topologies for NNLO Higgs boson production identified by TopoID. In order to distinguish propagators more clearly we allowed interchange of external outgoing momenta.

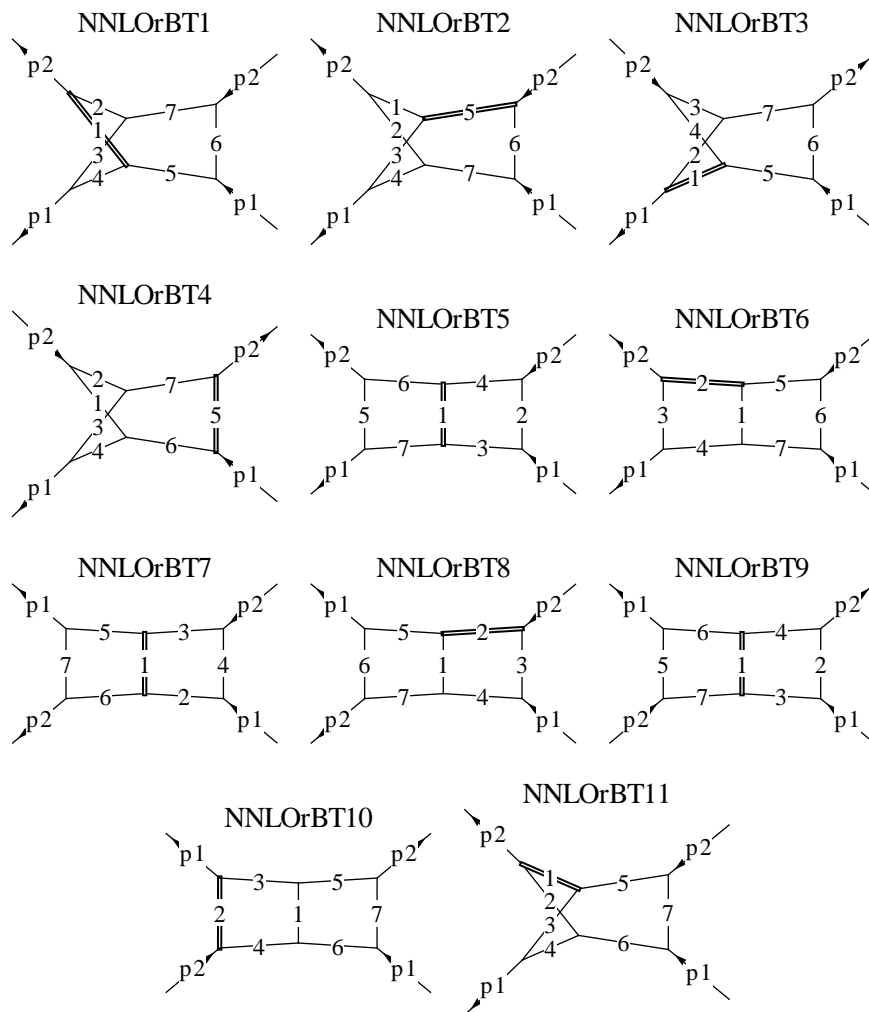


**Figure 15:** Minimal set of 11 basic topologies for NNLO Higgs boson production. Note that each topology has 7 lines which means that no irreducible scalar product or pseudo-propagator needs to be included.

for each generic topology (named  $\text{NNLOrGT1s1}$ ,  $\text{NNLOrGT1s2}$ , ...). In the set of these independent topologies duplicates appear. Thus, in the next step a minimal set of 11 independent topologies is constructed, see Fig. 15. Usually, the last step in this scheme is completion of topologies. However, in this particular case each topology in the minimal set of independent topologies is already complete and therefore constitutes a basic topology (named  $\text{NNLOrBT1}$ ,  $\text{NNLOrBT2}$ , ...).

The organization of topologies as just stated is also depicted in Fig. 16. Note that throughout this scheme it was made use of the cuts of the topologies, otherwise linearly independent subtologies without cut would occur, for example without the Higgs boson line. As one can see in Fig. 16, some generic topologies are also basic topologies, for example  $\text{NNLOrGT1} \rightarrow \text{NNLOrGT1s1} \rightarrow \text{NNLOrBT8}$ . The other cases demonstrate that many generic topologies share common linearly independent subtologies. The FORM code realizing this scheme in the calculation of all diagrams for NNLO

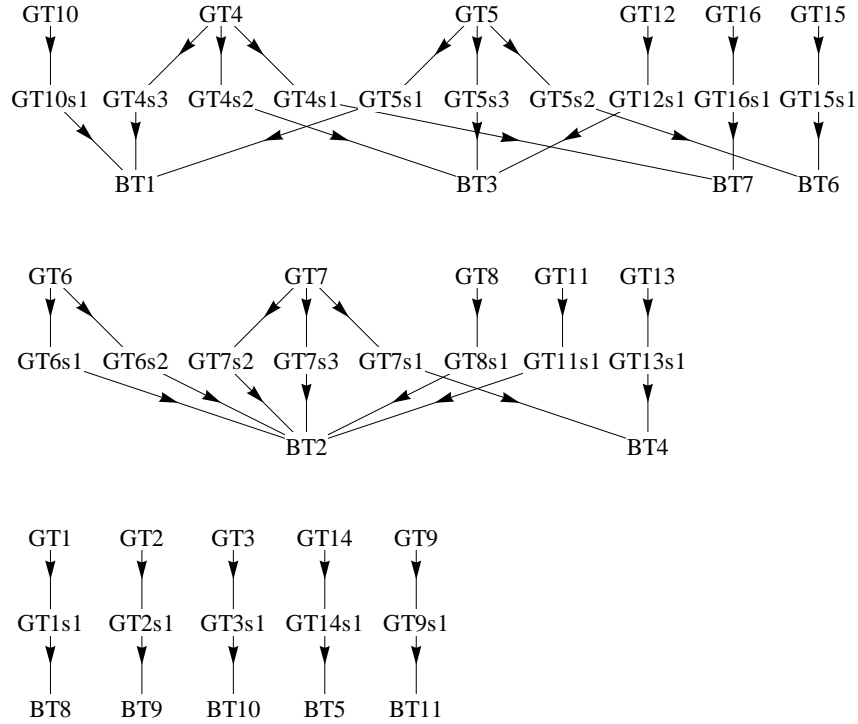


**Figure 16:** Graphical representation of the mapping scheme. We intentionally left out the prefix NNLOr of topology names. Generic topologies are arranged at the top level of each cluster in the graph, followed by their individual linearly independent set of subtopologies. At the bottom of each cluster topologies from the minimal set of linearly independent ones appear.

Higgs boson production is explained in Appendix C.1 for generic and in Appendix C.2 for basic topologies.

### 4.3.3 Results

Using the topologies defined above in Section 4.3.2, we found agreement with our results from a previous calculation, see Ref. [90]. In the main text, we only exemplify the results for the finite partonic cross sections up to NNLO including higher orders in  $\epsilon$ . The complete set of expressions can be found in electronic form in Refs. [34, 150]. Renormalization is performed for the operator  $\mathcal{O}_1$  and the strong coupling  $\alpha_s$  as explained in Section 4.2.1.1 on Page 115. Collinear counterterms are used to remove remaining singularities and topic of the upcoming Section 4.4.2 on Page 139. Terms to  $\mathcal{O}(\epsilon^2)$  are

given for  $\tilde{\sigma}_{q\bar{q}}^{(1)}$  and terms to  $\mathcal{O}(\epsilon)$  for  $\tilde{\sigma}_{qq'}^{(2)} = \tilde{\sigma}_{qq'}^{(2),0} + \epsilon \tilde{\sigma}_{qq'}^{(2),1}$ . In the latter, we set  $\mu = m_H$  to shorten the result.

$$\begin{aligned}
 \tilde{\sigma}_{q\bar{q}}^{(1)} &= \frac{32}{27}(1-x)^3 \\
 &\times \left\{ 1 + \epsilon \left[ 2\text{H}_1(x) + \text{H}_0(x) + \frac{2}{3} + \ln\left(\frac{\mu^2}{m_H^2}\right) \right] \right. \\
 &\quad + \epsilon^2 \left[ 4\text{H}_{1,1}(x) + 2\text{H}_{1,0}(x) + 2\text{H}_2(x) + \text{H}_{0,0}(x) \right. \\
 &\quad + \frac{4}{3}\text{H}_1(x) + \frac{2}{3}\text{H}_0(x) - \frac{\pi^2}{4} + \frac{13}{9} \\
 &\quad + \left( 2\text{H}_1(x) + \text{H}_0(x) + \frac{2}{3} \right) \ln\left(\frac{\mu^2}{m_H^2}\right) \\
 &\quad \left. \left. + \frac{1}{2}\ln^2\left(\frac{\mu^2}{m_H^2}\right) \right] \right\}, \tag{191}
 \end{aligned}$$

$$\begin{aligned}
 \tilde{\sigma}_{qq'}^{(2),0} &= -(x+2)^2 \left[ \frac{16}{9}\text{H}_3(x) + \frac{32}{9}\text{H}_{2,1}(x) + \frac{8}{3}\text{H}_{2,0}(x) + \frac{8}{9}\text{H}_{0,0,0}(x) \right] \\
 &\quad - (x+3)(1-x) \left[ \frac{64}{9}\text{H}_{1,1}(x) - \frac{16}{3}\text{H}_{1,0}(x) \right] \\
 &\quad + \frac{8}{9}(5x^2 + 8x - 12)\text{H}_2(x) + \frac{16}{9}(x^2 + 4x - 3)\text{H}_{0,0}(x) \\
 &\quad - \frac{4}{3}(5x + 17)(1-x)\text{H}_1(x) \\
 &\quad + \left[ \frac{2}{9}(29x^2 + 44x - 59) + \frac{4}{27}(x+2)^2\pi^2 \right] \text{H}_0(x) \\
 &\quad - \frac{4}{27}(3x^2 + 4x - 6)\pi^2 - \frac{2}{9}(11x + 105)(1-x), \tag{192}
 \end{aligned}$$

$$\begin{aligned}
 \tilde{\sigma}_{qq'}^{(2),1} &= -(x+2)^2 \left[ \frac{64}{3}\text{H}_{2,1,1}(x) + \frac{128}{9}\text{H}_{2,1,0}(x) + \frac{128}{9}\text{H}_{2,2}(x) \right. \\
 &\quad + 8\text{H}_{2,0,0}(x) + \frac{32}{3}\text{H}_{3,1}(x) + \frac{64}{9}\text{H}_{3,0}(x) \\
 &\quad \left. + \frac{16}{3}\text{H}_4(x) + \frac{8}{3}\text{H}_{0,0,0,0}(x) \right] \\
 &\quad - (x+3)(1-x) \left[ \frac{128}{3}\text{H}_{1,1,1}(x) + \frac{256}{9}\text{H}_{1,1,0}(x) + \frac{256}{9}\text{H}_{1,2}(x) \right. \\
 &\quad \left. + 16\text{H}_{1,0,0}(x) \right] \\
 &\quad + \frac{16}{9}(13x^2 + 16x - 44)\text{H}_{2,1}(x) + \frac{8}{9}(17x^2 + 20x - 60)\text{H}_{2,0}(x) \\
 &\quad + \frac{8}{9}(11x^2 + 32x - 44)\text{H}_3(x) + \frac{8}{9}(5x^2 + 20x - 22)\text{H}_{0,0,0}(x) \\
 &\quad - \frac{8}{9}(53x + 177)(1-x)\text{H}_{1,1}(x) - \frac{32}{3}(3x + 10)(1-x)\text{H}_{1,0}(x) \\
 &\quad + \left[ \frac{4}{9}(84x^2 + 140x - 193) + \frac{44}{27}(x+2)^2\pi^2 \right] \text{H}_2(x)
 \end{aligned}$$

$$\begin{aligned}
& + \left[ \frac{14}{27}(2+x)^2\pi^2 + \frac{2}{9} + (99x^2 + 172x - 193) \right] H_{0,0}(x) \\
& + \left[ \frac{88}{27}(x+3)(1-x)\pi^2 - \frac{2}{9}(131x + 727)(1-x) \right] H_1(x) \\
& + \left[ \frac{8}{3}(2+x)^2\zeta(3) - \frac{1}{27}(23x^2 + 104x - 100)\pi^2 \right. \\
& \quad \left. + \frac{1}{9}(229x^2 + 880x - 711) \right] H_0(x) \\
& + \frac{2}{405}(x+2)^2\pi^4 - \frac{8}{9}(5x^2 + 28x - 18)\zeta(3) \\
& - \frac{1}{54}(245x^2 + 348x - 469)\pi^2 - 2(8x + 65)(1-x). \tag{193}
\end{aligned}$$

Below, we describe the procedure of inserting master integrals into the reduction, see Ref. [73]. Moreover, we give a short review of harmonic polylogarithms which appear in the partonic cross sections and in the splitting functions, see Section 4.2.2.4.

**SINGULAR BEHAVIOR** Having the reduction to master integrals and analytic expressions for the  $\epsilon$ -expansion of these master integrals at hand, one has to carefully insert the second into the first. The reason is the following: the boundary condition of a master integral in the soft limit has in general terms with different singular behavior

$$\sum_{\{i\}} (1-x)^{-a_i+b_i\epsilon}, \tag{194}$$

where  $\{a_i > 0\}$  and  $\{b_i\}$  are integers, that are factored off before performing the expansion in  $\epsilon$  in the integrand and evaluating integrals order-by-order. First, we need to combine the expression for a master integral in the soft limit  $I(x \rightarrow 1)$ , exposing above form of singularities, with the expression containing the full  $x$ -dependence  $I(x)$ . In the latter, the singular factors are usually not apparent anymore since they were expanded to allow for the matching of the differential equation to a boundary value. The form of  $I(x)$  and  $I(x \rightarrow 1)$  is

$$I(x \rightarrow 1) = \sum_{\{i\}} (1-x)^{-a_i+b_i\epsilon} \sum_{j=j_{\min,i}}^{j_{\max,i}+1} \epsilon^j I_i^{(j)}(x \rightarrow 1), \tag{195}$$

$$I(x) = \sum_{j=j_{\min}}^{j_{\max}} \epsilon^j I^{(j)}(x), \tag{196}$$

where  $j_{\min}$  and  $j_{\max}$  give the highest pole and the needed depth of the expansion, respectively. Thus, we need to apply the following replacement to the reduced result:

$$I(x) \rightarrow I(x) - I(x) \Big|_{x \rightarrow 1} + I(x \rightarrow 1), \tag{197}$$

where  $I(x) \Big|_{x \rightarrow 1}$  denotes the Taylor expansion of the full kinematics result. We subtract the behavior in the soft limit expanded naively in  $\epsilon$  and add

the correct behavior. The coefficients of a master integral in the reduced result can contain additional factors of  $(1-x)^{-c_i}$  whose powers need to be combined with the singular behaviors of the master integral to be then expanded in terms of delta- and plus-distributions such that singularities are properly regularized, see Eqs. (118) and (161). This expansion can generate a shift of orders in the  $\epsilon$ -expansion (we wrote  $j_{\max,i} + 1$  as upper bound in Eq. (195) for this reason) and one needs to evaluate the soft limit of a master integral one order higher compared to the solution of the differential equation. By their coefficients in the reduced result, master integrals not singular on their own, can therefore give rise to singular terms. We emphasize that this procedure has to be followed only for the  $gg$ -channel where delta- and plus-distributions are relevant.

#### 4.3.3.1 Harmonic polylogarithms

Harmonic polylogarithms, in short HPLs, were introduced by Remiddi and Vermaseren in Ref. [151]. They form the basis for many analytic results for higher-order corrections and related quantities. For convenience, we list here their most important properties.

- HPLs are denoted by  $H_{\vec{w}}(x)$  where  $\vec{w} = (w_1, \dots, w_m)$  is the vector of indices and its length  $m$  is called weight. They are defined in a recursive fashion as nested integrals over the weight functions  $f_w(x)$  where  $\vec{w}_{n-1} = (w_2, \dots, w_n)$  is the weight vector with the first component dropped,

$$\begin{aligned}
 H_{\vec{w}}(x) &= \int_0^x dx' f_{w_1}(x') H_{\vec{w}_{n-1}}(x') \quad \text{with} \\
 f_0(x) &= \frac{1}{x}, \quad H_0(x) = \ln x, \\
 f_1(x) &= \frac{1}{1-x}, \quad H_1(x) = -\ln(1-x), \\
 f_{-1}(x) &= \frac{1}{1+x}, \quad H_{-1}(x) = \ln(1+x).
 \end{aligned} \tag{198}$$

The denominators of the weight functions are also referred to as the alphabet of the HPLs. From this definition, relations for derivatives of HPLs follow directly. Index vectors allow for a shorter notation by increasing the absolute values of the weights  $\pm 1$  by the length of a sequence of pure zeros directly to their left. For example:

$$H_{0,1,1,0,0,-1}(x) = H_{2,1,-2}(x).$$

- HPLs through weight three can be represented by Nielsen polylogarithms (by linear combinations with algebraic arguments). Beginning from weight four they cover a larger class of functions than polylogarithms  $\text{Li}_n(x)$  or Nielsen polylogarithms  $S_{n,m}(x)$  which are defined via:

$$\text{Li}_0(x) = \frac{x}{1-x}, \quad \text{Li}_n(x) = \int_0^x dx' \frac{1}{x'} \text{Li}_{n-1}(x'), \tag{199}$$

$$S_{n,m}(x) = \frac{(-1)^{n+m+1}}{(n-1)! m!} \int_0^1 dx' \frac{1}{x'} \ln^{n-1}(x') \ln^m(1-x x'). \quad (200)$$

For example,  $H_{-1,3}(x)$  cannot be expressed in terms of  $S_{n,m}(x)$ , even when permitting algebraically transformed arguments.

- HPLs follow a product algebra called “shuffle algebra”. Products of HPLs can be expressed as sum of HPLs where the weight of each term equals the combined weight of the former product. This can be denoted as:

$$H_{\vec{w}_1}(x) H_{\vec{w}_2}(x) = \sum_{\vec{w} \in \vec{w}_1 \uplus \vec{w}_2} H_{\vec{w}}(x), \quad (201)$$

where  $\uplus$  is the “shuffling” operation on indices, preserving the relative order within each initial set, e.g.

$$\begin{aligned} H_{0,1}(x) H_{1,-1}(x) &= 2 H_{0,1,1,-1}(x) + H_{0,1,-1,1}(x) + H_{1,0,1,-1}(x) \\ &\quad + H_{1,0,-1,1}(x) + H_{1,-1,0,1}(x). \end{aligned}$$

The same algebra holds for harmonic sums which are closely related to HPLs in a one-to-one correspondence.

- Identities from the product algebra can be used in conjunction with integration-by-parts identities to transform arbitrary HPLs to a minimal set. Also by this method, singularities behaving like  $\ln^i x$  or  $\ln^i(1-x)$  can be extracted and made explicit.
- There exist relations among HPLs with transformed arguments for  $x \rightarrow x'$  with  $x' \in \{-x, 1-x, 1/x, x^2, (1-x)/(1+x)\}$ .
- HPLs evaluated at  $x = 1$  can be expressed as combination of multiple zeta values (MZVs) which are transcendental numbers. For example,  $H_3(x) = \zeta(3)$  and  $H_{-4}(x) = 7/8 \zeta(4)$  where  $\zeta(n)$  is the Riemann zeta-function.
- HPLs have convergent power series expansions which allow for stable numerical evaluation.
- There exist convenient implementations in computer algebra systems. The `harmpl` package for FORM, see Refs. [152, 153], and the HPL package for Mathematica, see Refs. [154, 155].

**Example 46.** The HPLs through weight one are related to ordinary logarithms by:

$$\begin{aligned} H(x) &= 1, \\ H_0(x) &= \ln x, \\ H_1(x) &= -\ln(1-x), \\ H_{-1}(x) &= \ln(1+x). \end{aligned} \quad (202)$$

HPLs up to weight three can still be mapped to combinations of Nielsen polylogarithms, e.g.

$$\begin{aligned}
 H_{0,0}(x) &= \frac{1}{2} \ln^2(x), \\
 H_2(x) &= \text{Li}_2(x), \\
 H_{1,0}(x) &= -\text{Li}_2(x) - \ln(1-x) \ln(x), \\
 H_{-1,1}(x) &= \text{Li}_2\left(\frac{1+x}{2}\right) - \ln(2) \ln(1+x) - \text{Li}_2\left(\frac{1}{2}\right), \\
 H_{1,-1,-1}(x) &= \text{Li}_3\left(\frac{1+x}{2}\right) - \text{Li}_3\left(\frac{1}{2}\right) - \text{Li}_2\left(\frac{1+x}{2}\right) \ln(1+x) \\
 &\quad - \frac{1}{2} \ln^2(1+x) \ln\left(\frac{1-x}{2}\right), \\
 H_{2,1}(x) &= S_{1,2}(x),
 \end{aligned}$$

where  $\text{Li}_2(x)$  is Euler's dilogarithm and  $\text{Li}_3(x)$  the trilogarithm.

#### 4.4 CONVOLUTIONS OF NNLO CROSS SECTIONS

To render partonic cross sections finite, those singularities associated with collinear initial state radiation need to be subtracted from the sum of real and virtual corrections which is free of soft singularities. As we motivated in Section 4.2.2 on Page 117, collinear singularities can be absorbed into a redefinition of the parton distribution functions  $\phi_i(x)$  by so-called transition functions  $\Gamma_{ij}(x)$ . At each order of perturbation theory the transition functions are constructed from convolution integrals of the parton splitting functions  $P_{ij}^{(k)}(x)$  including those from lower orders and coefficients of the QCD beta-function. The infrared counterterms to the cross sections  $\sigma_{ij}^{(k)}(x)$  are then given by the (double-)convolution with the (inverse) transition functions.

##### 4.4.1 Transition functions to $N^3\text{LO}$

The transition functions  $\Gamma_{ij}(x)$  describe all collinear emissions off a parton and are used to define parton distributions  $\phi_i(x)$  in a renormalization scheme. The redefinition is carried out via a convolution integral:

$$\phi_i(x) = \left[ \Gamma_{ij} \otimes \phi_j^0 \right](x), \quad (203)$$

where  $\phi_i(x)$  denotes a PDF in the  $\overline{\text{MS}}$ -scheme and  $\phi_i^0$  a bare quantity. In this subsection all quantities with superscript zero are to be understood as infrared-bare quantities. We suppressed here the dependence on the factorization scale  $\mu$  that  $\phi_i(x)$  acquires. The renormalization group equation (RGE) for  $\phi_i(x)$  reads:



$$0 = \frac{d}{d \ln \mu^2} \phi_i^0 = \frac{d}{d \ln \mu^2} \left[ \Gamma_{ij}^{-1} \otimes \phi_j \right] (x) = \pi \beta^D(\alpha_s) \left[ \frac{\partial \Gamma_{ij}^{-1}}{\otimes} \partial \alpha_s \right] (x) \phi_j + \left[ \Gamma_{ij}^{-1} \otimes \frac{d \phi_j}{d \ln \mu^2} \right] (x), \quad (204)$$

where  $\pi \beta^D(\alpha_s) = d\alpha_s / d \ln \mu^2$  defines the  $D$ -dimensional beta-function of QCD and we made use of the fact that within the  $\overline{\text{MS}}$ -scheme the transition function must not depend on any scale explicitly:  $\partial \Gamma_{ij}^{-1}(x) / \partial \mu^2 = 0$ . Since  $\Gamma_{ij}^{-1}(x)$  is allowed to have poles in  $\epsilon$  starting at order  $\alpha_s$ , we need to include terms of  $\mathcal{O}(\epsilon)$  in  $\beta^D(\alpha_s)$ . As usual, we have

$$\alpha_s^0 = Z_{\alpha_s} \alpha_s \mu^{2\epsilon} \quad \text{with} \quad Z_{\alpha_s} = 1 + \sum_{i=1}^{\infty} \frac{1}{\epsilon^i} Z_{\alpha_s}^{(i)}, \quad (205)$$

where we wrote the expansion in poles and not the coupling. From this and RGE-invariance we obtain the following:

$$0 = \frac{d}{d \ln \mu^2} \alpha_s^0 = \left[ \frac{d \alpha_s}{d \ln \mu^2} \frac{\partial Z_{\alpha_s}}{\partial \alpha_s} \alpha_s + Z_{\alpha_s} \frac{d \alpha_s}{d \ln \mu^2} + Z_{\alpha_s} \alpha_s \epsilon \right] \mu^{2\epsilon}. \quad (206)$$

The  $D$ -dimensional beta-function  $\beta^D(\alpha_s)$  is then entirely determined by the coefficient of the first pole  $Z_{\alpha_s}^{(1)}$  in Eq. (205):

$$\beta^D(\alpha_s) = -\frac{\alpha_s}{\pi} \epsilon Z_{\alpha_s} \left( \frac{\partial Z_{\alpha_s}}{\partial \alpha_s} \alpha_s + Z_{\alpha_s} \right)^{-1} = -\frac{\alpha_s}{\pi} \epsilon - \frac{\alpha_s}{\pi} \frac{\partial}{\partial \alpha_s} \alpha_s Z_{\alpha_s}^{(1)} = -\frac{\alpha_s}{\pi} \epsilon + \beta(\alpha_s). \quad (207)$$

Equation (207) can be obtained by expansion in  $\alpha_s$  and the requirement to be free of poles in  $\epsilon$ . The  $\mathcal{O}(\epsilon)$  term is usually omitted since it vanishes for  $\epsilon \rightarrow 0$ . The 4-dimensional beta-function  $\beta(\alpha_s)$  in Eq. (207) is given in Eq. (131) on Page 115.

The evolution of physical, i.e. renormalized, PDFs with an energy scale is governed by the DGLAP equations (we use a different convention for  $P_{ij}$  in comparison to Eq. (157) on Page 121) given by

$$\frac{d}{d \ln \mu^2} \phi_i(x) = [P_{ij} \otimes \phi_j](x), \quad (208)$$

where the splitting functions  $P_{ij}(x)$  do not depend explicitly on the scale  $\mu$ , assuming the  $\overline{\text{MS}}$ -scheme. Plugging Eq. (208) into Eq. (204) and realizing that the equation must hold also for the integrand of the common convolution integral leads to

$$\pi \beta^D(\alpha_s) \frac{\partial \Gamma_{ij}^{-1}(x)}{\partial \alpha_s} + \left[ \Gamma_{ik}^{-1} \otimes P_{kj} \right] (x) = 0. \quad (209)$$

The perturbative expansion of the splitting functions can be written as

$$P_{ij}(x) = \frac{\alpha_s}{\pi} P_{ij}^{(1)}(x) + \left( \frac{\alpha_s}{\pi} \right)^2 P_{ij}^{(2)}(x) + \left( \frac{\alpha_s}{\pi} \right)^3 P_{ij}^{(3)}(x) + \mathcal{O}(\alpha_s^4). \quad (210)$$

In Ref. [90], the expansion of  $P_{ij}(x)$  had in addition to Eq. (208) the term  $\delta_{ij}\delta(1-x)$ . With this term we could form all convolutions entering the N<sup>3</sup>LO calculation. But in order to describe PDF evolution in Eq. (208) correctly, it must be omitted. Note that in Eq. (208) we absorbed a factor  $\alpha_s/\pi$  in  $P_{ij}$  to obtain the form of Eq. (210). At lowest order no interaction or splitting takes place. In a hard process each collinear radiation comes with a pole in  $\epsilon$  and splitting functions are extracted from the coefficients of these poles. Thus, we make an ansatz for the transition function and its inverse analogously to a  $\overline{\text{MS}}$ -scheme renormalization constant:

$$\begin{aligned} \Gamma_{ij}(x) = & \delta_{ij}\delta(1-x) + \frac{\alpha_s}{\pi} \frac{\Gamma_{ij}^{(1,1)}(x)}{\epsilon} + \left(\frac{\alpha_s}{\pi}\right)^2 \left[ \frac{\Gamma_{ij}^{(2,2)}(x)}{\epsilon^2} + \frac{\Gamma_{ij}^{(2,1)}(x)}{\epsilon} \right] \\ & + \left(\frac{\alpha_s}{\pi}\right)^3 \left[ \frac{\Gamma_{ij}^{(3,3)}(x)}{\epsilon^3} + \frac{\Gamma_{ij}^{(3,2)}(x)}{\epsilon^2} + \frac{\Gamma_{ij}^{(3,1)}(x)}{\epsilon} \right] + \mathcal{O}(\alpha_s^4). \end{aligned} \quad (211)$$

Using Eqs. (131), (207) and (210) as well as the expansion for  $\Gamma_{ij}^{-1}$ , we can expand Eq. (209) and solve for the coefficients in the ansatz for  $\Gamma_{ij}^{-1}(x)$  at each order in  $\alpha_s$ . To order  $\alpha_s^3$  the solution reads:

$$\begin{aligned} \Gamma_{ij}^{-1}(x) = & \delta_{ij}\delta(1-x) + \frac{\alpha_s}{\pi} \frac{1}{\epsilon} P_{ij}^{(1)}(x) \\ & + \left(\frac{\alpha_s}{\pi}\right)^2 \left\{ \frac{1}{2\epsilon^2} \left( [P_{ik}^{(1)} \otimes P_{kj}^{(1)}](x) - \beta_0 P_{ij}^{(1)}(x) \right) + \frac{1}{2\epsilon} P_{ij}^{(2)}(x) \right\} \\ & + \left(\frac{\alpha_s}{\pi}\right)^3 \left\{ \frac{1}{6\epsilon^3} \left( [P_{ik}^{(1)} \otimes P_{kl}^{(1)} \otimes P_{lj}^{(1)}](x) \right. \right. \\ & \quad \left. \left. - 3\beta_0 [P_{ik}^{(1)} \otimes P_{kj}^{(1)}](x) + 2\beta_0^2 P_{ij}^{(1)}(x) \right) \right. \\ & \quad \left. + \frac{1}{6\epsilon^2} \left( 2 [P_{ik}^{(1)} \otimes P_{kj}^{(2)}](x) + [P_{ik}^{(2)} \otimes P_{kj}^{(1)}](x) \right. \right. \\ & \quad \left. \left. - 2\beta_0 P_{ij}^{(2)}(x) - 2\beta_1 P_{ij}^{(1)}(x) \right) \right. \\ & \quad \left. + \frac{1}{3\epsilon} P_{ij}^{(3)}(x) \right\}. \end{aligned} \quad (212)$$

To get  $\Gamma_{ij}(x)$ , we simply invert the above result using  $[\Gamma_{ik}^{-1} \otimes \Gamma_{kj}](x) = \delta_{ij}\delta(1-x)$ :

$$\begin{aligned} \Gamma_{ij}(x) = & \delta_{ij}\delta(1-x) - \frac{\alpha_s}{\pi} \frac{1}{\epsilon} P_{ij}^{(1)}(x) \\ & + \left(\frac{\alpha_s}{\pi}\right)^2 \left\{ \frac{1}{2\epsilon^2} \left( [P_{ik}^{(1)} \otimes P_{kj}^{(1)}](x) + \beta_0 P_{ij}^{(1)}(x) \right) - \frac{1}{2\epsilon} P_{ij}^{(2)}(x) \right\} \\ & + \left(\frac{\alpha_s}{\pi}\right)^3 \left\{ -\frac{1}{6\epsilon^3} \left( [P_{ik}^{(1)} \otimes P_{kl}^{(1)} \otimes P_{lj}^{(1)}](x) \right. \right. \\ & \quad \left. \left. + 3\beta_0 [P_{ik}^{(1)} \otimes P_{kj}^{(1)}](x) + 2\beta_0^2 P_{ij}^{(1)}(x) \right) \right. \\ & \quad \left. + \frac{1}{6\epsilon^2} \left( [P_{ik}^{(1)} \otimes P_{kj}^{(2)}](x) + 2 [P_{ik}^{(2)} \otimes P_{kj}^{(1)}](x) \right. \right. \\ & \quad \left. \left. + 2\beta_0 P_{ij}^{(2)}(x) + 2\beta_1 P_{ij}^{(1)}(x) \right) \right\} \end{aligned}$$

$$\left. -\frac{1}{3\epsilon}P_{ij}^{(3)}(x) \right\}. \quad (213)$$

We agree with the result presented in Ref. [156]. In comparison to Eq. (2.8) of Ref. [114] where the same collinear singularities are discussed, there is a discrepancy in the  $\alpha_s^3/\epsilon^2$ -term. In our notation for the  $P_{ij}^{(k)}$ , they have the combination  $\frac{3}{2}P_{ik}^{(1)} \otimes P_{kj}^{(2)} + \frac{3}{2}P_{ik}^{(2)} \otimes P_{kj}^{(1)}$  instead of  $P_{ik}^{(1)} \otimes P_{kj}^{(2)} + 2P_{ik}^{(2)} \otimes P_{kj}^{(1)}$  in Eq. (213). This typo in Ref. [114] was also mentioned in the first footnote of Ref. [125].

It should be kept in mind that the transition functions are process independent quantities, as universal as the parton distributions, but perturbatively computable. They can be interpreted as one-particle reducible version of the splitting functions. Higher orders contain irreducible parts of the same order and reducible parts composed of splitting functions and self energy insertions at lower orders.

#### 4.4.2 Collinear counterterms to $N^3LO$

In Section 4.2.2 we saw that the hadronic cross section  $\sigma_h(x_h)$  with the dimensionless variable  $x_h = m_H^2/s_h$  related to the hadronic process, can be written as

$$\sigma_h(x_h) = x_h \left[ \phi_i^0 \otimes \frac{\sigma_{ij}^0(x)}{x} \otimes \phi_j^0 \right] (x_h). \quad (214)$$

All quantities on the right-hand side taken separately contain collinear singularities whereas the left-hand side is finite. We define cross sections divided by dimensionless variables  $\hat{\sigma}_h = \sigma_h/x_h$  and  $\hat{\sigma}_{ij}^0 = \sigma_{ij}^0/x$ . We insert the renormalization of PDFs via  $\phi_i^0 = \Gamma_{ij}^{-1}\phi_j$  and find:

$$\hat{\sigma}_h(x_h) = \left[ \phi_i^0 \otimes \hat{\sigma}_{ij}^0 \otimes \phi_j^0 \right] (x_h) = \left[ \phi_i \otimes \hat{\sigma}_{ij} \otimes \phi_j \right] (x_h) \quad \text{with} \quad (215)$$

$$\hat{\sigma}_{ij}(x) = \left[ \Gamma_{ik}^{-1,T} \otimes \hat{\sigma}_{kl}^0 \otimes \Gamma_{lj}^{-1} \right] (x), \quad \hat{\sigma}_{ij}^0(x) = \left[ \Gamma_{ik}^T \otimes \hat{\sigma}_{kl} \otimes \Gamma_{lj} \right] (x). \quad (216)$$

We expand the finite cross section  $\hat{\sigma}_{ij}$  in the usual manner as

$$\begin{aligned} \hat{\sigma}_{ij}(x) &= \hat{\sigma}_{ij}^{(0)}(x) + \frac{\alpha_s}{\pi} \hat{\sigma}_{ij}^{(1)}(x) + \left(\frac{\alpha_s}{\pi}\right)^2 \hat{\sigma}_{ij}^{(2)}(x) \\ &\quad + \left(\frac{\alpha_s}{\pi}\right)^3 \hat{\sigma}_{ij}^{(3)}(x) + \mathcal{O}(\alpha_s^4). \end{aligned} \quad (217)$$

The same form holds for the divergent version  $\hat{\sigma}_{ij}^0$  and the counterterm  $\delta\hat{\sigma}_{ij}$  which we define via  $\hat{\sigma}_{ij} = \hat{\sigma}_{ij}^0 + \delta\hat{\sigma}_{ij}$ . We can solve Eq. (216) order by order for the mass factorization counterterms  $\delta\hat{\sigma}_{ij}$  and find:

$$-\delta\hat{\sigma}_{ij}^{(0)} = 0, \quad (218)$$

$$-\delta\hat{\sigma}_{ij}^{(1)} = \left[ \Gamma_{ik}^{(1)} \otimes \hat{\sigma}_{kj}^{(0)} \right] (x) + \left[ \hat{\sigma}_{ik}^{(0)} \otimes \Gamma_{kj}^{(1)} \right] (x), \quad (219)$$

$$-\delta\hat{\sigma}_{ij}^{(2)} = \left[ \Gamma_{ik}^{(1)} \otimes \hat{\sigma}_{kl}^{(0)} \otimes \Gamma_{lj}^{(1)} \right] (x) + \left[ \Gamma_{ik}^{(1)} \otimes \hat{\sigma}_{kj}^{(1)} \right] (x) + \left[ \Gamma_{ik}^{(2)} \otimes \hat{\sigma}_{kj}^{(0)} \right] (x)$$

$$\begin{aligned}
 & + \left[ \hat{\sigma}_{ik}^{(0)} \otimes \Gamma_{kj}^{(2)} \right] (x) + \left[ \hat{\sigma}_{ik}^{(1)} \otimes \Gamma_{kj}^{(1)} \right] (x), \quad (220) \\
 -\delta\hat{\sigma}_{ij}^{(3)} = & \left[ \Gamma_{ik}^{(1)} \otimes \hat{\sigma}_{kl}^{(0)} \otimes \Gamma_{lj}^{(2)} \right] (x) + \left[ \Gamma_{ik}^{(1)} \otimes \hat{\sigma}_{kl}^{(1)} \otimes \Gamma_{lj}^{(1)} \right] (x) \\
 & + \left[ \Gamma_{ik}^{(2)} \otimes \hat{\sigma}_{kl}^{(0)} \otimes \Gamma_{lj}^{(1)} \right] (x) + \left[ \Gamma_{ik}^{(1)} \otimes \hat{\sigma}_{kj}^{(2)} \right] (x) \\
 & + \left[ \Gamma_{ik}^{(2)} \otimes \hat{\sigma}_{kj}^{(1)} \right] (x) + \left[ \Gamma_{ik}^{(3)} \otimes \hat{\sigma}_{kj}^{(0)} \right] (x) + \left[ \hat{\sigma}_{ik}^{(0)} \otimes \Gamma_{kj}^{(3)} \right] (x) \\
 & + \left[ \hat{\sigma}_{ik}^{(2)} \otimes \Gamma_{kj}^{(1)} \right] (x) + \left[ \hat{\sigma}_{ik}^{(1)} \otimes \Gamma_{kj}^{(2)} \right] (x). \quad (221)
 \end{aligned}$$

Next, we specify the generic formulae Eqs. (218), (219), (220) and (221) to the channels we have in Higgs boson production. Due to symmetries of cross sections  $\hat{\sigma}_{ij} = \hat{\sigma}_{ji}$  and convolution integrals, non-trivial combinatorical factors arise. In addition, we have equivalence for different quark-flavors, e.g.  $\hat{\sigma}_{q'g} = \hat{\sigma}_{\bar{q}g} = \hat{\sigma}_{qg}$  or  $P_{q'g} = P_{\bar{q}g} = P_{qg}$ . We also need to account for the number of light flavors  $n_l$  when summing free parton indices over quarks. For example, from  $P_{kg}^{(1)} \otimes P_{gk}^{(1)} \otimes \hat{\sigma}_{gg}^{(0)}$  we get a term  $2n_l P_{qg}^{(1)} \otimes P_{gq}^{(1)} \otimes \hat{\sigma}_{gg}^{(0)}$  since quarks and antiquarks give the same contribution. Diagrammatically different chains of collinear emission can be related to the same convolution integral. Or the other way around, there are different ways to visualize a convolution integral, each corresponds to a collinear divergence of a cut in the four-point function diagrams we compute.

In this way we constructed all infrared counterterms needed for N<sup>3</sup>LO Higgs boson production. The results up to NNLO are given below in terms of convolutions of finite partonic cross sections and splitting functions.

$$\delta\hat{\sigma}_{gg}^{(0)} = \delta\hat{\sigma}_{q\bar{q}}^{(1)} = 0, \quad (222)$$

$$\delta\hat{\sigma}_{qg}^{(1)} = \frac{1}{\epsilon} \left[ P_{gq}^{(1)} \otimes \hat{\sigma}_{gg}^{(0)} \right] (x), \quad (223)$$

$$\delta\hat{\sigma}_{gg}^{(1)} = \frac{2}{\epsilon} \left[ P_{gg}^{(1)} \otimes \hat{\sigma}_{gg}^{(0)} \right] (x), \quad (224)$$

$$\begin{aligned}
 \delta\hat{\sigma}_{qq'}^{(2)} = \delta\hat{\sigma}_{q\bar{q}}^{(2)} = & \\
 & - \frac{1}{\epsilon^2} \left[ P_{gq}^{(1)} \otimes \hat{\sigma}_{gg}^{(0)} \otimes P_{gq}^{(1)} \right] (x) + \frac{2}{\epsilon} \left[ P_{gq}^{(1)} \otimes \hat{\sigma}_{qg}^{(1)} \right] (x), \quad (225)
 \end{aligned}$$

$$\begin{aligned}
 \delta\hat{\sigma}_{q\bar{q}}^{(2)} = & - \frac{1}{\epsilon^2} \left[ P_{gq}^{(1)} \otimes \hat{\sigma}_{gg}^{(0)} \otimes P_{gq}^{(1)} \right] (x) \\
 & + \frac{2}{\epsilon} \left\{ \left[ P_{q\bar{q}}^{(1)} \otimes \hat{\sigma}_{q\bar{q}}^{(1)} \right] (x) + \left[ P_{gq}^{(1)} \otimes \hat{\sigma}_{qg}^{(1)} \right] (x) \right\}, \quad (226)
 \end{aligned}$$

$$\begin{aligned}
 \delta\hat{\sigma}_{qg}^{(2)} = & - \frac{1}{2\epsilon^2} \left\{ \left[ P_{q\bar{q}}^{(1)} \otimes P_{gq}^{(1)} \otimes \hat{\sigma}_{gg}^{(0)} \right] (x) + 3 \left[ P_{gq}^{(1)} \otimes P_{gg}^{(1)} \otimes \hat{\sigma}_{gg}^{(0)} \right] (x) \right. \\
 & \left. + \beta_0 \left[ P_{gq}^{(1)} \otimes \hat{\sigma}_{gg}^{(0)} \right] (x) \right\} \\
 & + \frac{1}{2\epsilon} \left\{ \left[ P_{gq}^{(2)} \otimes \hat{\sigma}_{gg}^{(0)} \right] (x) + 2 \left[ P_{qg}^{(1)} \otimes \hat{\sigma}_{q\bar{q}}^{(1)} \right] (x) \right. \\
 & + 2 \left[ P_{gg}^{(1)} \otimes \hat{\sigma}_{qg}^{(1)} \right] (x) + 2 \left[ P_{q\bar{q}}^{(1)} \otimes \hat{\sigma}_{qg}^{(1)} \right] (x) \\
 & \left. + 2 \left[ P_{gq}^{(1)} \otimes \hat{\sigma}_{gg}^{(1)} \right] (x) \right\}, \quad (227)
 \end{aligned}$$

$$\delta\hat{\sigma}_{gg}^{(2)} = - \frac{1}{\epsilon^2} \left\{ 2 \left[ P_{gg}^{(1)} \otimes P_{gg}^{(1)} \otimes \hat{\sigma}_{gg}^{(0)} \right] (x) + 2n_l \left[ P_{qg}^{(1)} \otimes P_{gq}^{(1)} \otimes \hat{\sigma}_{gg}^{(0)} \right] (x) \right.$$

$$\begin{aligned}
 & +\beta_0 \left[ P_{gg}^{(1)} \otimes \hat{\sigma}_{gg}^{(0)} \right] (x) \Big\} \\
 & + \frac{1}{\epsilon} \left\{ 2 \left[ P_{gg}^{(1)} \otimes \hat{\sigma}_{gg}^{(1)} \right] (x) + \left[ P_{gg}^{(2)} \otimes \hat{\sigma}_{gg}^{(0)} \right] (x) \right. \\
 & \quad \left. + 4n_l \left[ P_{qg}^{(1)} \otimes \hat{\sigma}_{qg}^{(1)} \right] (x) \right\}. \tag{228}
 \end{aligned}$$

The N<sup>3</sup>LO expressions are quite lengthy and for this reason we exemplify them in the main text only by the counterterm to the  $qq'$ -channel. This expression will be used in Section 4.5.1, all remaining expressions can be found in Appendix B.2. The complete set of expressions is also provided in electronic form in Ref. [34].

$$\begin{aligned}
 \delta\hat{\sigma}_{qq'}^{(3)} = & \frac{1}{\epsilon^3} \left\{ \left[ P_{qq}^{(1)} \otimes P_{gq}^{(1)} \otimes \hat{\sigma}_{gg}^{(0)} \otimes P_{gq}^{(1)} \right] (x) \right. \\
 & + \left[ P_{gq}^{(1)} \otimes P_{gg}^{(1)} \otimes \hat{\sigma}_{gg}^{(0)} \otimes P_{gq}^{(1)} \right] (x) \\
 & \left. + \beta_0 \left[ P_{gq}^{(1)} \otimes \hat{\sigma}_{gg}^{(0)} \otimes P_{gq}^{(1)} \right] (x) \right\} \\
 & - \frac{1}{\epsilon^2} \left\{ \left[ P_{gq}^{(1)} \otimes P_{qg}^{(1)} \otimes \hat{\sigma}_{q\bar{q}}^{(1)} \right] (x) + 3 \left[ P_{q\bar{q}}^{(1)} \otimes P_{gq}^{(1)} \otimes \hat{\sigma}_{qg}^{(1)} \right] (x) \right. \\
 & + \left[ P_{gq}^{(1)} \otimes P_{gg}^{(1)} \otimes \hat{\sigma}_{qg}^{(1)} \right] (x) + \left[ P_{gq}^{(1)} \otimes \hat{\sigma}_{gg}^{(1)} \otimes P_{gq}^{(1)} \right] (x) \\
 & + \left[ P_{gq}^{(1)} \otimes \hat{\sigma}_{gg}^{(0)} \otimes P_{gq}^{(2)} \right] (x) + \beta_0 \left[ P_{gq}^{(1)} \otimes \hat{\sigma}_{qg}^{(1)} \right] (x) \Big\} \\
 & + \frac{1}{\epsilon} \left\{ 2 \left[ P_{qq}^{(1)} \otimes \hat{\sigma}_{qq'}^{(2)} \right] (x) + 2 \left[ P_{gq}^{(1)} \otimes \hat{\sigma}_{qg}^{(2)} \right] (x) \right. \\
 & \quad \left. + \left[ P_{qq'}^{(2)} \otimes \hat{\sigma}_{q\bar{q}}^{(1)} \right] (x) + \left[ P_{gq}^{(2)} \otimes \hat{\sigma}_{qg}^{(1)} \right] (x) \right\}. \tag{229}
 \end{aligned}$$

Here, it is rather obvious why we needed to evaluate higher orders in  $\epsilon$  for the cross sections up to NNLO. The collinear counterterms cancel not only singularities in the N<sup>3</sup>LO cross sections but give also finite contributions. Therefore, as can be seen in Eq. (229) where only  $\hat{\sigma}_{ij}^{(k)}$  retains dependence on  $\epsilon$ , we need the LO cross section to  $\mathcal{O}(\epsilon^3)$ , the NLO cross sections to  $\mathcal{O}(\epsilon^2)$  and the NNLO cross section to  $\mathcal{O}(\epsilon)$ . The same is true for the ultraviolet counterterms.

#### 4.4.3 Systematic approach to convolution integrals

Having at hand expressions for the collinear subtraction terms, given by convolutions of cross sections and splitting functions, the task of their evaluations remains. We only have to consider five different types of convolutions which are pictured in Fig. 17. For mass factorization at NLO only 2 different convolutions are needed, at NNLO 15 more convolutions must be considered and 63 more for N<sup>3</sup>LO accuracy (exploiting all symmetries). It stands to reason to evaluate them in a systematic fashion. Note that some of the convolutions of up to three splitting functions involve only the LO cross section. Since  $\hat{\sigma}_{gg}^{(0)}$  is proportional to  $\delta(1-x)$  one of these convolutions is trivial. On the other hand, convolutions involving essentially only splitting functions have universal character for QCD corrections to the parton model.

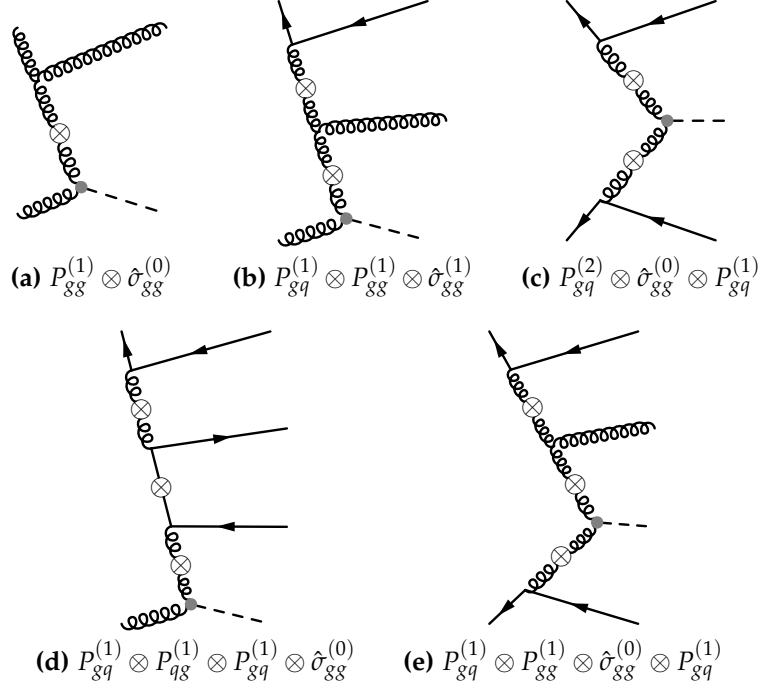


**Figure 17:** Examples for the five convolution topologies we need to consider for Higgs boson production at  $N^3\text{LO}$ . Note that we only showed convolutions involving LO quantities. In the one-fold and two-fold convolutions in Figs. a, b and c they can be replaced by their contributions up to NNLO and NLO, respectively. The figure labels state the specific sequence of convolutions indicated by the  $\otimes$  symbol connecting splitting function and cross section lines. Apart from that, the notation is as before. Cross sections can be distinguished by the effective coupling to a Higgs line. Each convolution comes with a pole in  $\epsilon$ . Figure d shows the case of a convolution that comes with a factor  $2n_f$ , accounting for an internal quark line which represents light quarks and antiquarks of all flavors. Figure a appears first at NLO, Figs. b and c first at NNLO, Figs. d and e only at  $N^3\text{LO}$ .

The following building blocks arise in the splitting functions and in our case also in the cross sections: constant terms or terms proportional to one of the distributions  $\delta(1-x)$  and  $\left[\frac{\ln^k(1-x)}{1-x}\right]_+$ , containing HPLs of argument  $x$  up to some maximum weight (weight four in the  $\mathcal{O}(\epsilon)$  terms of the NNLO Higgs boson production cross sections), multiplied by polynomials in  $x$ , factors of  $\frac{1}{1-x}$ ,  $\frac{1}{x}$  and  $\frac{1}{1+x}$ .

#### 4.4.3.1 Mellin transform and harmonic sums

The Mellin transform of an  $x$ -space function  $f(x)$  to  $n$ -space is defined as

$$M_n[f(x)] = \int_0^1 dx x^{n-1} f(x), \quad (230)$$

where  $M_n$  is also called the  $n$ -th Mellin moment. Once transformed to Mellin space, convolution integrals turn into ordinary products

$$M_n[[f \otimes g](x)] = M_n[f(x)] M_n[g(x)]. \quad (231)$$

This is because integrations in Eq. (151) are bounded by  $[0, 1]$  and therefore also the product  $x_1 x_2$ . The Mellin transform links HPLs and their derivatives to harmonic sums  $S_{\bar{w}}(n)$ . Harmonic sums are defined as nested sums, similarly to the HPLs:

$$S(n) = 1, \quad S_{\bar{w}_m}(n) = \sum_{i=1}^n f_{w_1}(i) S_{\bar{w}_{m-1}}(i),$$

$$\text{with } f_w(i) = \begin{cases} i^{-w}, & w \geq 0, \\ (-1)^i i^w, & w < 0. \end{cases} \quad (232)$$

But in contrast to HPLs, the weight of harmonic sums is the sum of absolute values of indices, not their number.

**Example 47.** The Mellin transforms of HPLs through weight one read:

$$\begin{aligned} M_n[1] &= \frac{1}{n}, \\ M_n[H_0(x)] &= -\frac{1}{n^2}, \\ M_n[H_1(x)] &= \frac{S_1(n)}{n}, \\ M_n[H_{-1}(x)] &= -\frac{(-1)^n}{n} (S_{-1}(n) + \ln 2) + \frac{\ln 2}{n}. \end{aligned} \quad (233)$$

Note that in general on the right-hand sides transcendental numbers from HPLs evaluated at  $x = 1$  appear.

From the definition of the Mellin transform in Eq. (230), we trivially have an index-shift identity:

$$M_n[x^k f(x)] = M_{n+k}[f(x)]. \quad (234)$$

For the derivative  $df(x)/dx$  of a function  $f(x)$  we have the integration-by-parts relation:

$$\begin{aligned} M_n\left[\frac{df(x)}{dx}\right] &= x^{n-1} f(x) \Big|_0^1 - (n-1) M_{n-1}[f(x)] \\ &= f(1) - (n-1) M_{n-1}[f(x)], \end{aligned} \quad (235)$$

assuming  $f(x)$  is regular in the limit  $x \rightarrow 1$  and  $n$  is larger than the highest pole of  $f(x)$  for  $x \rightarrow 0$ .

#### 4.4.3.2 Regularized derivative

In case  $f(x)$  is not regular for  $x \rightarrow 1$ , we need to treat logarithmic singularities in Eq. (235) properly. This can be achieved by introducing ‘‘regularized derivatives’’, denoted  $\hat{\partial}_x$ , as follows:

$$M_n[\hat{\partial}_x 1] = 1, \quad M_n[\hat{\partial}_x f(x)] = R[f(x)] - (n-1) M_{n-1}[f(x)], \quad (236)$$

where  $R$  regulates the boundary term for  $x \rightarrow 1$ . To see the precise action of  $R$ , let us assume  $f(x)$  has the form

$$f(x) = \sum_{i=0}^m f_i(x) \ln^i(1-x), \quad (237)$$

where  $m$  corresponds to the highest power of a logarithm. The effect of  $R$  is just to drop all logarithmically divergent contributions:

$$R[f(x)] = f_0(1). \quad (238)$$

Another way to regulate these singularities is by the more common delta- and plus-distributions. Let us demonstrate in a simple example that these two approaches are equivalent.

**Example 48.** The Mellin transform  $M_n[df(x)/dx]$  in the case  $df(x)/dx = 1/(1-x)$  is not defined because  $f(x) = H_1(x) = -\ln(1-x)$  is divergent in the limit  $x \rightarrow 1$ . Sticking to our definitions in Eqs. (236) and (238), we observe:

$$\begin{aligned} M_n \left[ \hat{\partial}_x H_1(x) \right] &= R[-\ln(1-x)] - (n-1) M_{n-1}[-\ln(1-x)] \\ &= 0 - (n-1) \frac{S_1(n-1)}{n-1} = -S_1(n-1). \end{aligned}$$

Apart from that, making the replacement  $\frac{1}{1-x} \rightarrow \left[ \frac{1}{1-x} \right]_+$ , we can directly evaluate the Mellin transform:

$$\begin{aligned} M_n \left[ \left[ \frac{1}{1-x} \right]_+ \right] &= \int_0^1 dx x^{n-1} \left[ \frac{1}{1-x} \right]_+ = \int_0^1 dx \frac{x^{n-1} - 1}{1-x} \\ &= \sum_{i=0}^{\infty} \int_0^1 dx (x^{n+i-1} - x^i) = \sum_{i=0}^{\infty} \left( \frac{1}{n+i} - \frac{1}{i+1} \right) \\ &= - \sum_{i=1}^{n-1} \frac{1}{i} = -S_1(n-1), \end{aligned}$$

where we used the definition of the plus-distribution in Eq. (158) on Page 121, the infinite geometric series  $1/(1-x) = \sum_{i=0}^{\infty} x^i$  and identified the harmonic sum  $S_1(n-1)$ . As we can see, regularization with the plus-distribution and subsequent explicit evaluation of the Mellin moment gives the same result as application of the regularized derivative.

**Example 49.** In addition, the regularized derivative reduces to the ordinary derivative when applied to a function without divergence in the limit  $x \rightarrow 1$ , e.g.:

$$\begin{aligned} \hat{\partial}_x H_0(x) &= \frac{d}{dx} H_0(x) = \frac{1}{x}, \\ \hat{\partial}_x H_{-1}(x) &= \frac{d}{dx} H_{-1}(x) = \frac{1}{1+x}, \end{aligned} \quad (239)$$



$$\hat{\partial}_x H_{-1,1}(x) = \frac{d}{dx} H_{-1,1}(x) = \frac{H_1(x)}{1+x}.$$

Some other applications of the regularized derivative give:

$$\boxed{\begin{aligned} \hat{\partial}_x 1 &= \delta(1-x), \\ \hat{\partial}_x H_1(x) &= \left[ \frac{1}{1-x} \right]_+, \end{aligned}} \quad (240)$$

$$\hat{\partial}_x H_{1,1}(x) = - \left[ \frac{\ln(1-x)}{1-x} \right]_+,$$

$$\hat{\partial}_x H_{1,1,1}(x) = \frac{1}{2} \left[ \frac{\ln^2(1-x)}{1-x} \right]_+,$$

$$\hat{\partial}_x H_{1,2}(x) = \frac{\pi^2}{6} \left[ \frac{1}{1-x} \right]_+ + \frac{H_2(x) - \frac{\pi^2}{6}}{1-x}.$$

Note that  $\hat{\partial}_x 1 = \delta(1-x)$  by the definition in Eq. (236), although  $f(x) = 1$  does not diverge for  $x \rightarrow 1$ . Otherwise we would have  $M_n \left[ \frac{d}{dx} 1 \right] = 0$  but  $M_n \left[ \hat{\partial}_x 1 \right] = 1$  is needed to incorporate convolutions involving also delta-functions.

In conclusion, the notion of the regularized derivative gives us a handle to treat Mellin transforms of derivatives of HPLs in a consistent way, regardless whether they diverge for  $x \rightarrow 1$  or not. This is related to regularization by means of delta- and plus-distributions and therefore Mellin transforms containing these generalized functions are accessible within our framework.

Before coming finally to the description of an algorithm that allows for computing convolutions of the type described in the beginning of the subsection, we elaborate on the examples for quantities of weight one. They will serve as illustration of the way the algorithm works.

**Example 50.** Mellin transforms of regularized derivatives of quantities up to weight one read:

$$\boxed{\begin{aligned} M_n \left[ \hat{\partial}_x 1 \right] &= 1, \\ M_n \left[ \hat{\partial}_x H_0(x) \right] &= \frac{1}{n-1}, \\ M_n \left[ \hat{\partial}_x H_1(x) \right] &= -S_1(n-1), \\ M_n \left[ \hat{\partial}_x H_{-1}(x) \right] &= (-1)^{n-1} S_{-1}(n-1) + (-1)^{n-1} \ln 2. \end{aligned}} \quad (241)$$

For completion, we also list the inverse Mellin transforms of weight-one quantities:

$$\begin{aligned}
 \mathbf{M}_x^{-1}[1] &= \hat{\partial}_x 1, \\
 \mathbf{M}_x^{-1}\left[\frac{1}{n}\right] &= 1, \\
 \mathbf{M}_x^{-1}\left[\frac{1}{n^2}\right] &= -\mathbf{H}_0(x), \\
 \mathbf{M}_x^{-1}[\mathbf{S}_1(n)] &= -x\hat{\partial}_x \mathbf{H}_1(x), \\
 \mathbf{M}_x^{-1}\left[\frac{\mathbf{S}_1(n)}{n}\right] &= \mathbf{H}_1(x).
 \end{aligned}
 \tag{242}$$

**Algorithm 4** (MT). With our formalism laid out, we set up a linear system of relations that is restricted by the maximum weight of the considered expressions. One input are Mellin images of HPLs and their regularized derivatives, see for example Eqs. (233) and (241). The other input are index-shift and integration-by-parts identities, see Eqs. (234) and (235), relating the just mentioned Mellin transforms. Solving this system for monomials of the form

$$\left\{ \frac{1}{n^k}, \frac{\mathbf{S}_{\bar{w}}(n)}{n^k}, (-1)^n \frac{\mathbf{S}_{\bar{w}}(n)}{n^k} \right\}
 \tag{243}$$

gives consequently the inverse Mellin transforms, see Eq. (242). In more detail, the convolution  $[f \otimes g](x)$  of two functions  $f(x)$  and  $g(x)$  can be found by the following procedure:

1. Transform expressions for  $f(x)$  and  $g(x)$  to Mellin space where the convolution integral turns into a simple product, see Eq. (231).
2. For HPLs up to a weight that is fixed by the sum of maximum weights in  $f(x)$  and  $g(x)$ , compute the table of Mellin transforms, see Eq. (233).
3. Provide the corresponding table of regularized derivatives for the HPLs from Step 2, see Eq. (241).
4. Solve the linear system of equations built from the two tables of Step 2 and Step 3, see Eq. (242).
5. Inserting the results from Step 4 allows evaluation of the inverse Mellin transform and thereby the convolution integral initially asked for:

$$[f \otimes g](x) = \mathbf{M}_x^{-1}[\mathbf{M}_n[f(x)] \mathbf{M}_n[g(x)]].
 \tag{244}$$

**Example 51.** We list some results for convolutions of building blocks appearing in the calculation of the infrared counterterms and involving plus-distributions. They were found with the help of Algorithm 4.

$$\begin{aligned}
 & \left[ \left[ \frac{\ln^3(1-x)}{1-x} \right]_+ \otimes \left[ \frac{1}{1-x} \right]_+ \right] (x) = \\
 & \quad \frac{5}{4} \left[ \frac{\ln^4(1-x)}{1-x} \right]_+ - \frac{\pi^2}{2} \left[ \frac{\ln^2(1-x)}{1-x} \right]_+ \\
 & \quad + 6\zeta(3) \left[ \frac{\ln(1-x)}{1-x} \right]_+ - \frac{\pi^4}{15} \left[ \frac{1}{1-x} \right]_+ + 6\zeta(5)\delta(1-x) \\
 & \quad + \frac{6}{1-x} (\text{H}_{1,1,2}(x) + \text{H}_{1,2,1}(x) + \text{H}_{2,1,1}(x) + \text{H}_{1,1,1,0}(x)), \\
 & \left[ \left[ \frac{\ln^4(1-x)}{1-x} \right]_+ \otimes \left[ \frac{1}{1-x} \right]_+ \right] (x) = \\
 & \quad \frac{6}{5} \left[ \frac{\ln^5(1-x)}{1-x} \right]_+ - \frac{2\pi^2}{3} \left[ \frac{\ln^4(1-x)}{1-x} \right]_+ + 12\zeta(3) \left[ \frac{\ln^2(1-x)}{1-x} \right]_+ \\
 & \quad - \frac{4\pi^4}{15} \left[ \frac{\ln(1-x)}{1-x} \right]_+ + 24\zeta(5) \left[ \frac{1}{1-x} \right]_+ - \frac{8\pi^6}{315} \delta(1-x) \\
 & \quad - \frac{24}{1-x} (\text{H}_{1,1,1,2}(x) + \text{H}_{1,1,2,1}(x) + \text{H}_{1,2,1,1}(x) + \text{H}_{2,1,1,1}(x) \\
 & \quad \quad + \text{H}_{1,1,1,1,0}(x)), \\
 & \left[ \text{H}_{1,1,1,0}(x) \otimes \left[ \frac{1}{1-x} \right]_+ \right] (x) = \\
 & \quad - \text{H}_{1,1,1,0,0}(x) - 3\text{H}_{1,1,1,1,0}(x) - \text{H}_{1,1,1,2}(x) - \text{H}_{1,1,2,0}(x) \\
 & \quad - \text{H}_{1,2,1,0}(x) - \text{H}_{2,1,1,0}(x) + \frac{\pi^2}{6} \text{H}_{1,1,1}(x) - 2\zeta(3) \text{H}_{1,1}(x) \\
 & \quad - \frac{\pi^4}{72} \text{H}_1(x) - 3\zeta(5) + \frac{\pi^2}{6} \zeta(3).
 \end{aligned}$$

#### CONCLUDING REMARKS

- Results for the convolution integrals relevant to N<sup>3</sup>LO Higgs boson production contain HPLs up to weight five, even though in intermediate steps quantities of weight six occur. Inverse Mellin transforms of the form  $(-1)^n/n$  are not listed in Eq. (243) since they cannot be expressed in terms of HPLs. For the same reason they cannot be determined from the system of Step 4 but they cancel in the final results for convolutions of splitting functions and cross sections. Both observations can be linked to the fact that integrals of specific order in perturbation theory and in  $\epsilon$  give rise only to quantities of a certain maximum weight.
- In Refs. [90, 115, 150, 157], we presented explicit results for all convolutions of LO to NNLO cross sections needed for physical Higgs boson

production cross sections at  $N^3LO$ . In Refs. [115, 157], we made our implementation of above algorithm publicly available together with a full-fledged user manual and convolutions needed for vector boson production to  $N^3LO$ . Convolutions involving quark flavor dependent splitting functions were missing in Refs. [90, 150]; these were supplemented together with Refs. [115, 157].

- Our implementation of Algorithm 4 in *Mathematica*, called MT, is built upon the HPL package, see Refs. [154, 155]. It originated from an earlier version due to A. Pak and was used in Ref. [73] where also a sketch of the algorithm was first published. Mellin transforms of HPLs were obtained via the FORM package `harmpol`, see Refs. [152, 153]. All Mellin images we had to deal with can also be found in Refs. [158, 159].
- An alternative approach is described in Ref. [114] and agreement can be found with our results. In intermediate steps it is made use of multiple polylogarithms which form an even more generic class of functions compared to HPLs.

#### 4.5 CONTRIBUTIONS TO HIGGS BOSON PRODUCTION AT $N^3LO$

The calculation of the total Higgs boson production rate at  $N^3LO$ , that is at three loops within the EFT, is without any doubt a highly demanding and formidable task. This required the build-up of a powerful toolchain. Those parts concerned with the calculation of diagrams, management of topologies and reduction of scalar integrals were presented in Chapters 2 and 3. The calculation of master integrals is not part of this thesis. The  $qq'$ -channel at  $N^3LO$  serves as testing ground for our approach and will be discussed in Sections 4.5.1 and 4.5.2. In Section 4.5.3, we give an outlook for the calculation of the remaining partonic channels.

Table 4 gives an overview of the total number of diagrams in each partonic channel and the dissection into fermionic contributions at  $N^3LO$ . For channels with gluons in the initial state, these numbers also account for the corresponding subchannels initiated by ghosts. As on lower loop orders, the  $gg$ -channel has by far the largest number of diagrams. On the other side, one can expect that most topologies and master integrals already appear in the  $q\bar{q}$ - and  $qg$ -channels since they involve already all classes of cuts, see Tab. 2, apart from purely virtual corrections which are known, see Refs. [116, 117].

The numbers in Tab. 4 cannot be produced directly with QGRAF. When setting up the needed forward scattering process, a large excess of diagrams that are not relevant for Higgs boson production is the outcome. Therefore, we use a filter, see Ref. [160], that implements Algorithm 3 in order to select diagrams with valid cuts and a non-zero color factor only. As described before, valid cuts go through the Higgs line and up to three partons in the  $s$ -channel (separating incoming from outgoing momenta). It proved more practical to check first for valid cuts and only then, if a diagram passed, to compute the color factor. Table 5 compares the original numbers of diagrams given by QGRAF to the numbers of diagrams accepted by the filter.

**Table 4:** Number of diagrams appearing at N<sup>3</sup>LO in each channel and in their sum. The numbers in the right columns indicate dissection in fermionic contributions. Gluonic channels include also diagrams with ghosts as incoming and outgoing particles. Purely virtual diagrams in the  $gg$ -channel are listed for completeness.

Channel	Number of diagrams (fermionic loops)			
$qq'$	#220	= #216	+ #4 $n_l$	
$qq$	#404	= #396	+ #8 $n_l$	
$q\bar{q}$	#4889	= #4438	+ #445 $n_l$	+ #6 $n_l^2$
$qg$	#9591	= #8976	+ #612 $n_l$	+ #3 $n_l^2$
$gg_{\text{virt}}$	#9538	= #7266	+ #2180 $n_l$	+ #92 $n_l^2$
$gg_{\text{real}}$	#150246	= #128676	+ #21196 $n_l$	+ #374 $n_l^2$
$\Sigma$	#174938	= #150014	+ #24449 $n_l$	+ #475 $n_l^2$

#### 4.5.1 Fermionic contribution in the $qq'$ -channel

One of the simplest independent contributions to the N<sup>3</sup>LO Higgs boson production cross section from genuine three-loop diagrams is the fermionic contribution in the  $qq'$ -channel, cf. Tab. 4. The  $qq'$ -channel starts at NNLO with a single diagram. Hence, at N<sup>3</sup>LO only four diagrams exist with an additional fermion insertion in different places, see Fig. 18a on Page 154. They only have a three-particle cut and consequently belong to the VR<sup>2</sup> class. This subchannel is on its own a physical contribution. It can be UV and IR renormalized independently and is gauge independent. The NNLO  $qq'$ -channel cross section enters via UV renormalization of  $\alpha_s$  and  $\mathcal{O}_1$  because  $\beta_0$  has a term proportional to the number of light quark flavors  $n_l$ . For mass factorization already 7 of the 13 convolution integrals in Eq. (229) become relevant. The dependence on  $n_l$  of

$$\begin{aligned}
 & \left[ P_{gq}^{(1)} \otimes P_{gg}^{(1)} \otimes \hat{\sigma}_{gg}^{(0)} \otimes P_{gq}^{(1)} \right] (x), \beta_0 \left[ P_{gq}^{(1)} \otimes \hat{\sigma}_{gg}^{(0)} \otimes P_{gq}^{(1)} \right] (x), \\
 & \left[ P_{gq}^{(1)} \otimes P_{gg}^{(1)} \otimes \hat{\sigma}_{qg}^{(1)} \right] (x), \left[ P_{gq}^{(1)} \otimes \hat{\sigma}_{gg}^{(0)} \otimes P_{gq}^{(2)} \right] (x), \beta_0 \left[ P_{gq}^{(1)} \otimes \hat{\sigma}_{qg}^{(1)} \right] (x), \\
 & \left[ P_{gq}^{(1)} \otimes \hat{\sigma}_{qg}^{(2)} \right] (x), \left[ P_{gq}^{(2)} \otimes \hat{\sigma}_{qg}^{(1)} \right] (x)
 \end{aligned}$$

is implicit in Eq. (229).

Based on the four diagrams with 10 propagators each, it is possible to infer a single topology with 7 propagators and 5 irreducible scalar products, see Fig. 18b. This was accomplished with the package TopoID. In this process, three propagators in each of the initial diagrams were identified due to identical momentum flow. In Fig. 18a the three vertical propagators on the left with labels 5, 6 and 7 are contracted. The two lines 6 and 7 connected to the fermionic insertion can be identified in a first step. The two subsequent identifications can be understood analogously to Example 2 on Page 15. In particular, propagators 3 and 5 carry the same momentum since  $p_2$  enters at the lower left external leg and exits at the lower right external leg. Then one arrives at the topology in Fig. 18b, up to a horizontal mirroring. All propa-

**Table 5:** Statistics for filtering diagrams from LO to N<sup>3</sup>LO. The first figure indicates the number of diagrams which exhibit a valid cut and a non-zero color factor. The figures in parentheses show the number of diagrams generated initially by QGRAF, followed by the numbers of discarded diagrams due to missing cuts and zero color factor, respectively.

Order	Channel	Number of diagrams (initial, no cut, no color)			
LO	$g\bar{g}$	1	(3	-2	-0)
	$q\bar{q}$	1	(4	-3	-0)
NLO	$qg$	1	(18	-17	-0)
	$g\bar{g}_{\text{virt}}$	10	(48	-32	-6)
	$g\bar{g}_{\text{real}}$	38	(202	-164	-0)
	$\Sigma$	50	(272	-216	-6)
	$qq'$	1	(154	-153	-0)
NNLO	$qq$	2	(298	-296	-0)
	$q\bar{q}$	84	(280	-182	-14)
	$qg$	124	(1515	-1377	-14)
	$g\bar{g}_{\text{virt}}$	294	(1368	-909	-165)
	$g\bar{g}_{\text{real}}$	2458	(12289	-9623	-208)
	$\Sigma$	2964	(15922	-12549	-409)
	$qq'$	220	(8818	-8572	-26)
N <sup>3</sup> LO	$qq$	404	(16100	-15616	-80)
	$q\bar{q}$	4889	(15392	-9207	-1296)
	$qg$	9591	(84286	-72840	-1855)
	$g\bar{g}_{\text{virt}}$	9538	(44190	-29342	-5310)
	$g\bar{g}_{\text{real}}$	150246	(690624	-513385	-26993)
	$\Sigma$	174938	(860118	-649316	-35864)

gators are linearly dependent and no partial fractioning is needed. This is true also for the topologies of the full  $qq'$ -channel.

The factors of the topology N3L0qpn1BT1 found in the way described above are given by

$$\begin{aligned}
 1: d_7 &= m_H^2 - s - 2p_1 \cdot v_1 - 2p_2 \cdot v_1 + v_1^2 && (p_1 + p_2 - v_1 - v_2) \\
 &\quad - 2p_1 \cdot v_2 - 2p_2 \cdot v_2 + 2v_1 \cdot v_2 + v_2^2, \\
 2: d_9 &= -2p_2 \cdot v_2 + v_2^2 + 2p_2 \cdot v_3 - 2v_2 \cdot v_3 + v_3^2, && (p_2 - v_2 + v_3) \\
 3: n_{10} &= v_1^2 - 2v_1 \cdot v_3 + v_3^2, \\
 4: d_5 &= -2p_2 \cdot v_2 + v_2^2, && (p_2 - v_2) \\
 5: n_4 &= -2p_1 \cdot v_2 + v_2^2, \\
 6: d_4 &= v_2^2, && (v_2) \\
 7: n_2 &= -2p_2 \cdot v_1 + v_1^2, \\
 8: d_2 &= -2p_1 \cdot v_1 + v_1^2, && (p_1 - v_1) \\
 9: n_9 &= -2p_2 \cdot v_3 + v_3^2, \\
 10: n_8 &= -2p_1 \cdot v_3 + v_3^2, \\
 11: d_{10} &= v_3^2, && (v_3) \\
 12: d_1 &= v_1^2, && (v_1) \tag{245}
 \end{aligned}$$

where the first column of numbers are the positions of powers of these factors in the function notation N3L0qpn1BT1( $\mathbf{a}_1, \mathbf{a}_2, \dots, \mathbf{a}_{12}$ ). Symbols on the left-hand side in the second column indicate whether the factor is a denominator  $d_i$  or a numerator  $n_i$  with the labels  $i$  fixed by TopoID. The right-hand sides show the defining quadratic forms of scalar products of external and internal momenta and the Higgs boson mass  $m_H$ . External invariants have been identified in these definitions by  $p_1^2 = p_2^2 = 0$  and  $p_1 \cdot p_2 = s/2$ . For propagators  $d_i$  the attached flows of momenta are shown in parentheses and the corresponding directed edges in Fig. 18b. Pseudo-propagators  $n_i$  were introduced with the prescription  $n_i = (v_k - v_l)^2$  in case  $v_k \cdot v_l$  was irreducible for the external or internal momenta  $v_k$  and  $v_l$ .

The reduction of N3L0qpn1BT1 with rows, see Ref. [49], reveals only three master integrals which are defined by

$$\begin{aligned}
 \text{N3L0qpn1BT1m1} &= \text{N3L0qpn1BT}(1, 1, 0, 0, 0, 1, 0, 0, 0, 0, 1, 1), \\
 \text{N3L0qpn1BT1m2} &= \text{N3L0qpn1BT}(1, 1, -1, 0, 0, 1, 0, 0, 0, 0, 1, 1), \\
 \text{N3L0qpn1BT1m3} &= \text{N3L0qpn1BT}(1, 1, 0, 0, 0, 1, 0, 1, 0, 0, 1, 1). \tag{246}
 \end{aligned}$$

They were calculated by C. Anzai, M. Höschele and T. Ueda in preparation of Ref. [161]. We exemplify results for the three master integrals by N3L0qpnlBT1m1 to  $\mathcal{O}(\epsilon^2)$ :

$$\begin{aligned}
 \text{N3L0qpnlBT1m1} = & \tag{247} \\
 & -\frac{1}{\epsilon} \left\{ H_0(x) x + \frac{(x+1)(1-x)}{2} \right\} \\
 & -5x H_2(x) + x H_{0,0}(x) - \frac{5}{2}(x+1)(1-x) H_1(x) \\
 & + \frac{(x-12)x}{2} H_0(x) + \frac{5}{6}x\pi^2 - \frac{(11x+10)(1-x)}{2} \\
 & + \epsilon \left\{ x \left[ -25 H_{2,1}(x) - 3 H_{2,0}(x) + 5 H_3(x) - H_{0,0,0}(x) \right] \right. \\
 & \quad - \frac{(x+1)(1-x)}{2} [25 H_{1,1}(x) + 3 H_{1,0}(x)] \\
 & \quad + \frac{(x-12)x}{2} [5 H_2(x) - H_{0,0}(x)] - \frac{5}{2}(11x+10)(1-x) H_1(x) \\
 & \quad + \left[ \frac{(11x-47)x}{2} + \frac{2}{3}\pi^2 x \right] H_0(x) + 14x\zeta(3) \\
 & \quad \left. - \frac{14x^2 - 60x - 9}{12}\pi^2 - \frac{(77x+64)(1-x)}{2} \right\} \\
 & + \epsilon^2 \left\{ x \left[ -125 H_{2,1,1}(x) + 3 H_{2,0,0}(x) + 25 H_{3,1}(x) + 3 H_{3,0}(x) \right] \right. \\
 & \quad - 5 H_4(x) + H_{0,0,0,0}(x) - 15x [H_{2,1,0}(x) + H_{2,2}(x)] \\
 & \quad + \frac{(x+1)(1-x)}{2} [125 H_{1,1,1}(x) + 15 H_{1,1,0}(x) + 15 H_{1,2}(x) \\
 & \quad \quad - 3 H_{1,0,0}(x)] \\
 & \quad + \frac{(x-12)x}{2} [25 H_{2,1}(x) + 3 H_{2,0}(x) - 5 H_3(x) + H_{0,0,0}(x)] \\
 & \quad - \frac{(11x+10)(1-x)}{2} [25 H_{1,1}(x) + 3 H_{1,0}(x)] \\
 & \quad + \left[ 2\pi^2 + \frac{11x-47}{2} \right] 5x H_2(x) - \left[ \frac{11x-47}{2} + \frac{2}{3}\pi^2 \right] x H_{0,0}(x) \\
 & \quad + \left[ (1+x)\pi^2 - \frac{77x+64}{2} \right] 5(1-x) H_1(x) \\
 & \quad + \left[ 8\zeta(3) - \frac{x-12}{3}\pi^2 + \frac{7}{2}(11x-21) \right] x H_0(x) \\
 & \quad - \frac{3}{8}x\pi^4 - (18x^2 - 84x - 11)\zeta(3) - \frac{77x^2 - 122x - 45}{6}\pi^2 \\
 & \quad \left. - \frac{(439x+336)(1-x)}{2} \right\}.
 \end{aligned}$$

Results to higher orders in  $\epsilon$  for all three master integrals are included in Ref. [34] in electronic form. Only the  $gg$ -channel has a singular behaviour in the soft limit where denominators of form  $(1-x)$  must be handled with care. Therefore, master integrals can be inserted in this case naively, ignoring the prescriptions in Eqs. (161) and (197) on Pages 123 and 133. For the finite



fermionic contribution  $\tilde{\sigma}_{qq',n_l}^{(3)}$  in the  $qq'$ -channel, defined by  $\tilde{\sigma}_{qq'}^{(3)} = \tilde{\sigma}_{qq',0}^{(3)} + n_l \tilde{\sigma}_{qq',n_l}^{(3)}$  we obtain:

$$\begin{aligned}
 \tilde{\sigma}_{qq',n_l}^{(3)} = & (x+2)^2 \left[ \frac{8}{9} H_{2,1,1}(x) + \frac{40}{27} H_{2,1,0}(x) + \frac{40}{27} H_{2,2}(x) \right. \\
 & + \frac{16}{9} H_{2,0,0}(x) + \frac{4}{3} H_{3,1}(x) + \frac{40}{27} H_{3,0}(x) \\
 & \left. + \frac{32}{27} H_4(x) + \frac{8}{9} H_{0,0,0,0}(x) \right] \\
 & + (x+3)(1-x) \left[ \frac{16}{9} H_{1,1,1}(x) + \frac{80}{27} H_{1,2}(x) + \frac{80}{27} H_{1,1,0}(x) \right. \\
 & \left. + \frac{32}{9} H_{1,0,0}(x) \right] \\
 & + \frac{2}{27} (43x^2 + 184x + 268) H_{2,1}(x) \\
 & + \frac{20}{81} (7x^2 + 40x + 76) H_{2,0}(x) + \frac{4}{81} (23x^2 + 80x + 284) H_3(x) \\
 & + \frac{4}{81} (11x^2 - 40x + 188) H_{0,0,0}(x) \\
 & + (1-x) \left( \frac{1}{27} (319x + 771) H_{1,1}(x) + \frac{70}{81} (13x + 33) H_{1,0}(x) \right) \\
 & - \left[ \frac{4}{81} (x+2)^2 \pi^2 + \frac{2}{243} (896x^2 + 260x - 3247) \right] H_2(x) \\
 & - \left[ \frac{2}{243} (772x^2 + 1156x - 2213) + \frac{4}{81} (x+2)^2 \pi^2 \right] H_{0,0}(x) \\
 & - \left[ \frac{8}{81} (x+3)(1-x) \pi^2 - \frac{41}{486} (169x + 519)(1-x) \right] H_1(x) \\
 & - \left[ \frac{4}{27} (x+2)^2 \zeta(3) + \frac{16}{81} (x^2 + x + 4) \pi^2 \right. \\
 & \left. + \frac{1}{243} (3139x^2 + 5218x - 7620) \right] H_0(x) \\
 & - \frac{49}{2430} (x+2)^2 \pi^4 + \frac{2}{81} (13x^2 + 184x + 4) \zeta(3) \\
 & + \frac{1}{729} (215x^2 - 904x - 1402) \pi^2 + \frac{1}{324} (2549x + 15343)(1-x) \\
 & + \left[ \frac{4}{27} (x+2)^2 H_0(x) + \frac{8}{27} (x+3)(1-x) \right] \ln^3 \left( \frac{\mu^2}{m_H^2} \right) \\
 & + \left[ (x+2)^2 \left( \frac{16}{27} H_2(x) + \frac{4}{9} H_{0,0}(x) - \frac{8}{81} \pi^2 \right) \right. \\
 & + \frac{32}{27} (x+3)(1-x) H_1(x) \\
 & - \frac{2}{81} (x^2 - 56x - 188) H_0(x) \\
 & \left. + \frac{1}{81} (227x + 615)(1-x) \right] \ln^2 \left( \frac{\mu^2}{m_H^2} \right)
 \end{aligned}$$

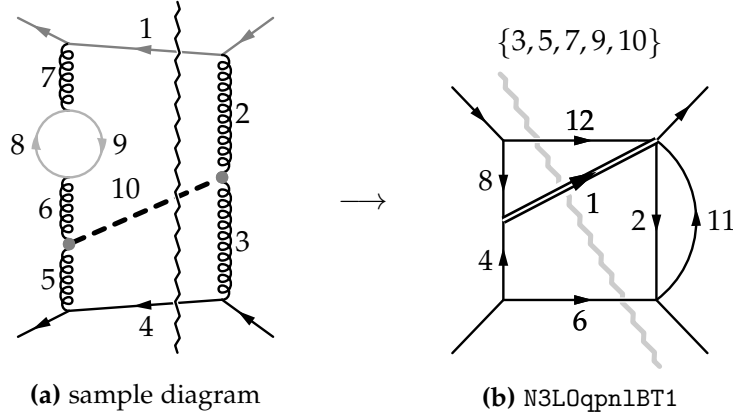


**Figure 18:** Figure a shows the only type of diagram in the fermionic contribution to the  $qq'$ -channel. The four existing diagrams differ only by the position of the fermionic insertion. We accentuated the external quark of different flavor and the internal quark by different shades of gray. The single topology sufficient to calculate the four diagrams is shown in Fig. b. Thin black lines stand for massless propagators, the thick black line is massive. Integer labels on the lines correspond to the propagators defined in Eq. (245). Arrows on external legs mark the routing the momentum  $p_1$ , on internal lines they denote the flows of propagator momenta. The integers in braces are a reminder of the irreducible scalar products that are not represented by graph lines, in this case. The only 3-particle cut is shown by a gray zigzag line in the background.

$$\begin{aligned}
 & + \left[ (x+2)^2 \left( \frac{4}{3} H_{2,1}(x) + \frac{40}{27} H_{2,0}(x) + \frac{32}{27} H_3(x) \right. \right. \\
 & \quad \left. \left. + \frac{8}{9} H_{0,0,0}(x) \right) \right. \\
 & + (x+3)(1-x) \left( \frac{8}{3} H_{1,1}(x) + \frac{80}{27} H_{1,0}(x) \right) \\
 & + \frac{4}{81} (17x^2 + 128x + 284) H_2(x) \\
 & + \frac{4}{81} (5x^2 + 8x + 188) H_{0,0}(x) \\
 & + \frac{2}{81} (341x + 885)(1-x) H_1(x) \\
 & - \left( \frac{4}{81} (x+2)^2 \pi^2 + \frac{2}{243} (724x^2 + 460x - 2213) \right) H_0(x) \\
 & + \frac{4}{9} (x+2)^2 \zeta(3) - \frac{2}{243} (53x^2 + 200x + 176) \pi^2 \\
 & \left. + \frac{2}{243} (1027x + 3714)(1-x) \right] \ln \left( \frac{\mu^2}{m_H^2} \right). \quad (248)
 \end{aligned}$$

The topology N3L0qpnlBT1 can be embedded easily in topologies of the full  $qq'$ -channel which provided a welcome (and fulfilled) check for our methodology.

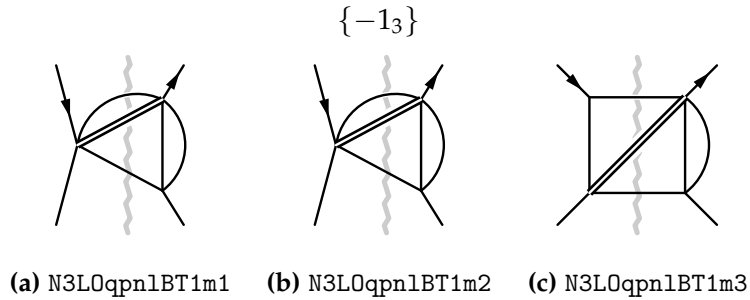


**Figure 19:** The tree master integrals of the topology N3L0qpnlBT1 are defined in Eq. (246). N3L0qpnlBT1m1 in Fig. a and N3L0qpnlBT1m2 in Fig. b have only five propagators and belong to the simpler class of triangle diagrams compared to N3L0qpnlBT1m3 in Fig. c. N3L0qpnlBT1m3 is a box diagram with six propagators. N3L0qpnlBT1m2 has in contrast to N3L0qpnlBT1m1 an irreducible scalar product of power one from the third factor of the topology which is denoted by  $\{-1_3\}$ .

#### 4.5.2 The complete $qq'$ -channel

As at NNLO, the easiest channel at N<sup>3</sup>LO in terms of the number of diagrams is the scattering of two quarks of different flavor, denoted as  $qq'$ -channel. At NNLO only one diagram has to be calculated, at N<sup>3</sup>LO 220 appear. Our calculation is organized as follows: we first define topologies onto which we can match all the Feynman diagrams and then we perform the reduction of all appearing integrals within these topologies. In the result expressed in terms of master integrals of each topology many of these integrals can be eliminated. This means there still exist identities and even linear relations among the master integrals of all families appearing in this preliminary result for the reduction. The third step of the calculation is to eliminate these redundancies as far as possible. This simplifies the final step of calculating the bare forward amplitude, namely the computation of the (almost) minimal number of master integrals. In addition, it helps to establish gauge-parameter independence which must hold even before the master integrals have been computed and substituted into the result.

##### 4.5.2.1 Definition of topologies

For the first step of our calculation we used two differently defined sets of topologies based on the diagrams of the  $qq'$ -channel and obtained with the code TopoID. The first set, in the following referred to as set  $A$ , is constructed by the following steps:

1. Propagators carrying the same momentum are identified on scalar diagram level. MapDiagramTo-  
Topology
2. The set of corresponding topologies is minimized concerning possible line contractions. MinimizeTopolo-  
gies
3. All topologies are completed by including the irreducible scalar products directly. The way topologies are completed can be controlled via the option Method. Here, we assign it the value "ScalarProducts". CompleteTopology  
ScalarProducts

MapTopologyToIn-  
dependents

4. The complete topologies are mapped onto linearly independent topologies.
5. The resulting set is minimized again.

This set of topologies is illustrated in Fig. 20. The second set, denoted as set B, was obtained in contrast with the following modifications:

Keep

1. Propagators carrying the same momentum are *not* identified in the diagrams. This can be controlled by assigning the option `Method` the value "Keep".

MinusPropagator

3. Topologies are completed by including irreducible scalar products in the form of pseudopropagators, see e.g. Section 2.7. This can be accomplished by using "MinusPropagator" as value for `Method`.

The reason of the first modification was of purely technical nature connected to mapping diagrams onto topologies via the program `exp`, see Refs. [23, 24]. Aforementioned program is not able to perform this identification of propagators on graph level.

The result should of course be independent of how irreducible scalar products are included. This makes the comparison of results obtained in sets *A* and *B* a powerful cross-check. Completion of topologies in set *B* with unidentified equal propagators and subsequent partial fractioning lead to other topologies than those in set *A*. In general, the topologies were simpler concerning the numbers of denominators but their total amount was larger. We found 17 topologies in set *A* and 29 in set *B*. We refrain from inspecting set *B* more closely since we stick to set *A* as basis for the coming discussions.

Some remarks on the topologies of set *A* in Fig. 20 are in order:

- The order of topologies is chosen by `TopoID` and not necessarily intuitive or appealing. The same holds for the order of propagators within each topology. This is a direct consequence of the canonical ordering procedure presented in Section 2.4.2.
- Topologies `N3L0qpBT1` to `N3L0qpBT5` and `N3L0qpBT9` have 10 lines which is the maximum for graphs in this process at this order, see Tab. 1 on Page 16. In this sense, they represent complete or maximal graphs. The remaining topologies have vertices of degree four and 9 lines or only 8 in the case of `N3L0qpBT17`.
- Especially those topologies mentioned lastly can be embedded into more generic topologies appearing in the *gg*-channel. During this process merging of topologies is possible, see for example `N3L0qpBT10` and `N3L0qpBT17` in Fig. 20. Suppose we stretch the bubble of lines 1 and 2 in `N3L0qpBT10` into a triangle and do the same for the differently oriented bubble of lines 2 and 3 in `N3L0qpBT17`. Then, the modified `N3L0qpBT17` becomes a subtopology to the modified `N3L0qpBT10` if line 5 is contracted there.

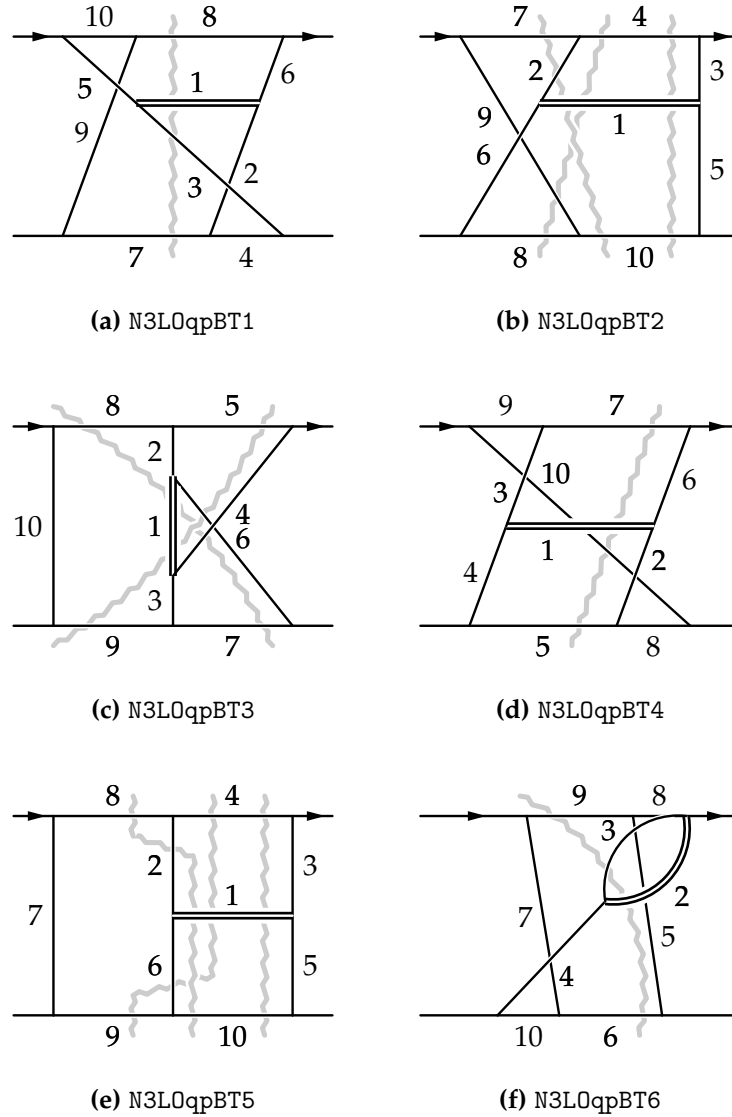
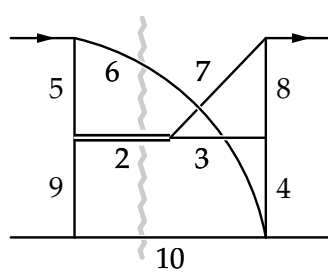
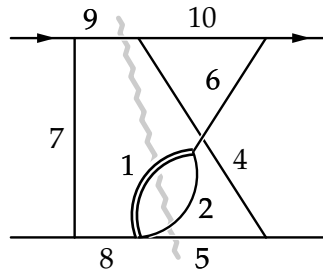


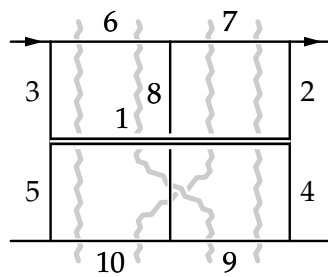
**Figure 20:** Set of 17 topologies derived from the 220 diagrams appearing in the  $qq'$ -channel at  $N^3LO$ . The name of a topology is given below each picture. As before, arrows mark the flow of the external momentum  $p_1$ . Plain lines are massless, the double line is massive. Underlaid grey zigzag lines hint at the allowed cuts of a topology. Number labels denote the indices linked to a propagator line. Since each topology has in total 12 indices, numbers missing in a picture correspond to irreducible numerators.



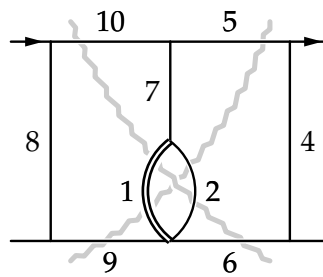
(g) N3LOqpBT7



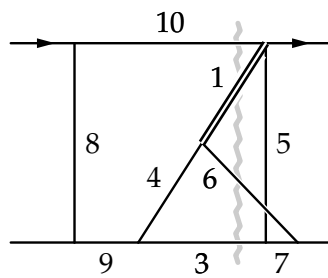
(h) N3LOqpBT8



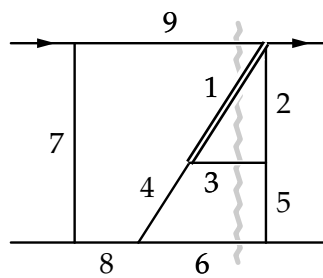
(i) N3LOqpBT9



(j) N3LOqpBT10



(k) N3LOqpBT11



(l) N3LOqpBT12

Figure 20: Continued.

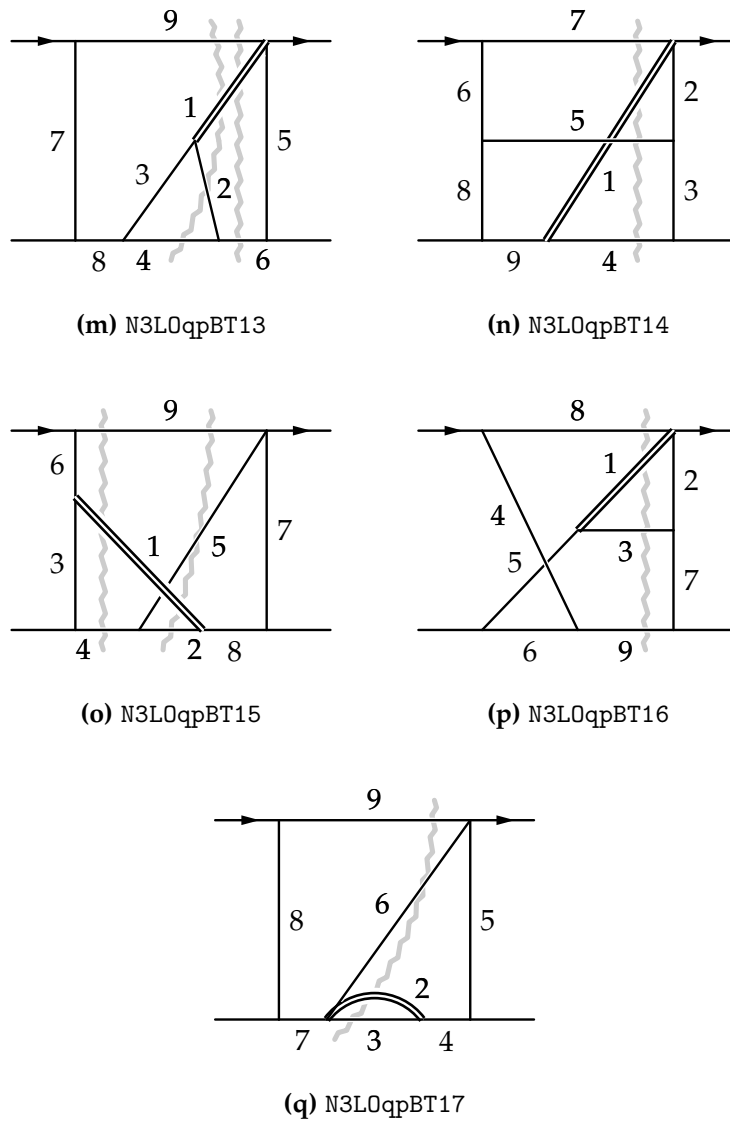


Figure 20: Concluded.

We performed the reduction of integrals in the two sets of topologies A and B separately. In each case we used the combination of the programs rows, see Ref. [49], and FIRE, see Refs. [44–46]. We observed that FIRE is more efficient in reducing integrals with higher absolute values on particular indices. But rows on the other side handles symmetries better and provides results in a form that can be recycled more conveniently, e.g. when updating the reduction for a new set of integrals. For illustration, we show N3L0qpBT4 together with its 11 master integrals revealed by rows in Fig. 21. This topology is also called the “sea snake” topology. To see the reason for this name it was drawn in a slightly different way as in Fig. 20d. The sea snake topology was subject of the studies performed in Ref. [19]. In this paper we constructed the canonical basis of master integrals and solved the differential equations in terms of HPLs up to  $\mathcal{O}(\epsilon^5)$ . This topology governs purely real contributions of the class  $R^3$ . Our analytic results with full  $x$ -dependence for this class of cuts are unique in the literature so far.

#### 4.5.2.2 Finding additional relations

Once the reduction of all appearing integrals in each topology is done, a crucial step is to identify equal integrals. These can be encoded as different index vectors of the same topology or as different index vectors from different topologies.

The first kind of identification can for example be handled by the Mathematica code `tsort`, see Ref. [45]. However, reductions of integrals performed with rows show no sign of identical integrals which is a result of exploiting all existing symmetries to their full extent.

Identical integrals of the second kind have propagators which are defined within the routing of momenta of the corresponding original topology. Only after some unknown transformation of momenta identity of integrals can be established. The following algorithm gives a general solution to this problem, automatically including identities of the first kind.

---

**Algorithm 5** (minimize master integrals). Our strategy for finding a minimal basis of master integrals consists of the following procedure:

1. We collect all integrals  $\{I_i^j\}$  from all topologies  $\{T^j\}$  appearing in the reduced result.
2. We generate for each integral a representation that is independent of its parent topology but information on the routing of momenta is kept.
3. Now, we find for each integral  $I \in \{I_i^j\}$  systematically all possible representations within each topology  $T \in \{T^j\}$  in the following way (see also Section 2.4.5):
  - a) We neglect the numerator  $I_n$  of  $I$  and produce only for its denominator a canonical representation  $I_d$  with the techniques described in Section 2.4.

MapTopologyToIntegral

MapIntegralToTopology



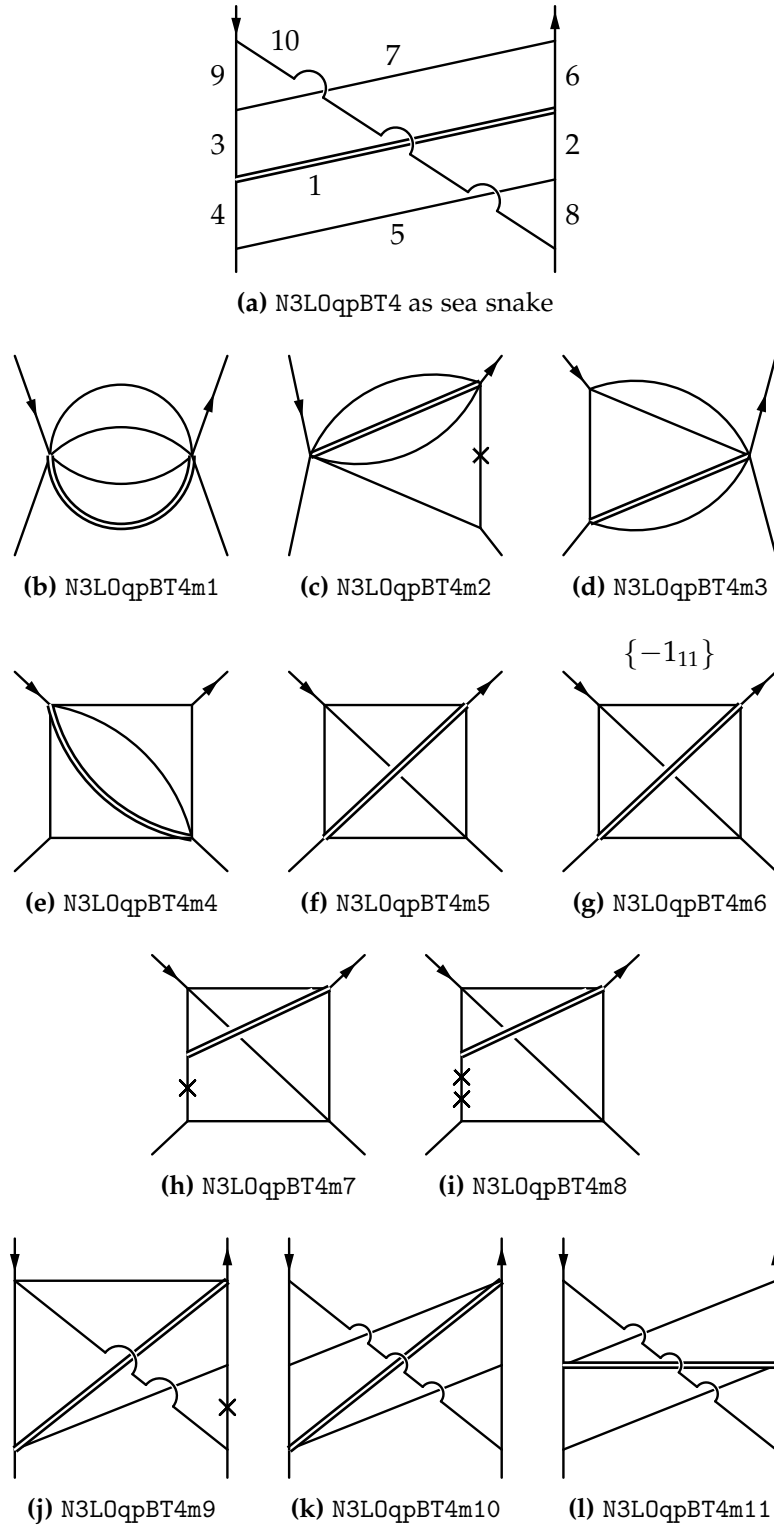


**Figure 21:** The sea snake topology  $N3L0qpBT4$  together with its 11 master integrals in the basis chosen by rows. The notation is as in Fig. 18b and Fig. 19 but we omitted drawing the four-particle cuts. Crosses on lines denote an index of  $-1$ .

- b) Assuming  $T$  is in a form where all relevant subtopologies are classified, we see immediately all those subtopologies  $\{T_d\}$  that match  $I_d$ , if there are any. This gives us essentially different momentum space representations  $I_d$  and  $\{T_d\}$  of the denominator of the same integral.
- c) Exploiting the canonical order in which  $I_d$  and all  $\{T_d\}$  are given, we know precisely which denominator of  $I_d$  is to be transformed into which of one of the  $\{T_d\}$ . We can basically read off the related shifts of loop momenta.
- d) These shifts of loop momenta are applied onto the numerator  $I_n$  of  $I$  to give its representations  $\{I_n^T\}$  within the topology  $T$ . Combined with the  $\{T_d\} = \{I_d^T\}$ , we have complete representations  $\{I^T\} = \{I_n^T I_d^T\}$  of  $I$  within  $T$ . Note that these representations are in general linear combinations of integrals from  $T$  due to the  $\{I_n\}$  being transformed and reexpressed in  $T$ .

TopologyToRules

4. These representations can contain (hidden) duplicates which we get rid of by applying symmetries of the topologies appearing on the right-hand sides. In addition also constraints due to scalelessness and cuts are imposed.

LookUp

5. Integrals appearing in these relations are not necessarily in reduced form. Therefore we apply the same reduction rules used to get the reduced result used for Step 1.
  6. In the end, we have a large overdetermined system of about  $\mathcal{O}(10^3)$  to  $\mathcal{O}(10^4)$  linear equations. This system can be solved in terms of a preferred set of variables, the set of *genuine* master integrals, to give relations one can apply in order to eliminate linear dependent integrals from the result of the reduction.
- 

#### CONCLUDING REMARKS

- The solution of the system is not unique. Hence, the choice of master integrals is arbitrary but it should somewhat reflect lower complexity compared to eliminated integrals.
- The solvability of the system is a strong consistency check of the reduction.
- The linear system is highly overdetermined, its rank is way less than the number of relations. This is because we use all representations of all integrals in all topologies. Alternatively, one could build the system up in an iterative fashion and restrict the set  $T$  in Step 3 to one topology. Algorithm 5 would then be iterated for the topologies  $\{T^j\}$  until all integrals from Step 2 have been mapped or until all topologies have been tested.

- Auxiliary integrals, absent in the preliminary reduced result used in Step 1 may also be present in this system. There may be several reasons (or combinations of them):
  - they do not appear in the reduction tables at all (i.e. they are unreduced),
  - they are master integrals from a sector of the topology which is not needed,
  - cancellations in the expression for Step 1 occurred.

In any case, we can solve the system in terms of the integrals  $\{I_i^j\}$  we started with. Thereby, auxiliary integrals are never among the set of true master integrals that are actually needed.

- In case auxiliary integrals can be expressed by true master integrals, two perspectives are possible. Either we obtained additional reduction relations for these integrals that are not anywhere in the reduction tables. Or one can try and apply the reduction algorithm again on these integrals. If this results in any new relation not yet in the described system, this could allow to reduce the number of master integrals even further.
- The same procedure can be applied in order to rewrite integrals defined in one set of topologies  $A$  into another set of topologies  $B$ , i.e. a *generic basis transformation*. The only modifications are to replace integrals and topologies in Step 1 and Step 2 with reference to set  $A$  and to apply the remaining steps with reference to set  $B$ .

One downside of the reduction via most Laporta-based algorithms is that one can never be sure if all the integrals remaining in the end are *true* master integrals. This statement holds even after identification of integrals, at least as long as the set of seed integrals is not considerably larger than the set of target integrals one wants to reduce. For complicated calculations one often cannot arbitrarily enlarge the set of seeds. From our experience, the described algorithm helps tremendously to cope with this issue. We also observed that the algorithm finds relations among the “master” integrals of a single topology in an intermediate reduction step where the selection of seeds does not allow yet for a complete reduction.

For the reduction within set  $A$  the algorithm reduced the initial 332 master integrals to only 108 in the very end. Moreover, we employed Algorithm 5 in its modified form to rewrite results obtained in set  $B$  to topology definitions of set  $A$  and found agreement of both calculations. Within set  $B$  the number of “master” integrals before changing to basis  $A$  was 161. In set  $B$  the reduction allowed to establish independence from the gauge parameter for the result. This was again done with Algorithm 5 which could express the 161 reduced integrals in the  $\zeta$ -term by only 27 master integrals. Each coefficient of a master integral in the  $\zeta$ -term is then independently zero.

**Example 52.** We demonstrate Steps 2 to 5 of Algorithm 5 on the master integral in Fig. 21c of the sea snake topology N3L0qpBT4 in Fig. 21a. The master integral is defined by rows as:

$$\text{N3L0qpBT4m2} = \text{N3L0qpBT4}[1, 0, 0, 0, 1, 0, 1, -1, 0, 1, 0, 0].$$

In Step 2 a canonical representation of this integral is generated. In Step 3 many representations are found for this integral which is just the four-particle phase space with an additional numerator. For clarity, we show only the three representations within topology N3L0qpBT1:

$$\begin{aligned} & \{ \text{N3L0qpBT1}[1, 0, 1, 0, 0, -1, 1, 1, 0, 0, 0, 0], \\ & \text{N3L0qpBT1}[1, 0, 0, 0, 0, 0, 1, 1, 0, 0, 0, 0] \\ & + 2 \text{N3L0qpBT1}[1, 0, 1, 0, 0, 0, 1, 1, 0, 0, 0, -1], \\ & \text{N3L0qpBT1}[1, 0, 1, 0, -1, 0, 1, 1, 0, 0, 0, 0] \\ & - \text{N3L0qpBT1}[1, 0, 1, 0, 0, -1, 1, 1, 0, 0, 0, 0] \\ & + \text{N3L0qpBT1}[1, 0, 1, 0, 0, 0, 0, 1, 0, 0, 0, 0] \\ & + \text{N3L0qpBT1}[1, 0, 1, 0, 0, 0, 1, 0, 0, 0, 0, 0] \\ & - \text{N3L0qpBT1}[1, 0, 1, 0, 0, 0, 1, 1, 0, -1, 0, 0] \\ & + \text{N3L0qpBT1}[1, 0, 1, 0, 0, 0, 1, 1, 0, 0, 0, 0] \}. \end{aligned}$$

We apply symmetries and constraints from vanishing subtopologies for N3L0qpBT1 in Step 4 and above representations become:

$$\begin{aligned} & \{ \text{N3L0qpBT1}[1, 0, 1, 0, 0, 0, 1, 1, -1, 0, 0, 0], \\ & 2 \text{N3L0qpBT1}[1, 0, 1, 0, 0, 0, 1, 1, 0, 0, 0, -1], \\ & \text{N3L0qpBT1}[1, 0, 1, 0, -1, 0, 1, 1, 0, 0, 0, 0] \\ & - \text{N3L0qpBT1}[1, 0, 1, 0, 0, 0, 1, 1, -1, 0, 0, 0] \\ & - \text{N3L0qpBT1}[1, 0, 1, 0, 0, 0, 1, 1, 0, -1, 0, 0] \\ & + \text{N3L0qpBT1}[1, 0, 1, 0, 0, 0, 1, 1, 0, 0, 0, 0] \}. \end{aligned}$$

Application of the reduction table for N3L0qpBT1 in Step 5 leaves in the end only one distinct representation for N3L0qpBT4m2 in terms of master integrals from N3L0qpBT1:

$$\begin{aligned} & \frac{1}{2} \text{N3L0qpBT1}[1, 0, 1, 0, -1, 0, 1, 1, 0, 0, 0, 0] \\ & + \frac{2+x}{6} \text{N3L0qpBT1}[1, 0, 1, 0, 0, 0, 1, 1, 0, 0, 0, 0]. \end{aligned}$$

Finding relations for master integrals with more denominators and numerators (including higher absolute values for indices) proceeds by the same steps but is less transparent. Automatization is inevitable for the above task when applied to large systems of master integrals from many topologies.

The reduction of integrals in the  $qq'$ -channel and the construction of canonical bases of master integrals is meanwhile completed. M. Höschele and T. Ueda found evidence that functions of different alphabet compared to HPLs, cf. Section 4.3.3.1, are needed for one of the topologies in this channel. See also Ref. [78]. The calculation of boundary conditions for VR<sup>2</sup> type integrals is underway. Integrals with a three-particle cut in the soft limit are not available in explicit form in the literature. Once the calculation of master integrals in this channel is finished, a large part of the master integrals with three- and four-particle cuts needed for the complete calculation of all channels should already be covered. These master integrals are the last missing piece for a full kinematics result for the Higgs boson production cross section at N<sup>3</sup>LO which should resolve the issue of convergence of the soft expansion, see Ref. [125].

#### 4.5.3 *Roadmap to the full calculation*

Our strategy is to advance channel-wise from easier contributions to more complicated ones. Building blocks encountered earlier will reappear later and can be reused. The order of channels in Tabs. 3, 4 and 5 reflects this complexity. For the remaining channels we classify topologies based on diagrams of the  $gg$ -channel. Therefore, we employ the same trick of purely gluonic interactions as in Section 2.5.1 on Page 62. All the code needed for the complete calculation is already prepared and can be found in the supplementary material, see Ref. [34]. There are altogether 188 topologies in the  $gg$ -channel.



## OTHER APPLICATIONS

---

In this chapter we describe two direct applications of the techniques presented or used in Chapters 2, 3 and 4. Higgs boson pair production, see Section 5.1, and Drell-Yan process, see Section 5.2, are from a technical point of view very similar to single Higgs boson production and require only few modifications or additions.

### 5.1 HIGGS BOSON PAIR PRODUCTION

To gain insight into the mechanism of electroweak symmetry breaking the Higgs boson self-interactions need to be probed. The process granting this possibility is production of a Higgs boson pair via gluon fusion which has two kinds of contribution, see Fig. 22. In the first kind, both Higgs bosons couple to top quarks. The second kind involves the cubic coupling  $\lambda$  of the SM Higgs potential

$$V(H) = \frac{1}{2}m_H^2 H^2 + \lambda v H^3 + \frac{1}{4}\lambda H^4, \quad (249)$$

with the Higgs mass  $m_H$ , the vacuum expectation value  $v$  and  $\lambda = m_H^2/2v^2$  for the SM. The influence of the second contribution is strongly suppressed compared to the first one but becomes noticeable through its large destructive interference. The process has a relatively small cross section of  $\mathcal{O}(10 \text{ fb})$  and suffers from large backgrounds, making the extraction of the Higgs self-interaction at the LHC a challenge. However, a number of studies suggest the prospect of measuring  $\lambda$ , see Refs. [162–165], some within an accuracy of about 30% with at least  $3000 \text{ fb}^{-1}$  accumulated luminosity, see Refs. [164, 165]. This amount of luminosity will be within reach after a future upgrade of the LHC.

The LO result with exact dependence on the top quark mass  $M_t$  has been known since long, see Refs. [166, 167]. Further terms in the perturbation series have been computed in the  $M_t \rightarrow \infty$  EFT at NLO, see Ref. [168], and just recently at NNLO, see Ref. [169]. It is important to remark that doing so, the exact LO result has been factored off in the NLO and NNLO contributions to improve convergence. In Ref. [170], the Wilson coefficient for the coupling of two Higgs bosons to gluons  $C_{HH}$  has been computed up to three loops where it deviates from  $C_H = C_1$  for the first time.  $C_{HH}$  was a missing piece in the NNLO calculation of Ref. [169] where  $C_{HH} = C_H$  was assumed. Moreover, in Ref. [170] virtual NNLO corrections were calculated in the full theory, confirming the EFT calculation of Ref. [169].

It is known that the expansion in  $1/M_t$  works extremely well for the case of a single Higgs boson, see Refs. [72, 76, 102], employing the aforesaid factorization procedure. For that reason we computed for Higgs boson pair

production at NLO power corrections due to a finite top quark mass, also factoring off the exact LO dependence on  $M_t$ . In Ref. [171] we presented results expanded up to  $\mathcal{O}(1/M_t^8)$ , in Ref. [172] to  $\mathcal{O}(1/M_t^{10})$  and in Ref. [173] they were available to  $\mathcal{O}(1/M_t^{12})$ . The discussion of results has not changed by including new terms:

- Including  $1/M_t$  corrections is necessary to detect deviations in  $\lambda$  of  $\mathcal{O}(10\%)$ .
- Compared to the prediction in the  $M_t \rightarrow \infty$  limit

$$\sigma_{HH}^{\text{NLO}} = 19.7^{\text{LO}} + 19.0^{\text{NLO}, M_t \rightarrow \infty} \text{ fb},$$

we obtained for the LHC at 14 TeV

$$\sigma_{HH}^{\text{NLO}} = 19.7^{\text{LO}} + (27.3 \pm 5.9)^{\text{NLO}, 1/M_t^{12}} \text{ fb},$$

where the error refers to the difference of the two highest orders in the expansion in  $1/M_t$  (scale variation underestimates the theoretical uncertainty at NLO).

- Above contributions up to  $\mathcal{O}(1/M_t^{12})$  can be seen either as an improvement of current precision with corrections of about 20% or at least as reliable error estimate for a NLO computation in this process.

We refrain from discussing the phenomenological studies of Ref. [171] in more detail. Instead we refer to the PhD thesis of J. Grigo, see Ref. [174], whose main subject is Higgs boson pair production. In the following we give a short account of some technical aspects.

### 5.1.1 Top quark mass corrections

Being interested mainly in the total cross section for  $gg \rightarrow HH$ , we make use of the optical theorem (see Chapter 3) as first ingredient. We compute imaginary parts or discontinuities of the forward scattering amplitude  $\mathcal{M}(gg \rightarrow gg)$  related to a Higgs boson pair instead of having to square  $\mathcal{M}(gg \rightarrow HH)$  and perform the phase space integrations. This is sketched in Fig. 22. Note that in contrast to single Higgs boson production a valid cut now goes through two Higgs bosons and additional partons. On the one hand, this method simplifies the calculation, namely: forward scattering kinematics, common treatment of contributions related to different phase space integrations and computation of the latter only in the very end at master integral level. On the other hand, one has to compute a larger number of diagrams with more loops. Purely virtual corrections are cross-checked in a direct calculation via squaring the amplitude for  $\mathcal{M}(gg \rightarrow HH)$  and performing the two-particle phase space integrals.

The second ingredient making this calculation feasible is the asymptotic expansion at diagrammatic level. See, e.g., Ref. [175]. This procedure effectively reduces the number of loops and scales in the integrals to be evaluated, thus diminishing some of the drawbacks connected to use of the optical theorem. We give a precise formulation of the asymptotic expansion procedure for large masses in the following.



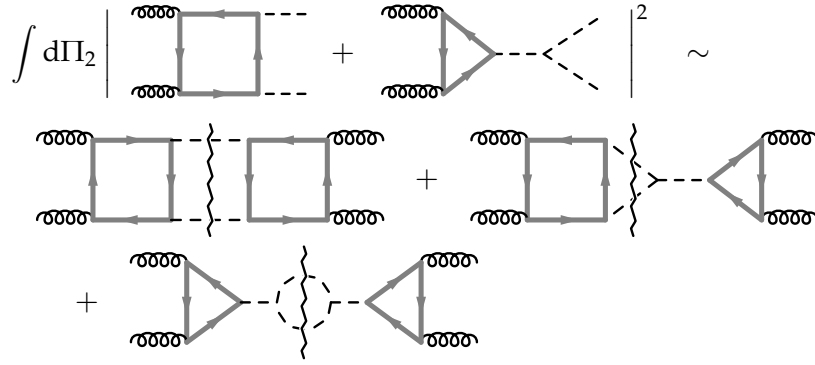


**Figure 22:** The correspondence of the total cross section and the imaginary parts or discontinuities of the forward scattering amplitude is depicted for the LO order contributions. For Higgs boson pair production we only need to consider cuts through two Higgs bosons and, beginning at NLO, additional partons. Thick gray lines represent the top quark, apart from that the notation is as before.

#### 5.1.1.1 Large mass expansion

There exists a universal prescription to perform an expansion of a Feynman diagram in a given hierarchy of scales at *integrand level*. The result of this prescription is equivalent to the expansion of an exact analytic result. However, for complicated problems it is often impossible to compute the result analytically with exact dependence on all scales and this prescription must be employed. For Higgs boson pair production we assume the hierarchy  $M_t \gg m_H, \sqrt{s}$  or the expansion parameter  $\rho = m_H^2/M_t^2$  together with the variable  $x = 4m_H^2/s$ .

The prescription for an “expansion by subgraphs” consists of two steps:

1. selection of subgraphs  $\gamma$ ,
2. expansion of propagators in  $\gamma$ .

The selection of “asymptotically irreducible” or “hard” subgraphs in Step 1 can be formulated in graph theoretical language: valid graphs  $\gamma$  *contain all heavy lines* (with mass  $M_t$  in our case) and each of their connectivity components is *one-particle irreducible (1PI)* with respect to light lines. Thus, removing a light line must not disjoin any connectivity component of  $\gamma$  (in general there can be multiple).

In Step 2 a Taylor expansion in small masses and small external momenta of  $\gamma$  is performed in the propagators of the subgraph. Among small external momenta are also loop momenta of the initial graph  $\Gamma$  that are not completely routed through  $\gamma$ . Loop momenta running through lines of  $\gamma$  only are assumed to be of the same scale as the large mass.

Formally, we have:

$$\Gamma \sim \sum_{\{\gamma\}} \Gamma \setminus \{\gamma\} \circ \mathcal{T}[\gamma], \quad (250)$$

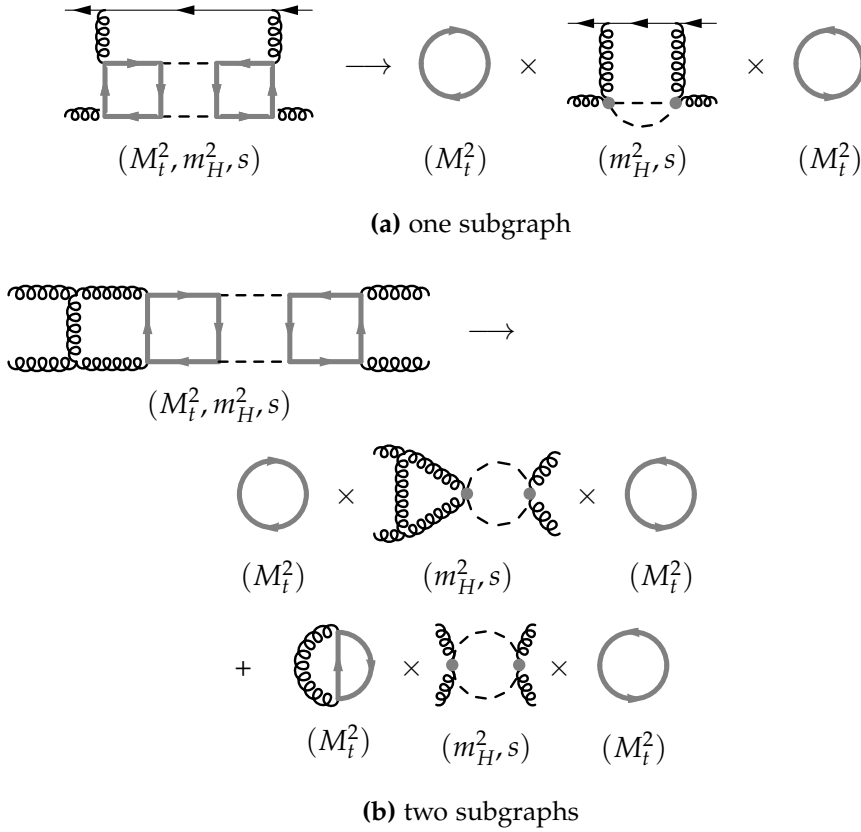


**Figure 23:** Applying the rules for asymptotic expansion to a Feynman diagram results in general in a sum of contributions (there is only one in Fig. a). Each contribution in turn is a product of subgraphs (containing the hard scale;  $M_t^2$  in our case) and co-subgraphs (containing the soft scales;  $m_H^2, s$ ). The notation is as in Fig. 22. Figure a shows a real contribution in the  $qg$ -channel at NLO, Fig. b a virtual contribution in the  $gg$ -channel at NLO.

where  $\mathcal{T}$  denotes the Taylor expansion in small parameters in Step 2 ( $\rho$  in our case) and  $\{\gamma\}$  is the set of valid subgraphs obtained in Step 1. The co-subgraph  $\Gamma \setminus \{\gamma\}$  is obtained from  $\Gamma$  by contracting all lines that are assigned to  $\gamma$ .

An OPE separates physics of different scales at the level of the Lagrangian and its outcome corresponds to an expansion by subgraphs. Expansion by subgraphs can also be applied successively to transform a multi-scale integral entirely to single-scale integrals which gives a nested series in the expansion parameters.

Application of the asymptotic expansion to examples from Higgs boson pair production can be found in Fig. 23. At NLO (NNLO) massive tadpole diagrams up to two (three) loops and box diagrams with two scales and up to two (three) loops appear after the asymptotic expansion which is performed with `exp`, see Refs. [23, 24]. Massive tadpoles can be calculated with `MATAD`, see Ref. [39], and topologies for the box diagrams can be generated with `TopoID`, see Ref. [28].

### 5.1.2 Towards NNLO corrections

For advancing in this process towards NNLO, further automatization is needed. Our toolchain for the various steps of the calculation looks as follows:

1. generation of Feynman diagrams with QGRAF, see Ref. [33],
2. selection of diagrams which have valid cuts with a filter, see Ref. [160],
3. asymptotic expansion with q2e and exp, see Refs. [23, 24],
4. reduction to scalar integrals with FORM, see Refs. [30, 32], or TFORM, see Ref. [31],
5. reduction to master integrals with rows, see Ref. [49], and FIRE, see Refs. [44, 45],
6. minimization of the set of master integrals with TopoID, see Ref. [28].

Step 2 is necessary since one cannot steer QGRAF in such a way that only diagrams with a specific cut structure are generated. Therefore, we filter the diagrams provided by QGRAF for those which exhibit an appropriate cut in the  $s$ -channel corresponding to an interference term from squaring the amplitude  $\mathcal{M}(gg \rightarrow HH)$ . At NLO, Step 4 turned out to be the bottleneck of the calculation for going to higher orders in the expansion parameter  $\rho$ . The input for Steps 3 to 6 in the above list is provided in an automatic fashion by TopoID. More precisely: all the graphs corresponding to a topology as “mapping patterns” for Step 3, FORM code processing aforementioned topologies in Step 4 and definitions of topologies suitable for reduction with the programs listed for Step 5.

#### 5.1.2.1 Mapping of topologies

We briefly discuss the mapping scheme for topologies which is realized with exp and TopoID. The same scheme can also be used for single Higgs boson production in the EFT, see Chapter 4.

The asymptotic expansion we apply for Higgs boson pair production comes with a small complication: the number of loops can vary for different (co-)subdiagrams. To identify needed topologies we use EFT diagrams from different loop orders as input to TopoID.

Another issue is the following: exp does not map factorizing topologies to more generic topologies (that may factorize only after contracting lines). The co-subgraph in the second line of Fig. 23b is such an example. This is rather inconvenient since there are non-factorizing numerators which require a tensor reduction if topology factors are treated individually. Instead, we recombine topology factors with the help of TopoID after the mapping with exp is performed. Also, exp is not capable to detect propagators with identical flow of momenta which must be circumvented with TopoID.

The mapping process consists of the following steps (examples we refer to in Appendix C are related to single Higgs boson production):

1. A `topsel.<set>` file is generated with the graph data from *all* EFT diagrams. The corresponding topologies can have propagators of equal momenta flow which are left unidentified, hence we call them “(uncontracted) diagram topologies”. In case of factorizing topologies, separate entries are written for each topology factor to the configuration file. See Appendix C.3.1.
2. The full theory diagrams are asymptotically expanded, subgraphs are mapped to massive tadpoles and co-subgraphs to EFT diagram topologies from Step 1 with `exp`. Note that the order of entries for topologies in the `<topsel>.<set>` file reflects their complexity. (In case of Higgs boson production in the EFT, `exp` performs only the mapping of a diagram to a topology and no asymptotic expansion is performed.)
3. In Step 2 only few topologies from the `topsel.<set>` file are actually used by `exp`. Information on these topologies (and their combinations in the case of factorizing topologies) are extracted from the `<diagram>.src` files generated by `exp` with the Perl script `post-EXP.pl` included with `TopoID`. This script gives a Mathematica readable list which can be passed (e.g. as signature file `EXP.<set>.m`) to `TopoID` or rather to the wrapper package `AuTopo` (whose name refers to **A**utomatic **T**opologies), see Appendix C.3.2.
4. For the topologies from aforementioned `EXP.<set>.m` file, the mapping to a generic topology is constructed and corresponding FORM code can be generated. For factorizing topologies this step can be quite intricate if `exp` picks factors from different diagram topologies which need to be combined properly. The code for non-factorizing topologies is written in `<set>GT.EXP` files and for factorizing ones in `<set>FT.exp` files. See also Appendices C.3.3 and C.3.4.

In the above `<set>` denotes a set of diagrams which can be a complete process or a particular (sub)channel.

## 5.2 DRELL-YAN PROCESS

The Drell-Yan process, i.e. the production of a lepton pair in hadronic collisions mediated by a vector boson, constitutes an important benchmark process at hadron colliders. In particular, it provides information about the PDFs and is a useful tool in searches for heavier gauge bosons by examining the invariant mass of the produced leptons.

The Drell-Yan process is induced at leading order by the transition of a quark-antiquark-pair  $q\bar{q}$  into a massive/virtual vector boson  $\gamma$ ,  $W^\pm$  or  $Z^0$ . For the calculation, we consider a generic coupling for the vector boson  $V$  from the electroweak sector to the quark flavors  $q_i$  and  $q_j$ :

$$q_i\bar{q}_jV \sim Q_{ij}^v \gamma_\mu + Q_{ij}^a \gamma_\mu \gamma_5, \quad (251)$$

where  $Q_{ij}^v$  and  $Q_{ij}^a$  encode the couplings of flavors  $i$  and  $j$  to the vector and axial-vector component of the boson  $V = \gamma, W^\pm, Z^0$ . Note that we consider

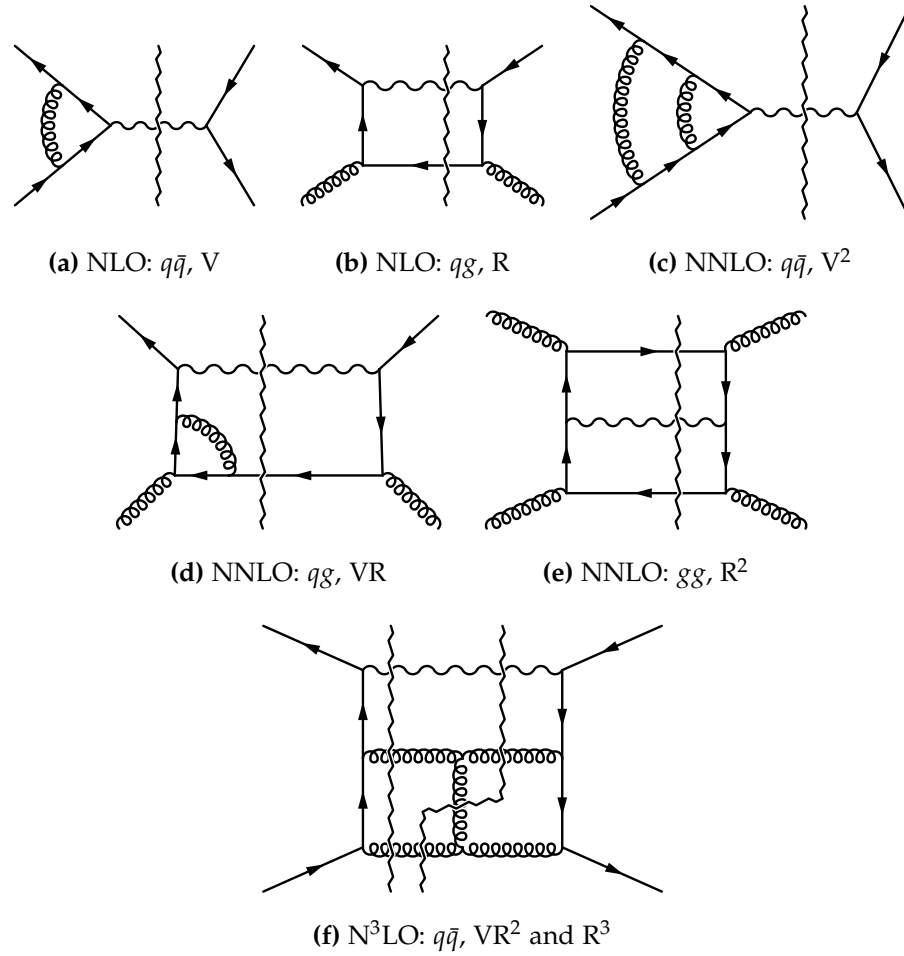


**Figure 24:** Sample Feynman diagrams up to  $N^3\text{LO}$  contributing to the Drell-Yan process. The wiggly lines denote a generic vector boson, i.e.  $\gamma$ ,  $W^\pm$  or  $Z^0$ . The zigzag lines mark the considered cuts through a massive vector boson and additional massless particles. The captions state the perturbative order, the channel and the type of contributions (“R” for real, “V” for virtual or their interference).

QCD corrections to this process, hence the renormalization of the coupling in Eq. (251) is of higher orders in  $\sqrt{G_F}$ .

The calculation of total cross sections can be performed with the same techniques as for Higgs boson production, see Chapter 4. We use the optical theorem where a valid cut goes in this case through the heavy gauge boson and additional light quark and gluon lines. In particular, the same families of scalar Feynman integrals, see Section 4.3, and master integrals occur, see Refs. [73, 113]. Apart from the treatment of  $\gamma_5$ , to be explained below, all other aspects of the calculation are analogous to Higgs boson production.

Our aim is to evaluate all convolution integrals relevant to  $N^3\text{LO}$  with the help of MT, see Section 4.4.3 and Ref. [115]. Therefore, we need to evaluate partonic cross sections in the following orders and channels to the indicated order in  $\epsilon$ :

$$\text{LO } q\bar{q} \text{ to } \mathcal{O}(\epsilon^3),$$

$$\text{NLO } qg \text{ and } q\bar{q} \text{ to } \mathcal{O}(\epsilon^2),$$

NNLO  $gg, qg, qq', qq, \text{ and } q\bar{q}$  to  $\mathcal{O}(\epsilon)$ .

See Fig. 24 for sample diagrams for single- and double-real corrections which are considered simultaneously.

Using the same notation as in Ref. [176], the LO result for the Drell-Yan process, including its full  $\epsilon$ -dependence, reads

$$\Delta_{q_i\bar{q}_j}^{(0)} = \left( Q_{ij}^v + Q_{ij}^a \right) \delta(1-x)(1-\epsilon). \quad (252)$$

The  $\epsilon$ -dependence originates from the trace over gamma-matrices of the only diagram at this order, i.e.  $\text{Tr}[\gamma_\mu\gamma^\mu]$  for the vector coupling and  $\text{Tr}[\gamma_\mu\gamma_5\gamma^\mu\gamma_5]$  for the axial-vector coupling.

### 5.2.1 Treatment of $\gamma_5$

Singlet diagrams which exhibit the vector boson's  $\gamma_\mu\gamma_5$  vertices in two distinct quark lines or traces begin to contribute at NNLO. Since diagrams of this type are not present at lower loops they are manifestly finite and could be evaluated within  $D = 4$  dimensions. However, for us this is not an option since we are interested in the terms of  $\mathcal{O}(\epsilon)$ .

For each non-singlet diagram one has always zero or two  $\gamma_5$  in a fermion trace. Therefore,  $\gamma_5$  can be anticommutated with any  $\gamma_\mu$  until it cancels with a second  $\gamma_5$ . All non-singlet diagrams are completely unproblematic and can be treated with this “naive”  $\gamma_5$ .

For singlet diagrams two points of view are possible. On the one hand, one can make explicit use of the fact that the SM is free of triangle-anomalies when taking whole fermion families into account, see Refs. [177, 178], and set all singlet diagrams to zero.

The other point of view employs the definition given by 't Hooft and Veltman in Refs. [20, 179]. This is also known as Larin's scheme, see Refs. [180, 181], and affects *only singlet* contributions:

- Axial-vector couplings are replaced by:

$$\gamma_\mu\gamma_5 = \frac{i}{3!}\epsilon_{\mu\nu\rho\sigma}\gamma^{[\nu\rho\sigma]}. \quad (253)$$

- Fermion traces are computed with these antisymmetrized products of gamma-matrices:

$$\begin{aligned} \gamma^{[\nu\rho\sigma]} &= \frac{1}{3!}(\gamma^\nu\gamma^\rho\gamma^\sigma - \gamma^\nu\gamma^\sigma\gamma^\rho \pm (\dots)) \\ &= \frac{1}{2}(\gamma^\nu\gamma^\rho\gamma^\sigma - \gamma^\sigma\gamma^\rho\gamma^\nu). \end{aligned} \quad (254)$$

- Finally, indices of epsilon-tensors are contracted in  $D$  dimensions using

$$\epsilon^{\alpha\beta\gamma\delta}\epsilon_{\mu\nu\rho\sigma} = -g_\mu^{[\alpha}g_\nu^\beta g_\rho^\gamma g_\sigma^{\delta]}, \quad (255)$$

where parentheses denote total antisymmetrization of indices.

As cross-check we implemented this prescription in two variants: one uses the FORM built-in epsilon-tensor and its contractions, for the other one contractions are done “manually”.

In Larin’s scheme the LO result takes the form

$$\Delta_{q_i\bar{q}_j}^{(0)} = \delta(1-x) \left[ Q_{ij}^v (1-\epsilon) + Q_{ij}^a \left( 1 - \frac{8}{3}\epsilon + \frac{1}{3}\epsilon^2 + \frac{8}{3}\epsilon^3 - \frac{4}{3}\epsilon^4 \right) \right]. \quad (256)$$

Note, one has to include the finite renormalization of the axial-vector current to find within this scheme agreement with the finite vector coupling contributions stemming from non-singlet diagrams (always with two  $\gamma_5$  in a fermion trace). The renormalization constant for the non-singlet axial-vector current is, see Refs. [180, 181],

$$\begin{aligned} Z_5^{ns} = & 1 - \frac{\alpha_s}{\pi} C_F + \left( \frac{\alpha_s}{\pi} \right)^2 \left( \frac{11}{8} C_F^2 - \frac{107}{144} C_F C_A + \frac{1}{36} C_F T_F n_l \right) \\ & + \left( \frac{\alpha_s}{\pi} \right)^3 \left[ C_F^3 \left( -\frac{185}{96} + \frac{3}{2} \zeta_3 \right) + C_F^2 C_A \left( \frac{2917}{864} - \frac{5}{2} \zeta_3 \right) \right. \\ & \quad + C_F^2 T_F n_l \left( -\frac{31}{432} - \frac{1}{3} \zeta_3 \right) + C_F C_A^2 \left( -\frac{2147}{1728} + \frac{7}{8} \zeta_3 \right) \\ & \quad \left. + C_F C_A T_F n_l \left( \frac{89}{648} + \frac{1}{3} \zeta_3 \right) + \frac{13}{324} C_F T_F^2 n_l^2 \right]. \quad (257) \end{aligned}$$

### 5.2.2 Results

For convenience, we treated purely virtual corrections separately. The NNLO expression for the resulting quark form factor can be found in Refs. [182–185], N<sup>3</sup>LO results are presented in Refs. [116, 117, 186]. Higher orders in  $\epsilon$  for purely virtual corrections agree with the results given in Ref. [185].

We checked that at the level of bare amplitudes, before using results for the master integrals, the dependence on the gauge parameter  $\zeta$  dropped out in the sum of all diagrams. It was possible to extract some of the correction terms in different ways from the calculated forward scattering amplitudes. This served as inner consistency check for our setup. Moreover, the vector part can be compared to the axial-vector part, using Eq. (257) in Larin’s scheme.

We found agreement with Ref. [176], after implementing the information given in the erratum and in Ref. [100] and rewriting all polylogarithms in terms of HPLs. Concerning the  $\mathcal{O}(\epsilon)$  terms of the NLO correction terms  $\Delta_{q\bar{q}}^{(1)}$  and  $\Delta_{qg}^{(1)}$ , one has to pay attention in two aspects. First, in Ref. [176] the definition  $D = 4 + \epsilon$  and not  $D = 4 - 2\epsilon$  is used. Second, from the complete series in  $\alpha_s$  the dependence of the LO coefficient on  $\epsilon$  is factored out (one is always free to do so as long as the factor has no poles in  $\epsilon$ ). In the notation of Ref. [176] this means:

$$\Delta_{ij} = (1-\epsilon) \left( \Delta_{ij}^{(0)} + \frac{\alpha_s}{4\pi} \Delta_{ij}^{(1)} + \left( \frac{\alpha_s}{4\pi} \right)^2 \Delta_{ij}^{(2)} + \mathcal{O}(\alpha_s^3) \right). \quad (258)$$

However, we found a discrepancy for  $\Delta_{q\bar{q},AB}^{(2),A}$  and our result (including  $\mathcal{O}(\epsilon)$  terms) reads

$$\begin{aligned} \Delta_{q\bar{q},AB}^{(2),A} = & \left(\frac{\alpha_s}{4\pi}\right)^2 C_F \left\{ 1 - x + \frac{1+2x}{2} H_0(x) \right. \\ & + \epsilon \left[ -\frac{3x^2 - 3x - 2}{1-x} H_2(x) + H_{1,0}(x) - \frac{4x^2 - 3x - 5}{2(1-x)} H_{0,0}(x) \right. \\ & + (5 - 3x) H_1(x) + \frac{3x^2 - 13x + 6}{2(1-x)} H_0(x) \\ & + \frac{\pi^2(3x^2 - 4x - 1)}{6(1-x)} + \frac{7(1-x)}{2} \\ & \left. \left. + (2(1-x) + (1+2x) H_0(x)) \ln\left(\frac{\mu^2}{m_V^2}\right) \right] \right\}. \quad (259) \end{aligned}$$

Note that we stick to the notation of Ref. [176] which uses  $\alpha_s/(4\pi)$  as expansion parameter. The symbol  $m_V$  is used for the mass or virtuality of the vector boson. All expressions for the correction terms to higher orders in  $\epsilon$  (one version in the naive scheme, one in Larin's scheme for  $\gamma_5$ ) can be found in electronic form in Ref. [34].

All convolution integrals of correction terms to the partonic cross section and splitting functions can be computed with MT, see Ref. [115]. The transition function, see Eq. (213) on Page 139, and the generic expression for collinear counterterms, see Eq. (218) to Eq. (221) on Page 139, can be specified to the structure of channels in the Drell-Yan process. Thus, the collinear subtraction terms to N<sup>3</sup>LO are also known for the Drell-Yan process.



## CONCLUSION

---

The main topics of this thesis are Higgs boson production discussed in Chapter 4 and the program package TopoID.

We published results for all collinear counterterms up to  $N^3\text{LO}$  (which give also finite contributions) in Refs. [90, 115, 150, 157]. For a particular class of triple-real integrals we obtained results with full dependence on  $x$ , see Ref. [19]. A full kinematics calculation for further triple-real and also double-real contributions is underway and was discussed in Section 4.5, see also Ref. [161]. Aforementioned contributions are the only missing ingredients for the full  $N^3\text{LO}$  Higgs boson production cross section. We emphasize that all the code to finally tackle the calculation of the  $gg$ -channel at  $N^3\text{LO}$  is available now.

The package TopoID is designed to be a process independent tool for topology identification, FORM code generation and finding non-trivial relations among integrals that remain after applying a reduction algorithm. Techniques that are implemented in TopoID are carefully explained in Chapters 2 and 3. Several algorithms that are given in this thesis proved to be invaluable in real calculations.

Methods needed for Higgs boson production were also transferred to Higgs boson pair production and the Drell-Yan process in Chapter 5. For Higgs boson pair production we computed corrections due to a finite top quark mass in Refs. [171–173]. For the Drell-Yan process we provided all convolutions for the collinear counterterms up to  $N^3\text{LO}$ , see Refs. [115, 157].



## FEYNMAN INTEGRAL FAMILIES

### A.1 MASSLESS PROPAGATORS AT FIVE LOOPS

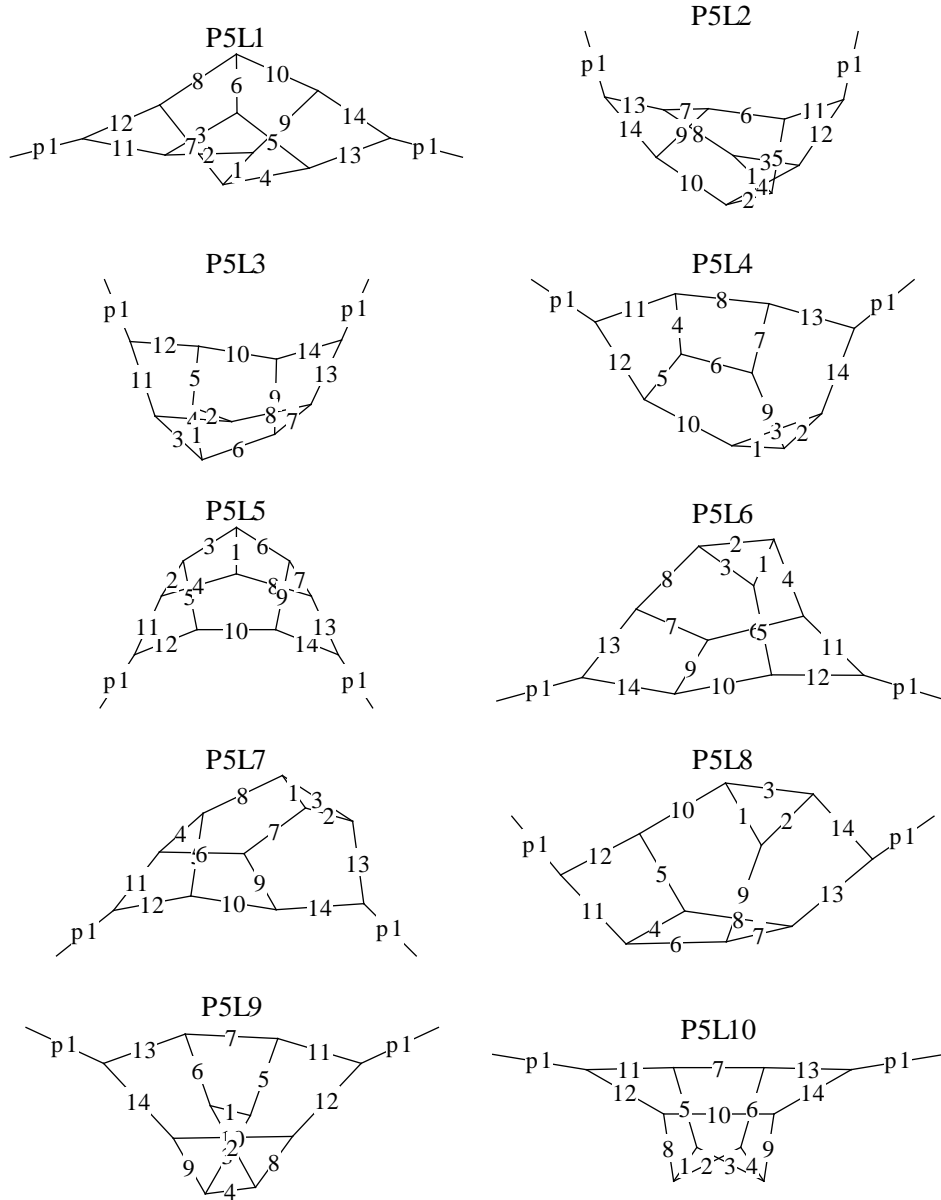


**Figure 25:** Minimal set of massless propagator topologies at five loops.

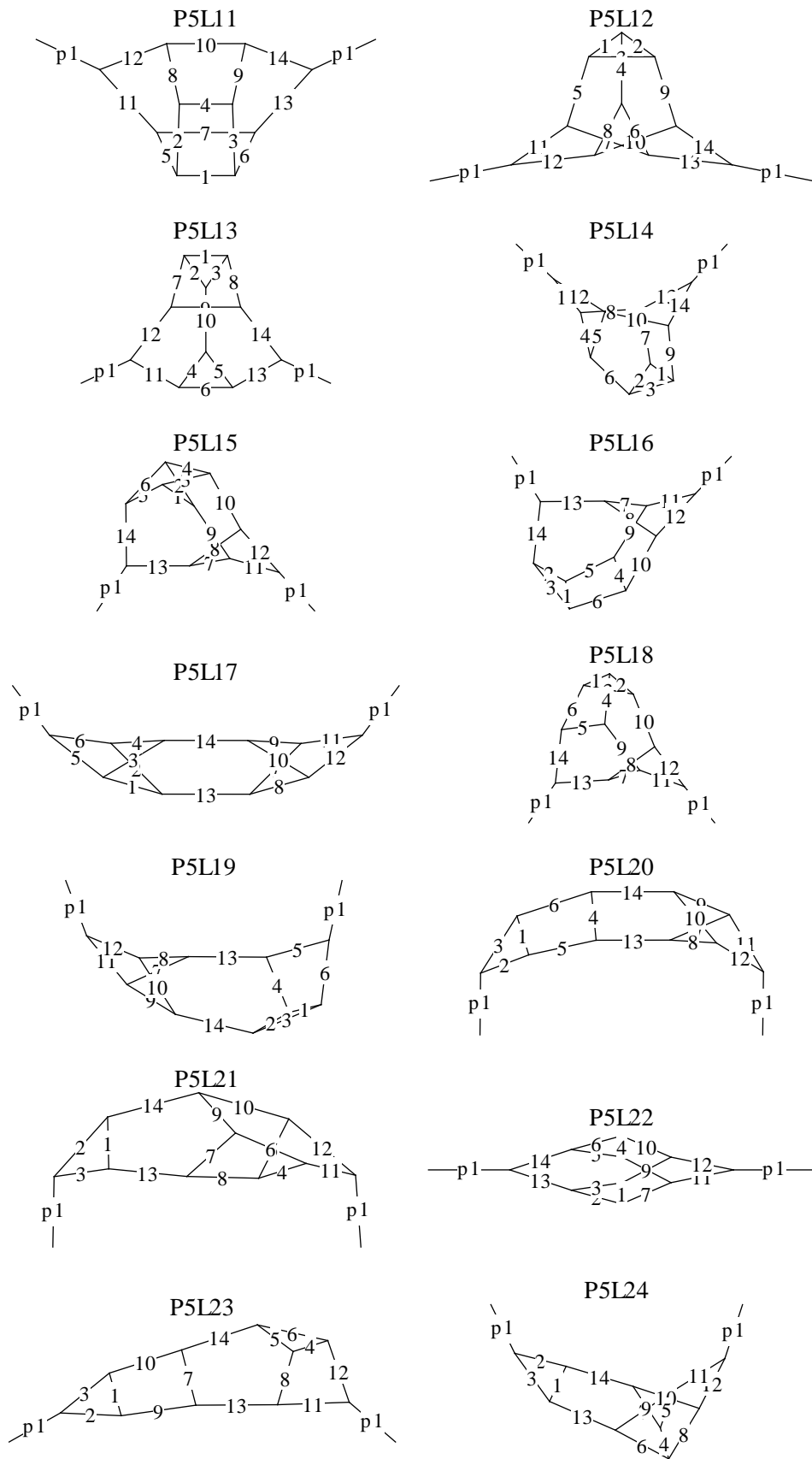


Figure 25: Continued.

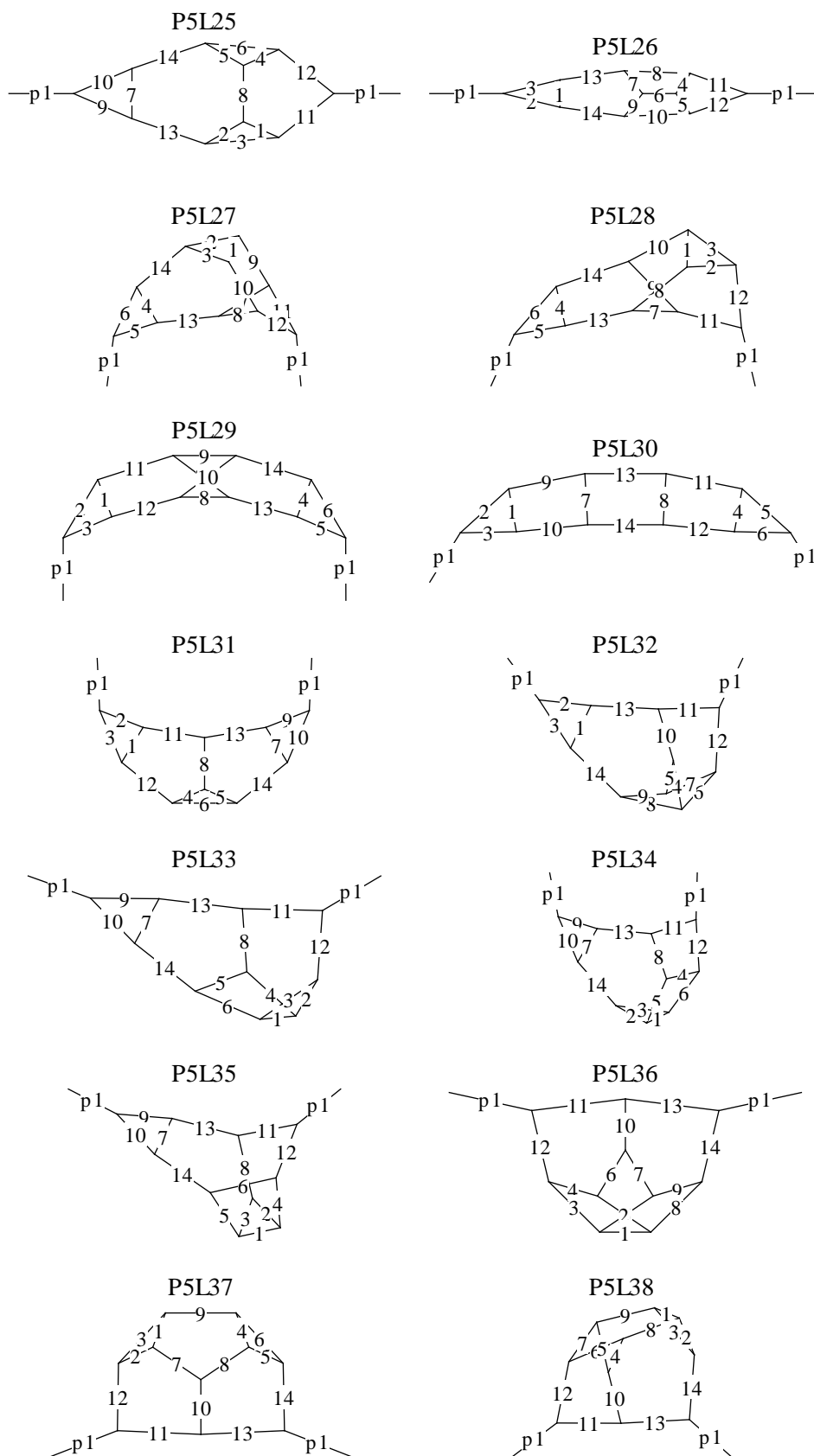


Figure 25: Continued.

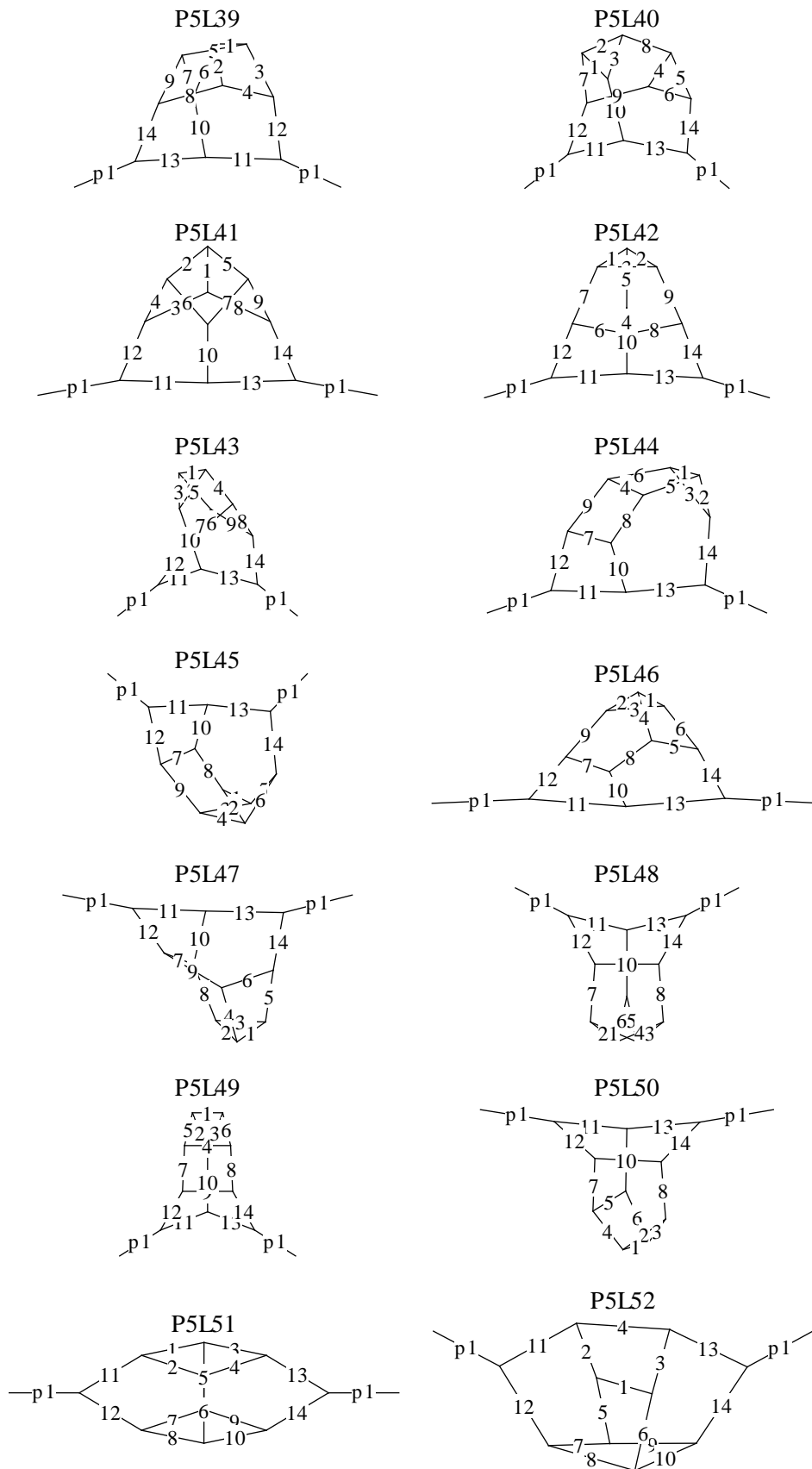


Figure 25: Continued.

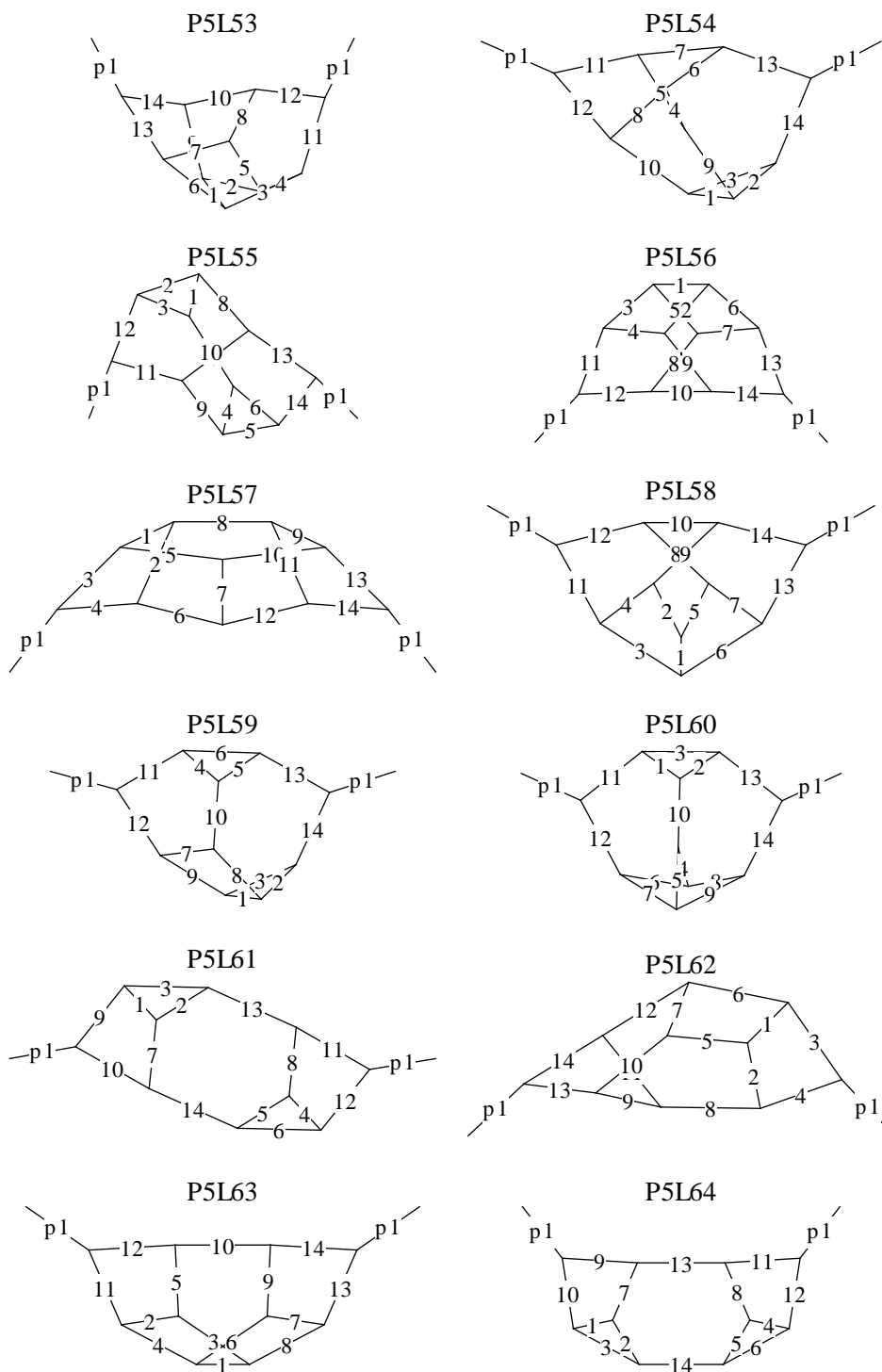


Figure 25: Concluded.





## HIGGS BOSON PRODUCTION

---

### B.1 SPLITTING FUNCTIONS AT NNLO

The splitting functions to three loops were computed in Refs. [111, 112]. We list the results up to two loops with regularized singularities in terms of delta- and plus-distributions. Moreover, we show the combinations of singlet and non-singlet quark contributions corresponding to the partonic channels  $qq$ ,  $qq'$  and  $q\bar{q}$ . For  $P_{ij}^{(1)}$ ,  $P_{qq'}^{(2)}$  and  $P_{q\bar{q}}^{(2)}$  see Section 4.2.2.4 on Page 125.

$$\begin{aligned}
P_{qg}^{(2)} = & C_F \left( \frac{2x^2 - 2x + 1}{4} H_2(x) + \frac{2x^2 - 2x + 1}{4} H_{1,1}(x) \right. \\
& + \frac{2x^2 - 2x + 1}{4} H_{1,0}(x) + \frac{4x^2 - 2x + 1}{8} H_{0,0}(x) \\
& - \frac{(1-x)x}{2} H_1(x) + \frac{8x^2 - 4x + 3}{16} H_0(x) \\
& \left. - \frac{\pi^2(2x^2 - 2x + 1)}{24} + \frac{20x^2 - 29x + 14}{16} \right) \\
& + C_A \left( -\frac{2x^2 - 2x + 1}{4} H_{1,1}(x) - \frac{2x^2 + 2x + 1}{4} H_{-1,0}(x) \right. \\
& - \frac{2x + 1}{4} H_{0,0}(x) + \frac{(1-x)x}{2} H_1(x) \\
& + \frac{44x^2 + 24x + 3}{24} H_0(x) - \frac{\pi^2 x}{12} \\
& \left. - \frac{218x^3 - 225x^2 + 18x - 20}{72x} \right), \tag{260}
\end{aligned}$$

$$\begin{aligned}
P_{gq}^{(2)} = & + C_F^2 \left( -\frac{x^2 - 2x + 2}{2x} H_{1,1}(x) + \frac{x - 2}{4} H_{0,0}(x) \right. \\
& \left. + \frac{5x^2 - 6x + 6}{4x} H_1(x) + \frac{7x + 4}{8} H_0(x) - \frac{7x + 5}{8} \right) \\
& + C_F C_A \left( \frac{x^2 - 2x + 2}{2x} H_2(x) + \frac{x^2 - 2x + 2}{2x} H_{1,1}(x) \right. \\
& + \frac{x^2 + 2x + 2}{2x} H_{-1,0}(x) + \frac{x^2 - 2x + 2}{2x} H_{1,0}(x) \\
& + \frac{x + 2}{2} H_{0,0}(x) - \frac{17x^2 - 22x + 22}{12x} H_1(x) \\
& - \frac{8x^2 + 15x + 36}{12} H_0(x) + \frac{\pi^2}{6} \\
& \left. + \frac{44x^3 + 37x^2 + 19x + 9}{36x} \right)
\end{aligned}$$

$$+ C_F T_F n_l \left( \frac{x^2 - 2x + 2}{3x} H_1(x) - \frac{2(4x^2 - 5x + 5)}{9x} \right), \quad (261)$$

$$\begin{aligned} P_{g8}^{(2)} = & C_F T_F n_l \left( -(1+x) H_{0,0}(x) - \frac{5x+3}{2} H_0(x) \right. \\ & \left. - \frac{(1-x)(5x^2+11x-1)}{3x} \right) \\ & + C_A T_F n_l \left( -\frac{x+1}{3} H_0(x) + \frac{23x^3-19x^2+29x-23}{18x} \right) \\ & + C_A^2 \left( \frac{(1-x+x^2)^2}{(1-x)x} H_2(x) + \frac{(1+x+x^2)^2}{(1+x)x} H_{-1,0}(x) \right. \\ & + \frac{(1-x+x^2)^2}{(1-x)x} H_{1,0}(x) + \frac{(-1-x+x^2)^2}{(1-x)(1+x)} H_{0,0}(x) \\ & + \frac{-25+11x-44x^2}{12} H_0(x) + \frac{\pi^2(2x^3+2x^2+4x+3)}{12(1+x)} \\ & \left. - \frac{25+109x}{72} \right) \\ & + \left[ \frac{1}{1-x} \right]_+ \left( C_A^2 \left( -\frac{\pi^2}{12} + \frac{67}{36} \right) - C_A T_F n_l \frac{5}{9} \right) \\ & + \delta(1-x) \left( -C_F T_F n_l \frac{1}{4} + C_A^2 \left( \frac{2}{3} + \frac{3\zeta(3)}{4} \right) - C_A T_F n_l \frac{1}{3} \right), \quad (262) \end{aligned}$$

$$\begin{aligned} P_{qq}^{(2)} = & \left[ \frac{1}{1-x} \right]_+ \left( -C_F T_F n_l \frac{5}{9} + C_F C_A \left( \frac{67}{36} - \frac{\pi^2}{12} \right) \right) \\ & + \delta(1-x) \left( C_F^2 \left( \frac{3\zeta(3)}{2} - \frac{\pi^2}{8} + \frac{3}{32} \right) \right. \\ & + C_F C_A \left( -\frac{3\zeta(3)}{4} + \frac{11\pi^2}{72} + \frac{17}{96} \right) \\ & \left. + C_F T_F n_l \left( -\frac{\pi^2}{18} - \frac{1}{24} \right) \right) \\ & + C_F^2 \left( \frac{x^2+1}{2(1-x)} H_2(x) + \frac{x^2+1}{2(1-x)} H_{1,0}(x) - \frac{x+1}{4} H_{0,0}(x) \right. \\ & \left. + \frac{2x^2-2x-3}{4(1-x)} H_0(x) - \frac{5}{4}(1-x) \right) \\ & + C_F C_A \left( \frac{x^2+1}{4(1-x)} H_{0,0}(x) + \frac{5x^2+17}{24(1-x)} H_0(x) + \frac{\pi^2(x+1)}{24} \right. \\ & \left. - \frac{187x-53}{72} \right) \\ & + C_F T_F \left( -\frac{x+1}{2} H_{0,0}(x) + \frac{8x^2+15x+3}{12} H_0(x) \right. \\ & + \frac{(1-x)(28x^2+10+x)}{18x} \\ & \left. + n_l \left( -\frac{1+x^2}{6(1-x)} H_0(x) + \frac{11x-1}{18} \right) \right). \quad (263) \end{aligned}$$

B.2 COLLINEAR COUNTERTERMS AT N<sup>3</sup>LO

The N<sup>3</sup>LO collinear counterterm, see Section 4.4.2, for the  $qq'$ -channel was given in Eq. (229) on Page 141. Here, we give Eq. (221) evaluated for the remaining partonic channels.

$$\begin{aligned}
 \delta\hat{\sigma}_{qq'}^{(3)} = \delta\hat{\sigma}_{qq}^{(3)} = & \frac{1}{\epsilon^3} \left\{ \left[ P_{gq}^{(1)} \otimes P_{gq}^{(1)} \otimes P_{qq}^{(1)} \otimes \hat{\sigma}_{gg}^{(0)} \right] (x) \right. \\
 & + \left[ P_{gg}^{(1)} \otimes P_{gq}^{(1)} \otimes P_{gq}^{(1)} \otimes \hat{\sigma}_{gg}^{(0)} \right] (x) \\
 & \left. + \beta_0 \left[ P_{gq}^{(1)} \otimes P_{gq}^{(1)} \otimes \hat{\sigma}_{gg}^{(0)} \right] (x) \right\} \\
 & - \frac{1}{\epsilon^2} \left\{ \left[ P_{gq}^{(1)} \otimes P_{qg}^{(1)} \otimes \hat{\sigma}_{q\bar{q}}^{(1)} \right] (x) + 3 \left[ P_{gq}^{(1)} \otimes P_{q\bar{q}}^{(1)} \otimes \hat{\sigma}_{qg}^{(1)} \right] (x) \right. \\
 & + \left[ P_{gg}^{(1)} \otimes P_{gq}^{(1)} \otimes \hat{\sigma}_{qg}^{(1)} \right] (x) + \left[ P_{gq}^{(1)} \otimes P_{gq}^{(1)} \otimes \hat{\sigma}_{gg}^{(1)} \right] (x) \\
 & + \left[ P_{gq}^{(1)} \otimes P_{gq}^{(2)} \otimes \hat{\sigma}_{gg}^{(0)} \right] (x) + \beta_0 \left[ P_{gq}^{(1)} \otimes \hat{\sigma}_{qg}^{(1)} \right] (x) \left. \right\} \\
 & + \frac{1}{\epsilon} \left\{ 2 \left[ P_{qg}^{(1)} \otimes \hat{\sigma}_{qg}^{(2)} \right] (x) + 2 \left[ P_{qq}^{(1)} \otimes \hat{\sigma}_{qq}^{(2)} \right] (x) \right. \\
 & \left. + \left[ P_{q\bar{q}}^{(2)} \otimes \hat{\sigma}_{q\bar{q}}^{(1)} \right] (x) + \left[ P_{qg}^{(2)} \otimes \hat{\sigma}_{qg}^{(1)} \right] (x) \right\}, \tag{264}
 \end{aligned}$$

$$\begin{aligned}
 \delta\hat{\sigma}_{q\bar{q}}^{(3)} = \frac{1}{\epsilon^3} \left\{ \left[ P_{gq}^{(1)} \otimes P_{gq}^{(1)} \otimes P_{qq}^{(1)} \otimes \hat{\sigma}_{gg}^{(0)} \right] (x) \right. \\
 & + \left[ P_{gg}^{(1)} \otimes P_{gq}^{(1)} \otimes P_{gq}^{(1)} \otimes \hat{\sigma}_{gg}^{(0)} \right] (x) \\
 & \left. + \beta_0 \left[ P_{gq}^{(1)} \otimes P_{gq}^{(1)} \otimes \hat{\sigma}_{gg}^{(0)} \right] (x) \right\} \\
 & - \frac{1}{\epsilon^2} \left\{ 2 \left[ P_{qq}^{(1)} \otimes P_{qq}^{(1)} \otimes \hat{\sigma}_{q\bar{q}}^{(1)} \right] (x) + \left[ P_{gq}^{(1)} \otimes P_{qg}^{(1)} \otimes \hat{\sigma}_{q\bar{q}}^{(1)} \right] (x) \right. \\
 & + 3 \left[ P_{gq}^{(1)} \otimes P_{q\bar{q}}^{(1)} \otimes \hat{\sigma}_{qg}^{(1)} \right] (x) + \left[ P_{gg}^{(1)} \otimes P_{gq}^{(1)} \otimes \hat{\sigma}_{qg}^{(1)} \right] (x) \\
 & + \left[ P_{gq}^{(1)} \otimes P_{gq}^{(1)} \otimes \hat{\sigma}_{gg}^{(1)} \right] (x) + \left[ P_{gq}^{(1)} \otimes P_{gq}^{(2)} \otimes \hat{\sigma}_{gg}^{(0)} \right] (x) \\
 & \left. + \beta_0 \left( \left[ P_{q\bar{q}}^{(1)} \otimes \hat{\sigma}_{q\bar{q}}^{(1)} \right] (x) + \left[ P_{gq}^{(1)} \otimes \hat{\sigma}_{qg}^{(1)} \right] (x) \right) \right\} \\
 & + \frac{1}{\epsilon} \left\{ 2 \left[ P_{qq}^{(1)} \otimes \hat{\sigma}_{q\bar{q}}^{(2)} \right] (x) + 2 \left[ P_{gq}^{(1)} \otimes \hat{\sigma}_{qg}^{(2)} \right] (x) \right. \\
 & \left. + \left[ P_{q\bar{q}}^{(2)} \otimes \hat{\sigma}_{q\bar{q}}^{(1)} \right] (x) + \left[ P_{gq}^{(2)} \otimes \hat{\sigma}_{qg}^{(1)} \right] (x) \right\}, \tag{265}
 \end{aligned}$$

$$\begin{aligned}
 \delta\hat{\sigma}_{qg}^{(3)} = \frac{1}{6\epsilon^3} \left\{ \left[ P_{gq}^{(1)} \otimes P_{q\bar{q}}^{(1)} \otimes P_{q\bar{q}}^{(1)} \otimes \hat{\sigma}_{gg}^{(0)} \right] (x) \right. \\
 & + 4 \left[ P_{gg}^{(1)} \otimes P_{gq}^{(1)} \otimes P_{q\bar{q}}^{(1)} \otimes \hat{\sigma}_{gg}^{(0)} \right] (x) \\
 & + 7 \left[ P_{gg}^{(1)} \otimes P_{gg}^{(1)} \otimes P_{gq}^{(1)} \otimes \hat{\sigma}_{gg}^{(0)} \right] (x) \\
 & + 8n_l \left[ P_{gq}^{(1)} \otimes P_{gq}^{(1)} \otimes P_{qg}^{(1)} \otimes \hat{\sigma}_{gg}^{(0)} \right] (x) \\
 & \left. + \beta_0 \left( 3 \left[ P_{gq}^{(1)} \otimes P_{q\bar{q}}^{(1)} \otimes \hat{\sigma}_{gg}^{(0)} \right] (x) \right. \right.
 \end{aligned}$$

$$\begin{aligned}
 & +9 \left[ P_{gg}^{(1)} \otimes P_{gq}^{(1)} \otimes \hat{\sigma}_{gg}^{(0)} \right] (x) \\
 & +2\beta_0^2 \left[ P_{gq}^{(1)} \otimes \hat{\sigma}_{gg}^{(0)} \right] (x) \} \\
 - \frac{1}{6\epsilon^2} & \left\{ 9 \left[ P_{qg}^{(1)} \otimes P_{qq}^{(1)} \otimes \hat{\sigma}_{q\bar{q}}^{(1)} \right] (x) + 3 \left[ P_{gg}^{(1)} \otimes P_{qg}^{(1)} \otimes \hat{\sigma}_{q\bar{q}}^{(1)} \right] (x) \right. \\
 & + 3 \left[ P_{q\bar{q}}^{(1)} \otimes P_{qq}^{(1)} \otimes \hat{\sigma}_{qg}^{(1)} \right] (x) + 12 \left[ P_{gq}^{(1)} \otimes P_{qg}^{(1)} \otimes \hat{\sigma}_{qg}^{(1)} \right] (x) \\
 & + 6 \left[ P_{gg}^{(1)} \otimes P_{qq}^{(1)} \otimes \hat{\sigma}_{qg}^{(1)} \right] (x) + 3 \left[ P_{gg}^{(1)} \otimes P_{gg}^{(1)} \otimes \hat{\sigma}_{qg}^{(1)} \right] (x) \\
 & + 3 \left[ P_{gq}^{(1)} \otimes P_{qq}^{(1)} \otimes \hat{\sigma}_{gg}^{(1)} \right] (x) + 9 \left[ P_{gg}^{(1)} \otimes P_{gq}^{(1)} \otimes \hat{\sigma}_{gg}^{(1)} \right] (x) \\
 & + 4 \left[ P_{gq}^{(1)} \otimes P_{q\bar{q}}^{(2)} \otimes \hat{\sigma}_{gg}^{(0)} \right] (x) + 2 \left[ P_{gq}^{(1)} \otimes P_{q\bar{q}}^{(2)} \otimes \hat{\sigma}_{gg}^{(0)} \right] (x) \\
 & + 2 \left[ P_{gq}^{(1)} \otimes P_{qq}^{(2)} \otimes \hat{\sigma}_{gg}^{(0)} \right] (x) + \left[ P_{gq}^{(2)} \otimes P_{qq}^{(1)} \otimes \hat{\sigma}_{gg}^{(0)} \right] (x) \\
 & + 5 \left[ P_{gg}^{(1)} \otimes P_{gq}^{(2)} \otimes \hat{\sigma}_{gg}^{(0)} \right] (x) + 4 \left[ P_{gg}^{(2)} \otimes P_{gq}^{(1)} \otimes \hat{\sigma}_{gg}^{(0)} \right] (x) \\
 & + 18n_l \left[ P_{gq}^{(1)} \otimes P_{qg}^{(1)} \otimes \hat{\sigma}_{qg}^{(1)} \right] (x) \\
 & + \beta_0 \left( 3 \left[ P_{qg}^{(1)} \otimes \hat{\sigma}_{q\bar{q}}^{(1)} \right] (x) + 3 \left[ P_{q\bar{q}}^{(1)} \otimes \hat{\sigma}_{qg}^{(1)} \right] (x) \right. \\
 & \quad + 3 \left[ P_{gg}^{(1)} \otimes \hat{\sigma}_{qg}^{(1)} \right] (x) + 3 \left[ P_{gq}^{(1)} \otimes \hat{\sigma}_{gg}^{(1)} \right] (x) \\
 & \quad \left. + 2 \left[ P_{gq}^{(2)} \otimes \hat{\sigma}_{gg}^{(0)} \right] (x) \right) \\
 & + 2\beta_1 \left[ P_{gq}^{(1)} \otimes \hat{\sigma}_{gg}^{(0)} \right] (x) \} \\
 + \frac{1}{6\epsilon} & \left\{ 12 \left[ P_{qg}^{(1)} \otimes \hat{\sigma}_{q\bar{q}}^{(2)} \right] (x) + 6 \left[ P_{qg}^{(1)} \otimes \hat{\sigma}_{q\bar{q}}^{(2)} \right] (x) \right. \\
 & + 6 \left[ P_{qg}^{(1)} \otimes \hat{\sigma}_{q\bar{q}}^{(2)} \right] (x) + 6 \left[ P_{q\bar{q}}^{(1)} \otimes \hat{\sigma}_{qg}^{(2)} \right] (x) \\
 & + 6 \left[ P_{gg}^{(1)} \otimes \hat{\sigma}_{qg}^{(2)} \right] (x) + 6 \left[ P_{gq}^{(1)} \otimes \hat{\sigma}_{gg}^{(2)} \right] (x) \\
 & + 3 \left[ P_{qg}^{(2)} \otimes \hat{\sigma}_{q\bar{q}}^{(1)} \right] (x) + 6 \left[ P_{q\bar{q}}^{(2)} \otimes \hat{\sigma}_{qg}^{(1)} \right] (x) \\
 & + 3 \left[ P_{q\bar{q}}^{(2)} \otimes \hat{\sigma}_{qg}^{(1)} \right] (x) + 3 \left[ P_{q\bar{q}}^{(2)} \otimes \hat{\sigma}_{qg}^{(1)} \right] (x) \\
 & + 3 \left[ P_{gg}^{(2)} \otimes \hat{\sigma}_{qg}^{(1)} \right] (x) + 3 \left[ P_{gq}^{(2)} \otimes \hat{\sigma}_{gg}^{(1)} \right] (x) \\
 & \left. + 2 \left[ P_{gq}^{(3)} \otimes \hat{\sigma}_{gg}^{(0)} \right] (x) \right\}, \tag{266}
 \end{aligned}$$

$$\begin{aligned}
 \delta\hat{\sigma}_{gg}^{(3)} & = \frac{1}{3\epsilon^3} \left\{ 4 \left[ P_{gg}^{(1)} \otimes P_{gg}^{(1)} \otimes P_{gg}^{(1)} \otimes \hat{\sigma}_{gg}^{(0)} \right] (x) \right. \\
 & + n_l \left( 10 \left[ P_{gg}^{(1)} \otimes P_{gq}^{(1)} \otimes P_{qg}^{(1)} \otimes \hat{\sigma}_{gg}^{(0)} \right] (x) \right. \\
 & \quad \left. + 2 \left[ P_{gq}^{(1)} \otimes P_{qg}^{(1)} \otimes P_{q\bar{q}}^{(1)} \otimes \hat{\sigma}_{gg}^{(0)} \right] (x) \right) \\
 & + 6\beta_0 \left[ P_{gg}^{(1)} \otimes P_{gg}^{(1)} \otimes \hat{\sigma}_{gg}^{(0)} \right] (x) \\
 & + 6n_l\beta_0 \left[ P_{gq}^{(1)} \otimes P_{qg}^{(1)} \otimes \hat{\sigma}_{gg}^{(0)} \right] (x) + 2\beta_0^2 \left[ P_{gg}^{(1)} \otimes \hat{\sigma}_{gg}^{(0)} \right] (x) \} \\
 - \frac{1}{3\epsilon^2} & \left\{ 6 \left[ P_{gg}^{(1)} \otimes P_{gg}^{(1)} \otimes \hat{\sigma}_{gg}^{(1)} \right] (x) + 6 \left[ P_{gg}^{(1)} \otimes P_{gg}^{(2)} \otimes \hat{\sigma}_{gg}^{(0)} \right] (x) \right. \\
 & \left. + n_l \left( 6 \left[ P_{qg}^{(1)} \otimes P_{qg}^{(1)} \otimes \hat{\sigma}_{q\bar{q}}^{(1)} \right] (x) \right) \right\}
 \end{aligned}$$

$$\begin{aligned}
 & + 6 \left[ P_{qg}^{(1)} \otimes P_{qq}^{(1)} \otimes \hat{\sigma}_{qg}^{(1)} \right] (x) \\
 & + 18 \left[ P_{gg}^{(1)} \otimes P_{qg}^{(1)} \otimes \hat{\sigma}_{qg}^{(1)} \right] (x) \\
 & + 6 \left[ P_{gq}^{(1)} \otimes P_{qg}^{(1)} \otimes \hat{\sigma}_{gg}^{(1)} \right] (x) \\
 & + 4 \left[ P_{gq}^{(1)} \otimes P_{qg}^{(2)} \otimes \hat{\sigma}_{gg}^{(0)} \right] (x) \\
 & + 2 \left[ P_{gq}^{(2)} \otimes P_{qg}^{(1)} \otimes \hat{\sigma}_{gg}^{(0)} \right] (x) \\
 & + \beta_0 \left( 3 \left[ P_{gg}^{(1)} \otimes \hat{\sigma}_{gg}^{(1)} \right] (x) + 2 \left[ P_{gg}^{(2)} \otimes \hat{\sigma}_{gg}^{(0)} \right] (x) \right. \\
 & \quad \left. + 6n_l \left[ P_{qg}^{(1)} \otimes \hat{\sigma}_{qg}^{(1)} \right] (x) \right) \\
 & + 2\beta_1 \left[ P_{gg}^{(1)} \otimes \hat{\sigma}_{gg}^{(0)} \right] (x) \Big\} \\
 & + \frac{1}{3\epsilon} \left\{ 6 \left[ P_{gg}^{(1)} \otimes \hat{\sigma}_{gg}^{(2)} \right] (x) + 3 \left[ P_{gg}^{(2)} \otimes \hat{\sigma}_{gg}^{(1)} \right] (x) \right. \\
 & \quad + 2 \left[ P_{gg}^{(3)} \otimes \hat{\sigma}_{gg}^{(0)} \right] (x) \\
 & \quad \left. + n_l \left( 12 \left[ P_{qg}^{(1)} \otimes \hat{\sigma}_{qg}^{(2)} \right] (x) + 6 \left[ P_{qg}^{(2)} \otimes \hat{\sigma}_{qg}^{(1)} \right] (x) \right) \right\}. \quad (267)
 \end{aligned}$$



## SAMPLE CODE

The following variables need to be defined in FORM:

$d_1, d_2, \dots$ : denominator (symbol),  
 $n_1, n_2, \dots$ : numerator (symbol),  
 $p_1, p_2, \dots$ : external momentum (vector),  
 $v_1, v_2, \dots$ : internal momentum (vector),  
 $NNL\text{OrGT}1, NNL\text{OrGT}2, \dots$ : generic topology (function),  
 $NNL\text{OrBT}1, NNL\text{OrBT}2, \dots$ : basic topology (function),  
 $x, [1-x], [1+x], \dots$ : kinematic variable (symbol),  
 $s, m_h$ : dimensionful quantity (symbol).

## C.1 GENERIC TOPOLOGIES

For a graphical representation of the topology  $NNL\text{OrGT}6$ , see Fig. 14 on Page 129. The FORM code below is an excerpt from  $NNL\text{OrGT}.inc$ .

```
*--#[ NNLOrGT6 :
*
* Generated by TopoID-1.2 (2014-10-16) on 2014-12-02 13:05:14.
*
* Note: Delete this comment on modification.
*
#+
* topology line definitions :
* 1: d7 (gl), -p2 - v1 - v2, 6 --- 5
* 2: d5 (gl), -v2, 5 --- 4
* 3: d6 (gl), p1 + v2, 6 --- 4
* 4: d3 (hb), -p2 - v1, 5 --- 2
* 5: d1 (gl), -v1, 2 --- 1
* 6: d4 (gl), -p1 + p2 + v1, 6 --- 3
* 7: d2 (gl), -p1 + v1, 3 --- 1
* (scheme w/o completion)
#-

#include NNLOrBT2.def

#procedure zNNLOrGT6
* vanishing sub-topologies
if ((count(d7,1) >= 0))
discard;
```

```

    if ((count(d3,1) >= 0))
        discard;
    if ((count(d2,1) >= 0))
        discard;
    if ((count(d5,1) >= 0) &&
        (count(d6,1) >= 0))
        discard;
#endprocedure

#procedure pNNLorGT6(MM)
* partial fraction decomposition:
*  $-d_1 + d_2 + d_3 - d_4 + s - s*x$ 
    id d2 = d1 - d3 + d4 - ('MM)*[1-x];
    id d4/d2 = -((d1 - d2 - d3 - ('MM)*[1-x])/d2);
    id d1/(d2*d4) = (d2 + d3 - d4 + ('MM)*[1-x])/(d2*d4);
    id d3/(d1*d2*d4) = (d1 - d2 + d4 - ('MM)*[1-x])/(d1*d2*d4);
    id 1/(d1*d2*d3*d4) = (d1 - d2 - d3 + d4)/(d1*d2*d3*d4*('MM)\
        *[1-x]);
* kinematic constraints
    id p3 = p2;
    id p4 = p1;
    id p1.p1 = 0;
    id p2.p2 = 0;
    id p1.p2 = -('MM)/2;
#endprocedure

#procedure mNNLorGT6tNNLorBT2(marker,MM,Mzep)
* subset 1
* map from (1,2,3,4,5,7) to (1,3,4,5,6,7)
    if ((count(d4,1) == 0));
        id ('marker') = NNLorBT2;
        mu replace_(d7,d7, d5,d5, d6,d4, d3,d3, d1,d1, d2,d2);
        mu replace_(v1,v1, v2,-p1 - v2);
    endif;
* subset 2
* map from (1,2,3,4,6,7) to (3,1,2,5,6,7)
    if ((count(d1,1) == 0));
        id ('marker') = NNLorBT2;
        mu replace_(d7,d5, d5,d7, d6,d6, d3,d3, d4,d1, d2,d2);
        mu replace_(p1,p2, p2,p1);
        mu replace_(v1,-p1 + p2 + v1, v2,p1 - p2 - v1 + v2);
    endif;
    .sort
    #call cNNLorBT2(('MM'))
    .sort
    #call gNNLorBT2(('MM'),('Mzep'))
    .sort
    #call zNNLorBT2
    .sort
#endprocedure

#procedure NNLorGT6
    #message this is "NNLorGT6"...
* apply simplifications
    #message apply simplifications...
    repeat;
        #call zNNLorGT6
        #call pNNLorGT6(s)

```



```

    endrepeat;
    .sort
* map to independents
  #message map to independents...
  mu marker;
  #call mNNLorGT6tNNLorBT2(marker,s,[(mu^2/s)^ep])
  .sort
  if (count(marker,1) != 0)
    exit "Error: \"NNLorGT6\" not completely mapped to \
      independents.";
* symmetrize
  #ifdef 'symNNLorBT2'
    #message symmetrize "NNLorBT2"...
    #call yNNLorBT2
    .sort
  #endif
* load reduction tables
  #ifdef 'useNNLorBT2'
    #message read table for "NNLorBT2"...
    #include NNLorBT2.inx
    .sort
  #endif
#endprocedure

* perform mapping, change notation
  #call initlines
* trigger topology
  #call NNLorGT6

*--#] NNLorGT6 :

```

In this sample code, the procedure `zNNLorGT6` discards zero subtopologies, `pNNLorGT6` performs partial fractioning, `mNNLorGT6tNNLorBT2` the mapping from `NNLorGT6` to `NNLorBT2` whose FORM code is included at the beginning. In this case two linearly independent subtopologies (which are isomorphic) emerge after the partial fractioning of the generic topology.

## C.2 BASIC TOPOLOGIES

For a graphical representation of the topology `NNLorBT2`, see Fig. 15 on Page 130. The FORM code below is an excerpt from `NNLorBT.def`.

```

*--#[ NNLorBT2 :

*
* Generated by TopoID-1.2 (2014-10-16) on 2014-11-17 12:57:54.
*
* Note: Delete this comment on modification.
*

* topology line definitions :
* 1: d7 (gl), -p1 + p2 + v1 - v2, 6 — 4
* 2: d6 (gl), p1 - v1 + v2, 5 — 4
* 3: d5 (gl), p1 + v2, 6 — 3
* 4: d4 (gl), -v2, 5 — 3
* 5: d3 (hb), -p2 - v1, 6 — 2

```

```

* 6: d1 (g1), -v1,          2 --- 1
* 7: d2 (g1), -p1 + v1,    5 --- 1

#include fsymm.prc
#ifndef 'symNNLorBT2'
#define symNNLorBT2 "o"
#endif

#define top "NNLorBT2"
#define pNNLorBT2 "p1,p2"
#define kNNLorBT2 "v1,v2"
#define dNNLorBT2 "d1,d2,d3,d4,d5,d6,d7"
#define vNNLorBT2 "x,[1-x]"

#procedure fNNLorBT2(MM,Mzep)
* write as factors
id NNLorBT2(a1?,a2?,a3?,a4?,a5?,a6?,a7?)
= NNLorBT2*('Mzep')^(-2)*('MM')^(-2*2 - a1 - a2 - a3 - a4 \
- a5 - a6 - a7)
*d7^(-a1)*d6^(-a2)*d5^(-a3)*d4^(-a4)*d3^(-a5)*d1^(-a6)\
*d2^(-a7);
#endprocedure

#procedure gNNLorBT2(MM,Mzep)
* write as function
id NNLorBT2*d7^a1*d6^a2*d5^a3*d4^a4*d3^a5*d1^a6*d2^a7?
= ('Mzep')^(+2)*('MM')^(+2*2 + a1 + a2 + a3 + a4 + a5 + a6 \
+ a7)
*NNLorBT2(-a1,-a2,-a3,-a4,-a5,-a6,-a7);
#endprocedure

#procedure eNNLorBT2(MM)
* expansion of factors
if (match(NNLorBT2))
id d7 = ('MM') - 2*p1.v1 + 2*p1.v2 + 2*p2.v1 - 2*p2.v2 + \
v1.v1 - 2*v1.v2 + v2.v2;
.sort
if (match(NNLorBT2))
id d6 = -2*p1.v1 + 2*p1.v2 + v1.v1 - 2*v1.v2 + v2.v2;
.sort
if (match(NNLorBT2))
id d5 = 2*p1.v2 + v2.v2;
.sort
if (match(NNLorBT2))
id d4 = v2.v2;
.sort
if (match(NNLorBT2))
id d3 = ('MM')*x + 2*p2.v1 + v1.v1;
.sort
if (match(NNLorBT2))
id d1 = v1.v1;
.sort
if (match(NNLorBT2))
id d2 = -2*p1.v1 + v1.v1;
.sort
* kinematic constraints
id p1.p1 = 0;
id p2.p2 = 0;

```

```

    id p1.p2 = -(MM)/2;
    .sort
#endprocedure

#procedure cNNLorBT2(MM)
* reduction of scalar products
  if (match(NNLorBT2))
    id p1.v1 = (d1 - d2)/2;
    .sort
  if (match(NNLorBT2))
    id p2.v1 = (-d1 + d3 - (MM)*x)/2;
    .sort
  if (match(NNLorBT2))
    id v1.v1 = d1;
    .sort
  if (match(NNLorBT2))
    id p1.v2 = (-d4 + d5)/2;
    .sort
  if (match(NNLorBT2))
    id p2.v2 = (-d1 + d3 + d6 - d7 + (MM)*[1-x])/2;
    .sort
  if (match(NNLorBT2))
    id v1.v2 = (d2 + d5 - d6)/2;
    .sort
  if (match(NNLorBT2))
    id v2.v2 = d4;
    .sort
* kinematic constraints
  id p1.p1 = 0;
  id p2.p2 = 0;
  id p1.p2 = -(MM)/2;
  .sort
#endprocedure

#procedure zNNLorBT2
* vanishing sub-topologies
  id NNLorBT2(a1?, a2?, a3?, a4?, a5?nego_, a6?, a7?) = 0;
  id NNLorBT2(a1?nego_, a2?nego_, a3?, a4?, a5?, a6?, a7?) = 0;
  id NNLorBT2(a1?, a2?nego_, a3?, a4?, a5?, a6?, a7?nego_) = 0;
  id NNLorBT2(a1?, a2?, a3?nego_, a4?nego_, a5?, a6?, a7?) = 0;
  id NNLorBT2(a1?, a2?, a3?, a4?nego_, a5?, a6?, a7?nego_) = 0;
#endprocedure

#procedure yNNLorBT2
  #redefine top "NNLorBT2"
* change notation
  #call fNNLorBT2(1, 1);
* symmetries
  if (match(NNLorBT2));
    repeat;

      #if ('symNNLorBT2' <= 6)
        #call fsymm(d7\\, d6\\, d5\\, d4\\, d3\\, d2\\, \
                    d5\\, d4\\, d7\\, d6\\, d3\\, d2)
      #endif

      #if ('symNNLorBT2' <= 5)
        #call fsymm(d7\\, d5\\, d3\\, d1\\, d2\\, \

```

```
                d5\\,d7\\,d3\\,d1\\,d2)
# call fsymm(d7\\,d4\\,d3\\,d1\\,d2\\,
            d4\\,d7\\,d3\\,d1\\,d2)
# call fsymm(d6\\,d5\\,d3\\,d1\\,d2\\,
            d5\\,d6\\,d3\\,d1\\,d2)
# call fsymm(d6\\,d4\\,d3\\,d1\\,d2\\,
            d4\\,d6\\,d3\\,d1\\,d2)
#endif

# if ('symNNLorBT2' <= 4)
# call fsymm(d7\\,d4\\,d3\\,d2\\,
            d6\\,d5\\,d3\\,d2\\,
            d5\\,d6\\,d3\\,d2\\,
            d4\\,d7\\,d3\\,d2)
#endif

    endrepeat;
endif;
* change notation
# call gNNLorBT2(1,1);
#endprocedure

#procedure sNNLorBT2
* discard vanishing sub-topologies
# call zNNLorBT2
. sort
* apply symmetries
# call yNNLorBT2
. sort
* substitute variables
mu replace_([1-x],1 - x);
. sort
#endprocedure

*--#] NNLorBT2 :
```

In the above code, the procedures `fNNLorBT2` and `gNNLorBT2` switch between function and factor notation, `eNNLorBT2` and `cNNLorBT2` express topology factors as scalar products and vice versa. The procedure `yNNLorBT2` performs total symmetrization using `fsymm.prc` which is also included in `TopoID`.

### C.3 MAPPING TOPOLOGIES

#### C.3.1 Configuration for `exp`

Configuration files for `exp` contain entries of the form:

```
{ A [<options>]; B; C; D; E; F; H; I [; I] }
```

where symbols `A`, `B`, ... denote:

**A:** name of the topology,

**B:** number of lines,

**C:** number of loops,

D: number of external momenta,

E: number of masses,

F: scales information,

H: simplified line specifications,

I: mass distribution.

Scales information will not be relevant for the examples given below. An entry for H has the form

$$(W : Y, Z)$$

where  $W$  is a line momentum  $q_1, q_2, \dots$  and  $Y$  and  $Z$  are vertex numbers. By convention, a line momentum is directed from  $Y$  to  $Z$ . Also, only one external momentum is outgoing, all others are incoming.

An excerpt from `topsel.NNLOr`:

```
{NNLORTT108f1, copy_scale , poco_scale ; 3 ; 1 ; 3 ; 1 ; ;
  (q1 : 1 , 2)(q2 : 1 , 2)(q3 : 3 , 2)(p1 : 1 , 3)(p2 : 3 , 2)(p3 : 1 , 2); 200}
{NNLORTT109f1, copy_scale , poco_scale ; 3 ; 1 ; 3 ; 1 ; ;
  (q1 : 1 , 2)(q2 : 1 , 2)(q3 : 3 , 2)(p1 : 1 , 2)(p2 : 3 , 2)(p3 : 1 , 3); 200}
...
{NNLORTT51f2, copy_scale , poco_scale ; 3 ; 1 ; 3 ; 1 ; ;
  (q1 : 2 , 1)(q2 : 3 , 1)(q3 : 1 , 1)(p1 : 1 , 2)(p2 : 3 , 2)(p3 : 1 , 3); 200}

{NNLORTT108f2, copy_scale , poco_scale ; 3 ; 1 ; 3 ; 1 ; ;
  (q1 : 1 , 3)(q2 : 2 , 3)(q3 : 3 , 3)(p1 : 3 , 1)(p2 : 3 , 2)(p3 : 2 , 1); 000}
{NNLORTT110f2, copy_scale , poco_scale ; 3 ; 1 ; 3 ; 1 ; ;
  (q1 : 1 , 2)(q2 : 1 , 2)(q3 : 3 , 2)(p1 : 1 , 2)(p2 : 1 , 3)(p3 : 3 , 2); 000}
{NNLORTT49f2, copy_scale , poco_scale ; 3 ; 1 ; 3 ; 1 ; ;
  (q1 : 2 , 1)(q2 : 3 , 1)(q3 : 1 , 1)(p1 : 1 , 2)(p2 : 1 , 3)(p3 : 3 , 2); 000}

{NNLORTT46f1, copy_scale , poco_scale ; 2 ; 1 ; 3 ; 1 ; ;
  (q1 : 1 , 2)(q2 : 1 , 2)(q3 : 2 , 2)(p1 : 2 , 1)(p2 : 2 , 1); 20}
{NNLORTT49f1, copy_scale , poco_scale ; 2 ; 1 ; 3 ; 1 ; ;
  (q1 : 2 , 1)(q2 : 2 , 1)(q3 : 1 , 1)(p1 : 2 , 1)(p2 : 2 , 1); 20}
{NNLORTT4f1, copy_scale , poco_scale ; 2 ; 1 ; 3 ; 1 ; ;
  (q1 : 1 , 2)(q2 : 1 , 2)(q3 : 2 , 2)(p1 : 1 , 2)(p2 : 1 , 2); 20}
{NNLORTT108f1, copy_scale , poco_scale ; 3 ; 1 ; 3 ; 1 ; ;
  (q1 : 1 , 2)(q2 : 1 , 2)(q3 : 3 , 2)(p1 : 1 , 3)(p2 : 3 , 2)(p3 : 1 , 2); 200}
{NNLORTT109f1, copy_scale , poco_scale ; 3 ; 1 ; 3 ; 1 ; ;
  (q1 : 1 , 2)(q2 : 1 , 2)(q3 : 3 , 2)(p1 : 1 , 2)(p2 : 3 , 2)(p3 : 1 , 3); 200}
...
{NNLORTT51f2, copy_scale , poco_scale ; 3 ; 1 ; 3 ; 1 ; ;
  (q1 : 2 , 1)(q2 : 3 , 1)(q3 : 1 , 1)(p1 : 1 , 2)(p2 : 3 , 2)(p3 : 1 , 3); 200}

{NNLORTT4, copy_scale , poco_scale ; 4 ; 2 ; 3 ; 1 ; ;
  (q1 : 1 , 2)(q2 : 1 , 2)(q3 : 2 , 2)(p1 : 3 , 2)(p2 : 3 , 2)(p3 : 3 , 1)(p4 : 3 , 1); 2000}
...
{NNLORTT99, copy_scale , poco_scale ; 7 ; 2 ; 3 ; 1 ; ;
  (q1 : 1 , 4)(q2 : 2 , 4)(q3 : 3 , 4)(p1 : 6 , 5)(p2 : 5 , 3)(p3 : 4 , 3)(p4 : 6 , 4)(p5 : 5 , 1)
  (p6 : 2 , 1)(p7 : 6 , 2); 0200000}
...
```

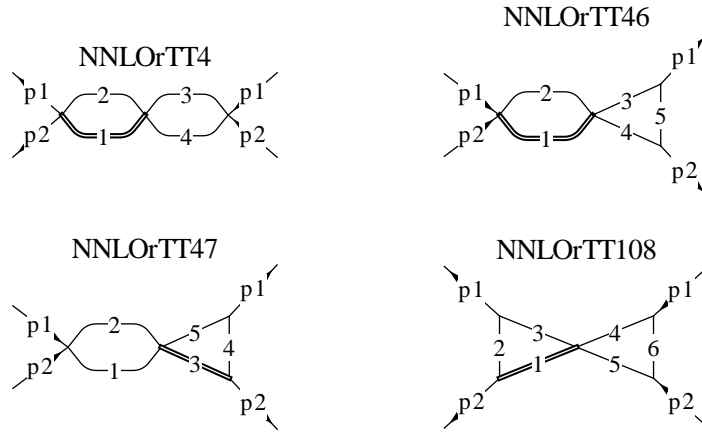


**Figure 26:** Selection of factorizing diagram topologies for NNLO Higgs boson production. Note that these topologies are picked from the topologies with unidentified propagators of equal flow of momenta since these are passed to `exp`, see Section 5.1.2.1.

```
{NNLOrTT18, copy_scale , poco_scale ;6;2;3;1;;
  (q1:1,2)(q2:1,2)(q3:3,2)(p1:5,4)(p2:5,3)(p3:4,3)(p4:5,1)(p5:4,2)
  (p6:1,2);000200}
{NNLOrTT22, copy_scale , poco_scale ;6;2;3;1;;
  (q1:1,3)(q2:1,3)(q3:2,3)(p1:5,4)(p2:5,3)(p3:4,3)(p4:5,1)(p5:4,2)
  (p6:1,2);000200}
{NNLOrTT26, copy_scale , poco_scale ;6;2;3;1;;
  (q1:2,1)(q2:3,1)(q3:1,1)(p1:5,4)(p2:5,3)(p3:4,3)(p4:5,1)(p5:4,2)
  (p6:1,2);000200}
{NNLOrTT30, copy_scale , poco_scale ;6;2;3;1;;
  (q1:3,1)(q2:2,1)(q3:1,1)(p1:5,4)(p2:5,3)(p3:4,3)(p4:5,1)(p5:4,2)
  (p6:1,2);000200}
...
{NNLOrTT35, copy_scale , poco_scale ;6;2;3;1;;
  (q1:2,1)(q2:3,1)(q3:1,1)(p1:5,4)(p2:5,4)(p3:1,2)(p4:4,2)(p5:5,3)
  (p6:1,3);002000}
{NNLOrTT114, copy_scale , poco_scale ;7;2;3;1;;
  (q1:1,3)(q2:2,3)(q3:4,3)(p1:6,5)(p2:5,4)(p3:6,4)(p4:5,2)(p5:2,1)
  (p6:6,3)(p7:3,1);0002000}
{NNLOrTT118, copy_scale , poco_scale ;7;2;3;1;;
  (q1:1,4)(q2:2,4)(q3:3,4)(p1:6,5)(p2:5,4)(p3:6,4)(p4:5,2)(p5:2,1)
  (p6:6,3)(p7:3,1);0002000}
...
{NNLOrTT167, copy_scale , poco_scale ;7;2;3;1;;
  (q1:4,1)(q2:3,1)(q3:2,1)(p1:6,5)(p2:6,5)(p3:3,1)(p4:2,1)(p5:5,3)
  (p6:6,4)(p7:4,2);0020000}
...
```

In this configuration file for `exp`, factors of factorizing diagram topologies appear first, see Figs. 26 and 27. Identical factors due to different topologies are arranged in groups. Thereafter come non-factorizing diagram topologies grouped by their corresponding generic topology. We show ellipses for large parts of the original file. The last block gives the mapping patterns for `NNLOrGT6`. Sample graphs for diagram topologies are depicted in Fig. 28.

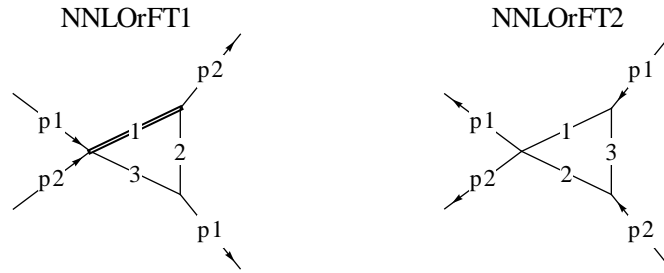


**Figure 27:** Minimal set of topology factors from the factorizing diagram topologies for NNLO Higgs boson production. For each of these factor topologies all representations from factorizing diagram topologies, cf. Fig. 26, are written to the `topsel.<set>` file.

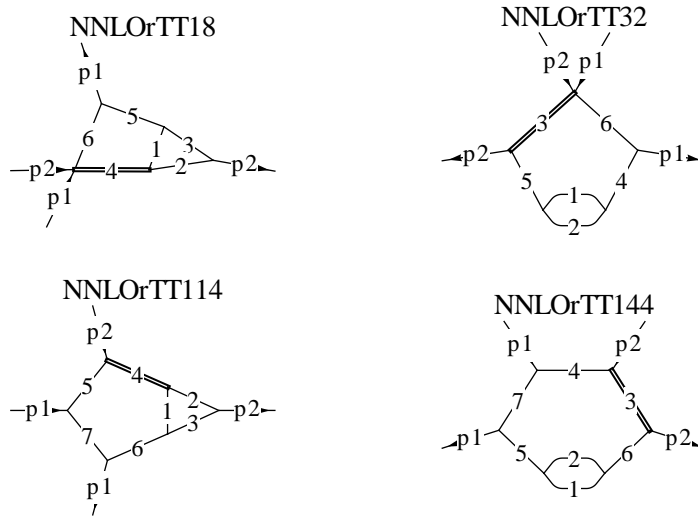


**Figure 28:** Selection of non-factorizing diagram topologies for NNLO Higgs boson production that map all to NNLOrGT6. For NNLOrTT114 we give sample code that performs the mapping to NNLOrGT6 in Appendix C.3.3.

### C.3.2 Signature file

If the script `post-EXP.pl` is on the `$PATH`, it can be called via

```
post-EXP.pl [-i REGEX] SRC...
```

to scan the source files `SRC...` for (combinations of) used topologies. The option `-i` allows to ignore topology names matching the regular expression `REGEX`, e.g., in order to omit from the output tadpole topologies (`tad11, ...`) that do not have to be handled with `TopoID`.

The file `EXP.NNLOr.m` can be created by invoking

```
post-EXP.pl *.src > EXP.NNLOr.m
```

and results in the following:

```
{
  {"NNLOrTT1"},
  {"NNLOrTT10"},
  {"NNLOrTT100"},
}
```

```

{"NNLorTT101"},
{"NNLorTT102"},
{"NNLorTT103"},
{"NNLorTT104"},
{"NNLorTT105"},
{"NNLorTT106"},
{"NNLorTT107"},
{"NNLorTT108f1", "NNLorTT108f2"},
{"NNLorTT108f1", "NNLorTT110f2"},
{"NNLorTT109f1", "NNLorTT108f2"},
{"NNLorTT110f1", "NNLorTT108f2"},
{"NNLorTT110f1", "NNLorTT110f2"},
{"NNLorTT111f1", "NNLorTT108f2"},
{"NNLorTT111f1", "NNLorTT110f2"},
{"NNLorTT112"},
{"NNLorTT113"},
{"NNLorTT114"},
{"NNLorTT115"},
{"NNLorTT116"},
{"NNLorTT117"},
{"NNLorTT118"},
...
}

```

where combinations of topology factors appear, for example

```

{"NNLorTT108f1", "NNLorTT108f2"}

```

and single topologies, for example

```

{"NNLorTT114"}

```

which is related to NNLOrGT6.

### C.3.3 *Non-factorizing topologies*

The part of the file NNLOrGT.EXP relevant for NNLOrTT114, shown in Fig. 28, is given below:

```

* — NNLOrGT6 —
*--#[ NNLOrTT114 :
* target topology
  #define INTCOMBINED "NNLOrGT6"
* immediate notation change
  mu replace_(p'JH1'1,p'JH'1,
              p'JH1'2,p'JH'2,
              p'JH1'3,p'JH'3,
              p'JH1'4,p'JH'4,
              p'JH1'5,p'JH'5,
              p'JH1'6,p'JH'6,
              p'JH1'7,p'JH'7);
* convert MATAD notation
#procedure MATADtoNNLOrTT114
* propagators

```



```

id (p1.p1)^(-1) = d7^(-1);
id (p2.p2)^(-1) = d5^(-1);
id (p3.p3)^(-1) = d6^(-1);
id s4m2 = d3^(-1);
id (p5.p5)^(-1) = d1^(-1);
id (p6.p6)^(-1) = d4^(-1);
id (p7.p7)^(-1) = d2^(-1);
.sort
* line momenta
id p1 = -ptmp2 - v1 - v2;
id p2 = -v2;
id p3 = tmp2 + v2;
id p4 = -ptmp2 - v1;
id p5 = -v1;
id p6 = v1;
id p7 = -ptmp1 + v1;
.sort
* external momenta
id Q1 = tmp1;
id Q2 = tmp2;
.sort
* temporary symbols
mu replace_(tmp1,p1, tmp2,p2);
.sort
#endprocedure

#procedure mNNLorTT114tNNLorGT6
* rename denominators
mu replace_(d7,d7, d5,d5, d6,d6, d3,d3, d1,d4, d4,d4, d2,d2);
* apply momenta shifts
id p1 = tmp2;
id p2 = tmp1;
id v1 = -ptmp1 + tmp2 + tmp3;
id v2 = tmp4;
* replace temporary symbols
mu replace_(tmp1,p1, tmp2,p2, tmp3,v1, tmp4,v2);
#endprocedure

* to be called later
#procedure initlines
#call MATADtoNNLorTT114
#call mNNLorTT114tNNLorGT6
#endprocedure

*--#] NNLorTT114 :

...

```

This kind of code acts as interface between `exp` and generic topologies created with `TopoID`. The line

```
mu replace_(d7,d7, d5,d5, d6,d6, d3,d3, d1,d4, d4,d4, d2,d2);
```

is a typical example for an identification of identical propagators (`d1` and `d4` in this case) which `exp` cannot handle out of the box.

## C.3.4 Factorizing topologies

For factorizing diagrams, it occurs that factors from one diagram are mapped to topology factors that stem from different “parent” topologies. These factors need to be mapped properly to a generic topology. Therefore, in an intermediate step, the minimal set of topology factors needs to be identified from factorizing topologies. Figure 26 shows some of the factorizing diagram topologies in NNLO Higgs boson production, Fig. 27 the corresponding minimal set.

From NNLOrFT.EXP:

```

*--#[ NNLOrTT108f1xNNLOrTT11of2 :

  #define FACTOR "2"

* target topology
  #define INTCOMBINED "NNLOrGT1"

* immediate notation change
  mu replace-(p'JH1'1,p'JH'1, p'JH1'2,p'JH'2, p'JH1'3,p'JH'3,
              p'JH2'1,p'JH'4, p'JH2'2,p'JH'5, p'JH2'3,p'JH'6);

* convert MATAD notation
#procedure MATADtoNNLOrTT108f1xNNLOrTT11of2
* propagators
  id s1m2 = d1^(-1);
  id (p2.p2)^(-1) = d2^(-1);
  id (p3.p3)^(-1) = d3^(-1);
  id (p4.p4)^(-1) = d4^(-1);
  id (p5.p5)^(-1) = d5^(-1);
  id (p6.p6)^(-1) = d6^(-1);
  .sort
* line momenta
  id p1 = ptmp2 - v1;
  id p2 = -v1;
  id p3 = ptmp1 + v1;
  id p4 = ptmp1 + v2;
  id p5 = ptmp2 - v2;
  id p6 = -v2;
  .sort
* external momenta
  id Q1 = ptmp1;
  id Q2 = ptmp2;
  .sort
* temporary symbols
  mu replace-(ptmp1,p1, ptmp2,p2);
  .sort
#endprocedure

#procedure mNNLOrTT108f1xNNLOrTT11of2tNNLOrGT1
* rename denominators
  mu replace-(d1,d3, d2,d1, d3,d2, d4,d6, d5,d5, d6,d4);
* apply momenta shifts
  id v1 = -ptmp3;
  id v2 = -ptmp4;

```

```
* replace temporary symbols
  mu replace_(ptmp1,p1, ptmp2,p2, ptmp3,v1, ptmp4,v2);
#endprocedure

* to be called later
#procedure initlines
  #call MATADtoNNLorTT1o8f1xNNLorTT11of2
  #call mNNLorTT1o8f1xNNLorTT11of2tNNLorGT1
#endprocedure

*--#] NNLorTT1o8f1xNNLorTT11of2 :
```

This snippet of code recombines a massless triangle graph and a triangle with a massive Higgs boson line, see Fig. 27, back into a single graph (as the last one in Fig. 26).



## BIBLIOGRAPHY

---

- [1] **ATLAS Collaboration** Collaboration, G. Aad *et al.*, *Observation of a new particle in the search for the Standard Model Higgs boson with the ATLAS detector at the LHC*. Phys.Lett. **B716** (2012) 1–29, arXiv:1207.7214 [hep-ex].
- [2] **CMS Collaboration** Collaboration, S. Chatrchyan *et al.*, *Observation of a new boson at a mass of 125 GeV with the CMS experiment at the LHC*. Phys.Lett. **B716** (2012) 30–61, arXiv:1207.7235 [hep-ex].
- [3] A. Pak, *The Toolbox of modern multi-loop calculations: novel analytic and semi-analytic techniques*. J.Phys.Conf.Ser. **368** (2012) 012049, arXiv:1111.0868 [hep-ph].
- [4] B. Buchberger, *An Algorithmic Criterion for the Solvability of Algebraic Systems of Equations*.
- [5] B. Buchberger, *An Algorithm for Finding the Basis Elements in the Residue Class Ring Modulo a Zero Dimensional Polynomial Ideal*. PhD thesis, 3, 2006.
- [6] B. Buchberger, “Gröbner bases: A short introduction for systems theorists,” vol. 2178 of *Lecture Notes in Computer Science*, pp. 1 – 19. Springer Verlag, Berlin, 2001.
- [7] B. Buchberger and M. Kauers, *Gröbner basis*. Scholarpedia **5** (2010) no. 10, 7763. revision 128998.
- [8] B. Sturmfels, *What is ... a Gröbner basis?* Notices Amer. Math. Soc. **52** (2005) no. 10, 1199–1200.
- [9] A. Smirnov and V. A. Smirnov, *Applying Gröbner bases to solve reduction problems for Feynman integrals*. JHEP **0601** (2006) 001, arXiv:hep-lat/0509187 [hep-lat].
- [10] A. Smirnov, *An Algorithm to construct Gröbner bases for solving integration by parts relations*. JHEP **0604** (2006) 026, arXiv:hep-ph/0602078 [hep-ph].
- [11] A. Smirnov and V. Smirnov, *S-bases as a tool to solve reduction problems for Feynman integrals*. Nucl.Phys.Proc.Suppl. **160** (2006) 80–84, arXiv:hep-ph/0606247 [hep-ph].
- [12] V. A. Smirnov, *Evaluating Feynman integrals*. Springer Tracts Mod.Phys. **211** (2004) 1–244.
- [13] V. Smirnov, *Feynman integral calculus*.

- [14] V. A. Smirnov, *Analytic tools for Feynman integrals*. Springer Tracts Mod.Phys. **250** (2012) 1–296.
- [15] C. Bogner and S. Weinzierl, *Feynman graph polynomials*. Int.J.Mod.Phys. **A25** (2010) 2585–2618, arXiv:1002.3458 [hep-ph].
- [16] E. Panzer, *On the analytic computation of massless propagators in dimensional regularization*. Nucl.Phys. **B874** (2013) 567–593, arXiv:1305.2161 [hep-th].
- [17] E. Panzer, *On hyperlogarithms and Feynman integrals with divergences and many scales*. JHEP **1403** (2014) 071, arXiv:1401.4361 [hep-th].
- [18] J. M. Henn, *Lectures on differential equations for Feynman integrals*. arXiv:1412.2296 [hep-ph].
- [19] M. Höschele, J. Hoff, and T. Ueda, *Adequate bases of phase space master integrals for  $gg \rightarrow h$  at NNLO and beyond*. JHEP **1409** (2014) 116, arXiv:1407.4049 [hep-ph].
- [20] G. 't Hooft and M. Veltman, *Regularization and Renormalization of Gauge Fields*. Nucl.Phys. **B44** (1972) 189–213.
- [21] A. Pak and A. Smirnov, *Geometric approach to asymptotic expansion of Feynman integrals*. Eur.Phys.J. **C71** (2011) 1626, arXiv:1011.4863 [hep-ph].
- [22] H. Cheng and T. Wu, *EXPANDING PROTONS: SCATTERING AT HIGH-ENERGIES*.
- [23] R. Harlander, T. Seidensticker, and M. Steinhauser, *Complete corrections of Order  $\alpha_s$  to the decay of the Z boson into bottom quarks*. Phys.Lett. **B426** (1998) 125–132, arXiv:hep-ph/9712228 [hep-ph].
- [24] T. Seidensticker, *Automatic application of successive asymptotic expansions of Feynman diagrams*. arXiv:hep-ph/9905298 [hep-ph].
- [25] D. M. B. Nickel and G. Baker, *University of Guelph Report*, <http://users.physik.fu-berlin.de/~kleinert/nickel/guelph.pdf>, 1977. Preprint.
- [26] J. Hoff and A. Pak, “reg – a tool for expansion by regions.” unpublished.
- [27] A. von Manteuffel and C. Studerus, *Reduze 2 - Distributed Feynman Integral Reduction*. arXiv:1201.4330 [hep-ph].
- [28] J. Hoff and A. Pak, “TopoID - a Mathematica package for topology identification.” unpublished.
- [29] S. Wolfram, *Mathematica : a system for doing mathematics by computer*. Addison-Wesley, Redwood City, Calif., 2. ed., 1991.

- 
- [30] J. Vermaseren, *New features of FORM*. arXiv:math-ph/0010025 [math-ph].
- [31] M. Tentyukov and J. Vermaseren, *The Multithreaded version of FORM*. Comput.Phys.Commun. **181** (2010) 1419–1427, arXiv:hep-ph/0702279 [hep-ph].
- [32] J. Kuipers, T. Ueda, J. Vermaseren, and J. Vollinga, *FORM version 4.0*. Comput.Phys.Commun. **184** (2013) 1453–1467, arXiv:1203.6543 [cs.SC].
- [33] P. Nogueira, *Automatic Feynman graph generation*. J.Comput.Phys. **105** (1993) 279–289.
- [34] J. Hoff, *result files*, see attachments.
- [35] F. Tkachov, *A Theorem on Analytical Calculability of Four Loop Renormalization Group Functions*. Phys.Lett. **B100** (1981) 65–68.
- [36] K. Chetyrkin and F. Tkachov, *Integration by Parts: The Algorithm to Calculate beta Functions in 4 Loops*. Nucl.Phys. **B192** (1981) 159–204.
- [37] S. Gorishnii, S. Larin, L. Surguladze, and F. Tkachov, *Mincer: Program for Multiloop Calculations in Quantum Field Theory for the Schoonschip System*. Comput.Phys.Commun. **55** (1989) 381–408.
- [38] S. Larin, F. Tkachov, and J. Vermaseren, *The FORM version of MINCER*.
- [39] M. Steinhauser, *MATAD: A Program package for the computation of MAssive TADpoles*. Comput.Phys.Commun. **134** (2001) 335–364, arXiv:hep-ph/0009029 [hep-ph].
- [40] R. Lee, *Group structure of the integration-by-part identities and its application to the reduction of multiloop integrals*. JHEP **0807** (2008) 031, arXiv:0804.3008 [hep-ph].
- [41] A. Smirnov and A. Petukhov, *The Number of Master Integrals is Finite*. Lett.Math.Phys. **97** (2011) 37–44, arXiv:1004.4199 [hep-th].
- [42] S. Laporta, *High precision calculation of multiloop Feynman integrals by difference equations*. Int.J.Mod.Phys. **A15** (2000) 5087–5159, arXiv:hep-ph/0102033 [hep-ph].
- [43] C. Anastasiou and A. Lazopoulos, *Automatic integral reduction for higher order perturbative calculations*. JHEP **0407** (2004) 046, arXiv:hep-ph/0404258 [hep-ph].
- [44] A. Smirnov, *Algorithm FIRE – Feynman Integral REduction*. JHEP **0810** (2008) 107, arXiv:0807.3243 [hep-ph].
- [45] A. Smirnov and V. Smirnov, *FIRE4, LiteRed and accompanying tools to solve integration by parts relations*. Comput.Phys.Commun. **184** (2013) 2820–2827, arXiv:1302.5885 [hep-ph].

- [46] A. V. Smirnov, *FIRE5: a C++ implementation of Feynman Integral REDuction*. arXiv:1408.2372 [hep-ph].
- [47] C. Studerus, *Reduze-Feynman Integral Reduction in C++*. Comput.Phys.Commun. **181** (2010) 1293–1300, arXiv:0912.2546 [physics.comp-ph].
- [48] A. Pak, *Precision Calculations in Heavy Fermion Decays*. Ph.d. thesis, University of Alberta, 2008.
- [49] J. Hoff and A. Pak, “rows – an implementation of Laporta’s algorithm.” unpublished.
- [50] C. W. Bauer, A. Frink, and R. Kreckel, *Introduction to the GiNaC framework for symbolic computation within the C++ programming language*. arXiv:cs/0004015 [cs-sc].
- [51] R. H. Lewis, *Fermat – A Computer Algebra System for Polynomial and Matrix Computation*, <http://home.bway.net/lewis/>.
- [52] P. Baikov, *Explicit solutions of the three loop vacuum integral recurrence relations*. Phys.Lett. **B385** (1996) 404–410, arXiv:hep-ph/9603267 [hep-ph].
- [53] P. Baikov, *Explicit solutions of the multiloop integral recurrence relations and its application*. Nucl.Instrum.Meth. **A389** (1997) 347–349, arXiv:hep-ph/9611449 [hep-ph].
- [54] P. Baikov and V. A. Smirnov, *Equivalence of recurrence relations for Feynman integrals with the same total number of external and loop momenta*. Phys.Lett. **B477** (2000) 367–372, arXiv:hep-ph/0001192 [hep-ph].
- [55] P. Baikov and M. Steinhauser, *Three loop vacuum integrals in FORM and REDUCE*. Comput.Phys.Commun. **115** (1998) 161–169, arXiv:hep-ph/9802429 [hep-ph].
- [56] V. A. Smirnov and M. Steinhauser, *Solving recurrence relations for multiloop Feynman integrals*. Nucl.Phys. **B672** (2003) 199–221, arXiv:hep-ph/0307088 [hep-ph].
- [57] R. Lee, *Presenting LiteRed: a tool for the Loop InTEgrals REDuction*. arXiv:1212.2685 [hep-ph].
- [58] R. N. Lee, *LiteRed 1.4: a powerful tool for reduction of multiloop integrals*. J.Phys.Conf.Ser. **523** (2014) 012059, arXiv:1310.1145 [hep-ph].
- [59] P. Kant, *Finding Linear Dependencies in Integration-By-Parts Equations: A Monte Carlo Approach*. Comput.Phys.Commun. **185** (2014) 1473–1476, arXiv:1309.7287 [hep-ph].
- [60] A. von Manteuffel and R. M. Schabinger, *A novel approach to integration by parts reduction*. arXiv:1406.4513 [hep-ph].



- [61] C. Anastasiou and K. Melnikov, *Higgs boson production at hadron colliders in NNLO QCD*. Nucl.Phys. **B646** (2002) 220–256, arXiv:hep-ph/0207004 [hep-ph].
- [62] M. E. Peskin and D. V. Schroeder, *An Introduction to quantum field theory*.
- [63] G. 't Hooft and M. Veltman, *DIAGRAMMAR*. NATO Sci.Ser.B **4** (1974) 177–322.
- [64] G. 't Hooft, *Under the spell of the gauge principle*. Adv.Ser.Math.Phys. **19** (1994) 1–683.
- [65] G. 't Hooft, *The Conceptual Basis of Quantum Field Theory*. Phys.Phil.A:661-729 (2002) .
- [66] R. Cutkosky, *Singularities and discontinuities of Feynman amplitudes*. J.Math.Phys. **1** (1960) 429–433.
- [67] L. Landau, *On analytic properties of vertex parts in quantum field theory*. Nucl.Phys. **13** (1959) 181–192.
- [68] C. Anastasiou, L. J. Dixon, and K. Melnikov, *NLO Higgs boson rapidity distributions at hadron colliders*. Nucl.Phys.Proc.Suppl. **116** (2003) 193–197, arXiv:hep-ph/0211141 [hep-ph].
- [69] C. Anastasiou, L. J. Dixon, K. Melnikov, and F. Petriello, *Dilepton rapidity distribution in the Drell-Yan process at NNLO in QCD*. Phys.Rev.Lett. **91** (2003) 182002, arXiv:hep-ph/0306192 [hep-ph].
- [70] C. Anastasiou, L. J. Dixon, K. Melnikov, and F. Petriello, *High precision QCD at hadron colliders: Electroweak gauge boson rapidity distributions at NNLO*. Phys.Rev. **D69** (2004) 094008, arXiv:hep-ph/0312266 [hep-ph].
- [71] C. Anastasiou, K. Melnikov, and F. Petriello, *Fully differential Higgs boson production and the di-photon signal through next-to-next-to-leading order*. Nucl.Phys. **B724** (2005) 197–246, arXiv:hep-ph/0501130 [hep-ph].
- [72] A. Pak, M. Rogal, and M. Steinhauser, *Finite top quark mass effects in NNLO Higgs boson production at LHC*. JHEP **1002** (2010) 025, arXiv:0911.4662 [hep-ph].
- [73] A. Pak, M. Rogal, and M. Steinhauser, *Production of scalar and pseudo-scalar Higgs bosons to next-to-next-to-leading order at hadron colliders*. JHEP **1109** (2011) 088, arXiv:1107.3391 [hep-ph].
- [74] A. Pak, M. Rogal, and M. Steinhauser, *Virtual three-loop corrections to Higgs boson production in gluon fusion for finite top quark mass*. Phys.Lett. **B679** (2009) 473–477, arXiv:0907.2998 [hep-ph].

- [75] R. V. Harlander and K. J. Ozeren, *Top mass effects in Higgs production at next-to-next-to-leading order QCD: Virtual corrections*. Phys.Lett. **B679** (2009) 467–472, arXiv:0907.2997 [hep-ph].
- [76] R. V. Harlander and K. J. Ozeren, *Finite top mass effects for hadronic Higgs production at next-to-next-to-leading order*. JHEP **0911** (2009) 088, arXiv:0909.3420 [hep-ph].
- [77] R. V. Harlander, H. Mantler, S. Marzani, and K. J. Ozeren, *Higgs production in gluon fusion at next-to-next-to-leading order QCD for finite top mass*. Eur.Phys.J. **C66** (2010) 359–372, arXiv:0912.2104 [hep-ph].
- [78] M. Höschele, *Phasenraum-Masterintegrale zur Berechnung der Higgsproduktion in Gluonfusion*. Ph.d. thesis, Karlsruhe Institute of Technology (KIT), 2015. in preparation.
- [79] A. Kotikov, *Differential equations method: New technique for massive Feynman diagrams calculation*. Phys.Lett. **B254** (1991) 158–164.
- [80] A. Kotikov, *Differential equation method: The Calculation of N point Feynman diagrams*. Phys.Lett. **B267** (1991) 123–127.
- [81] E. Remiddi, *Differential equations for Feynman graph amplitudes*. Nuovo Cim. **A110** (1997) 1435–1452, arXiv:hep-th/9711188 [hep-th].
- [82] T. Gehrmann and E. Remiddi, *Differential equations for two loop four point functions*. Nucl.Phys. **B580** (2000) 485–518, arXiv:hep-ph/9912329 [hep-ph].
- [83] M. Argeri and P. Mastrolia, *Feynman Diagrams and Differential Equations*. Int.J.Mod.Phys. **A22** (2007) 4375–4436, arXiv:0707.4037 [hep-ph].
- [84] J. M. Henn, *Multiloop integrals in dimensional regularization made simple*. Phys.Rev.Lett. **110** (2013) no. 25, 251601, arXiv:1304.1806 [hep-th].
- [85] M. Argeri, S. Di Vita, P. Mastrolia, E. Mirabella, J. Schlenk, *et al.*, *Magnus and Dyson Series for Master Integrals*. JHEP **1403** (2014) 082, arXiv:1401.2979 [hep-ph].
- [86] R. N. Lee, *Reducing differential equations for multiloop master integrals*. arXiv:1411.0911 [hep-ph].
- [87] B. Jantzen, A. V. Smirnov, and V. A. Smirnov, *Expansion by regions: revealing potential and Glauber regions automatically*. Eur.Phys.J. **C72** (2012) 2139, arXiv:1206.0546 [hep-ph].
- [88] C. Anastasiou, C. Duhr, F. Dulat, and B. Mistlberger, *Soft triple-real radiation for Higgs production at N<sub>3</sub>LO*. JHEP **1307** (2013) 003, arXiv:1302.4379 [hep-ph].

- 
- [89] C. Anastasiou, C. Duhr, F. Dulat, F. Herzog, and B. Mistlberger, *Real-virtual contributions to the inclusive Higgs cross-section at  $N^3LO$* . JHEP **1312** (2013) 088, arXiv:1311.1425 [hep-ph].
- [90] M. Höschele, J. Hoff, A. Pak, M. Steinhauser, and T. Ueda, *Higgs boson production at the LHC: NNLO partonic cross sections through order  $\epsilon$  and convolutions with splitting functions to  $N^3LO$* . Phys.Lett. **B721** (2013) 244–251, arXiv:1211.6559 [hep-ph].
- [91] **LHC Higgs Cross Section Working Group** Collaboration, S. Dittmaier *et al.*, *Handbook of LHC Higgs Cross Sections: 1. Inclusive Observables*. arXiv:1101.0593 [hep-ph].
- [92] **LHC Higgs Cross Section Working Group** Collaboration, S. Dittmaier, C. Mariotti, G. Passarino, R. Tanaka, *et al.*, *Handbook of LHC Higgs Cross Sections: 2. Differential Distributions*. arXiv:1201.3084 [hep-ph].
- [93] J. R. Ellis, M. K. Gaillard, and D. V. Nanopoulos, *A Phenomenological Profile of the Higgs Boson*. Nucl.Phys. **B106** (1976) 292.
- [94] F. Wilczek, *Decays of Heavy Vector Mesons Into Higgs Particles*. Phys.Rev.Lett. **39** (1977) 1304.
- [95] H. Georgi, S. Glashow, M. Machacek, and D. V. Nanopoulos, *Higgs Bosons from Two Gluon Annihilation in Proton Proton Collisions*. Phys.Rev.Lett. **40** (1978) 692.
- [96] T. G. Rizzo, *Gluon Final States in Higgs Boson Decay*. Phys.Rev. **D22** (1980) 178.
- [97] S. Dawson, *Radiative corrections to Higgs boson production*. Nucl.Phys. **B359** (1991) 283–300.
- [98] A. Djouadi, M. Spira, and P. Zerwas, *Production of Higgs bosons in proton colliders: QCD corrections*. Phys.Lett. **B264** (1991) 440–446.
- [99] M. Spira, A. Djouadi, D. Graudenz, and P. Zerwas, *Higgs boson production at the LHC*. Nucl.Phys. **B453** (1995) 17–82, arXiv:hep-ph/9504378 [hep-ph].
- [100] R. V. Harlander and W. B. Kilgore, *Next-to-next-to-leading order Higgs production at hadron colliders*. Phys.Rev.Lett. **88** (2002) 201801, arXiv:hep-ph/0201206 [hep-ph].
- [101] V. Ravindran, J. Smith, and W. L. van Neerven, *NNLO corrections to the total cross-section for Higgs boson production in hadron hadron collisions*. Nucl.Phys. **B665** (2003) 325–366, arXiv:hep-ph/0302135 [hep-ph].
- [102] S. Marzani, R. D. Ball, V. Del Duca, S. Forte, and A. Vicini, *Higgs production via gluon-gluon fusion with finite top mass beyond next-to-leading order*. Nucl.Phys. **B800** (2008) 127–145, arXiv:0801.2544 [hep-ph].

- [103] K. Chetyrkin, B. A. Kniehl, and M. Steinhauser, *Decoupling relations to  $O(\alpha_s^3)$  and their connection to low-energy theorems*. Nucl.Phys. **B510** (1998) 61–87, arXiv:hep-ph/9708255 [hep-ph].
- [104] M. Steinhauser, *Results and techniques of multiloop calculations*. Phys.Rept. **364** (2002) 247–357, arXiv:hep-ph/0201075 [hep-ph].
- [105] M. Krämer, E. Laenen, and M. Spira, *Soft gluon radiation in Higgs boson production at the LHC*. Nucl.Phys. **B511** (1998) 523–549, arXiv:hep-ph/9611272 [hep-ph].
- [106] Y. Schröder and M. Steinhauser, *Four-loop decoupling relations for the strong coupling*. JHEP **0601** (2006) 051, arXiv:hep-ph/0512058 [hep-ph].
- [107] K. Chetyrkin, J. H. Kühn, and C. Sturm, *QCD decoupling at four loops*. Nucl.Phys. **B744** (2006) 121–135, arXiv:hep-ph/0512060 [hep-ph].
- [108] V. Spiridonov, *Anomalous Dimension of  $g^2$  (Muon-neutrino) and Beta Function*.
- [109] O. Tarasov, A. Vladimirov, and A. Y. Zharkov, *The Gell-Mann-Low Function of QCD in the Three Loop Approximation*. Phys.Lett. **B93** (1980) 429–432.
- [110] S. Larin and J. Vermaseren, *The Three loop QCD Beta function and anomalous dimensions*. Phys.Lett. **B303** (1993) 334–336, arXiv:hep-ph/9302208 [hep-ph].
- [111] S. Moch, J. Vermaseren, and A. Vogt, *The Three loop splitting functions in QCD: The Nonsinglet case*. Nucl.Phys. **B688** (2004) 101–134, arXiv:hep-ph/0403192 [hep-ph].
- [112] A. Vogt, S. Moch, and J. Vermaseren, *The Three-loop splitting functions in QCD: The Singlet case*. Nucl.Phys. **B691** (2004) 129–181, arXiv:hep-ph/0404111 [hep-ph].
- [113] C. Anastasiou, S. Bühler, C. Duhr, and F. Herzog, *NNLO phase space master integrals for two-to-one inclusive cross sections in dimensional regularization*. JHEP **1211** (2012) 062, arXiv:1208.3130 [hep-ph].
- [114] S. Bühler and A. Lazopoulos, *Scale dependence and collinear subtraction terms for Higgs production in gluon fusion at  $N_3$ LO*. JHEP **1310** (2013) 096, arXiv:1306.2223 [hep-ph].
- [115] M. Höschele, J. Hoff, A. Pak, M. Steinhauser, and T. Ueda, *MT: A Mathematica package to compute convolutions*. Comput.Phys.Commun. **185** (2014) 528–539, arXiv:1307.6925.
- [116] P. Baikov, K. Chetyrkin, A. Smirnov, V. Smirnov, and M. Steinhauser, *Quark and gluon form factors to three loops*. Phys.Rev.Lett. **102** (2009) 212002, arXiv:0902.3519 [hep-ph].

- 
- [117] T. Gehrmann, E. Glover, T. Huber, N. Ikizlerli, and C. Studerus, *Calculation of the quark and gluon form factors to three loops in QCD*. JHEP **1006** (2010) 094, arXiv:1004.3653 [hep-ph].
- [118] W. B. Kilgore, *One-Loop Single-Real-Emission Contributions to  $pp \rightarrow H + X$  at Next-to-Next-to-Next-to-Leading Order*. Phys.Rev. **D89** (2014) 073008, arXiv:1312.1296 [hep-ph].
- [119] Y. Li and H. X. Zhu, *Single soft gluon emission at two loops*. JHEP **1311** (2013) 080, arXiv:1309.4391 [hep-ph].
- [120] C. Duhr and T. Gehrmann, *The two-loop soft current in dimensional regularization*. Phys.Lett. **B727** (2013) 452–455, arXiv:1309.4393 [hep-ph].
- [121] F. Dulat and B. Mistlberger, *Real-Virtual-Virtual contributions to the inclusive Higgs cross section at  $N_3LO$* . arXiv:1411.3586 [hep-ph].
- [122] C. Duhr, T. Gehrmann, and M. Jaquier, *Two-loop splitting amplitudes and the single-real contribution to inclusive Higgs production at  $N_3LO$* . arXiv:1411.3587 [hep-ph].
- [123] C. Anastasiou, C. Duhr, F. Dulat, E. Furlan, T. Gehrmann, *et al.*, *Higgs boson gluonfusion production at threshold in  $N^3LO$  QCD*. Phys.Lett. **B737** (2014) 325–328, arXiv:1403.4616 [hep-ph].
- [124] Y. Li, A. von Manteuffel, R. M. Schabinger, and H. X. Zhu,  *$N^3LO$  Higgs and Drell-Yan production at threshold: the one-loop two-emission contribution*. Phys.Rev. **D90** (2014) 053006, arXiv:1404.5839 [hep-ph].
- [125] C. Anastasiou, C. Duhr, F. Dulat, E. Furlan, T. Gehrmann, *et al.*, *Higgs boson gluon-fusion production beyond threshold in  $N_3LO$  QCD*. arXiv:1411.3584 [hep-ph].
- [126] Y. Li, A. von Manteuffel, R. M. Schabinger, and H. X. Zhu, *Soft-virtual corrections to Higgs production at  $N^3LO$* . arXiv:1412.2771 [hep-ph].
- [127] S. Catani, D. de Florian, M. Grazzini, and P. Nason, *Soft gluon resummation for Higgs boson production at hadron colliders*. JHEP **0307** (2003) 028, arXiv:hep-ph/0306211 [hep-ph].
- [128] S. Moch, J. Vermaseren, and A. Vogt, *Higher-order corrections in threshold resummation*. Nucl.Phys. **B726** (2005) 317–335, arXiv:hep-ph/0506288 [hep-ph].
- [129] S. Moch and A. Vogt, *Higher-order soft corrections to lepton pair and Higgs boson production*. Phys.Lett. **B631** (2005) 48–57, arXiv:hep-ph/0508265 [hep-ph].
- [130] A. Idilbi, X.-d. Ji, J.-P. Ma, and F. Yuan, *Threshold resummation for Higgs production in effective field theory*. Phys.Rev. **D73** (2006) 077501, arXiv:hep-ph/0509294 [hep-ph].

- [131] V. Ravindran, *Higher-order threshold effects to inclusive processes in QCD*. Nucl.Phys. **B752** (2006) 173–196, arXiv:hep-ph/0603041 [hep-ph].
- [132] V. Ahrens, T. Becher, M. Neubert, and L. L. Yang, *Renormalization-Group Improved Prediction for Higgs Production at Hadron Colliders*. Eur.Phys.J. **C62** (2009) 333–353, arXiv:0809.4283 [hep-ph].
- [133] V. Ahrens, T. Becher, M. Neubert, and L. L. Yang, *Updated Predictions for Higgs Production at the Tevatron and the LHC*. Phys.Lett. **B698** (2011) 271–274, arXiv:1008.3162 [hep-ph].
- [134] D. de Florian and M. Grazzini, *Higgs production at the LHC: updated cross sections at  $\sqrt{s} = 8$  TeV*. Phys.Lett. **B718** (2012) 117–120, arXiv:1206.4133 [hep-ph].
- [135] D. de Florian and J. Mazzitelli, *A next-to-next-to-leading order calculation of soft-virtual cross sections*. JHEP **1212** (2012) 088, arXiv:1209.0673 [hep-ph].
- [136] R. D. Ball, M. Bonvini, S. Forte, S. Marzani, and G. Ridolfi, *Higgs production in gluon fusion beyond NNLO*. Nucl.Phys. **B874** (2013) 746–772, arXiv:1303.3590 [hep-ph].
- [137] M. Bonvini, R. D. Ball, S. Forte, S. Marzani, and G. Ridolfi, *Updated Higgs cross section at approximate  $N^3LO$* . J.Phys. **G41** (2014) 095002, arXiv:1404.3204 [hep-ph].
- [138] M. Bonvini and S. Marzani, *Resummed Higgs cross section at  $N^3LL$* . JHEP **1409** (2014) 007, arXiv:1405.3654 [hep-ph].
- [139] S. Catani, L. Cieri, D. de Florian, G. Ferrera, and M. Grazzini, *Threshold resummation at  $N^3LL$  accuracy and soft-virtual cross sections at  $N^3LO$* . Nucl.Phys. **B888** (2014) 75–91, arXiv:1405.4827 [hep-ph].
- [140] D. de Florian, J. Mazzitelli, S. Moch, and A. Vogt, *Approximate  $N^3LO$  Higgs-boson production cross section using physical-kernel constraints*. JHEP **1410** (2014) 176, arXiv:1408.6277 [hep-ph].
- [141] M. Bonvini, S. Forte, G. Ridolfi, and L. Rottoli, *Resummation prescriptions and ambiguities in SCET vs. direct QCD: Higgs production as a case study*. arXiv:1409.0864 [hep-ph].
- [142] T. van Ritbergen, J. Vermaseren, and S. Larin, *The Four loop beta function in quantum chromodynamics*. Phys.Lett. **B400** (1997) 379–384, arXiv:hep-ph/9701390 [hep-ph].
- [143] B. A. Kniehl and M. Spira, *Low-energy theorems in Higgs physics*. Z.Phys. **C69** (1995) 77–88, arXiv:hep-ph/9505225 [hep-ph].
- [144] V. D. Barger and R. Phillips, *COLLIDER PHYSICS*.

- 
- [145] R. K. Ellis, W. J. Stirling, and B. Webber, *QCD and collider physics*. Camb.Monogr.Part.Phys.Nucl.Phys.Cosmol. **8** (1996) 1–435.
- [146] C. Anastasiou, F. Herzog, and A. Lazopoulos, *On the factorization of overlapping singularities at NNLO*. JHEP **1103** (2011) 038, arXiv:1011.4867 [hep-ph].
- [147] A. Vogt, S. Moch, and J. Vermaseren, *The three-loop splitting functions in QCD*. Nucl.Phys.Proc.Suppl. **152** (2006) 110–115, arXiv:hep-ph/0407321 [hep-ph].
- [148] S. Moch, J. Vermaseren, and A. Vogt, *The QCD splitting functions at three loops: Methods and results*. Nucl.Phys.Proc.Suppl. **135** (2004) 137–146, arXiv:hep-ph/0408075 [hep-ph].
- [149] P. Nogueira, *Abusing qgraf*. Nucl.Instrum.Meth. **A559** (2006) 220–223.
- [150] M. Höschele, J. Hoff, A. Pak, M. Steinhauser, and T. Ueda, *result files*, <http://www.ttp.kit.edu/Progdata/ttp12/ttp12-45/>.
- [151] E. Remiddi and J. Vermaseren, *Harmonic polylogarithms*. Int.J.Mod.Phys. **A15** (2000) 725–754, arXiv:hep-ph/9905237 [hep-ph].
- [152] J. Vermaseren, *Harmonic sums, Mellin transforms and integrals*. Int.J.Mod.Phys. **A14** (1999) 2037–2076, arXiv:hep-ph/9806280 [hep-ph].
- [153] J. Vermaseren, *harmopol*, <http://www.nikhef.nl/~form/maindir/packages/harmopol/>.
- [154] D. Maitre, *HPL, a mathematica implementation of the harmonic polylogarithms*. Comput.Phys.Commun. **174** (2006) 222–240, arXiv:hep-ph/0507152 [hep-ph].
- [155] D. Maitre, *Extension of HPL to complex arguments*. Comput.Phys.Commun. **183** (2012) 846, arXiv:hep-ph/0703052 [HEP-PH].
- [156] A. Vogt, *Resummation of small- $x$  double logarithms in QCD: semi-inclusive electron-positron annihilation*. JHEP **1110** (2011) 025, arXiv:1108.2993 [hep-ph].
- [157] M. Höschele, J. Hoff, A. Pak, M. Steinhauser, and T. Ueda, *result files*, <http://www.ttp.kit.edu/Progdata/ttp13/ttp13-027/>.
- [158] J. Blümlein and S. Kurth, *Harmonic sums and Mellin transforms up to two loop order*. Phys.Rev. **D60** (1999) 014018, arXiv:hep-ph/9810241 [hep-ph].
- [159] J. Ablinger, J. Blümlein, and C. Schneider, *Harmonic Sums and Polylogarithms Generated by Cyclotomic Polynomials*. J.Math.Phys. **52** (2011) 102301, arXiv:1105.6063 [math-ph].

- [160] J. Hoff and A. Pak, “gen – a filter for cut diagrams.” unpublished.
- [161] C. Anzai, A. Hasselhuhn, M. Höschele, J. Hoff, W. Kilgore, M. Steinhauser, and T. Ueda. in preparation.
- [162] J. Baglio, A. Djouadi, R. Gröber, M. Mühlleitner, J. Quevillon, *et al.*, *The measurement of the Higgs self-coupling at the LHC: theoretical status*. JHEP **1304** (2013) 151, arXiv:1212.5581 [hep-ph].
- [163] U. Baur, T. Plehn, and D. L. Rainwater, *Probing the Higgs selfcoupling at hadron colliders using rare decays*. Phys.Rev. **D69** (2004) 053004, arXiv:hep-ph/0310056 [hep-ph].
- [164] F. Goertz, A. Papaefstathiou, L. L. Yang, and J. Zurita, *Higgs Boson self-coupling measurements using ratios of cross sections*. JHEP **1306** (2013) 016, arXiv:1301.3492 [hep-ph].
- [165] V. Barger, L. L. Everett, C. Jackson, and G. Shaughnessy, *Higgs-Pair Production and Measurement of the Triscalar Coupling at LHC(8,14)*. Phys.Lett. **B728** (2014) 433–436, arXiv:1311.2931 [hep-ph].
- [166] E. N. Glover and J. van der Bij, *HIGGS BOSON PAIR PRODUCTION VIA GLUON FUSION*. Nucl.Phys. **B309** (1988) 282.
- [167] T. Plehn, M. Spira, and P. Zerwas, *Pair production of neutral Higgs particles in gluon-gluon collisions*. Nucl.Phys. **B479** (1996) 46–64, arXiv:hep-ph/9603205 [hep-ph].
- [168] S. Dawson, S. Dittmaier, and M. Spira, *Neutral Higgs boson pair production at hadron colliders: QCD corrections*. Phys.Rev. **D58** (1998) 115012, arXiv:hep-ph/9805244 [hep-ph].
- [169] D. de Florian and J. Mazzitelli, *Higgs Boson Pair Production at Next-to-Next-to-Leading Order in QCD*. Phys.Rev.Lett. **111** (2013) 201801, arXiv:1309.6594 [hep-ph].
- [170] J. Grigo, K. Melnikov, and M. Steinhauser, *Virtual corrections to Higgs boson pair production in the large top quark mass limit*. Nucl.Phys. **B888** (2014) 17–29, arXiv:1408.2422 [hep-ph].
- [171] J. Grigo, J. Hoff, K. Melnikov, and M. Steinhauser, *On the Higgs boson pair production at the LHC*. Nucl.Phys. **B875** (2013) 1–17, arXiv:1305.7340 [hep-ph].
- [172] J. Grigo, J. Hoff, K. Melnikov, and M. Steinhauser, *Higgs boson pair production at the LHC: top-quark mass effects at next-to-leading order*. PoS **RADCOR2013** (2013) 006, arXiv:1311.7425 [hep-ph].
- [173] J. Grigo and J. Hoff, *Mass-corrections to double-Higgs production & TopoID*. PoS **LL2014** (2014) 030, arXiv:1407.1617 [hep-ph].
- [174] J. Grigo, *Higgs boson pair production at the LHC*. Ph.d. thesis, Karlsruhe Institute of Technology (KIT), 2015. in preparation.



- 
- [175] V. A. Smirnov, *Applied asymptotic expansions in momenta and masses*. Springer Tracts Mod.Phys. **177** (2002) 1–262.
- [176] R. Hamberg, W. van Neerven, and T. Matsuura, *A Complete calculation of the order  $\alpha - s^2$  correction to the Drell-Yan K factor*. Nucl.Phys. **B359** (1991) 343–405.
- [177] S. L. Adler, *Axial vector vertex in spinor electrodynamics*. Phys.Rev. **177** (1969) 2426–2438.
- [178] J. Bell and R. Jackiw, *A PCAC puzzle:  $\pi \rightarrow \gamma \gamma$  in the sigma model*. Nuovo Cim. **A60** (1969) 47–61.
- [179] P. Breitenlohner and D. Maison, *Dimensional Renormalization and the Action Principle*. Commun.Math.Phys. **52** (1977) 11–38.
- [180] S. Larin and J. Vermaseren, *The  $\alpha$ - $s^3$  corrections to the Bjorken sum rule for polarized electroproduction and to the Gross-Llewellyn Smith sum rule*. Phys.Lett. **B259** (1991) 345–352.
- [181] S. Larin, *The Renormalization of the axial anomaly in dimensional regularization*. Phys.Lett. **B303** (1993) 113–118, arXiv:hep-ph/9302240 [hep-ph].
- [182] G. Kramer and B. Lampe, *Two Jet Cross-Section in  $e^+ e^-$  Annihilation*. Z.Phys. **C34** (1987) 497.
- [183] T. Matsuura and W. van Neerven, *Second Order Logarithmic Corrections to the Drell-Yan Cross-section*. Z.Phys. **C38** (1988) 623.
- [184] T. Matsuura, S. van der Marck, and W. van Neerven, *The Calculation of the Second Order Soft and Virtual Contributions to the Drell-Yan Cross-Section*. Nucl.Phys. **B319** (1989) 570.
- [185] T. Gehrmann, T. Huber, and D. Maitre, *Two-loop quark and gluon form-factors in dimensional regularisation*. Phys.Lett. **B622** (2005) 295–302, arXiv:hep-ph/0507061 [hep-ph].
- [186] R. Lee, A. Smirnov, and V. Smirnov, *Analytic Results for Massless Three-Loop Form Factors*. JHEP **1004** (2010) 020, arXiv:1001.2887 [hep-ph].



## DANKSAGUNG

---

Zunächst möchte ich mich bei Prof. Dr. Matthias Steinhauser und Prof. Dr. Johann Kühn für die Übernahme von Referat und Korreferat bedanken, aber auch für die Möglichkeit mich über die vergangenen Jahre hinweg am Institut für Theoretische Teilchenphysik (TTP) mit interessanten Fragestellungen befassen zu können. Ihre Förderung erlaubte mir den Einstieg in das Feld der theoretischen Teilchenphysik. Insbesondere möchte ich Herrn Steinhauser für das Angebot danken, eine Doktorarbeit unter seiner Betreuung zu verfassen und für Betrauung mit Aufgaben in Lehre und Computeradministration des Instituts. Auch die Zeit, die zahlreiche Diskussionen und das Debugging von TopoID in Anspruch nahmen, möchte ich nennen.

Im diesem Kontext ist Alexey Pak hervorzuheben. Auf ihn geht die erste Version des Programms zurück und er stellte mir desweiteren andere seiner Programme zur Verfügung, aus deren Code ich vieles über Programmieren lernen und auf denen ich aufbauen konnte.

Mein Dank gilt auch den Mitautoren der Papiere, die wir während der Zeit meiner Diplom- und Doktorarbeit veröffentlichen konnten. Dies sind Jonathan Grigo, Andrey Grozin, Maik Höschele, Peter Marquard, Kirill Melnikov, Matthias Steinhauser, Alexey Pak und Takahiro Ueda.

Jonathan Grigo, Maik Höschele, Wolfgang Hollik, Peter Marquard und Matthias Steinhauser haben Teile dieser Dissertation korrekturgelesen oder gaben mir zahlreiche hilfreiche Kommentare und Verbesserungsvorschläge.

In meiner Funktion als Administrator für die Rechenanlagen des TTP möchte ich mich bei allen "Admins" des TTP und des Instituts für Theoretische Physik (ITP) für die angenehme Zusammenarbeit bedanken. Von Seiten des TTP sind dies: Otto Eberhardt, Thomas Hermann, David Kunz, Peter Marquard, Jens Salomon und Christoph Wiegand, von Seiten des ITP: Johannes Bellm, Bastian Feigl, Christian Röhr und Robin Roth.

Ich konnte mich immer auf die freundschaftliche Arbeitsatmosphäre am TTP verlassen. Neben den vorher genannten Personen ist dies auch Anastasia Bierweiler, Franziska Schissler, Dominik Kara, Tobias Kasprzik, Alexander Kurz, Ulises Saldaña Salazar, Nikolai Zerf, Max Zoller und allen anderen Mitarbeitern zu verdanken. Auch der Verdienst der Sekretärinnen des TTP, allen voran Martina Schorn, soll an dieser Stelle erwähnt sein.

Ohne die Hilfe und Unterstützung meiner Eltern Monika und Rudi, sowie meiner Schwester Simone in den Dingen neben der Physik wäre diese Arbeit wahrscheinlich nicht möglich gewesen.